

19941129 054

DTIC QUALITY INSPECTED 5

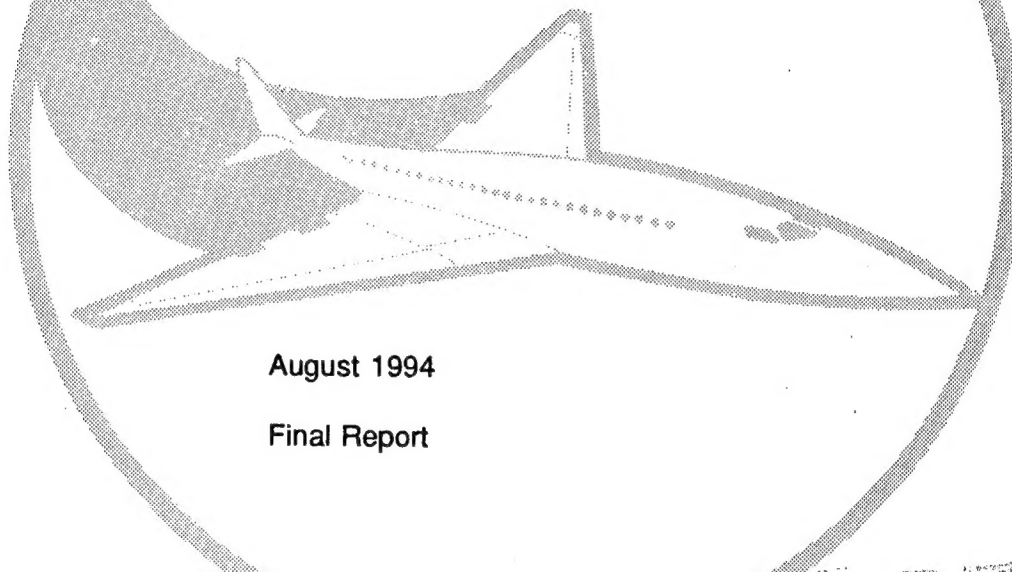
DOT/FAA/CT-94/56

FAA Technical Center  
Atlantic City International Airport,  
N.J. 08405

TP 11983E

Transportation Development Centre  
Montreal, Quebec, Canada

# Characterization of Corrosion and Development of a Breadboard Model of a D Sight Aircraft Inspection System: Phase I



August 1994

Final Report

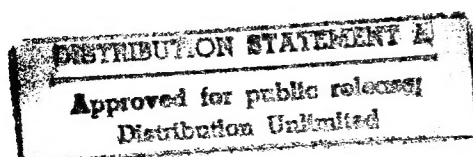
This document is available to the public  
through the National Technical Information  
Service, Springfield, Virginia 22161.



U.S. Department of Transportation  
Federal Aviation Administration



Transport Canada    Transports Canada



#### NOTICE

This document is disseminated under the sponsorship of the U.S. Department of Transportation in the interest of information exchange. The United States Government assumes no liability for the contents or use thereof.

The United States Government does not endorse products or manufacturers. Trade or manufacturers' names appear herein solely because they are considered essential to the objective of this report.

1. Report No. DOT/FAA/CT-94/56 * TP 11983E		2. Government Accession No.		3. Recipient's Catalog No.	
4. Title and Subtitle  CHARACTERIZATION OF CORROSION AND DEVELOPMENT OF A BREADBOARD MODEL OF A D SIGHT AIRCRAFT INSPECTION SYSTEM - PHASE I				5. Report Date  August 1994	
				6. Performing Organization Code	
7. Author(s)  F. Karpala and O.L. Hageniers				8. Performing Organization Report No.	
9. Performing Organization Name and Address  DiffRACTO Limited 2835 Kew Drive Windsor, Ontario N8T 3B7				10. Work Unit No. (TRAIS)	
				11. Contract or Grant No. PA-7	
12. Sponsoring Agency Name and Address  U.S. Department of Transportation Federal Aviation Administration Technical Center Atlantic City International Airport, NJ 08405				13. Type of Report and Period Covered  Final Report	
				14. Sponsoring Agency Code ACD-220	
15. Supplementary Notes  *Transportation Development Centre 800 René Levesque Blvd. W., 6th Floor Montreal, Quebec H3B 1X9  FAA Technical Center Project Manager: Dave Galella					
16. Abstract  This report presents Phase I results of a joint Project Arrangement between the FAA and Transport Canada Aviation for the development and testing of a nondestructive inspection (NDI) system for aircraft corrosion detection in fuselage lap joints. The process is based on D Sight, an optical technique developed by DiffRACTO Limited.  This research project had the following major components: identification of corrosion areas of concern, collection of corrosion samples, acceleration of specimen corrosion in the laboratory, construction and testing of a breadboard inspection device, and laboratory and field trials of the breadboard device.  The outcome can be summarized as follows: a library of aircraft corrosion samples has been established, a corrosion process has been developed that matches in-service corrosion well, a breadboard D Sight NDI system has been built and tested, and a proposal for follow-on work has been completed.					
17. Key Words  Aircraft, corrosion, nondestructive inspection, aging aircraft			18. Distribution Statement  This document is available to the public through the National Technical Information Service, Springfield, Virginia 22161		
19. Security Classif. (of this report)  Unclassified		20. Security Classif. (of this page)  Unclassified		21. No. of Pages  365	22. Price

## PREFACE

This report represents work accomplished under a Project Arrangement (PA-7) pursuant to Addendum 4, Aeronautics, of Memorandum of Understanding concerning Research and Development Cooperation in Transportation between the Department of Transportation of the United States of America and Transport Canada, signed November 2, 1981. Work accomplished under this project arrangement was conducted by Diffracto Limited as authorized by the Transportation Development Centre contract XSD92-00184-(621) T8200-2-2542/01-XSD.

The authors are grateful to the Transportation Development Centre (TDC) of Transport Canada and the Federal Aviation Administration (FAA) for their support in funding this project. The authors also wish to acknowledge the funding assistance of the National Research Council Canada, Institute for Aerospace Research under a collaborative research agreement.

Special thanks go to Mr. Pierre Hébert, Chief, Advanced Technology Division at TDC for his support and assistance, and Mr. Jean-Louis René, Senior Development Officer at TDC, who assumed the efficient coordination of this project. Further thanks go to Mr. William Miller of Transport Canada (Airworthiness) and Mr. David Galella, Project Engineer, at the FAA Technical Center for their input and guidance during the project.

We are especially thankful to Mr. Jerzy Komorowski and his research team from the National Research Council of Canada, Institute for Aerospace Research for their technical skill, enthusiasm, and timely execution of critical aspects of this project.

The research team members consisted of the following individuals from their respective organizations:

### Diffracto Limited

Dr. F. Karpala, Project Manager, Researcher  
Dr. O. L. Hageniers, Researcher  
Mr. Rodger Reynolds, Researcher  
Mr. W.G. James, Researcher  
Mr. Don Clarke, Senior Technician

### NRC/IAR

Mr. Jerzy P. Komorowski, Project Leader, Senior Research Officer  
Mr. Ronald W. Gould, Technical Officer  
Mr. Anton Marincak, Technical Officer  
Dr. Shankar Krishnakumar, Research Fellow

<b>Accession For</b>	
NTIS GRA&I	<input checked="checked" type="checkbox"/>
DTIC TAB	<input type="checkbox"/>
Unannounced	<input type="checkbox"/>
Justification	
By	
Distribution/Avail	
Availability Codes	
Dist	Avail and/or Special
A-1	

## TABLE OF CONTENTS

	<u>Page</u>
EXECUTIVE SUMMARY	ix
1 INTRODUCTION	1
2 SURVEY ACTIVITIES	2
3 SPECIMEN COLLECTION AND CHARACTERIZATION	2
4 SENSOR DESIGN AND CONSTRUCTION	4
5 SENSOR DEMONSTRATION	4
6 CONCLUSION	7
APPENDICES	
A Development of a D Sight Aircraft Inspection System - Phase 1. Task 5.1, Identify Representative Lap Splice Geometry, Task 5.2, Identify Materials of Interest, and Task 5.3, Review Corrosion Types to be Detected and Rank their Significance, Diffracto Limited.	
B Laboratory Technical Report, NRC-Diffracto Ltd. Collaborative Agreement: D Sight for Aircraft Corrosion Inspection, Report on Task 5.1, 5.2 and 5.3, J.P. Komorowski and R.W. Gould, Structures and Materials Laboratory, April 1993.	
C Summary On-Aircraft Non-Destructive Equipment Demonstration, Tinker Airforce Base Oklahoma City, Oklahoma, May 11 - 13, 1993, Diffracto Limited.	
D Modify Impact Detection Breadboard System, Task Report 5.9, October 1993, F. Karpala and R. Reynolds, Diffracto Limited.	
E Task 5.11, Part 1 of 2, DAIS-250C Field Trial, AANC - Albuquerque, NM, F. Karpala, October 1993, Diffracto Limited.	
F Task 5.11, Part 2 of 2, DAIS-250C Field Trial, Air Canada, Winnipeg, Manitoba, by J. P. Komorowski, Don Clarke, and F. Karpala, January 1994.	
G DAIS Applications, D Sight Aircraft Inspection System for Corrosion Inspection, Version 1.0, November 1993, Diffracto Limited.	
H NRC-CNRC Chemical Characterization of Corrosion Products in Fuselage Lap Joints, LTR-ST-1952, November 1993, S. Krishnakumar, J.P. Komorowski, I. Sproule.	
I Application of D Sight for Corrosion Detection in Fuselage Lap and Butt Joints, January 1994, J.P. Komorowski, R.W. Gould, A. Marincak, S. Krishnakumar, NRC/IAR.	

## LIST OF FIGURES

<u>Figure</u>		<u>Page</u>
1	D Sight Image of Corroded Lap Splice with DAIS-250C Sensor and Corresponding Eddy Current Image	6
2	Field Trial of DAIS-250C at AANC, Albuquerque, New Mexico	6

## LIST OF TABLES

<u>Table</u>		<u>Page</u>
1	Phase I Project Tasks	3

## ABBREVIATIONS

AANC	Aging Aircraft NDI Validation Center at Sandia National Laboratories
DAIS	D Sight Aircraft Inspection System
DND	Department of National Defense of Canada
D SIGHT	Diffraction Sight
FAA	Federal Aviation Administration
NRC/IAR	National Research Council Canada/Institute for Aerospace Research
NDI	Nondestructive Inspection
TCA	Transport Canada Aviation
TDC	Transportation Development Centre

## EXECUTIVE SUMMARY

In December 1992, an International Project Arrangement (PA-7) was established between Transport Canada Aviation (TCA) Transportation Development Centre (TDC) and the Federal Aviation Administration (FAA) Technical Center to conduct a Phase I effort to develop a breadboard prototype of a D Sight system for aircraft nondestructive inspection (NDI). The purpose of this research project was specifically to study the applicability of Diffracto's D Sight technology to the detection of interlayer corrosion in transport aircraft fuselage lap joints. To achieve this purpose, several tasks were identified and carried out (see table 1). This report details the results of those tasks and provides the basis for Phase II research.

The first step in this project was to carry out an airline survey to determine what types of corrosion problems occur most frequently on commercial transport aircraft, typical lap splice geometries, types of materials used by the aircraft manufacturers, and dimensional information on aircraft structures to establish geometrical inspection constraints. The survey results confirmed that corrosion in horizontal lap/stringer joints and rib joints comprised the most severe corrosion problems found on most commercial aircraft. This survey clearly justified the initial project focus on corrosion in lap splice joints.

A key aspect of the project was to collect aircraft lap splice samples, both corroded and uncorroded, for use in establishing sensor performance goals and to serve as test specimens in verifying sensor performance. A total of 150 specimens were cut and received from B-727, B-737, DC-9, DC-10, and L-1011 aircraft. Many of these specimens were inspected using other NDI methods. This project has allowed the National Research Council Canada, Institute for Aerospace Research (NRC/IAR) to establish an important library of aircraft specimens, many of which have been characterized for the degree of corrosion.

An accelerated corrosion program was also carried out on aircraft lap joint specimens by NRC/IAR. This program was carried out to produce specimens containing various levels of corrosion. Analysis of corrosion products from aircraft specimens and accelerated corrosion testing specimens has verified the similarity of the corrosion products in both cases, and thereby the validity of the accelerated corrosion process. An ancillary effort in this area has indicated that finite element modelling of lap joint corrosion may lead to prediction of surface bulging (pillowing) and thereby D Sight image prediction as a percentage of interlayer corrosion.

The design process of a breadboard D Sight corrosion sensor was based very heavily on a laboratory test program using the aircraft lap joint specimens collected by NRC/IAR. Seven of the dominant D Sight parameters were varied in this laboratory testing phase to arrive at optimal images of the corrosion pillowing. Based on these D Sight parameters, a breadboard sensor was designed and built. This sensor has been called the DAIS-250C. During laboratory testing of this sensor on corroded lap joints specimens, it was concluded that the sensitivity of D Sight in detecting corrosion rivals the sensitivity of eddy current inspection equipment used in everyday aircraft inspection. Furthermore, D Sight is much faster.

To conclude Phase I, two field trials were carried out using the breadboard DAIS-250C sensor. The first was at the FAA Aging Aircraft NDI Validation Center (AANC) operated by Sandia National Laboratories in Albuquerque, NM. The breadboard sensor was used to inspect 80 percent of the fuselage lap joints of the AANC B-737 aircraft. The total inspection and analysis time was only 13 percent of the suggested inspection time listed in the service bulletins for this aircraft. The second field trip was to an aircraft overhaul facility operated by Air Canada in Winnipeg, Manitoba. During this trip, partial inspections were carried out on a DC-9, A-320, and a B-727. Based on use of the equipment by Air Canada personnel, considerable feedback on method and ease of use was obtained.

## 1. INTRODUCTION.

The continued use of aircraft beyond their intended design life has led to the need for reliable inspections of aging aircraft. This need for added inspection has resulted in a requirement for the introduction of new nondestructive inspection (NDI) methods. One of the promising techniques is D Sight, a method of visualizing surface distortions, depressions, or protrusions. This method has been patented by Diffracto Ltd. of Windsor, Ontario. Previous experimentation has demonstrated the method's potential for use in detecting small defects, however, further development is required to establish a consistent defect detectability. It is also necessary to determine the relationship between the D Sight indication and the cause of the surface anomalies and, more specifically, the degree and type of corrosion where applicable. The establishment of defect detectability is very important to laying the groundwork for acceptance of this technique for corrosion detection.

For several years the Institute for Aerospace Research of the National Research Council Canada (IAR/NRC) has been working with Diffracto Limited on applying D Sight to aircraft inspection. Most of the effort has addressed composite material damage, primarily related to impact damage inspection. In October 1990, a limited D Sight inspection of a Boeing 727 fuselage lap joint recorded excessive pillowing. The area was opened and significant corrosion was found, confirming the D Sight indication. This success in locating the damage and the speed of the inspection provided a good indication of the potential of the D Sight as an inspection tool.

As a result of this successful and promising experiment, Transport Canada Aviation and the U.S. Federal Aviation Administration showed sufficient interest for the Transportation Development Centre to implement a research program which would lead to the development of a prototype capable of effectively functioning in an aircraft maintenance environment. In 1992, an international project arrangement was established between TC Aviation, TDC, and the FAA providing for research funds for Phase I of this project to develop a breadboard prototype D Sight system for aircraft nondestructive inspection.

Aging of aircraft structures is becoming a critically important consideration in aircraft safety as the number of aircraft operating beyond their 20-year design life increases. The use of proof pressure tests to ensure the safety of the fuselage of aging aircraft is impractical; consequently, there is a pressing need for the development of alternative methods of inspection and testing.

Inspection will increasingly be used as a means of keeping aging aircraft flying safely. Reliability and speed of inspection are the two factors of primary importance. D Sight technology has the potential to provide substantial improvement in both of these areas in comparison to current inspection techniques.

The project objective was to characterize corrosion in aircraft structures and to develop a D Sight based inspection system to inspect large aircraft structures. In this phase of the project, the goal was to develop an understanding of corrosion and its occurrence on commercial aircraft and to develop a breadboard corrosion sensor based on D Sight. To conduct this research, thirteen separate tasks (arbitrarily numbered 5.1 through 5.13) were identified and pursued by Diffracto LTD and IAR/NRC. The results of these Phase I tasks are primarily contained in stand-alone, unedited documents attached to this report as appendices. For a reference, table 1 shows the thirteen tasks, the researching organization, and the appendices containing respective task results.

To better understand corrosion, three activities were initiated. One

was a survey of airlines and aircraft structures to determine the types and level of corrosion found on current aircraft, the materials used, and the common lap splice geometries (tasks 5.1-5.3). The second was a procurement program to gather corroded and non-corroded specimens from decommissioned aircraft (tasks 5.4 and 5.7). The third was the testing of lap splice specimens in a laboratory accelerated corrosion testing program (tasks 5.5, 5.6, and 5.8)

The information and specimens obtained from these activities served as input to develop a breadboard corrosion sensor by providing physical constraints on the design, samples for optimizing the sensor optical configuration, and for testing the sensor's detection sensitivity (task 5.9).

To determine some of the human factors and inspection procedures associated with the breadboard corrosion sensor, two field trips were conducted (tasks 5.10 and 5.11). The experience gained from inspecting actual aircraft was used as feedback to suggest recommendations for future prototype development and to prepare the Phase I final report (tasks 5.12 and 5.13).

## 2. SURVEY ACTIVITIES.

Early in the program it was necessary to establish what types of corrosion problems occur most frequently on commercial aircraft, typical lap splice geometries, types of materials used by the aircraft manufacturers, and dimensional information for establishing inspection constraints. A number of different sources were used to compile this information including reference books, journals, conference proceedings, airworthiness directives (ADs), service bulletins (SBs), maintenance manuals, and a survey of aircraft carriers conducted specifically for this program. The detailed results of this effort are included as appendix A and appendix B to this report.

The survey results were particularly useful in confirming that corrosion in horizontal lap/stringer joints and rib joints was the most severe problem found on most commercial aircraft. These results were based on 21 responses from 16 North American airlines, including summaries of aircraft from Boeing, McDonnell Douglas, and Airbus. From the dimensional survey, it was also found that a 66-inch radius of curvature on the fuselage was the worst case curvature for inspection. The survey supported the basic premise of this program to develop a corrosion sensor primarily for horizontal and circumferential lap splices.

## 3. SPECIMEN COLLECTION AND CHARACTERIZATION.

The collection of corroded and non-corroded aircraft fuselage specimens was intended to provide laboratory samples for the optimization of the corrosion sensor, to verify the performance of the sensor after the samples were characterized by other NDI technologies and tear-down, and to provide specimens that could be used to accelerate the corrosion process by artificial means. In all, 150 specimens were cut and received from B-727, B-737, DC-9, DC-10, and L-1011 aircraft. Many of these specimens were characterized by eddy current, x-ray, shadow moire, tear-down, and by the newly developed corrosion sensor. Others were used for accelerated corrosion testing. This project has been instrumental in providing NRC/IAR with a large specimen library that will find uses beyond the scope of this program. Details of the specimen collection program are included in appendix I, prepared by NRC/IAR.

From chemical analysis of the corroded specimens and the accelerated corrosion specimens, it was found that the corrosion products had similar composition (see appendix H for details of this testing). From this composition, it was determined from preliminary modelling that deflection

TABLE 1 - PHASE I PROJECT TASKS

Task	Description	Performing Organization	Appendix
5.1	Identify Representative Lap Splice Geometry	Diffraeto/NRC	A/B
5.2	Identify Materials of Interest	Diffraeto/NRC	A/B
5.3	Review Corrosion Types to be Detected & Rank Their Significance	Diffraeto/NRC	A/B
5.4	Obtain Non-Corroded Specimens	NRC	I
5.5	Accelerated Corrosion Testing	NRC	H,I
5.6	Pre and Post Corrosion Testing NDI	NRC	I
5.7	Obtain Corroded Specimens (CS)	NRC	I
5.8	Characterize Corrosion Damage in CS by D Sight & Teardown	NRC	H,I
5.9	Modify Impact Detection Breadboard System	Diffraeto	D
5.10	Test Breadboard on Specimens to Verify Performance	Diffraeto/NRC	D,G/I
5.11	Demonstrate Breadboard D Sight System	Diffraeto/NRC	C,E/F
5.12	Document Recommendations for the Prototype System	Diffraeto/NRC	--
5.13	Prepare Report & Phase II Proposal	Diffraeto/NRC	--

height associated with pillowing (i.e., maximum pillow deflection) around rivets caused by the volume increase of aluminum to oxide was not only directly related to the amount of material loss due to corrosion, but was up to a factor of 4 greater. This result is a key finding in explaining why D Sight is so sensitive to the presence of corrosion in lap splices. Further theoretical modelling should be continued in future phases of the program.

#### 4. SENSOR DESIGN AND CONSTRUCTION.

The design of a sensor for corrosion detection started with the DAIS-500 optical geometry. The DAIS-500 sensor was developed under Contract #W2207-1-AF07/01-SV, "Location of Impact Damage Sites in Composite Aircraft Structure" sponsored by the Canadian Department of National Defence (DND). A number of field demonstrations from previous research indicated that this sensor was performing well in detecting corrosion even though its optics were designed for impact damage detection. Further details of this field testing success are included as appendix C, "On-Aircraft Non-Destructive Equipment Demonstration". Modification of this sensor to further improve its detectability of corrosion by making appropriate changes to the optical geometry was thought to be a logical starting point for optimization.

The process of optimization included both packaging and optics, keeping in mind that human factors issues are just as important as the sensor's sensitivity to corrosion indications. A hard aluminum skin enclosure with rigid handles was designed for the new sensor after the optical geometry was optimized and fixed. The optical geometry was determined by creating a bench setup of various optical arrangements based on a knowledge of the DAIS-500 deficiencies in detecting corrosion and a knowledge of D Sight. The resultant images were compared against the images from the DAIS-500 and those configurations that exhibited the best image signatures throughout the experiment. Seven dominant D Sight parameters were varied in the bench setups; camera to surface distance, retroreflector to surface distance, camera grazing angle, camera lens focal length, camera aspect ratio, light source to lens distance, and light source size. Ultimately, the camera grazing angle, aspect ratio, and light source size were the most significant changes from the DAIS-500 sensor. The new sensor was built and called the DAIS-250C. Details of the design process are discussed in appendix D, "Modify Impact Detection Breadboard System". Operational characteristics and sample images from the DAIS-250C are shown in appendix G, "DAIS Applications".

During the optimization phase of the program and a study of corroded specimens from actual aircraft, an understanding of corrosion indications began to emerge. The physical pillow indications of corrosion were consistently found on specimens, indicating that D Sight was an appropriate technology to detect its presence with sensitivity rivalling eddy current technology. The pillowing occurs because the corrosion products occupy a significantly larger volume than the original metal. Additional investigation of this process along with theoretical modelling could establish a calibration strategy for future development.

Figure 1 (left) shows a D Sight image from the DAIS-250C sensor with the bright signatures in the middle of the image indicating areas of corrosion. Figure 1 (right) shows the thresholded eddy current scan of the same specimen identifying corrosion in the same area as the D Sight image. Further examples are detailed in appendix I, "Application of D Sight for Corrosion Detection in Fuselage Lap and Butt Joints".

#### 5. SENSOR DEMONSTRATION.

The completed sensor was tested at the FAA's Aging Aircraft NDI

Validation Center (AANC), operated by Sandia National Laboratories in Albuquerque, New Mexico. An older B-737 is available at the facility for testing equipment and the human factors associated with hangar inspections. At present, this aircraft is not yet characterized for corrosion so that a comparison of inspection results could not be made on site. When this characterization is completed, a comparison could be made with the stored inspection results obtained during this field trip. The report "DAIS-250C Field Trial AANC - Albuquerque, NM" (attached as appendix E) details this field testing effort.

Two Boeing service bulletins were used as the basis for the inspections carried out with the new sensor. These bulletins called for a complete inspection of lap joints between body stations 259.5 and 1016 as well as the circumferential butt joints between these two body stations. Every attempt was made to perform a complete inspection of the entire aircraft according to the service bulletins. More than 80 percent of the aircraft was actually inspected while 20 percent was missed due to oversight and the lack of platforms to access the upper fuselage areas. Over 750 images were saved during the inspection. A full inspection was estimated to take a two man crew 11 man-hours followed by 25 man-hours of interpretation time. This time represents only 13 percent of the estimated 278 hours called for in the service bulletins. Based on these inspections, it was estimated that each sensor placement takes approximately 21 seconds and that the image acquisition rate is approximately 0.76 m/min (2.5-ft/min). A number of deficiencies in the sensor design and inspection procedure were identified during the field trip. Recommendations for resolving these problems were proposed for the prototype sensor (Phase II).

A second field trip to the Air Canada facilities at Mirabel Airport in Montreal was arranged to inspect a B-747 but was cancelled at the last moment by Air Canada production personnel for internal reasons. As an alternative, an inspection of a DC-9 at the overhaul facilities of Air Canada in Winnipeg was arranged. In addition to the DC-9, an A-320 and a B-727 were inspected during this trip. The B-727 had the greatest occurrence of corrosion and one large panel from the lower fuselage was donated by Air Canada to NRC for their specimen library. The report, "DAIS-250C Field Trial Air Canada, Winnipeg, Manitoba", attached as appendix F, provides details of the activities and results of this field demonstration. A new highlighter, called ELECTRON, was also used during the inspections. This highlighter is an environmentally friendly dielectric solvent having few health and safety hazards and no residue. Its only drawback is that it evaporates faster than the currently used Snoflake. This highlighter may be more easily approved for NDI than Snoflake and its use should continue in future field trials.

These field trips were extremely valuable in determining inspection procedures, inspection rates, and any shortcomings with the sensor or inspection equipment. Unfortunately, on-site confirmation of corrosion and detection sensitivity was not possible. The B-727 panel from Winnipeg, however, will be characterized fully at NRC and compared with the field inspections. Figure 2 shows the DAIS-250C being used to inspect the B-737 at the AANC.

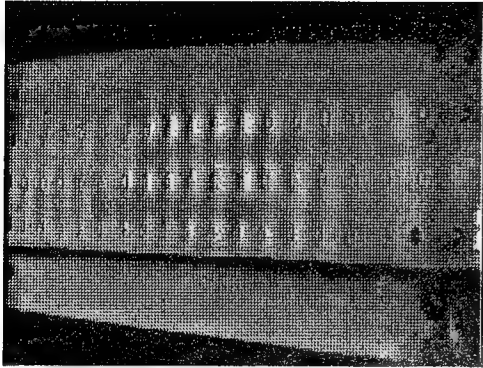


FIGURE 1.- D SIGHT IMAGE OF CORRODED LAP SPLICE WITH DAIS-250C SENSOR (LEFT) AND CORRESPONDING EDDY CURRENT IMAGE (RIGHT)

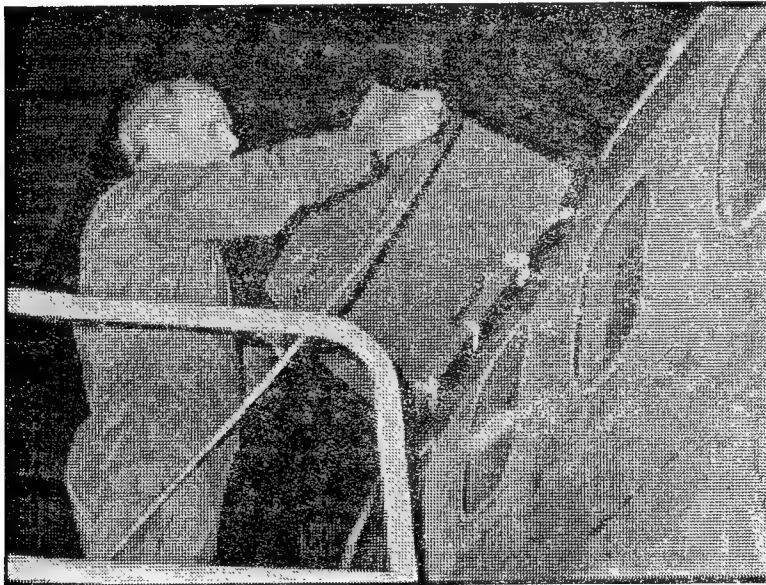


FIGURE 2.- FIELD TRIAL OF DAIS-250C AT AANC, ALBUQUERQUE, NEW MEXICO

## 6. CONCLUSION.

This project has been extremely successful in terms of accomplishments, budget, and scheduling. The procurement of specimens has been a difficult task with several unforeseen delays, but well worth the effort. The development of the breadboard sensor was also extremely successful and the sensor provides sensitivity to corrosion that rivals eddy current. Experience with the sensor on laboratory specimens and actual aircraft has indicated where areas of improvement and modification will be focused during the Phase II prototype development.

## APPENDIX A

Development of a D Sight Aircraft Inspection System - Phase 1. Task 5.1, Identify Representative Lap Splice Geometry, Task 5.2, Identify Materials of Interest, and Task 5.3, Review Corrosion Types to be Detected and Rank their Significance, Diffracto Limited.

**DEVELOPMENT OF A D SIGHT  
AIRCRAFT INSPECTION  
SYSTEM - PHASE 1**

**SSC FILE NO. XSD92-00184-(621)  
Contract No. T8200-2-2544/01-XSD**

**Report on**

**Task 5.1 - Identify Representative Lap Splice Geometry  
Task 5.2 - Identify Materials of Interest  
Task 5.3 - Review Corrosion Types to be Detected  
(exfoliation, interlayer, etc.) and  
Rank their Significance**

**by**

**Dr. Omer Hageniers  
Dr. Frank Karpala**

**Diffracto Limited  
2835 Kew Drive  
Windsor, Ontario  
Canada  
N8T 3B7  
519-945-1467**

**Ref:dsairisp**

## TABLE OF CONTENTS

- 1.0 Introduction
- 2.0 Aircraft Geometry
- 3.0 Lap Splice Geometry
- 4.0 Types and Location of Corrosion
- 5.0 Summary

- Attachment #1: Air Transport Dimensional Information
- Attachment #2: Typical Lap Splice Geometry Sketches
- Attachment #3: Airline Survey Letter & Mailing List
- Attachment #4: Survey Results

## **1.0 Introduction**

This report summarizes the first three tasks of the project. The combination of the first three tasks into a single report is based on two factors, first the tasks are highly interrelated and second, in combination they establish the detailed area of corrosion investigation for the project.

The particular goals of this combined task are as follows:

- 1) establish aircraft geometry, particularly fuselage curvature which will effect the design of the D Sight sensor.
- 2) establish the geometry of typical lap splice structures on aircraft construction.
- 3) establish the types and location of corrosion encountered on aircraft structures. This will be limited to exterior surface accessible structure where D Sight inspection can be of benefit. Furthermore, these corrosion types will be ranked in terms of significance both in relation to each other and to their degree.

## **2.0 Aircraft Geometry**

The overall aircraft geometry is important in terms of how the D Sight sensor head will interface with the surface being inspected. This information will be later used in Task 5.9, "Modify Impact Detection Breadboard D Sight System" to design the surface/sensor head interface.

The interface between the sensor head and the surface being inspected must be quasi light tight. An excessive amount of light leakage will reduce the contrast in the D Sight image and essentially reduce the sensitivity of the system. In order to provide maximum interlayer corrosion sensitivity, it will be necessary to have a surface following "skirt" on the sensor head to provide a light seal. The experience that Diffracto and IAR/NRC had during a field trial at Metro Tech in Oklahoma City, in July 1992, on a Boeing 727 lap joint inspection, made clear to us that in the bright sunlight conditions present, sealing of the surface/sensor head area was critical to successful inspection.

Since "flat" areas of the aircraft are expected to be present in the required surface regime for example, the near vertical sides of the Boeing 747, (in the region of the 2nd deck), the minimum radius of curvature across lap joints will set the other limit of the requirement.

This minimum radius of curvature must be accommodated both along the lap joint being inspected as well as across the lap joint being inspected, based on the presence of both vertical lap joints and horizontal lap joints in the aircraft fuselage structure.

Based on the information gathered in Attachment #1, "Air Transport Dimensional Information", the minimum radius of curvature to be considered is 66 inches based on the larger transport aircraft. To include the smaller commuter aircraft, it is necessary to reduce the minimum radius of curvature to 38 inches.

The design implications of the minimum radius to be inspected will be evaluated in the sensor head design Task 5.9.

### **3.0 Lap Splice Geometry**

Whereas the aircraft geometry outlined above is based on macro structural considerations, the geometry of the lap splice itself is of importance for several reasons. These can be summarized as follows:

- 1) The type and rate of corrosion can be dependent upon the lap splice geometry.
- 2) The width of the splice is important to the required D Sight field of view.
- 3) The number of metal layers in the lap splice (doublers, etc.) can influence the corrosion to D Sight signature effect.

There are a variety of lap splice joints in use throughout the aircraft industry. These vary from the simple two layers of metal riveted together to complex structures with doublers, longerons and rib intersection areas.

The most commonly encountered types of joints are sketched in Attachment No.2, "Typical Lap Splice Geometry Sketches".

The key conclusion from this variety of lap joints is that the strength of the interior structure of the lap joint will determine the extent of exterior pillowing in the lap joint. Since it is this exterior pillowing that we sense via the D Sight image, there is no doubt that the type of lap joint will influence the sensitivity of D Sight to the level of interior corrosion. This interaction will need study at some future point. In the research being carried out here, we will restrict our analysis of the D Sight - corrosion sensitivity interaction only to the simplest lap joint structure.

### **4.0 Types and Location of Corrosion**

There are several major types of aircraft corrosion: exfoliation, crevice, pitting, filiform and interlayer. It is the clear goal of this research to focus on interlayer corrosion, however, it is also important to rate the extent, importance and detectability with D Sight of the other corrosion forms.

The key area of D Sight inspection is the form that offers the greatest potential inspection advantage in terms of speed, is exterior aircraft surfaces, namely; fuselage, wings, tail and tail planes.

The best source of information on the real world of corrosion problems is the airlines who must deal with the corrosion inspection problem on a day to day basis. In order to obtain their input, a letter (see Attachment No. 3, "Airline Survey Letter) requesting information on corrosion problems relative to a selection of airframes was sent to all of the major North American Airlines (see list of names in Attachment No. 3). The source used for the airline NDI contacts

was the attendance lists of the 1991 and 1992 ATA conferences on NDI.

The results of the questionnaire have been summarized in Attachment No. 4, "Survey Results".

A brief recap of the survey results are given as follows:

- 48 NDI contacts were made at 22 North American Airlines requesting a corrosion severity rating on 11 locations for 29 types of aircraft.
- 21 responses were received representing 16 North American Airlines, giving information on 16 types of aircraft.
- Those aircraft types on which a significant response (greater than 3) was received include:

DC-8, DC-9, DC10 and MD-80  
B727, B737, B747, B757 and B767  
A300 and A320

- Analysis of the data on Aging Boeing Aircraft leads to ranking Horizontal Fuselage Lap Joint Corrosion as the #1 problem.
- Analysis of the data on Aging Douglas Aircraft leads to ranking Skin/Rib Fuselage Joints as the #1 problem.
- Analysis of data on all aircraft leads to the conclusion that Horizontal Fuselage Lap Joint Corrosion is the #1 problem.

Based on the survey results, it is possible to give the following ranking of relative importance of sub-surface corrosion locations on aircraft, when we limit ourselves to inspection from the outside of the aircraft:

- 1) Horizontal Fuselage Lap Joints
- 2) Skin/Stringer Fuselage Joints
- 3) Skin/Rib Fuselage Joints
- 4) Vertical Fuselage Lap Joints
- 5) Under Fastener Heads
- 6) Skin/Wing Spar Joints

**ATTACHMENT #1**

**AIR TRANSPORT**

**DIMENSIONAL INFORMATION**

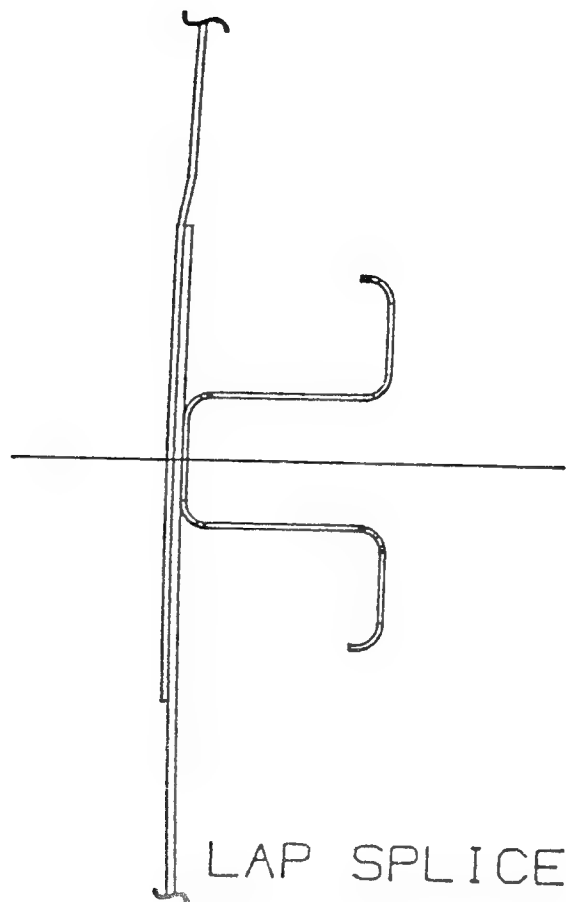
Aircraft Type	Wing Span (ft.)	Length (fuselage or overall [o.l.]) (ft.)	Fuselage diameter (ft.) [estimated from int. diam.]	Overall height (ft.)	Tailplane span (ft.)	Gross wing area (ft. <sup>2</sup> )	Vertical tail surfaces (ft. <sup>2</sup> )	Horizontal tail surfaces (ft. <sup>2</sup> )	Tailplane area (ft. <sup>2</sup> )	Fin area (ft. <sup>2</sup> )	Rudder area (ft. <sup>2</sup> )	Elevators area (ft. <sup>2</sup> )	Alcrons area (ft. <sup>2</sup> )
DC-8 30	142.3	150.5 [o.l.]	12.3	43.3		2758							
DC-9 50	93.3	133.5 [o.l.]	11.0	27.5	36.9	1001			275.6	161.0	65.3	105.8	38.0
DC-10	165.4	170.5	[19.8]	58.1	71.2	3958			1040.2	494.3	110.7	298.1	
MD-11	169.5	192.4	19.8	57.8	59.2	3648	605.0	920.0					
MD80	107.8	135.5	11.0	29.7	40.2	1270			314	102.4	65.3		38.0
MD90 - 40	107.8	171.7 [o.l.]	11.0	30.9		1209			314.0	102.4	65.3		38.0
B707 320-C	145.8	152.9 [o.l.]	12.3	42.4	45.8	3050			625.0	328.0	102.0	151.0	121.0
B720			12.3										
B727 - 200	108.0	136.2	12.3	34	35.8	1700			376.0	356.0	66.0	95.0	57.0
B737 - 200	93.0	96.9	12.3	37.0	36.0	1098			312.0	224.0	56.2	70.5	26.8
B747 - 100	195.7	225.2	21.2	63.4	72.8	5500			1470.0	830.0	247.0	350.0	222.0
B757 - 200	124.8	154.8	[12.6]	44.5	49.9	1994			542.0	370.0	125.0	135.0	48.0
B767 - 200	156.1	155.0	16.5	52.0	61.1	3050			644.5	325.0	171.7	191.7	124.6
L-1011 - 385	155.3	177.7 [o.l.]	19.8	55.3		3456			1282.0	550.0	128.0		160.0
A300	147.1	174.9	18.5	54.5	53.3	2799		688.9		486.5	146.1		
A310	144.0	148.0	18.5	51.8	53.3	2357			482.2	486.5	146.1	206.7	73.8
A320 - 200	111.3	123.3 [o.l.]	12.9 x 13.6	38.7	40.8	1318	231.4	333.7					29.5
BAe146	86.4	101.7 [o.l.]	11.7	28.3	36.4	832			168.0	167.0	57.0	108.0	39.0
BA111	93.5	107.0 [o.l.]	12.8	24.5									
BAe748 2B	102.5	67.0 [o.l.]	8.8	24.8	24.8	828.9			188.9	105.6	39.4	54.1	42.9
F27 MX 500	95.2	28.6 [o.l.]	8.9 x 9.1	28.2	32.0	735.5	153.0	172.0					37.8
F28 MX 5000	82.3	80.5	10.8	27.8	28.4	850.0			209.9	132.4	24.76	41.33	28.74
F50	95.1	82.8 [o.l.]	8.9	27.3	32.0	755.5			172.22	189.4	34.1	34.1	39.4
ATR42	80.6	74.5 [o.l.]	9.4	24.9	24.0	586.6			84.1	91.3	43.0	42.2	33.6
ATR72	88.7	89.1 [o.l.]	9.4	25.1	24.0	657			84.1	91.3	43.0	42.2	33.6
EMB120	64.9	61.5	7.5	20.9	22.8	424			65.7	61.8	27.9	42	31
DCH 6 300	65.0	51.8 [o.l.]	[6.3]	19.5	20.7	420			100.0	48.0	34.0	35.0	33.2
Shorts 360 - 300	74.8	70.8 [o.l.]	7.3	23.9	23.6	454	91.4	106.0	83.6	93.1	24.1	27.4	27.5
SAAB 340 - A	70.3	64.7	7.6	22.5	28.4	450			143.2	113.4	29.7	35.4	22.8

Sources: Jane's All The World's Aircraft, 1974-75 through 1991-1992; Aviation Week & Space Technology, Mar. 16, 1992

**ATTACHMENT #2**

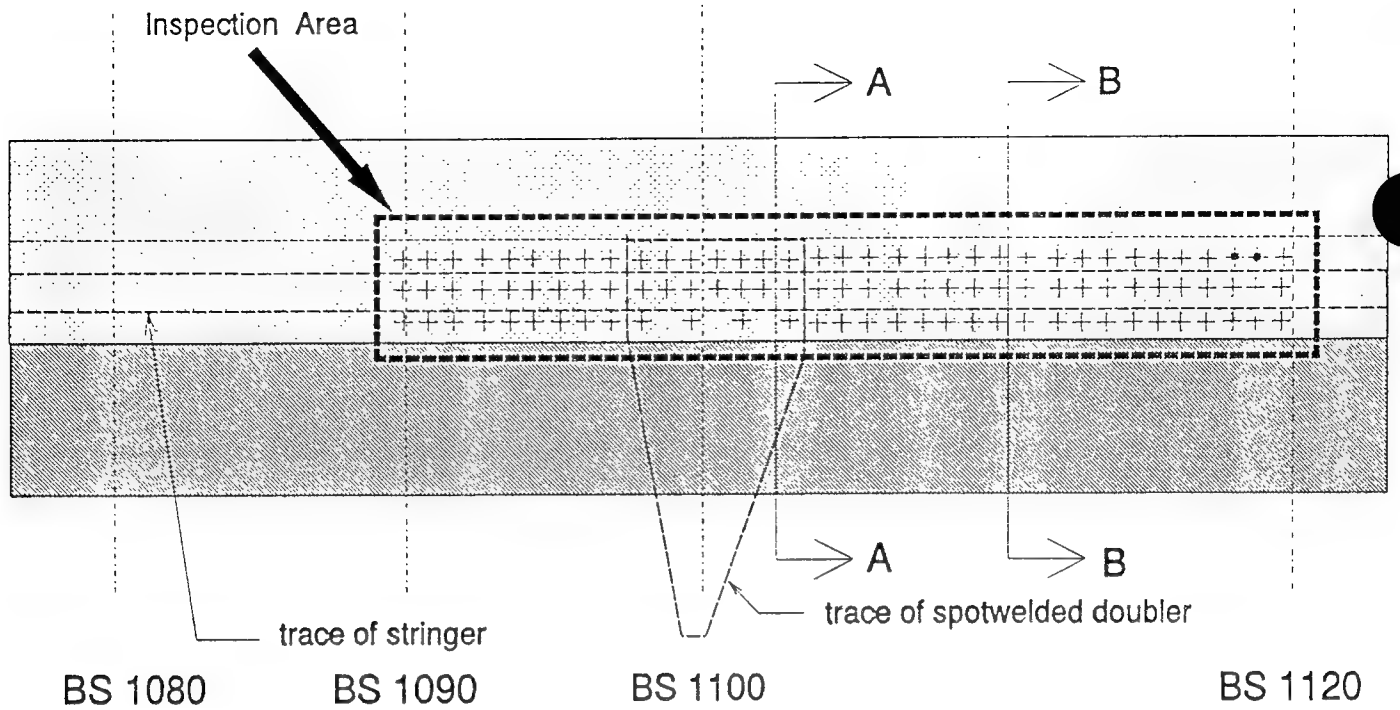
**TYPICAL LAP SPLICE**

**GEOMETRY SKETCHES**

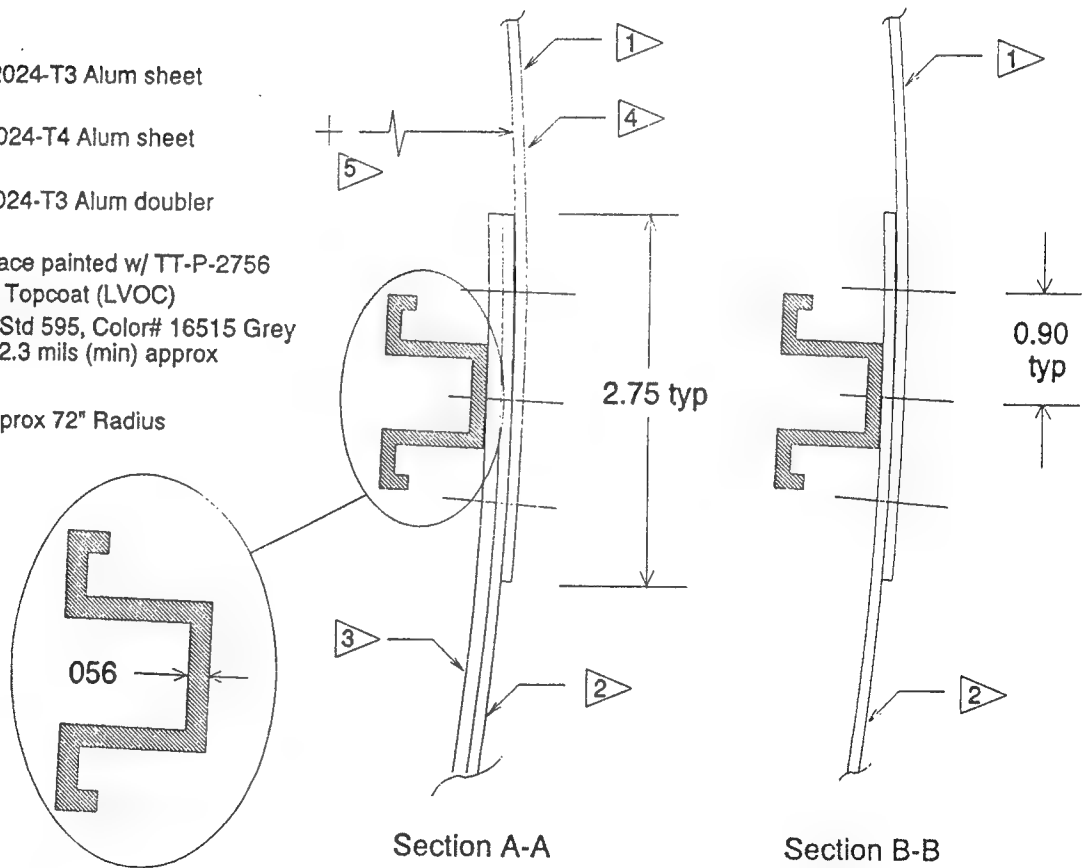


- THREE ROWS OF SOLID RIVETS, COUNTERSUNK HEADS, TYPICAL
- LAPS ARE ASSEMBLED WITHOUT SEALANT OR ADHESIVE. TYPICALLY, LAP IS PRIMED WITH EPOXY PRIMER/ZINC CHROMATE AND ALLOWED TO DRY BEFORE ASSEMBLY.
- DURING REWORK OF OPENED LAPS, MIL-S-81733 SEALANT USED AS FAY SEAL
- IN SOME LAPS, AN .040" DOUBLER IS SPOTWELDED BETWEEN INNER SKIN AND STIFFENER OR BETWEEN INNER SKIN AND OUTER SKIN
- SEE DIMENSION SHEETS FOR SKIN THICKNESSES

Figure 1.0



- 1 .064 Clad 2024-T3 Alum sheet
- 2 .051 Clad 2024-T4 Alum sheet
- 3 .025 Clad 2024-T3 Alum doubler
- 4 Exterior surface painted w/ TT-P-2756 Self-Priming Topcoat (LVOC)  
Shade: Fed Std 595, Color# 16515 Grey  
Thickness: 2.3 mils (min) approx
- 5 Fuselage approx 72" Radius

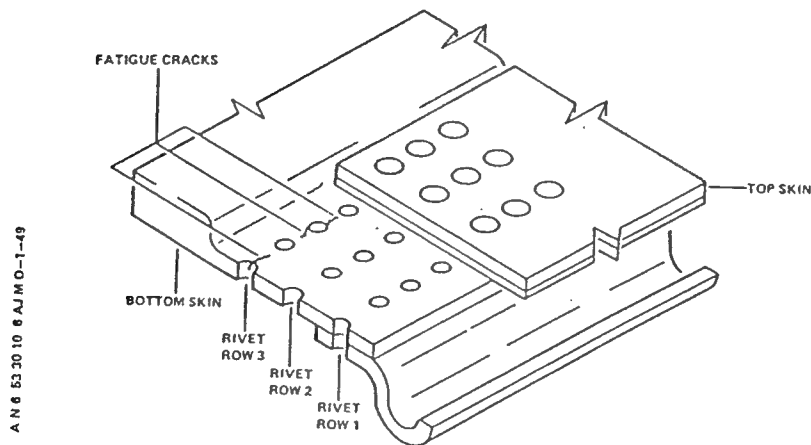
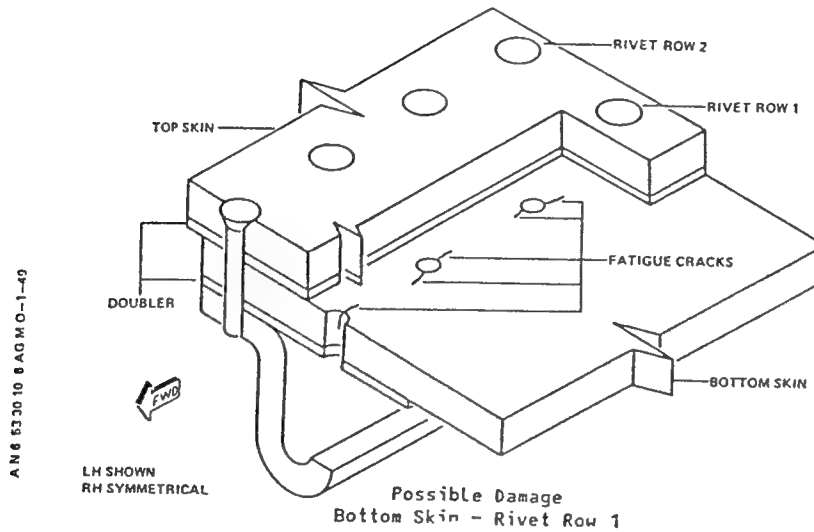


Not to Scale

Figure 2.0

PART 6 - EDDY CURRENT

NONE - SSI



Possible Damage  
Bottom Skin - Rivet Row 3

PART 6  
**53-30-10**  
CONFIG-1  
Page 9  
Mar 01/90

Printed in France

- 119 -

**Figure 3.0**

**ATTACHMENT #3**

**AIRLINE SURVEY LETTER  
& MAILING LIST**

17 March 1993

XXXXXXXXXXXXXXXXXX  
XXXXXXXXXXXXXXXXXX  
XXXXXXXXXXXXXXXXXX  
XXXXXXXXXXXXXXXXXX

Attention: XXXXXXXXXXXXXXXXXXXXXXXX

Dear XXXXXXXXXXXXXXXX:

Diffraeto Limited is under contract with the Canadian Department of Transportation and the FAA to develop subsurface corrosion inspection technology for Aging Aircraft exterior surface inspection. As part of this project we are trying to rate the most significant corrosion locations by aircraft type.

We have attached a simple questionnaire to establish the more common exterior areas of subsurface corrosion and would appreciate it if you could take a few moments to fill it out. Your input is important to the success of our survey, so please help us obtain an accurate survey result by providing us with your input.

Everyone who responds to this survey will receive a copy of the results of the survey. No airline names will be used in the survey results which will be given only by aircraft type.

Thank you for your assistance in this survey.

Sincerely,

**DIFFRACTO LIMITED**

Omer L. Hageniers  
President

OLH:cmg  
Encls.  
Ref:AirSurvey

March '93

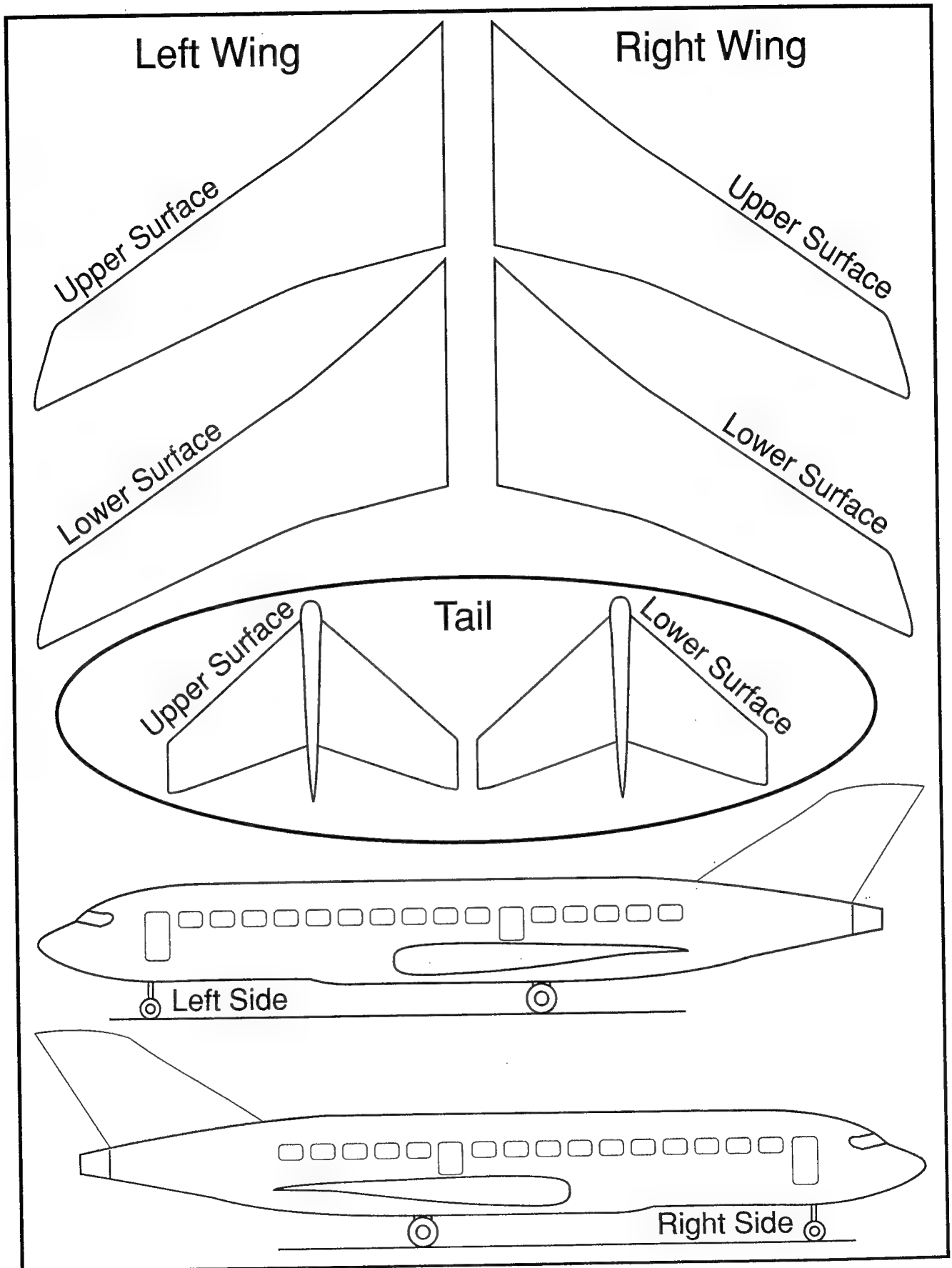
## AIRCRAFT CORROSION AIRLINE SURVEY

Diffraeto Limited, in collaboration with the Institute for Aerospace Research of the National Research Council of Canada (IAR/NRC) is under contract with Transport Canada (TDC) and the Federal Aviation Association (FAA) to develop technology for subsurface corrosion detection on the exterior structure on aging aircraft.

This survey is being carried out to determine which are the main corrosion problems by aircraft type. We would appreciate it if you could fill out the attached sheet for the aircraft types that you operate. Any information that you could provide would be extremely helpful in prioritizing our areas of corrosion Non Destructive Inspection research.

We have also attached a generic aircraft drawing and on it we would appreciate it if you could mark the areas that you feel are of major concern for exterior surface corrosion inspection.

<b>O P T I O N A L</b>	<b>Name:</b>	_____
	<b>Mailing</b>	_____
	<b>Address</b>	_____
	<b>for</b>	_____
	<b>Survey</b>	_____
	<b>Results</b>	_____



Aircraft Type	Operate ✓	Horizontal Fuselage Lap Joints	Vertical Fuselage Lap Joints	Under Fattener Heads	Skin/Stringer Fuselage Joints	Skin/Rib Fuselage Joints	Skin/Wing Rib Joints	Skin/Wing Spar Joints	Tailplane Skin Rivet Joints	Rudder Skin Rivet Joints	Engine Pylon Rivet Joints	Flaps	Other
DC-8													
DC-9													
DC-10													
MD-11													
MD80													
MD90													
B707													
B720													
B777													
B737													
B747													
B757													
B767													
L-1011													
A300													
A310													
A320													
BAe146													
BA111													
BAe748													
F77													
F78													
F50													
ATR42													
ATR72													
EMB120													
DHC-6													
Shorts 360													
SAAB 340													

Please provide a rating for each of the specified aircraft exterior surface corrosion locations for each of the aircraft types you operate, by placing a number from 0 to 10 in the chart.

10 meaning a severe corrosion problem  
5 meaning a moderate corrosion problem  
0 meaning no corrosion problem

Mr. Ernie Sawyer  
Training Rep.  
United Airlines  
San Francisco Int'l Airport  
San Francisco, CA.

Mr. Art Swiatek  
Quality Assurance Rep.  
United Airlines  
San Francisco Int'l Airport  
San Francisco, CA. 94128

Mr. Effren Copprue  
Technician  
Zantop Int'l Airlines  
22532 Hassel  
Detroit, MI. 48219

Mr. Roger Hendrickson  
NDT Inspector Level II  
Zantop Int'l Airlines  
East Airport Rd.,  
Lewis Wilson Airport  
Macon, GA. 31296

Mr. J. Robert Szucs  
Manager NDT Services  
Air Canada, Air Canada Base  
54A Montreal Int'l Airport  
Doval, Quebec HAY 1C2

Mr. Al D. "Smokey" Schnee  
Manager Quality Control  
Alaska Airlines  
PO Box 68900, SEAMQ  
Seattle, WA. 98168

Mr. Brian Vietri  
NDT Supervisor  
America West Airlines  
4000 E. Sky Harbor Blvd., HG-QUE  
Phoenix, AZ. 85034

Mr. Jerry Juba  
Maintenance Instructor  
United Airlines  
San Francisco Int'l Airport  
San Francisco, CA. 94128

Mr. Buck Kleb  
Tech III  
Canadian Airlines Int'l  
050 22nd St. NE  
Calgary, Alberta T2E 7H6

Mr. A. Mehlhaff  
NDT Supervisor  
United Airlines  
San Francisco Int'l Airport  
San Francisco, CA. 94128

Mr. Shawn Mulkin  
Automation  
United Airlines  
San Francisco Int'l Airport  
San Francisco, CA. 95128

Mr. Frank Pfeiffer  
NDT Testing Tech III  
Canadian Airlines Int'l  
One Gran McConachie Way, Vancouver  
Int'l Airport  
Vancouver, B.C. V7B 1V1

Mr. Jack Prall  
NDT Process Engineer  
United Airlines  
San Francisco Int'l Airport  
San Francisco, CA. 94128-3800

Mr. John Seckel  
Engineer, Maint. Supvr.  
Canadian Airlines Int'l  
6001 Grant McConachie Way,  
Vancouver Int'l Airport  
Vancouver, B.C. V7B 1V1

Mr. Jon Myers  
Instructor  
Continental Airlines  
15333 John F. Kennedy Blvd.  
Houston, TX. 77032

Mr. Jerome Recker  
NDT Supv  
Continental Airlines  
7300 World Way West  
Los Angeles, CA. 90045

Mr. Dan Dorr  
Materials & Process Engr.  
Delta Air Lines  
Hartsfield Int'l Airport  
Atlanta, GA. 30320

Mr. Kent Kinniburgh  
Sr. NDT Specialist  
Federal Express  
3101 Tchulahoma-COMBAT 5437  
Memphis, TN. 38118

Mr. Arie Koper  
Manager NDT  
Federal Express  
7401 World Way West  
Los Angeles, CA. 90045

Mr. Don Cline  
Manager NDT  
Hawaiian Airlines  
Honolulu Int'l Airport, PO Box 30008  
Honolulu, HI 96820

Mr. Burl W. Nethercutt  
Specialist NDT  
American Airlines  
P.O. Box 582809 MD 23  
Tulsa, OK 74158-2809

Mr. Dave Kline  
Manager - QC  
American Trans Air  
7661 N. Perimeter Road  
Indianapolis, IN. 46241

Mr. Robert J. Bonaventura  
Dir - Quality Control  
Continental Airlines  
8450 Travelair, Bldg. 2  
Houston, TX 77061

Mr. Richard Rohrig  
Inspection Supervisor  
Continental Airlines  
8250 E. Smith Rd.  
Denver, CO. 80207

Mr. Roy L. Bailey  
Foreman NDT  
Delta Airlines Dept. 521  
Hartsfield Int'l Airport  
Atlanta, GA. 30320

Mr. Richard Delano  
Chief Inspector  
Evergreen In'l Airline  
3850 Three Mile Lane  
McMinnville, OR 97128

Mr. Arie Koper  
Manager NDT Lab.  
Federal Express  
7401 World Way West  
Los Angeles, CA 90045

Mr. Norman C. Vaden, Jr.  
Senior NDT Specialist  
Federal Express  
3101 Tchulahoma - COMBAT 5437  
Memphis, TN. 38118

Mr. Philip Schnubb  
NDT Supervisor  
First Air  
CARP Airport  
CARP, IN, KOAULO, Canada

Mr. Drew A. Lewis  
Aircraft Inspector NDT  
Midwest Express  
555 W. Air Cargo Way  
Milwaukee, WI. 53220

Mr. Paul D. Zuleger  
NDT Inspector  
Midwest Express Airline  
555 Air Cargo Way  
Milwaukee, WI. 53207

Mr. Gerald Doetkott  
NDT Tech. Specialist  
Northwest Airlines  
5101 Northwest Drive, Dept. B-8840  
St. Paul, MN. 55111

Mr. Jeff Register  
Manager, NDT  
Northwest Airlines  
5101 Northwest Dr. MS C8840  
St. Paul, MN. 55111-3034

Mr. Frank T. Smith  
Mgr, NDT  
Northwest Airlines  
1000 Inner Loop Rd.  
Atlanta, GA. 30337

Mr. John P. Yuen  
NDT Tech Specialist  
Northwest Airlines  
5101 Northwest Drive  
St. Paul, MN 55111-3034

Mr. Mark M. Comeau  
NDT Supervisor  
Time Air  
770 McTavish Rd., N.E.  
Calgary, Alberta T4P 7G6

Mr. Ron Hannula  
QC Supervisor  
Tower Air  
Hanger 8 JFK Int'l Airport  
Jamaica, NY 11430

Mr. David Arms  
Instructor  
United Airlines  
S.F. Int'l Airport  
San Francisco, CA 94128

Mr. Gary Dean Davis  
Instructor  
Trans World Airlines  
G920 NW 77 Terr  
Kansas City, MO 64152

Mr. Tom Dreher  
NDT Process Engr  
United Airlines  
SFOEP San Francisco Int'l Airport  
San Francisco, CA. 94128-3800

Mr. James Morgan  
Manager NDT Inspection  
Trans World Airlines  
Kansas City Int'l Airport, RM 1-150  
Kansas City, MO 64195

Mr. Robert Scoble  
Manager, Inspection  
United Airlines SF01Q  
San Francisco Int'l Airport  
San Francisco, CA. 94128

Mr. Russell J. Jones  
Inspection Foreman NDT  
US Air  
Hanger 3 Room 310 Greater Pit Int'l  
Airport  
Pittsburgh, PA. 15231

Mr. Bob Schroeder  
Inspection Supervisor  
United Parcel Service  
801 Grade Ln  
Louisville, KY 40213

Dr. Raymond J. Leseck  
Technical Foreman  
US Air  
Pittsburgh Gtr. Int'l Aprt  
Pittsburgh, PA. 15231

Mr. Richard Butler  
NDT Inspector  
Zantop Int'l Airlines  
840 Willow Run Airport, Maint. Dept.  
Ypsilanti, MI. 48198

Mr. Karl J. Albert  
Inst'r Maint. Training  
United Airlines  
S.F. Int'l Airport SFOMT/PA  
San Francisco, CA. 94128

Mr. Tim Centivany  
Service Representative  
Gulfstream Aerospace Corp.  
824 Willow Run Airport  
Ypsilanti, MI. 48198

## MAILING LIST SUMMARY

<u>Airlines</u>	<u>Number of Contacts</u>
United	10
Canadian	3
Zantop	3
Air Canada	1
Alaska	1
America West	1
Continental	4
American Trans Air	1
Delta	2
Federal Express	4
Evergreen Int'l	1
Hawaiian	1
American	1
First Air	1
Time Air	1
Midwest Express	2
Tower Air	1
Northwest	4
TWA	2
US Air	2
UPS	1
Gulstream	1
<hr/> 22 Airlines	<hr/> 48

# **ATTACHMENT #4**

## **"SURVEY RESULTS"**

### **Survey of North American Airlines To Determine Ranking of Sub-Surface Corrosion Types by Aircraft Type**

**DiffRACTO Limited**

**March 1993**

**Dr. Omer L. Hageniers**

## TABLE OF CONTENTS

- 1.0 Introduction
- 2.0 Discussion of Survey Form
- 3.0 Sources of Survey Participants
- 4.0 Discussion of Results
- 5.0 Conclusions

### Tables

- I: Mailing/Response List
  - II: Summary of Responses of Aircraft Type
  - III: Average of Responses of Aircraft Type
  - IV: Average of Responses by Special Categories: All Responses, DC-8/9/10, and Boeing 727/37/47
  - V: Ranking of Corrosion Location for Aircraft Groupings
- Attachment: Survey Questionnaire

## **1.0 Introduction**

In order to obtain input on the types and location of sub-surface corrosion on aircraft structures, a survey of North American airlines was carried out via a questionnaire mailing. The survey form identified 11 locations for corrosion and requested input for 29 types of aircraft. The form requested that respondents rate each location on a scale from 0 to 10 (with zero representing no corrosion problem and 10 representing a severe corrosion problem) for the aircraft types that their airline operated.

## **2.0 Discussion of the Survey Form**

In arriving at the composition of the survey form several key assumptions were made that could have an influence on the survey results. These assumptions are listed as follows:

- The survey only related to corrosion that has an influence on the exterior aircraft skin and is therefore inspectable from the exterior of the aircraft.
- The survey only listed corrosion locations that relate to a joint of some type in the exterior aircraft structure. This joint could be a lap joint, a rivet location, etc.
- The aircraft types included in the survey form are all the major transport aircraft and a limited grouping of commuter aircraft.
- The rating of corrosion with 10 as severe, 5 as moderate, and 0 as no problem is somewhat vague, and there is a risk that respondents may have different opinions of what severe, moderate, and no problem mean.
- participation in the survey is purely voluntary with the only enticement offered for participation being a copy of the report on the results of the survey.

## **3.0 Sources of Survey Participants**

The survey was sent to 48 individuals at 22 Airlines in North America. It was decided that European and Asian Airline input would not be requested at this time. This choice may naturally have some influence on the survey results.

The 48 individual names were selected from the attendee lists of the 1991 and 1992 ATA/NDT Conferences. All of these participants had a clear connection to the maintenance and/or inspection of aircraft.

## **4.0 Discussion of Results**

Of the 48 questionnaires sent to 22 airlines, 21 responses were received representing 16 airlines. The details of the airlines contacted and respondents are shown in "Table I: Mailing/ Response List". The 21 responses represent a 44% response rate with participation of 73% of the airlines contacted. The elapsed time between the mailing of the questionnaires and the cut off date for

responses was 4.5 weeks.

The response data is listed in "Table II: Summary of Responses by Aircraft Type", the codes R1 thru R21 represent an identification number given to the respondent in the order that the responses were received at Diffracto.

The number of responses by aircraft type varied from a maximum of 12 to a minimum of zero. A summary is provided below:

<u># of Responses</u>	<u>Aircraft Type</u>
12	B727, B747
8	DC-9
6	DC-10
5	B737, B757, A320
4	MD80, A300, DC-8
3	B767
1	BAe748, F28, DHC-6, Shorts 360, L-1011
0	MD-11, MD90, B707, B720, A310, BAe146, BA111, F27, F50, ATR42, ATR72, EMB120, SAAB 340

The averages of the corrosion ratings given by each respondent are also given by aircraft type in Table II, and are summarized in "Table III: Average of Responses by Aircraft Type". Looking at this data (only for those aircraft types that have 3 or more responses), we can select the most severe corrosion areas as follows:

DC-8	Under Fastener Heads
DC-9	Skin/Rib Fuselage Joints
DC-10	Skin/Rib Fuselage Joints
MD80	Skin/Rib Fuselage Joints
B727	Horizontal Fuselage Lap Joints
B737	Horizontal Fuselage Lap Joints
B747	Horizontal Fuselage Lap Joints
B757	Horizontal Fuselage Lap Joints//Skin/Stringer Fuselage Joints
A300	Skin/Stringer Fuselage Joints//Under Fastener Heads
A320	Skin/Stringer Fuselage Joints

The clear conclusion from the above analysis is that the two key external sub-surface corrosion locations on large transport aircraft are the fuselage area at the Lap Joints, and the rib and stringer joint areas.

"Table IV: Average of Responses by Special Categories" contains the average response by three special groupings of aircraft. The first of these is the average of all aircraft, the second the average of the older Douglas Aircraft, namely the DC-8, DC-9 and DC-10, and the third group the average of the older Boeing aircraft, namely the B727, B737 and B747.

The results expressed numerically in Table IV are expressed in "Table V: Ranking of Corrosion Location for Aircraft Groupings" in order of importance relative to corrosion. Table V clearly illustrates that the most severe problem for Aging Boeing Aircraft is the Horizontal Fuselage Lap Joint (a rating of 6.8) while for the Douglas Aging Aircraft it is the Skin/Rib Fuselage Joints (a rating of 4.1).

What is particularly interesting is that the top 6 corrosion areas are the same for all three special categories, providing strong evidence that these are the critical areas to be watched for corrosion. It is further clear from the responses that the top 5 categories are all related to the fuselage area of the aircraft.

## **5.0 Conclusions**

Based on the survey results, it is possible to give the following ranking of relative importance of sub-surface corrosion locations on aircraft, when we limit ourselves to inspection from the outside of the aircraft:

- 1) Horizontal Fuselage Lap Joints
- 2) Skin/Stringer Fuselage Joints
- 3) Skin/Rib Fuselage Joints
- 4) Vertical Fuselage Lap Joints
- 5) Under Fastener Heads
- 6) Skin/Wing Spar Joints

**TABLE I**  
**MAILING/RESPONSE LIST**

<u>Airlines</u>	<u>Number of Contacts</u>	<u>Number of Responses</u>
United	10	
Canadian	3	
Zantop	3	
Air Canada	1	
Alaska	1	21 Responses
America West	1	
Continental	4	
American Trans Air	1	identities are
Delta	2	
Federal Express	4	
Evergreen Int'l	1	
Hawaiian	1	confidential
American	1	
First Air	1	
Time Air	1	
Midwest Express	2	
Tower Air	1	
Northwest	4	
TWA	2	
US Air	2	
UPS	1	
Gulstream	1	
<hr/> 22 Airlines	<hr/> 48	<hr/> 16 Airlines

Table II

Summary of  
Responses by  
Aircraft Type

	Operate ✓	Horizontal Fuselage Lap Joints	Vertical Fuselage Lap Joints	Under Fastener Heads	Skin/Stringer Fuselage Joints	Skin/Rib Fuselage Joints	Skin/Wing Rib Joints	Skin/Wing Spar Joints	Tailplane Skin Rivet Joints	Rudder Skin Rivet Joints	Engine Pylon Rivet Joints	Flaps	Other
DC-8													
R8		5	5	7	7	8	6	6	4	7	4	5	6
R13		0	2	3	2	0	0	0	0	0	0	0	
R19		0	0	0	0	0	0	0	0	0	0	0	
R21		5	2	8	3	3	4	4	2	2	2	4	
Average		2.5	2.3	4.5	3	2.8	2.5	2.5	1.5	2.3	1.5	2.3	
DC-9													
R1		8	8	5	8	8	1	2		0	1	0	
R2		2	3	3	7	4	1	6	4	5	1	6	5
R5		3	1	3	2	6	5	4	2	4	3	2	
R8		5	5	6	3	5	5	5	4	5	4	6	5
R16		3	4	2	5	5	4	5	3	2	4	5	
R18		5	7	7	7	6	1	3	3	0	1	1	
R19		0	0	0	0	0	0	0	0	0	0	0	
R21		6	1	8	2	2	3	3	2	2	2	5	
Average		4.0	3.6	3.6	4.3	4.5	2.5	3.5	2.6	2.6	2.0	3.1	
DC-10													
R1		8	8	5	8	8	1	2		0	2	0	
R3		1	1	3	1	1	0	0	0	0	0	0	0
R5		5	1	3	2	5	2	3	2	2	3	1	
R14		0	0	5	5	5	0	0	0	0	0	0	
R16		3	5	1	5	5	3	4	2	3	5	5	
R20		0	0	0	5	5	0	0	0	0	0	0	
Average		2.8	2.5	2.8	2.8	4.8	1.0	1.5	0.7	0.8	1.7	1.0	

	Operate ✓	Horizontal Fuselage Lap Joints	Vertical Fuselage Lap Joints	Under Fairer Heads	Skin/Stringer Fuselage Joints	Skin/Rib Fuselage Joints	Skin/Wing Rib Joints	Skin/Wing Spar Joints	Tailplane Skin Rivet Joints	Rudder Skin Rivet Joints	Engine Pylon Rivet Joints	Flaps	Other
MD80													
R1		8	8	5	8	8	1	2		0	0	0	
R5		2	1	1	1	2	1	1	0	1	1	2	
R16		2	2	0	3	3	2	2	2	2	2	2	
Average		4	3.7	2	4	4.3	1.3	1.7	1	1	1	1.3	
B727													
R1		10	10	8	10	10	1	6		0	0	0	
R4		5	5	3	6	5		3					
R5		10	1	5	5	3	2	3	2	2	3	1	
R6		5		5									
R8		8	6	6	7	7	5	5	4	5	5	6	5
R9		7	5	5	5	3	1	1	4	0	1	0	
R10		10											
R12		10											
R13		0	3	1	2	0	0	0	0	0	0	0	
R16		10	5	8	10	8	5	5	4	4	5	3	
R19		0	0	0	0	0	0	0	0	0	0	0	
R20		10	10	0	5	5	0	5	0	0	0	5	
Average		7.1	5.0	4.1	4.4	4.6	1.8	3.1	2.0	1.4	1.8	1.9	

	Operate ✓	Horizontal Fuselage Lap Joints	Vertical Fuselage Lap Joints	Under Fastener Heads	Skin/Stringer Fuselage Joints	Skin/Rib Fuselage Joints	Skin/Wing Rib Joints	Skin/Wing Spar Joints	Tailplane Skin Rivet Joints	Rudder Skin Rivet Joints	Engine Pylon Rivet Joints	Flaps	Other
<b>B737</b>													
R1		10	10	8	10	10	1	6		0	0	0	
R7		5	0	0	5	5	0	0	0	0	0	0	
R11		5	5	0	5	5	0	0	0	0	0	5	
R14		5	0	0	5	0	0	0	0	0	0	0	
R20		10	10	0	5	5	0	5	0	0	0	5	
Average		7.0	5.0	1.6	5.0	4.2	0.2	1.8	0	0	0	1.7	
<b>B747</b>													
R1		10	10	8	10	10	1	6		0	2	0	
R3		5	5	5	5	5	0	0	0	0	0	0	0
R4		5	5	3	6	5		3					
R5		10	1	5	5	5	3	3	1	1	4	2	
R8		8	5	8	4	4	6	8	6	6	5	6	6
R10		10											
R13		0	0	0	1	0	0	0	1	0	0	0	
R14		0	0	0	0	0	0	0	0	0	0	0	
R16		10	5	8	10	8	5	5	4	2	2	3	
R17		9	4	6	4	2	2	7	2	0	2	0	
R19		0	0	0	0	0	0	0	0	0	0	0	
R20		10	10	0	5	5	0	5	5	0	0	0	
Average		6.4	4.1	3.9	4.5	3.9	1.7	3.4	1.7	0.8	1.4	1.0	

	Operate ✓	Horizontal Fuselage Lap Joints	Vertical Fuselage Lap Joints	Under Fastener Heads	Skin/Spine Fuselage Joints	Skin/Rib Fuselage Joints	Skin/Wing Rib Joints	Skin/Wing Spar Joints	Tailplane Skin Rivet Joints	Rudder Skin Rivet Joints	Engine Pylon Rivet Joints	Flaps	Other
<b>B757</b>													
R5		3	0	1	1	1	0	1	1	0	1	1	
R7		0	0	0	0	0	0	0	0	0	0	0	
R13		0	0	0	0	0	0	0	0	0	0	0	
R16		2	2	2	4	3	2	1	1	1	1	1	
R20		0	0	0	0	0	0	0	0	0	0	0	
Average		1.0	0.4	0.6	1.0	0.8	0.4	0.4	0.4	0.2	0.4	0.4	
<b>B767</b>													
R14		0	0	0	0	0	0	0	0	0	0	0	
R19		0	0	0	0	0	0	0	0	0	0	0	
R20		0	0	0	0	0	0	0	0	0	0	0	
Average		0	0	0	0	0	0	0	0	0	0	0	
<b>L-1011</b>		4	2	3	3	3	1	1	1	1	1	2	
<b>A300</b>													
R1		8	8	8	8	8	1	1		0	0	0	
R3		1	1	1	1	1	1	0	0	0	0	0	0
R6				6	6						5		
Average		4.5	4.5	5	5	4.5	0.5	0.5	0	0	1.7	0	
<b>A320</b>													
R5		1	1	3	5	2	1	0	0	0	0	1	
R14		0	0	0	0	0	0	0	0	0	0	0	
R16		0	0	0	0	0	1	1	0	0		1	
R19		0	0	0	0	0	0	0	0	0	0	0	
Average		0.3	0.3	0.8	1.3	0.5	0.5	0.3	0	0	0	0.5	



Table III  
Average of  
Responses by  
Aircraft Type

Aircraft Type	# Responses	Horizontal Fuselage Lap Joints	Vertical Fuselage Lap Joints	Under Fattener Heads	Skin/Stinger Fuselage Joints	Skin/Rib Fuselage Joints	Skin/Wing Rib Joints	Skin/Wing Spar Joints	Tailplane Skin Rivet Joints	Rudder Skin Rivet Joints	Engine Pylon Rivet Joints	Flaps	Other
DC-8	4	2.5	2.3	4.5	3.0	2.8	2.5	2.5	1.5	2.3	1.5	2.3	
DC-9	8	4.0	3.6	3.6	4.3	4.5	2.5	3.5	2.6	2.6	2.0	3.1	
DC-10	6	2.8	2.5	2.8	2.8	4.8	1.0	1.5	0.7	0.8	1.7	1.0	
MD-11	0												
MD80	3	4	3.7	2	4	4.3	1.3	1.7	1	1	1	1.3	
MD90	0												
B707	0												
B720	0												
B727	12	7.1	5	4.1	4.4	4.6	1.8	3.1	2.0	1.4	1.8	1.9	
B737	5	7.0	5.0	1.6	5.0	4.2	0.2	1.8	0	0	0	1.7	
B747	12	6.4	4.1	3.9	4.5	3.9	1.7	3.4	1.7	0.8	1.4	1.0	
B757	5	1.0	0.4	0.6	1.0	0.8	0.4	0.4	0.4	0.2	0.4	0.4	
B767	3	0	0	0	0	0	0	0	0	0	0	0	
L-1011	1	4.0	2.0	3.0	3.0	3.0	1.0	1.0	1.0	1.0	1.0	2.0	
A300	3	4.5	4.5	5	5	4.5	0.5	0.5	0	0	1.7	0	
A310	0												
A320	4	0.3	0.3	0.8	1.3	0.5	0.5	0.3	0	0	0	0.5	
BAe146	0												
BA111	0												
BAe748	1	3	0	0	7	5	0	0	3	5	0	0	
F27	0												
F28	1	1	2	1	5	5	2	2	2	2	2	3	
F50	0												
ATR42	0												
ATR72	0												
EMB120	0												
DHC-6	1	0	0	0	0	0	0	0	0	0	7	0	
Shorts 360	1	1	1	1	1	1	1	1	1	1	1	1	
SAAB 340	0												

Average of  
Responses by  
Special  
Categories:  
ALL Responses,  
DC-8/9/10,  
Boeing 727/37/4

[illegible]

Table V: Ranking of Corrosion Location for Aircraft Groupings

	All Aircraft	Douglas DC-8/9/10	Boeing 727/37/47
Most Serious			
	1) Horizontal Fuselage Lap Joints (4.19)	Skin/Rib Fuselage Joints (4.1)	Horizontal Fuselage Lap Joints (6.8)
	2) Skin/Stringer Fuselage Joints (3.68)	Skin/Stringer Fuselage Joints (3.9)	Skin/Stringer Fuselage Joints (4.8)
	3) Skin/Rib Fuselage Joints (3.51)	Under Fastener Heads (3.8)	Vertical Fuselage Lap Joints (4.6)
	4) Vertical Fuselage Lap Joints (3.02)	Horizontal Fuselage Lap Joints (3.4)	Skin/Rib Fuselage Joints (4.4)
	5) Under Fastener Heads (2.88)	Vertical Fuselage Lap Joints (2.9)	Under Fastener Heads (3.6)
	6) Skin/Wing Spar Joints (2.09)	Skin/Wing Spar Joints (2.6)	Skin/Wing Spar Joints (3.0)
	7) Flaps (1.43)	Flaps (2.2)	Flaps (1.6)
	8) Skin/Wing Rib Joints (1.29)	Skin/Wing Rib Joints (2.0)	Tailplane Skin Rivet Joints (1.5)
	9) Tailplane Skin Rivet Joints (1.22)	Rudder Skin Rivet Joints (1.8)	Skin/Wing Rib Joints (1.4)
	10) Rudder Skin Rivet Joints (1.08)	Engine Pylon Rivet Joints (1.8)	Engine Pylon Rivet Joints (1.3)
	11) Engine Pylon Rivet Joints (0.98)	Tailplane Skin Rivet Joints (1.6)	Rudder Skin Rivet Joints (0.9)
Least Serious			

17 March 1993

XXXXXXXXXXXXXXXXXX  
XXXXXXXXXXXXXXXXXX  
XXXXXXXXXXXXXXXXXX  
XXXXXXXXXXXXXXXXXX

Attention: XXXXXXXXXXXXXXXXXXXXXXXX

Dear XXXXXXXXXXXXXXXX:

DiffRACTO Limited is under contract with the Canadian Department of Transportation and the FAA to develop subsurface corrosion inspection technology for Aging Aircraft exterior surface inspection. As part of this project we are trying to rate the most significant corrosion locations by aircraft type.

We have attached a simple questionnaire to establish the more common exterior areas of subsurface corrosion and would appreciate it if you could take a few moments to fill it out. Your input is important to the success of our survey, so please help us obtain an accurate survey result by providing us with your input.

Everyone who responds to this survey will receive a copy of the results of the survey. No airline names will be used in the survey results which will be given only by aircraft type.

Thank you for your assistance in this survey.

Sincerely,

**DIFFRACTO LIMITED**

Omer L. Hageniers  
President

OLH:cmg  
Encls.  
Ref:AirSurvey

March '93

## AIRCRAFT CORROSION AIRLINE SURVEY

Diffraeto Limited, in collaboration with the Institute for Aerospace Research of the National Research Council of Canada (IAR/NRC) is under contract with Transport Canada (TDC) and the Federal Aviation Association (FAA) to develop technology for subsurface corrosion detection on the exterior structure on aging aircraft.

This survey is being carried out to determine which are the main corrosion problems by aircraft type. We would appreciate it if you could fill out the attached sheet for the aircraft types that you operate. Any information that you could provide would be extremely helpful in prioritizing our areas of corrosion Non Destructive Inspection research.

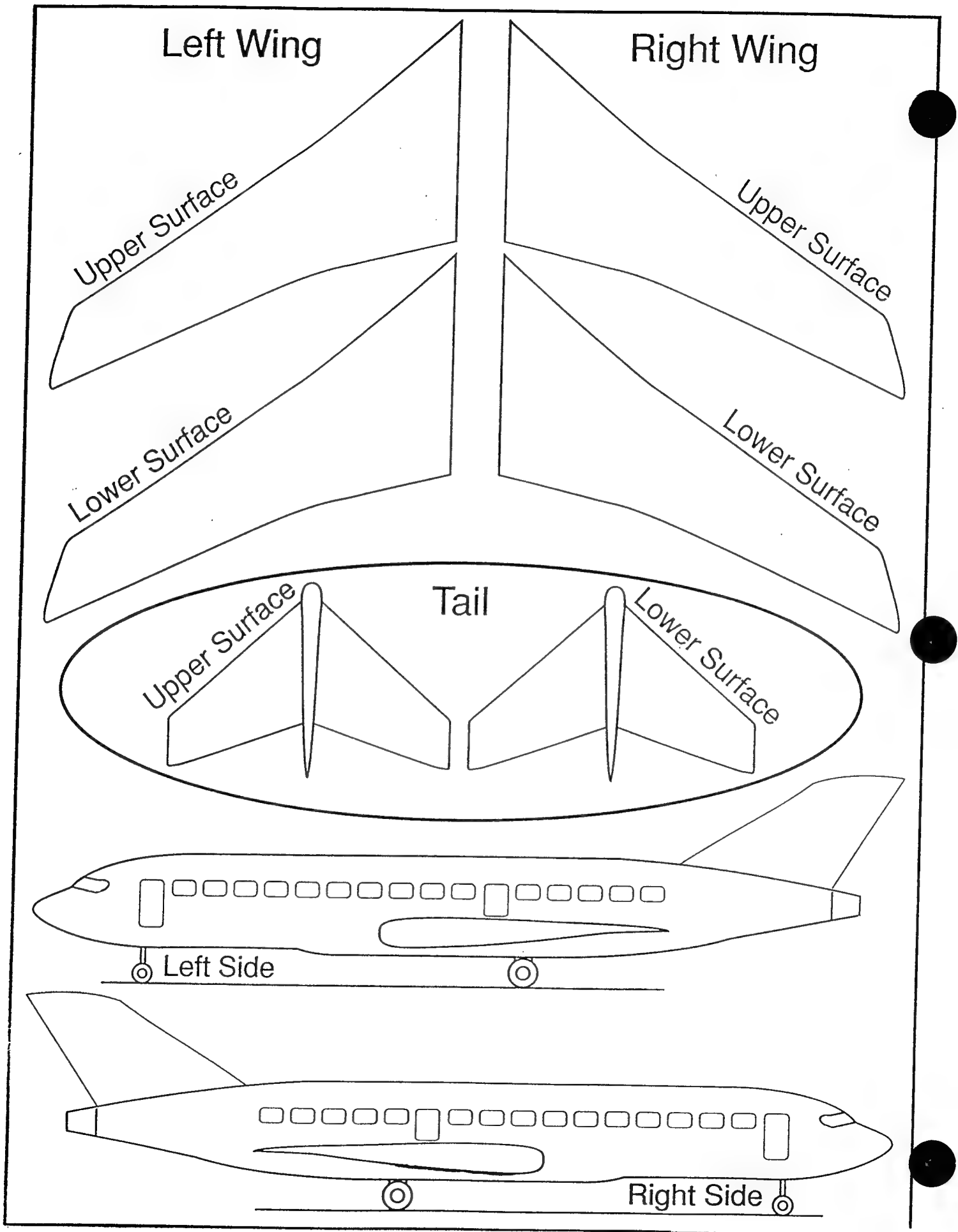
We have also attached a generic aircraft drawing and on it we would appreciate it if you could mark the areas that you feel are of major concern for exterior surface corrosion inspection.

<b>O P T I O N A L</b>	<b>Name:</b>	_____
	<b>Mailing</b>	_____
	<b>Address</b>	_____
	<b>for</b>	_____
	<b>Survey</b>	_____
	<b>Results</b>	_____

Aircraft Type	Operate ✓	Horizontal Fuselage Lap Joints	Vertical Fuselage Lap Joints	Under Fattener Heads	Skin/Stringer Fuselage Joints	Skin/Rib Fuselage Joints	Skin/Wing Rib Joints	Skin/Wing Spar Joints	Tailplane Skin Rivet Joints	Rudder Skin Rivet Joints	Engine Pylon Rivet Joints	Flaps	Other
DC-8													
DC-9													
DC-10													
MD-11													
MD80													
MD90													
B707													
B720													
B727													
B737													
B747													
B757													
B767													
L-1011													
A300													
A310													
A320													
BAe146													
BA111													
BAe748													
F77													
F28													
F50													
ATR42													
ATR72													
EMB120													
DHC-6													
Shore 360													
SAAB 340													

Please provide a rating for each of the specified aircraft exterior subsurface corrosion locations for each of the aircraft types you operate, by placing a number from 0 to 10 in the chart.

10 meaning a severe corrosion problem  
5 meaning a moderate corrosion problem  
0 meaning no corrosion problem



## APPENDIX B

Laboratory Technical Report, NRC-Diffracto Ltd. Collaborative Agreement: D  
Sight for Aircraft Corrosion Inspection, Report on Task 5.1, 5.2 and 5.3,  
J.P. Komorowski and R.W. Gould, Structures and Materials Laboratory, April  
1993.



National Research  
Council Canada

Conseil national  
de recherches Canada

Limited  
Unclassified

Institute for  
Aerospace Research

Institut de  
recherche aérospatiale

---

# ***NRC-CNRC***

---

## ***D Sight for Aircraft Corrosion Inspection***

**Report on Task 5.1, 5.2 and 5.3**

**LTR-ST-1943**

J.P. Komorowski, R.W. Gould

March 1994

**INSTITUTE FOR  
AEROSPACE RESEARCH**

**INSTITUT DE  
RECHERCHE AÉROSPATIALE**

Pages: 31

**REPORT  
RAPPORT**

Report  
Rapport LTR-ST-1943

Fig.  
Diag. 22

**STRUCTURES AND MATERIALS  
LABORATORY  
LABORATOIRE DES  
STRUCTURES ET DES  
MATÉRIAUX**

Date March 94

Limited  
Unclassified

For  
Pour Collaborative Research Agreement-Diffracto Ltd.  
Reference JGJ02

**LTR-ST-1943**

**D SIGHT FOR AIRCRAFT CORROSION  
INSPECTION**

**Report on Task 5.1, 5.2 and 5.3**

Submitted by  
Présenté par W. Wallace  
Director/Directeur

Approved  
Approuvé G.F. Marsters  
Director General

Authors  
Auteurs J.P. Komorowski  
R.W. Gould

THIS REPORT MAY NOT BE PUBLISHED WHOLLY  
OR IN PART WITHOUT THE WRITTEN CONSENT  
OF THE INSTITUTE FOR AEROSPACE RESEARCH

CE RAPPORT NE DOIT PAS ÊTRE REPRODUIT, NI EN  
ENTIER PARTIE SANS UNE AUTORISATION ÉCRITE  
DE L'INSTITUT DE RECHERCHE AÉROSPATIALE

### **ABSTRACT**

This report contains information collected as a fulfilment of Tasks 5.1 to 5.3 of a Collaborative Agreement between Diffracto Ltd. and NRC which involves work on behalf of Transport Canada and the Federal Aviation Administration: "D Sight for Aircraft Lap-joint Corrosion Detection". These tasks were to identify typical materials, typical fuselage lap joint designs and forms of corrosion. All large transport aircraft are constructed of nearly the same aluminium alloys. The lap joint designs are fairly different from one manufacturer to another and may include several layers of material (skins, doublers, tear-straps etc.). The fuselage, parts of the empennage and the control surfaces could be inspected with the aid of a D Sight based device for uniform, crevice, exfoliation and filiform corrosion.

## Table of Contents

1.0 INTRODUCTION .....	1
2.0 TYPICAL LAP-SPLICE CONSTRUCTION .....	1
2.1 Boeing Airplanes .....	2
2.2 Douglas Aircraft .....	8
2.3 Airbus .....	12
2.4 Fokker .....	15
3.0 MATERIALS OF INTEREST .....	16
4.0 CORROSION .....	17
4.1 Corrosion Prone Areas .....	17
4.2 Types Of Corrosion .....	24
5.0 CONCLUSIONS .....	30
6.0 REFERENCES .....	30

## 1.0 INTRODUCTION

The potential of the D Sight technique to locate corrosion damage in specimens and on aircraft has been successfully demonstrated at the Institute for Aerospace Research [1]. The current work aims to build on these experiences and through a comprehensive series of tests to evaluate D Sight as a future Non Destructive Inspection technique for aircraft lap-splice corrosion. Reported here is information gathered under the IAR work-share of tasks:

5.1 Identify Representative Lap Splice Geometry.

5.2 Identify Materials of Interest.

5.3 Review Corrosion Types to be Detected and Rank their Significance.

The information has been compiled from the references listed at the end of the report. In particular large excerpts from the Corrosion Handbook by Wallace et al. [2] are quoted in Chapter 4 (quoted text is in helvetica font). The authors have focused on the information which will be useful when addressing the remaining tasks of the current Phase I as well Phases II and III which could be funded in following years.

## 2.0 TYPICAL LAP-SPLICE CONSTRUCTION

Aging aircraft lap splice designs included in this section provide information which will be used in specimen selection for the accelerated corrosion Task 5.5. The structural arrangement drawings also contain information on depth of substructure. This will help in selection of tools used in removal of specimens from scrapped aircraft (Tasks 5.4 and 5.7 - Obtain Non-Corroded and Corroded Specimens). In Figure 1. Basic lap splice design concepts are shown.

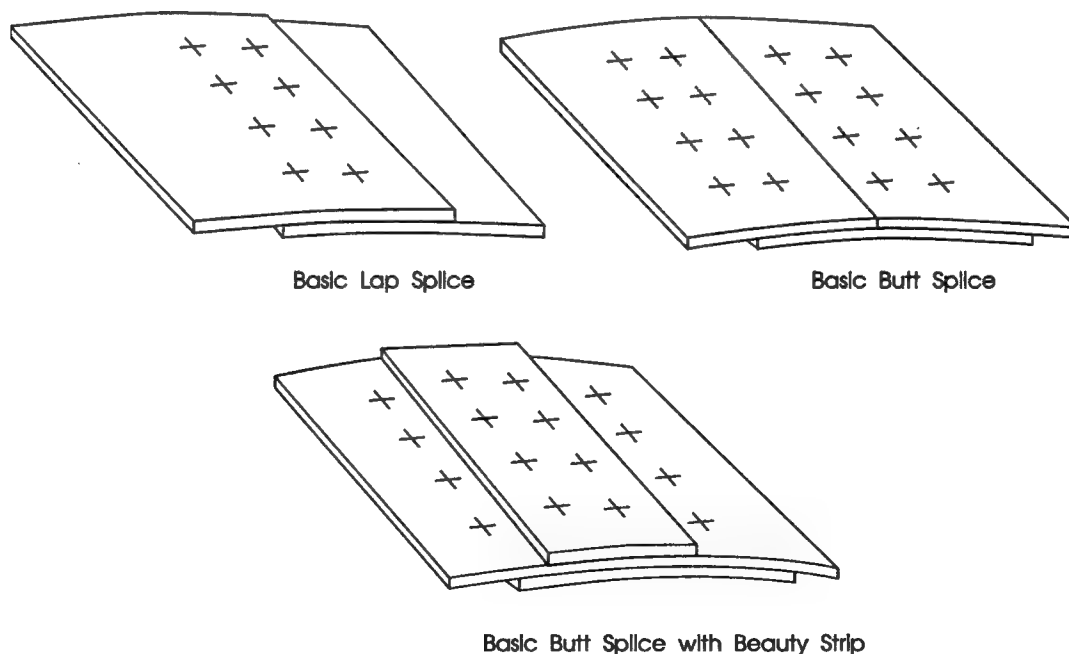


Figure 1. Basic splice design concepts.

## 2.1 Boeing Airplanes

Figures 2 to 7 contain drawings of typical fuselage joint designs found in B727, B737 and B747 airplanes. It should be noted that most splices were bonded and riveted. The fatigue critical rivet rows locations are also important for this study as corrosion increases fatigue crack growth rates (Fig. 3).

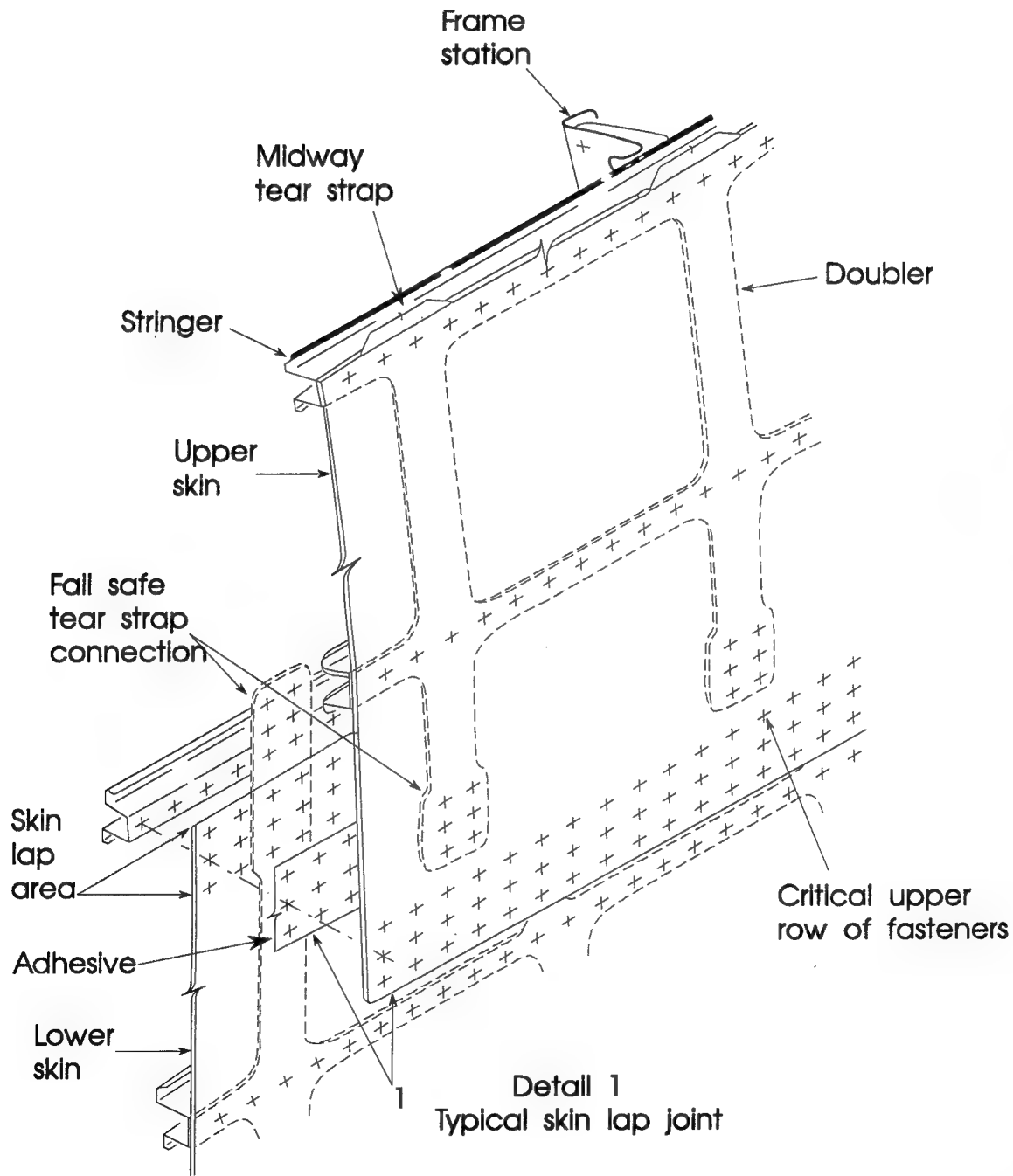


Figure 2. Typical B737 design.

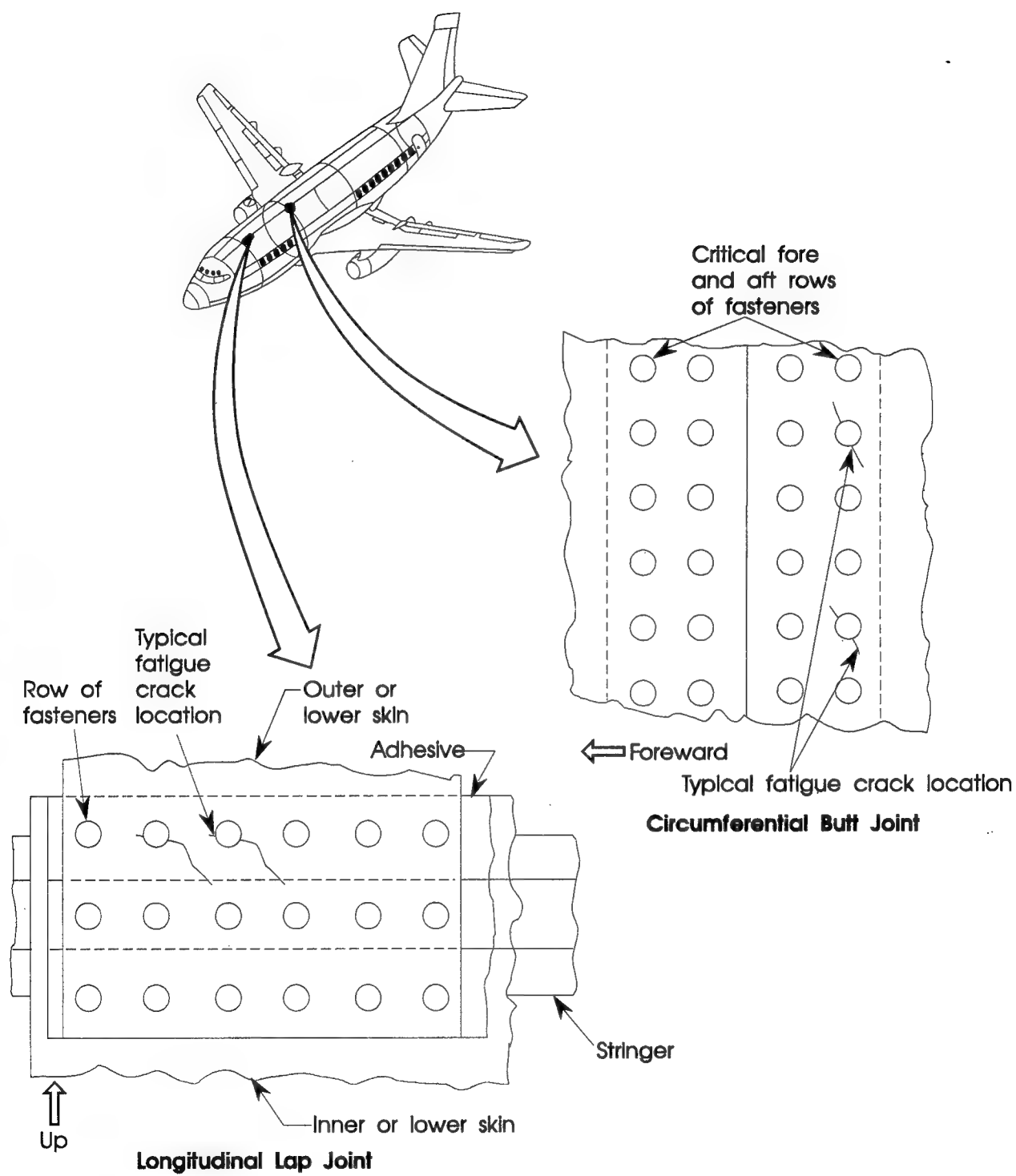


Figure 3. Fatigue critical rivet rows (B737).

Material: Skin and tear straps, 2024-T3 clad;  
stringer and frames, 7075-T6 clad

Radius: 74 in.

Skin: 0.036 in. thick

Tear Straps: 0.036 in. thick

Stringers: 0.028 in. thick hat sections  
9.25 in. spacing

Frames: 0.040 in. thick Z sections,  
20 in. spacing

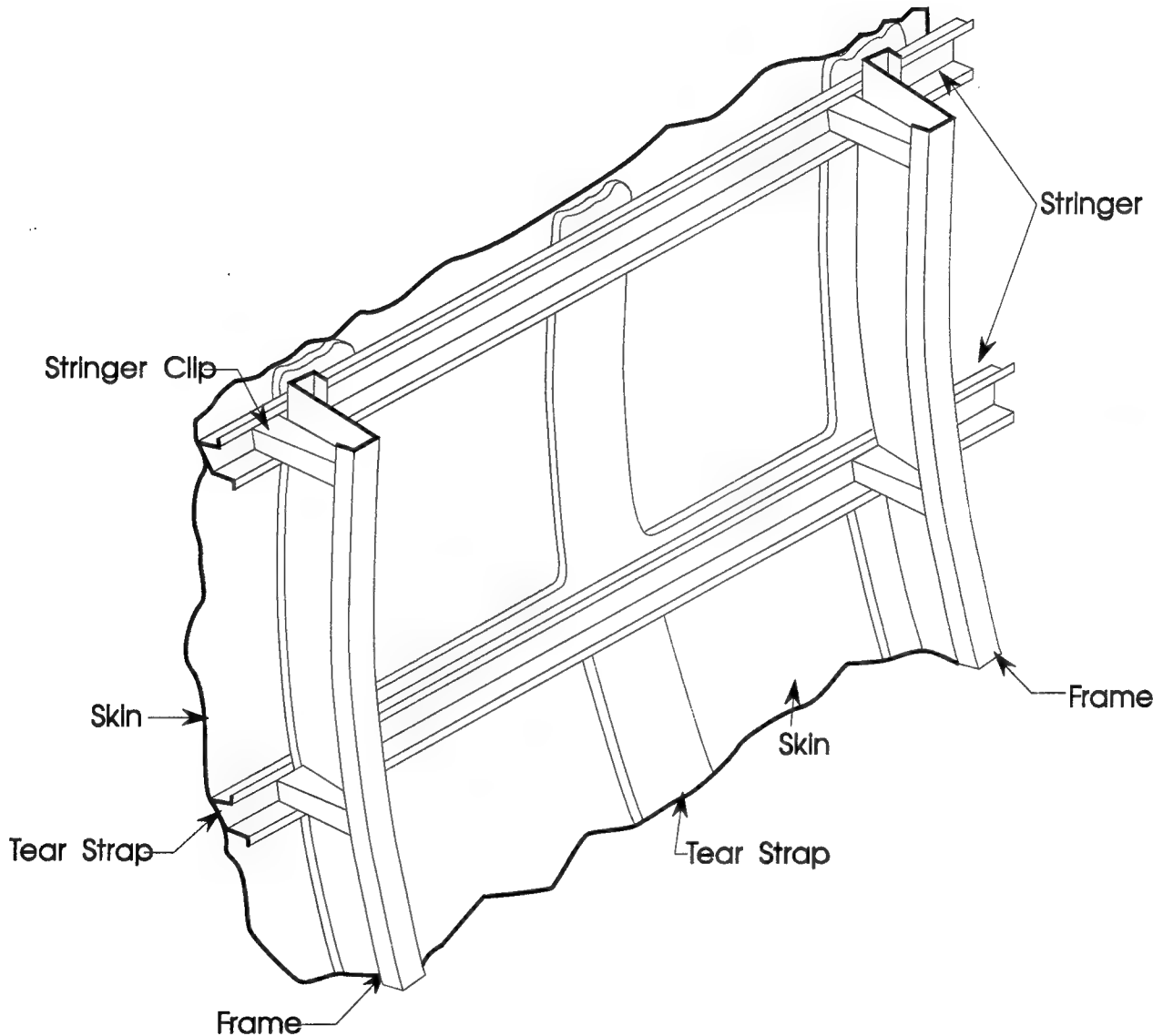


Figure 4. Structural features of a B737 body panel.

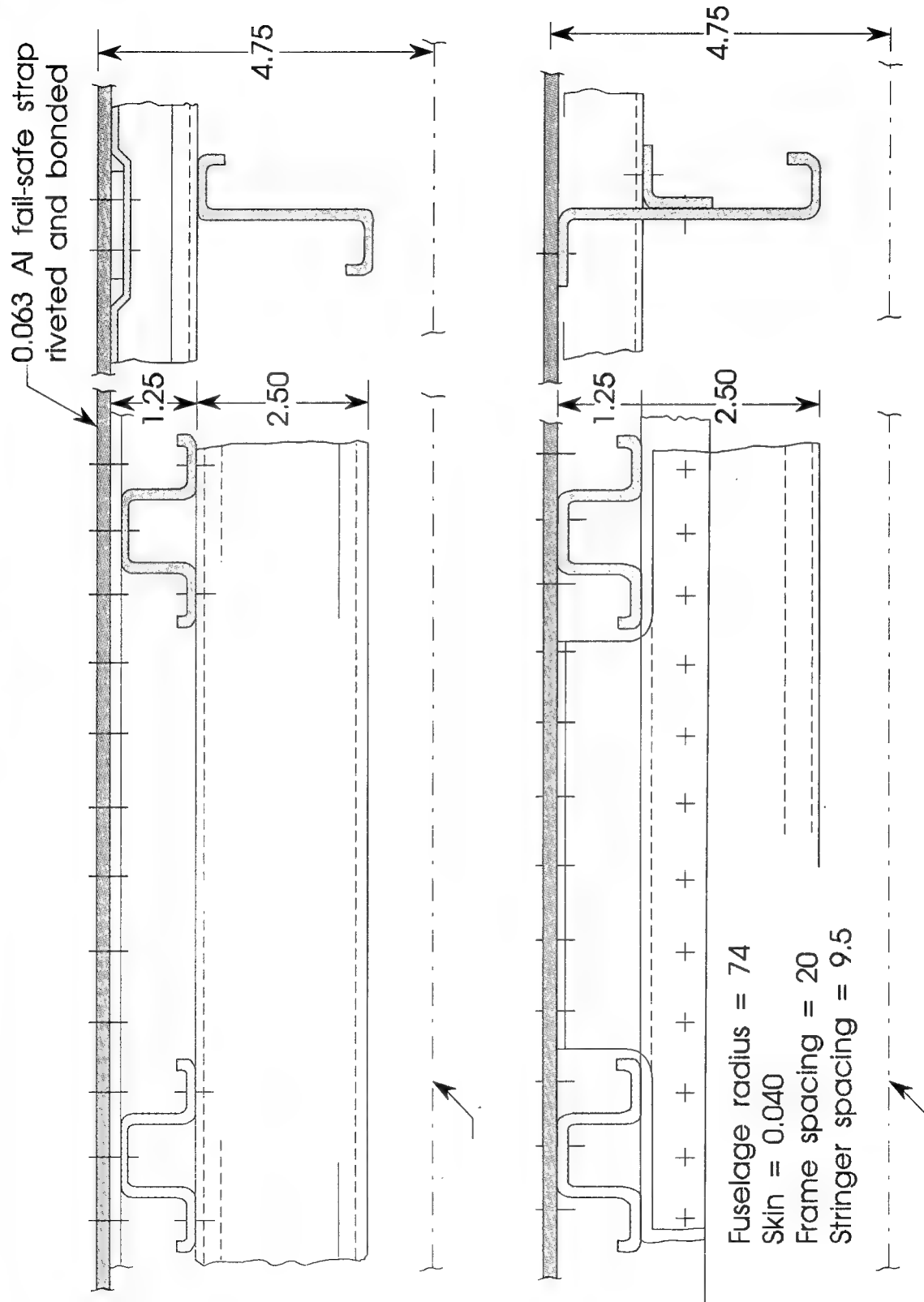
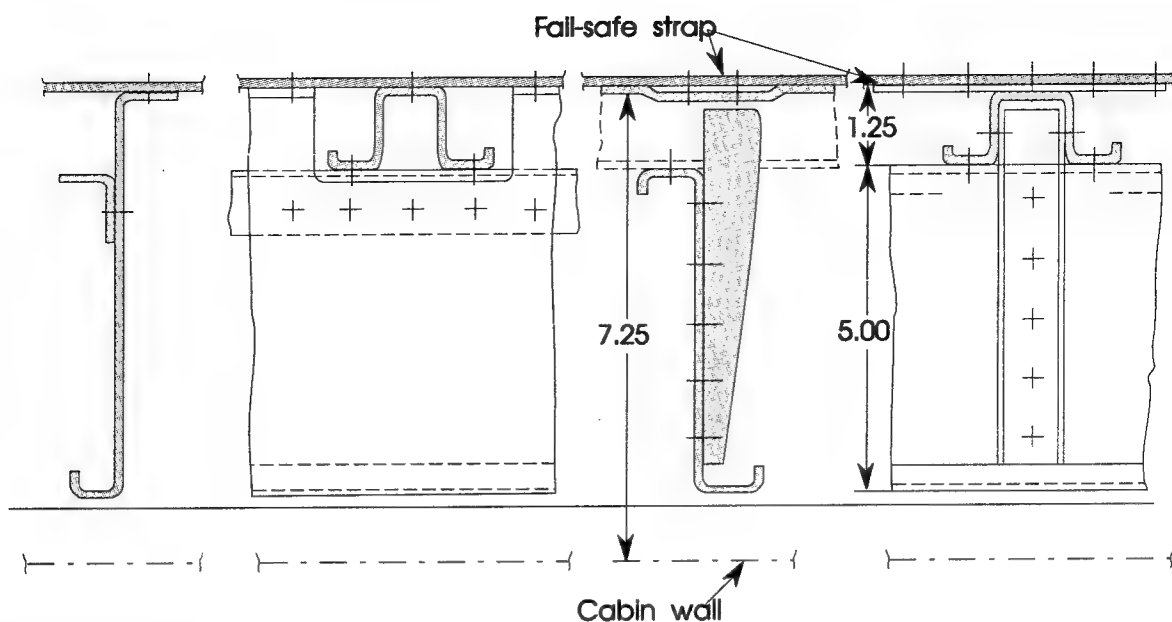
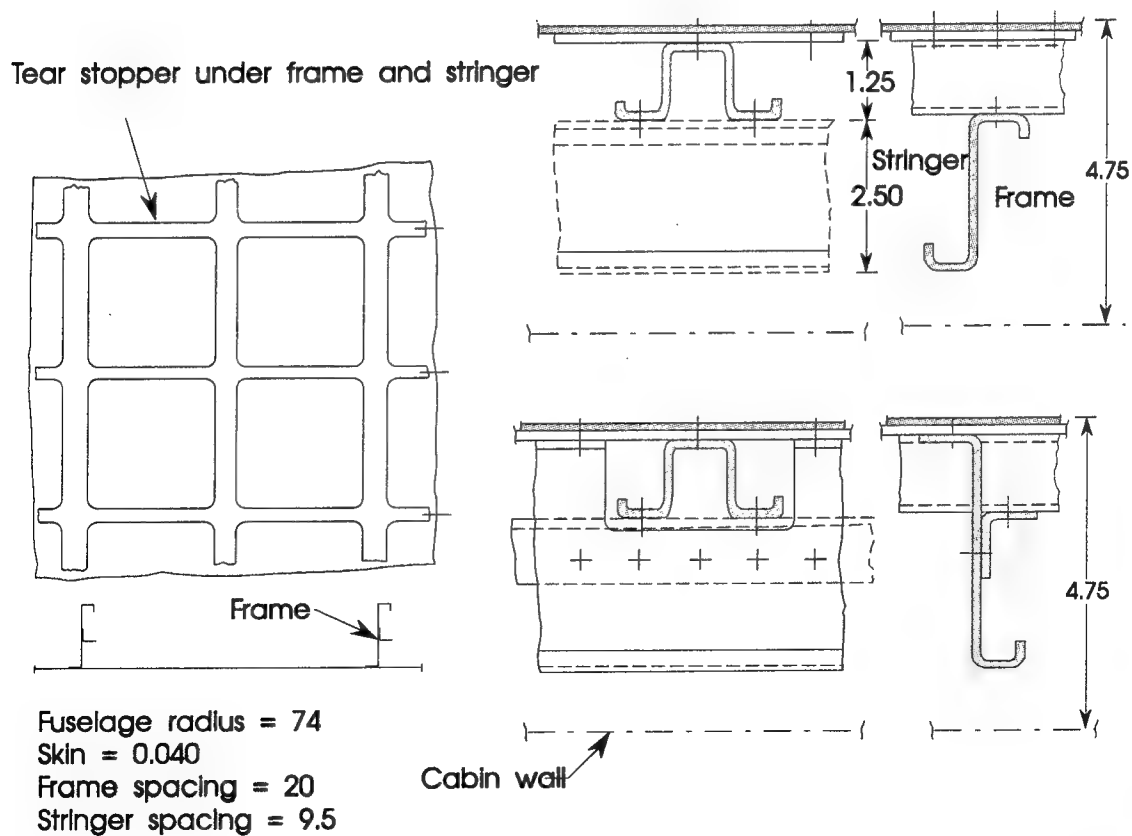


Figure 5. Typical B707 and B727 structural arrangement.



Fuselage radius = 128  
 Frame spacing = 20  
 Stringer spacing = 7.3 to 9.5

**B747**



**B737**

Figure 6. Typical 737 and 747 structural arrangement.

Material: Skin, 2024-T3 clad;  
 stiffeners and straps, 7075-T6 clad  
 Radius: 127 in.  
 Skin: 0.075 in. thick with 0.025 in. padup along  
 stringers and frames  
 Stringers: 0.050 in. thick Z-sections, 9.25 in. spacing  
 Shear Ties: 0.080 in. thick discrete shear ties  
 Frames: 0.063 in. thick Z-sections,  
 20 in. spacing  
 Filler Straps: 2 each, 1 by 0.063 in. continuoud  
 straps for fail safe chord

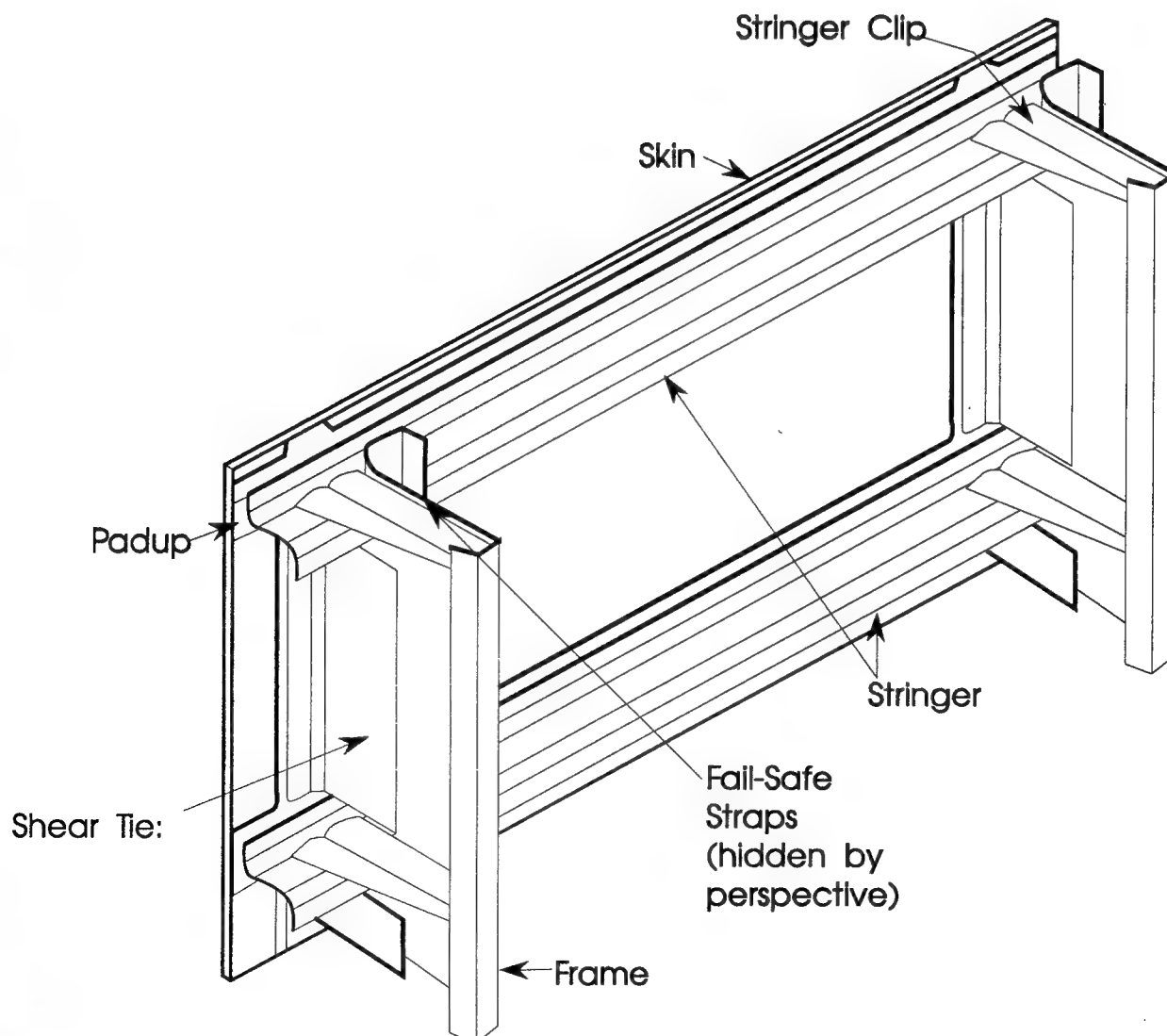


Figure 7. Structural features of B747 body panel.

## 2.2 Douglas Aircraft

Figure 8 to 12 are typical fuselage splices for McDonnell-Douglas aircraft (DC-8, DC-9/MD80 and DC-10/MD-11). The most characteristic features are the use of so called finger or scalloped doublers and external straps.

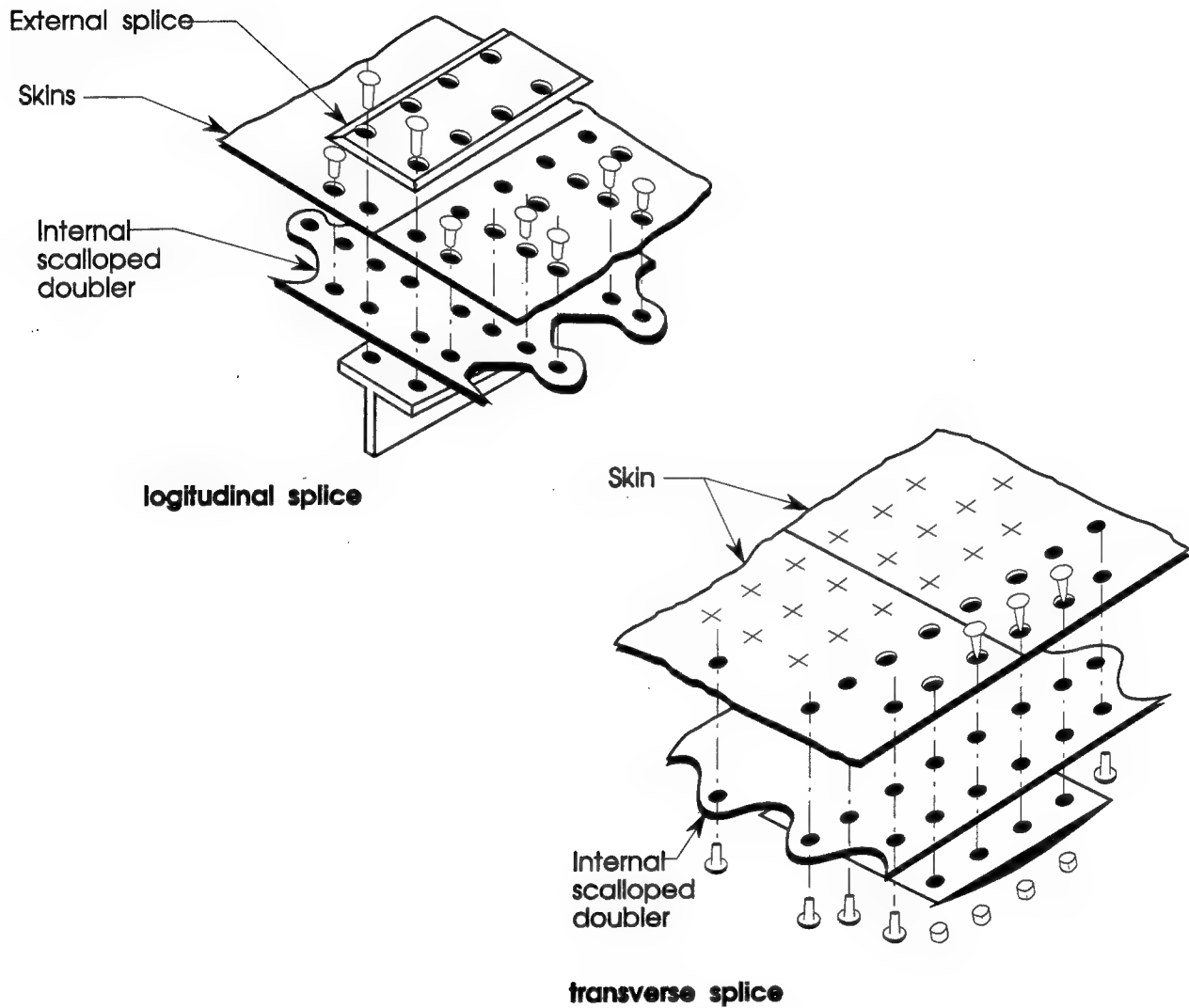
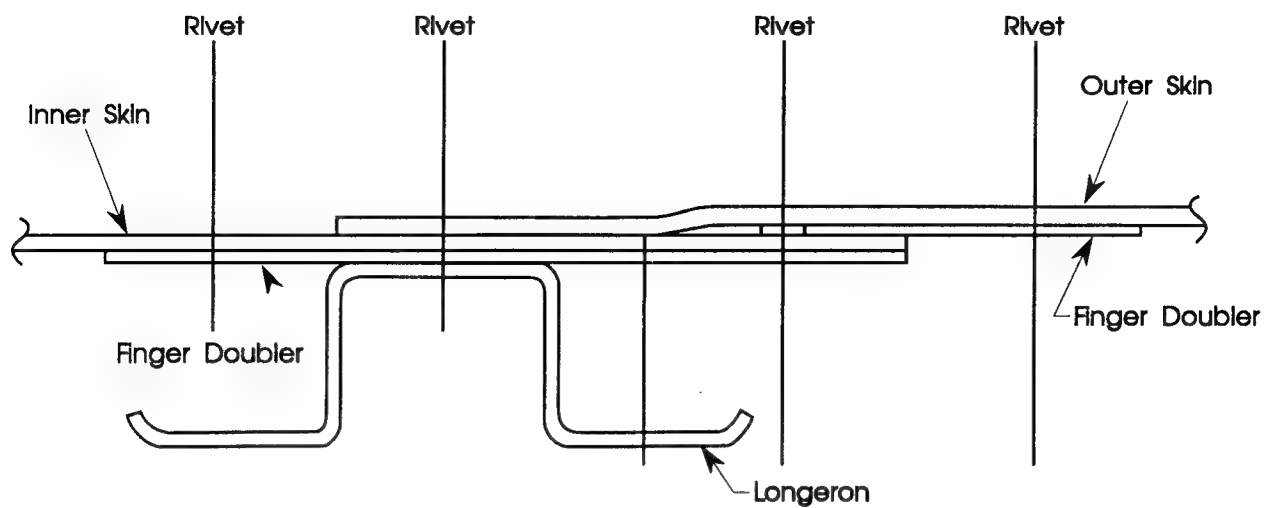


Figure 8. Fuselage splices with scalloped (finger) doubler. Typical Douglas design.



### Five-Element Splice

Figure 9. DC-9 longeron No.1.

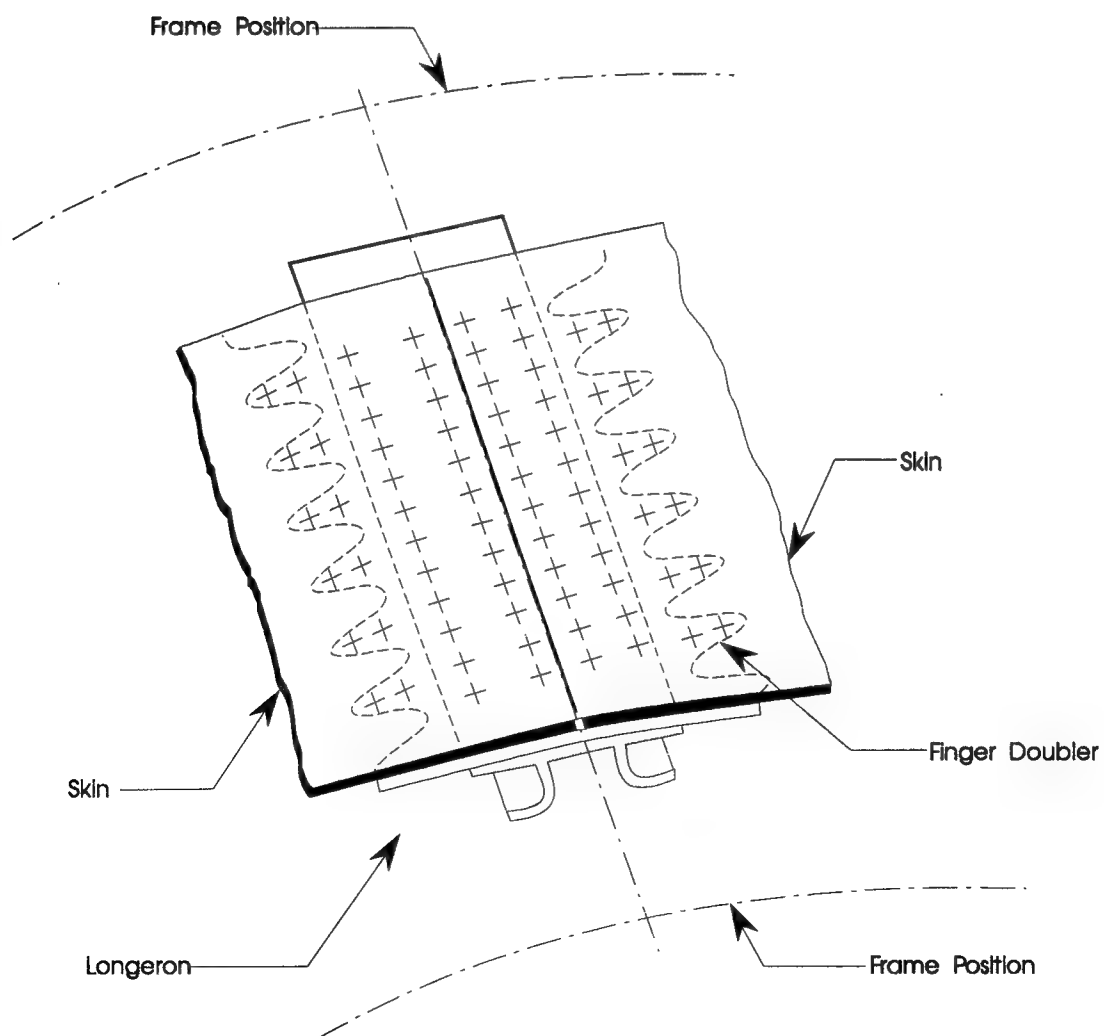
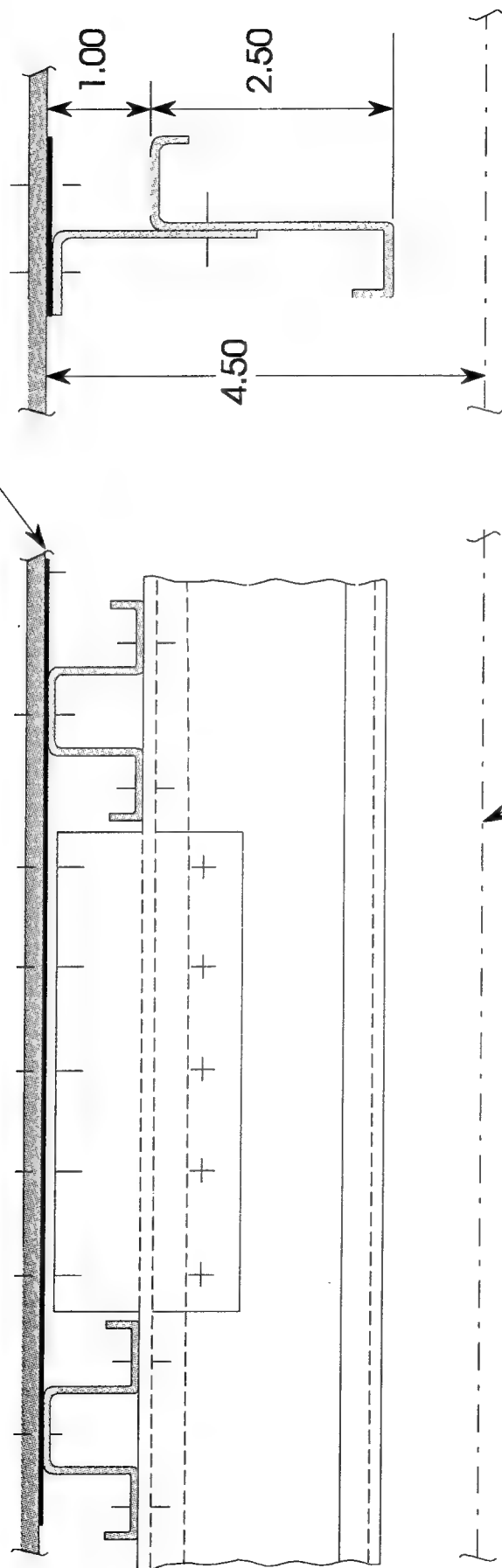


Figure 10. DC-8 longeron No.1.

Ti 0.025 fail-safe strap  
riveted to skin



Cabin wall

Fuselage radius = 73.5  
Skin = 0.050  
Frame spacing = 20  
Stringer spacing = 7.2

DC - 8

Figure 11. DC-8 structural arrangement.

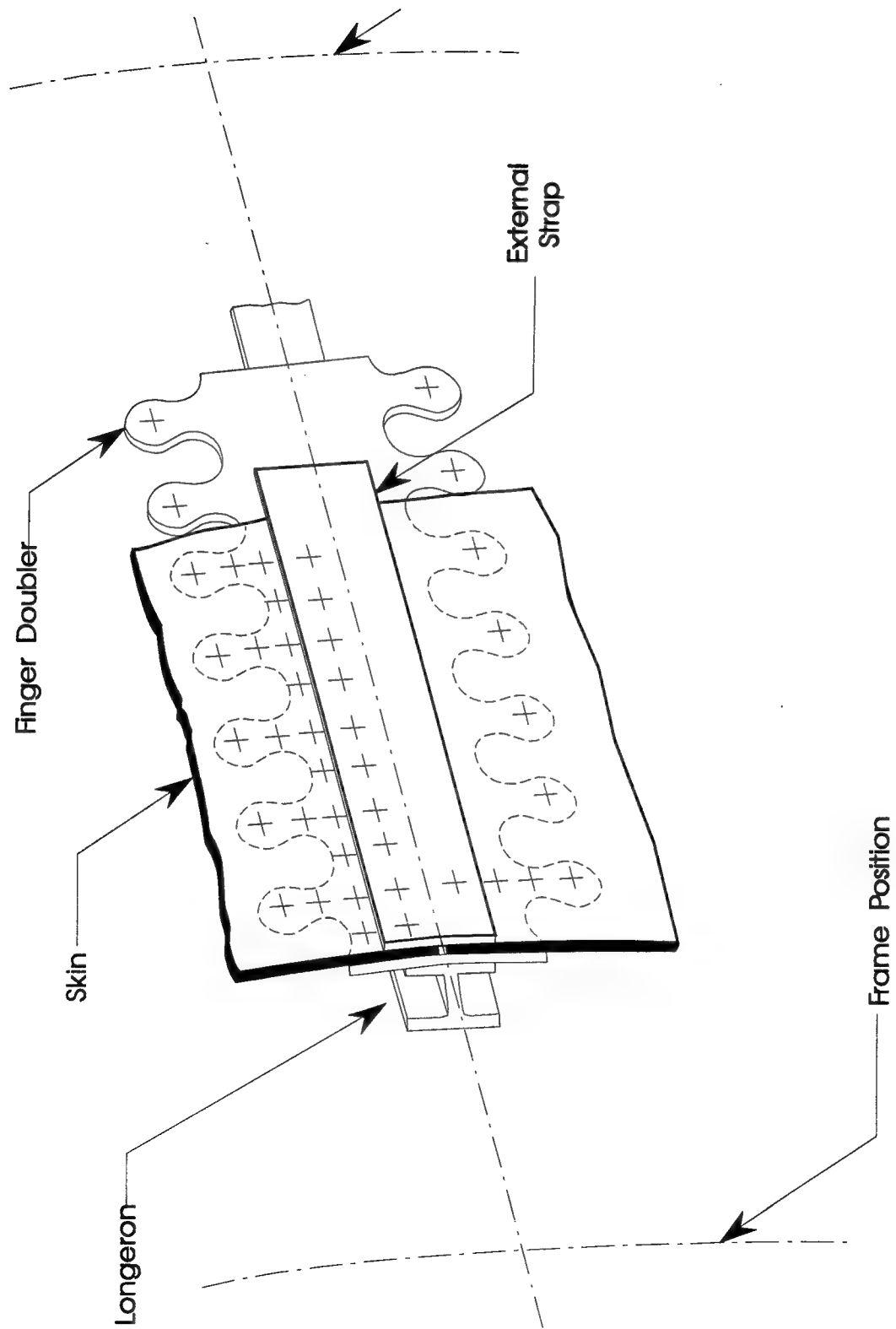


Figure 12. DC-10 longeron no.5.

## 2.3 Airbus

The Airbus splice designs illustrated in Figures 13 to 15 show more similarity with Boeing than Douglas designs. "J" stiffeners are used more commonly by Airbus where Boeing uses hat stiffeners. In Figure 15 the stiffener is attached to the outside rivet row while in the Boeing designs the middle row is typically used for stiffener attachment.

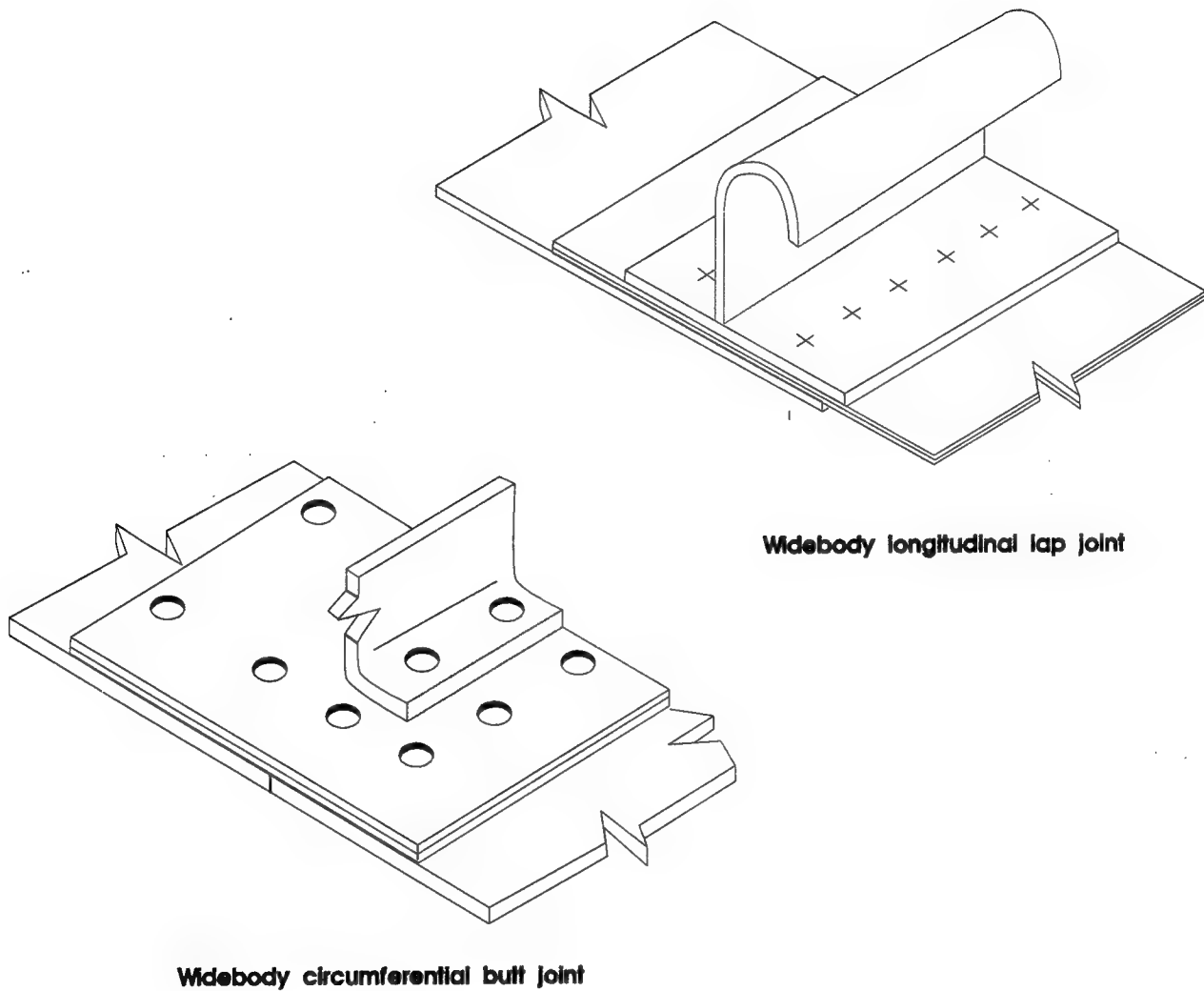


Figure 13. Typical A300 lap joints.

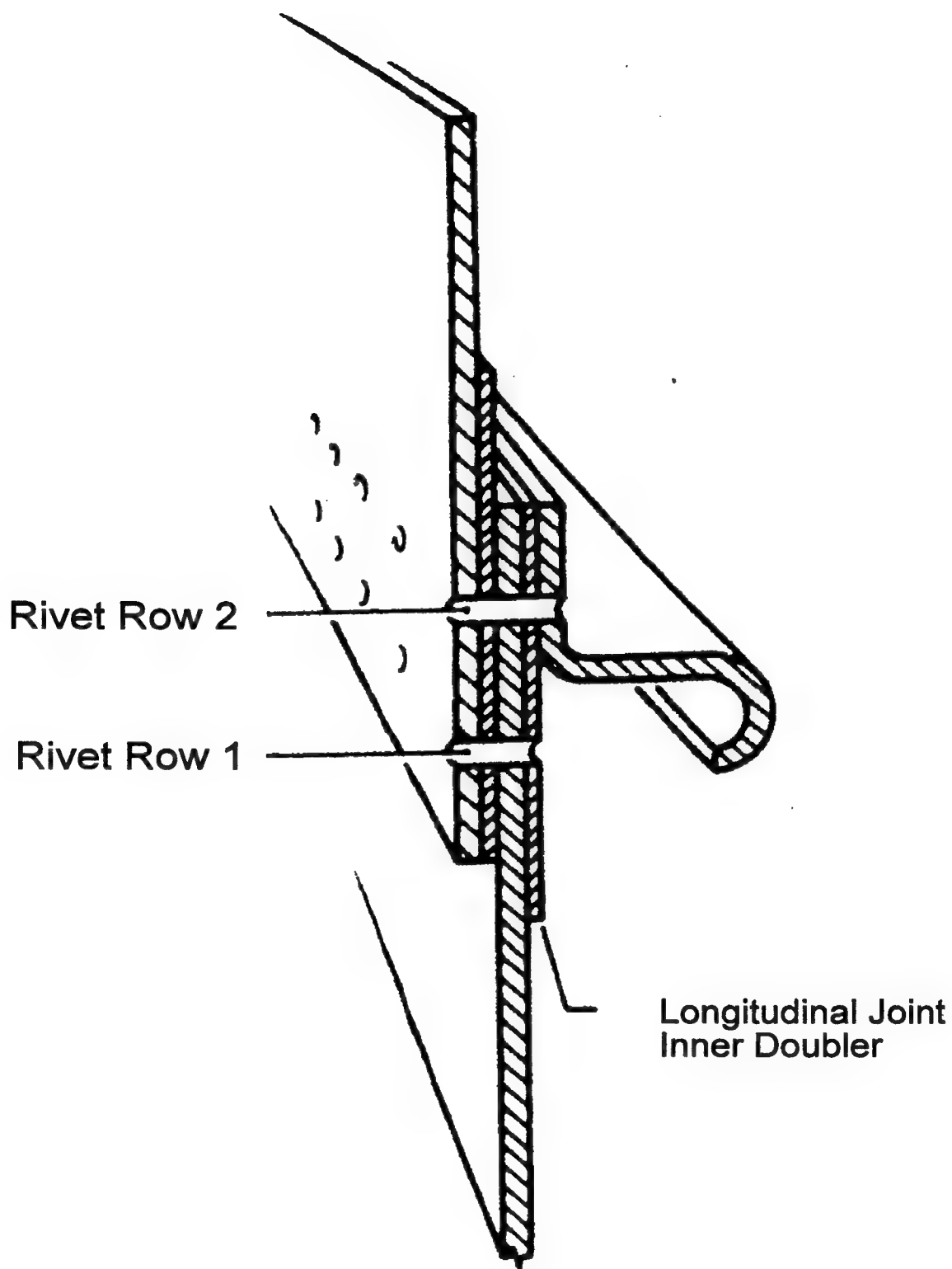
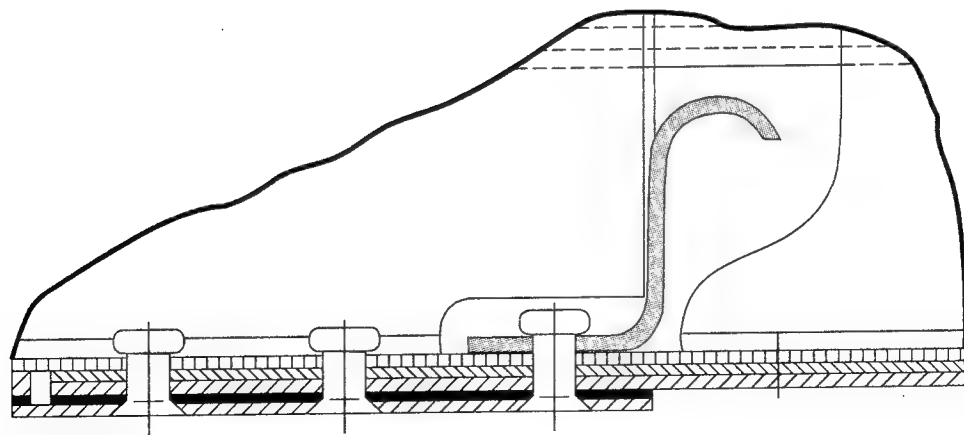
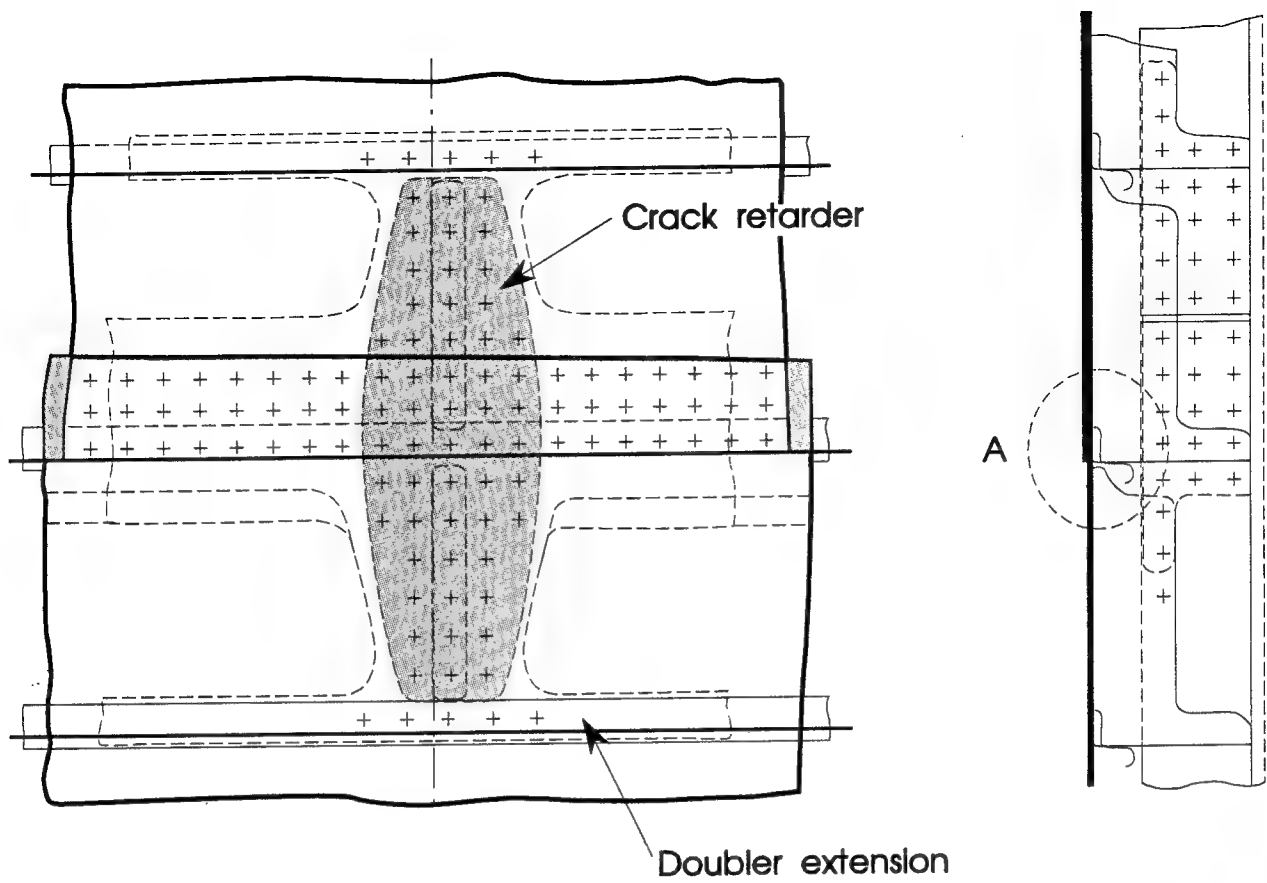


Figure 14. Airbus A300 longitudinal splice design.



Detail A (rotated 90°)

Figure 15. Longitudinal lap joint with crack retarder (A310).

## 2.4 Fokker

The Fokker is known for heavy use of bonding in their designs. The drawing in Figure 16 shows F-28 longitudinal lap joint with the stiffener bonded to the skin slightly off the overlapping spliced skins.

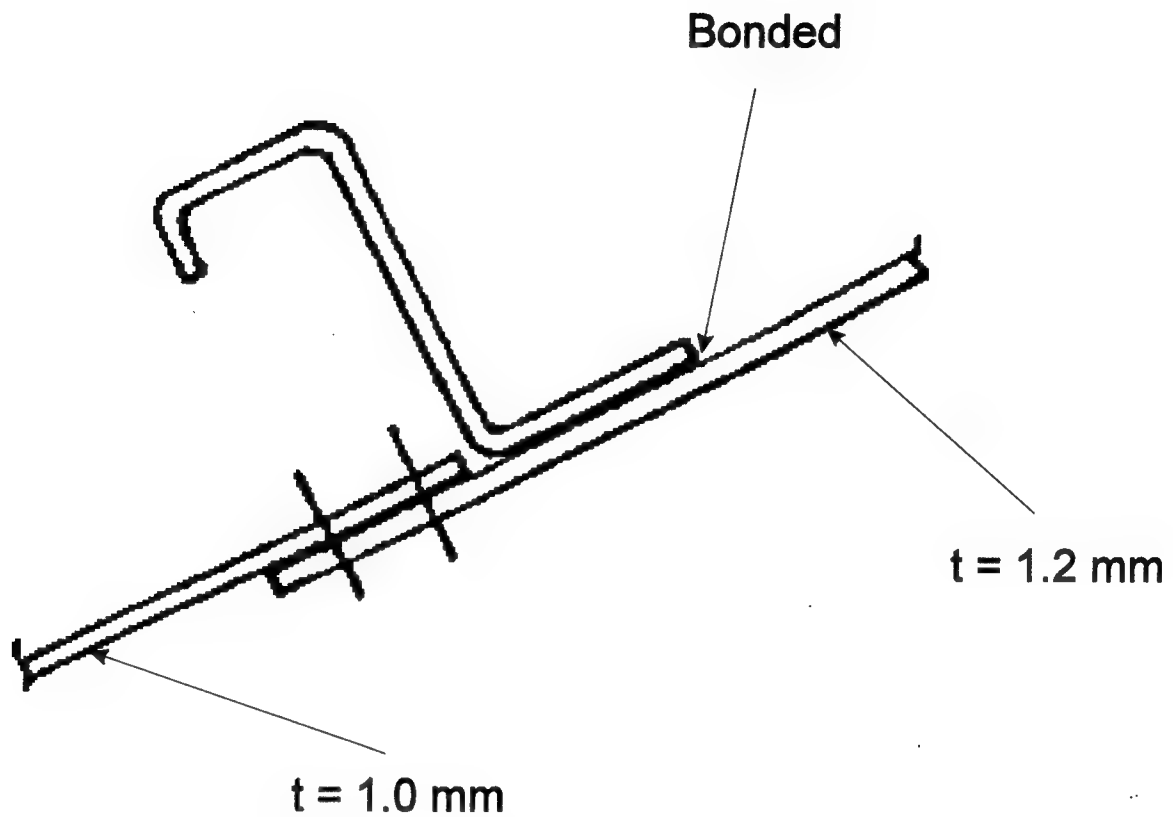


Figure 16. Fokker F-28 longitudinal lap joint.

### 3.0 MATERIALS OF INTEREST

The aging aircraft of interest were built from late 1950's to early 1970's. A complete materials list would be long and difficult to assemble. However, as Table 1 demonstrates, most manufacturers selected the same materials for fuselage construction. A similar uniformity can be observed in wing box material selection [6]. To reduce corrosion, manufacturers use cladding for aluminium alloys. Most fasteners used in the aircraft assembly are made from aluminium alloys, however in some areas other materials have been used (i.e. steel in highly stressed areas).

Aircraft	Material		
	Skin	Stringer	Tearstrap
B727	2024-T3	7075-T6	Alum
B737	2024-T3	7075-T6	
B747	2024-T3	7075-T6	2024-T3
DC9	2014-T6	7075-T6	Ti
DC10	2024-T3	7075-T6	Ti
DC8	2024-T3	7075-T6	Ti
L1011	2024-T3	7075-T6	Ti
A300			
F28	2024-T3	2024-T4	
BAC111	2024-T3		

**Table 1** Materials used in fuselage construction of aging aircraft.

Alloy	Form and condition		Tensile		%	Modulus	Brinell	Fatigue	Fracture
					Elongation	of elasticity	Hardness	strength	toughnees
			Yield	Ultimate	in	MPa x 10 <sup>3</sup>	500 Kg	MPa	MPa√m
					50 mm	(d)	load		(g)
			MPa	MPa			10 mm ball		
2014	T4	sheet(a)	290	428		73	105	140 (e)	
	T6	sheet(a)	414	483		73	135	125 (e)	23-26
2024	T3	sheet(a)	345	480	18	73	120	140 (e)	33-50
	T4	sheet(a)	325	470	20	73	120	140 (e)	
	T8	sheet(a)	460	480	6	73			22-27
7049	T73	forgings(c)	475	535	11.5	70	135	275-315 (f)	32-36
7075	T7351	plate(b)	435	500	10	72	160	159 (e)	31-35
	T661	sheet(a)	500	580	9	72			27-31

(a) 1.6 mm thick sheet.

(e) 6 x 10<sup>8</sup> cycles of completely reversed stress, R.R. Moore type, tests.

(b) 50 mm thick plate or extrusions.

(f) Axial tests on smooth specimens (R = 0.0). 50 mm thick plate.

(c) Properties of forgings across grain flow.

(g) Longitudinal-transverse orientation.

(d) Average of tension and compression values.

**Table 2** Typical room temperature mechanical properties of some common aerospace aluminium alloys [2]

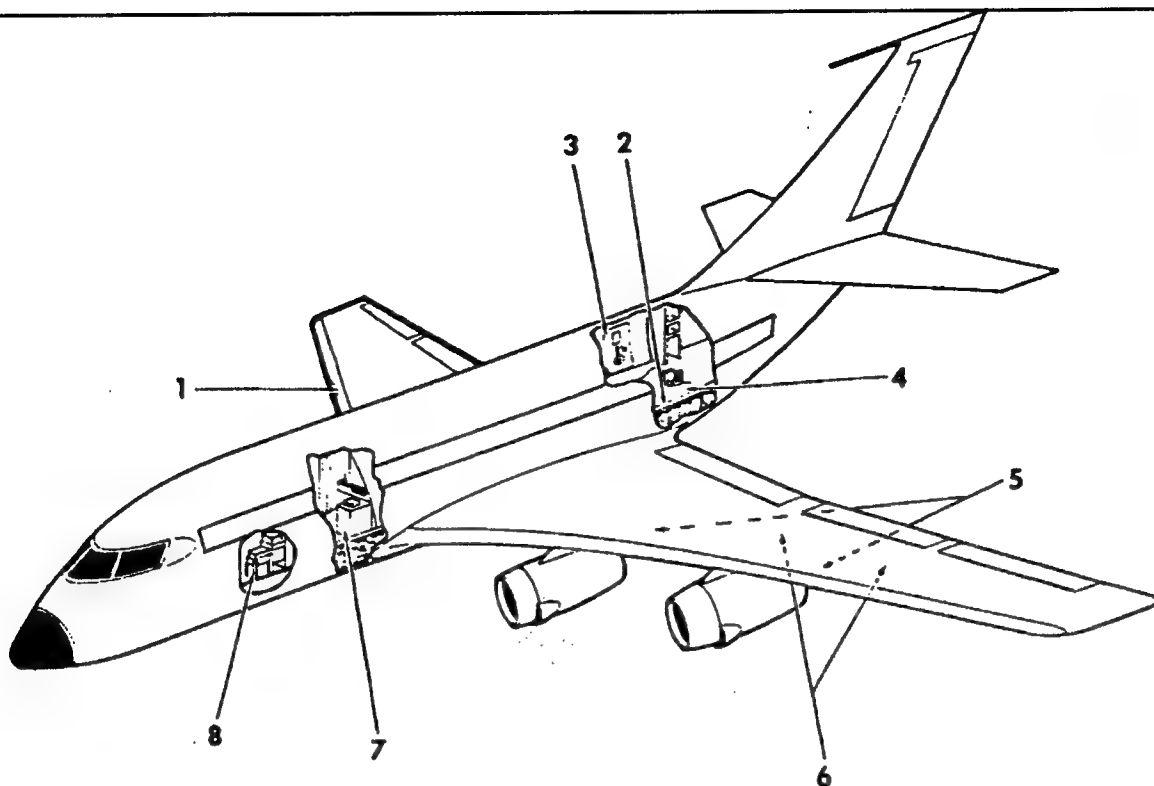
## 4.0 CORROSION

The chemical reactions by which metals revert back to their natural state are known as corrosion reactions and the detailed path followed by these reactions depends on the metal or alloy and the conditions under which the reactions occur. For simplicity it is convenient to consider two types of corrosion reactions:

- corrosion involving a liquid phase where an electrically conducting solution is present to assist in the transfer of metal ions and electrons between the oxidizing or anodic site of the metal and the reducing or cathodic site; and
- dry corrosion involving a metal/gas or metal/vapour reaction, where nonmetals such as oxygen, halogens, hydrogen sulphide or sulphur vapour lead to the formation of a film or scale on the metal surface without the intervention of a liquid electrolyte.

### 4.1 Corrosion Prone Areas

Recurring corrosion problems may appear in different areas of aircraft depending on the aircraft type and the local operating environment. Figure 17 shows some of the corrosion prone



#### **1 UNDER DE-ICER BOOTS**

Moisture may collect under the boots and result in corrosion.

#### **5 AREAS IN PATH OF EXHAUST GASES**

Exhaust gases on the nacelle and wing skins and seeping into the wing structure may permeate the protective finish and cause corrosion underneath.

#### **2 FLOOR SUPPORTS AND FLOORING**

Metal floors and substructure will corrode if continually in contact with moisture of any kind.

#### **6 INTEGRAL FUEL TANKS**

Corrosion may occur at load points inside the integral fuel tanks where water condensate gathers. Integrally stiffened panels do not have aluminum cladding and are more prone to corrode.

#### **3 PASSENGER CARGO AND CREW DOORS**

Floors and structure in these areas corrode as a result of exposure to rain water and condensate.

#### **7 LAVATORY AREAS**

Soapy water and human wastes in these areas promote rapid corrosion and deterioration of structure.

#### **4 GALLEY AREAS**

Spilled food, fruit juices, and other liquids in prolonged contact with metal structure will cause corrosion particularly when protective coatings are allowed to deteriorate.

#### **8 BATTERY AREAS**

Spilled battery electrolytes are extremely corrosive.

Figure 17. Areas most susceptible to corrosion [2]

areas in a typical transport aircraft [2]. Other corrosion prone areas that are not shown specifically in Figure 17 include:

- Main undercarriage.
- Nose undercarriage.
- Rudder and elevator shroud areas.
- Aileron and flap track area, flap tracks and trailing edges.
- Freight doors and ramps.
- Access doors.
- Control cables.
- Leading edges, hinge lines and air ducts.
- Radome area.

#### **4.1.1 D Sight Rating System**

In the following sections specific areas of aircraft and later various types of corrosion will be rated according to D Sight's potential as an inspection method in the given area or to identify the given type of corrosion:

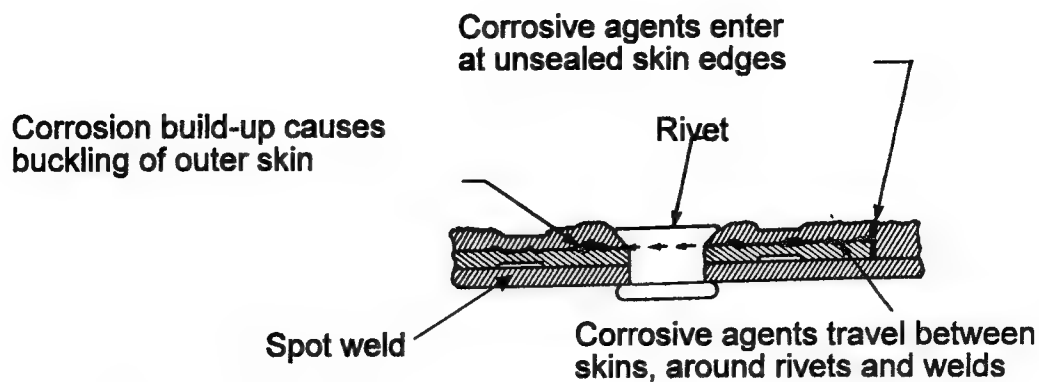
- DS++ strong candidate area or type of corrosion for D Sight inspection
- DS+ candidate area or type of corrosion for D Sight inspection
- DS— unlikely area or type of corrosion for D Sight inspection

#### **4.1.2 External Skins (DS++)**

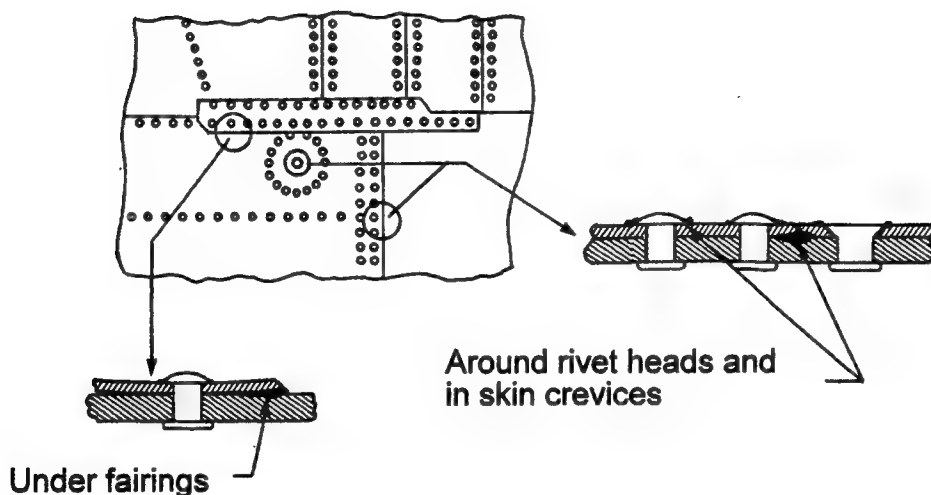
"The external surfaces of magnesium alloy or aluminium alloy skins are particularly susceptible to corrosion along rivet lines, lap joints, fasteners, faying surfaces, or where protective coatings have been damaged or neglected. These areas must be carefully examined by visual inspection, employing visual aids such as magnifying glasses, mirrors, fibre-optic probes, mechanical probes, and various other devices. These inspections would normally concentrate on to the following areas and damage mechanisms:

- Corrosion may be evident in spot-welded skins by corrosion products appearing at the crevices through which the corrosive agents entered and is usually more prevalent on external areas (Fig. 18);
- Piano-type hinges are also prime sites for corrosion as are edges of honeycomb panels and drilled holes;
- Lower fuselage, wing and flap areas aft of wheels suffer damage in protective coatings due to impact from particles thrown up from the runway on takeoff and landing;
- Canopy and passenger/crew/cargo door structures and associated hinges, fittings, and mechanisms may be damaged due to the combined effects of mechanical and corrosive action;
- Windows and door frames may be similarly affected." [2]

External surfaces are easily accessible and generally do not pose restriction on D Sight equipment placement. D Sight is an enhancement to visual inspection usually called for external skins examination.



### SPOT-WELDED SKIN CORROSION POINTS



### EXHAUST TRAIL AREA CORROSION POINTS

Figure 18. Corrosion prone areas.

#### 4.1.3 Exposed Hardware (DS—)

"Exposed hardware such as control surface actuating rods, fittings, attaching and hinge bolts, nuts, washers and cotter pins, are generally made from alloys different to those of the structure to which they are mounted, and several dissimilar metals may be used in the hardware itself. These items and the adjacent areas of airframe structure are therefore prime sites for galvanic corrosion. Corrosion may occur in these parts particularly when organic or chemical coatings have been damaged or have deteriorated, or when protective films or lubricants have been removed by cleaning solvents or detergents during cleaning. Protective films and lubricants can also be removed by de-icing fluids. Other areas requiring close inspection include:

- Bonding jumpers, grounding studs and receptacles, attaching hardware and adjacent areas.
- Access panels, antenna and radome attaching screws, countersink and adjacent areas.

- Navigation lights, landing lights and other external light installations and their attaching hardware and adjacent areas.
- Jacking pads, tie-down fittings, attaching hardware and adjacent areas.
- Boarding and access ladder mounting devices and attachments for engine run-up screens and blanking devices." [2]

Exposed hardware is an unlikely candidate for D Sight inspection because with D Sight it is difficult to inspect highly curved or small surface areas.

#### **4.1.4 Undercarriage Bays (DS—)**

"Wheel wells are exposed to flying debris from landing strips which damages paint work and lodges in inaccessible areas, between stiffeners, ribs and lower surfaces. Undercarriage assemblies must be examined with particular attention to magnesium wheels, paint work, exposed switches and electrical equipment. Frequent cleaning is required followed by treatment by water displacing fluids and re-lubrication to ensure continued safe operation. Other areas of the undercarriage require regular inspection and maintenance are:

- All pivot points including pivot and trunnion pins, lay shafts and securing hardware; bearings, bushings, attachment and pivot lugs, and attachment fittings.
- Exposed surfaces of shock strut and actuator pistons. These components should be extended to allow the piston surfaces to be inspected.
- Axles, wheels, wheel bearings, brake and their securing hardware.
- Opening and recesses where water and debris may collect.
- Surfaces of landing gear main members.
- All operating and locking mechanisms including bushings, bearings, rollers, springs, adjustment devices and securing hardware.
- Exposed tubing, especially at nuts and sleeves, and under clamps and identification tags.
- Valves and other fittings." [2]

D Sight optics dictate that the inspection head be constructed in such a way that minimum optical path length is maintained. This translates to a physical size of the head which generally will not allow inspections inside undercarriage bays.

#### **4.1.5 Battery Compartments and Vent Openings (DS+)**

"If not promptly treated, battery electrolyte spillage can cause severe corrosion particularly where protective paint work has been damaged. Inspections in these areas are performed for the following:

- Cleanliness and condition of protective coatings;
- Internal areas adjacent to battery compartments must be inspected since fumes from heated battery electrolytes are difficult to contain and will spread beyond the compartment;
- Supporting racks are examined for evidence of electrolyte spillage."

This is not a strong candidate area for D Sight inspections because of the inspection head size restrictions. However, severe consequences of electrolyte spillage should become evident

when the fuselage lap-splices in the area of battery compartments are inspected externally with D Sight.

#### **4.1.6 Fuel Tanks (DS+)**

"Top coating materials used in integral fuel cells are impervious to fuel but not completely impervious to water. Since it is impossible to keep fuel completely free of water, moisture may penetrate through the top coat material and cause intergranular corrosion on airframe structural parts. Microorganisms which live in fuel may become attached to the top coating and may result in deterioration of such materials. This is more likely to occur in warm climates, and the use of fuel system icing inhibitors in cold climates should reduce the likelihood of such corrosion. Fuel tanks are therefore inspected for the following:

- Condition of the top coating materials.
- For signs of active corrosion, particularly around water drainage points.
- For evidence of microbiological corrosion.
- To establish the condition of metal under loose or removed sealing and coating materials, and accumulated residues." [2]

This is not a strong candidate area for D Sight inspection. However, D Sight may be able to detect changes in the top coating material following penetration by moisture.

#### **4.1.7 Exhaust Trail Areas (DS+)**

"Fairings and drains located in engine exhaust areas are subject to highly corrosive exhaust gas. They should be examined and cleaned regularly to ensure that exhaust deposits do not accumulate in joints, crevices, seams or hinges. The following inspections are usually carried out:

- Fairings and access panels in the exhaust gas path are removed and all surfaces are inspected.
- Special attention is paid to skin joints, hinges, fasteners and fairings since deposits may become trapped and not be removed during routine cleaning.
- Internal areas of structure in the path of exhaust gases, such as wings, flaps and nacelles are inspected." [2]

D Sight might be applied to inspections especially in large high bi-pass jet engines where physical size of the inspection head would not be a restricting factor.

#### **4.1.8 Engines And Nacelles (DS+)**

"The protective finish on leading edges and engine intake areas may be subject to rain erosion and abrasion by dust. These areas should be cleaned, examined and re-protected as regularly as possible, particularly when operating in marine or desert environments. Problems occur both in jet engines and reciprocating engines and inspections usually include the following specific tasks:

- Frontal areas of engines are inspected, particularly cylinders and push rod housings on reciprocating engines.
- Accessory mounting brackets and particularly cadmium plated parts are examined for signs of corrosion or mechanical damage.

- Cooling air paths that can become obstructed are inspected, as are any crevices where salt deposits may build up.
- Carburetors and other air intake structures are examined, particularly at faying surfaces and fasteners.
- Propeller surfaces and particularly leading edges are examined for nicks, pits or other damage that might lead to corrosion or fatigue.
- Engine mounts and struts are examined, and particularly under clamps or tape, and at welded joints." [2]

Nacelles and pylons of large high bi-pass jet engines would be good candidates for D Sight inspections.

#### **4.1.9 Toilet And Galley Areas (DS—)**

"Fluid spillage in toilet and galley areas often gains access to inaccessible places beneath floor structure. Waste products from these areas are highly corrosive and should be removed as soon as possible. The inspections in these areas should ensure that:

- All areas, particularly deck areas behind toilets, sinks and ranges where spilled food and waste products may collect are clean, dry and free of corrosion.
- Bilge areas under galleys and toilets should likewise be inspected for cleanliness and to ensure integrity of protective treatments and coatings." [2]

These area are not good candidates for D Sight inspection because of restricted access.

#### **4.1.10 Miscellaneous Areas (DS—)**

"Any areas where foreign matter and moisture may accumulate are potential sites for corrosion. Containers or enclosures of all types, including housings for electrical and avionics equipment are prime areas for concern. Access panel seals may deteriorate to allow ingress of water, and the housings may be vented which may allow moist air or spray to enter and corrosion to occur. Electrical equipment may not be adequately designed to resist corrosion and therefore this should be inspected for signs of corrosion and performance at regular intervals. Potential corrosion areas exist in flaps, ailerons, elevators, spoilers and speed brake recesses where dirt and moisture may collect when such control surfaces are in the closed condition. Control cables are also prone to corrosion, particularly where they are exposed or where they pass through seals. Aircraft exposed directly to salt spray such as amphibious aircraft must be inspected more frequently than land based aircraft." [2]

These area are not good candidates for D Sight inspection because of restricted access.

#### **4.1.11 Corrosion Related ADs and SBs**

All Corrosion Prevention and Control Documents [9-14] list the numbers of corrosion related Airworthiness Directives (AD) and Service Bulletins (SB). For the Douglas DC-9 aircraft out of a total of 102 SBs, 28 were related to corrosion in the fuselage, 25 in the wings and 11 in the horizontal stabilizer. For the Boeing 727 out of 27 SBs, 14 pertained to the fuselage, 7 to the wing and 3 to the stabilizer. Only some Corrosion Control Documents and SBs were made available to the authors through Transport Canada, those that were indicate that all Aging Aircraft require repeat inspections of external surfaces (strong candidates for D Sight inspection).

## 4.2 Types Of Corrosion

### 4.2.1 Uniform Corrosion (DS++)

"Corrosion of metals by uniform chemical attack is the simplest and most common form of corrosion. It may occur in moist air or other gases, and in a wide variety of liquids including water. It is probably the most common form of corrosion in aircraft structures, occurring under normal service conditions and particularly in areas where water or condensation is apt to collect. High temperature oxidation is a special form of uniform attack. In uniform corrosion the anodes and cathodes of the electrolytic cells are numerous and closely spaced on the surface of a single piece of metal, and therefore uniform corrosion can be considered as localized electrolytic attack occurring consistently and evenly over the surface.

Uniform corrosion generally produces large areas of damage, and provided the corrosion prone area is accessible for visual inspection, it can usually be detected fairly early and remedial action taken. Uniform corrosion occurring in sealed interior areas, or other visually non-inspectable areas can lead to serious damage unless non-destructive inspection methods are used for early detection followed by corrective maintenance.

Most of the common engineering metals and alloys produce characteristic corrosion products which allow corrosion to be recognized fairly easily. Probably the best-known form of corrosion occurs on non-stainless iron and steel and is easily recognized by the familiar red iron rust.

The corrosion products of aluminium and magnesium alloys are evident as white to gray powdery deposits, the latter are often of a fluffy or granular nature. Early identification of aluminium or magnesium corrosion is essential, and frequently the first indications are flaking or blistering (D S++) of the surface finish. Early attention to uniform corrosion damage is particularly important where the metal skin is used as an outer layer of a honeycomb sandwich structure, or closed box structure. Failure to do so may lead to penetration of the skin by corrosion, and the entry of water or other corrosives into the internal structure." [2]

Flaking and blistering of surface finish are easily located by D Sight. This type of corrosion is a strong D Sight inspection candidate in areas where D Sight head access is possible.

### 4.2.2 Galvanic Corrosion (DS++)

"Galvanic corrosion occurs when metals of different electrochemical potential are in contact in a corrosive medium. Common examples of metal couples susceptible to galvanic corrosion include combinations such as a copper pipe connected to an iron pipe, a bronze propeller in contact with a steel hull, cold worked metal in contact with the same metal annealed, and grain boundaries in a metal in contact with the grains of the same metal. The less noble metal will form the anode of the electrolytic cell and will be corroded while the more noble metal will act as the cathode and will remain largely unaffected. The resulting damage to the anodic metal will be more severe than if the same metal were exposed to the corrosive environment without the presence of, and contact with the cathode.

Galvanic corrosion can often be identified from other forms of corrosion because the corrosive attack is usually more severe at the interface between the two dissimilar metals. Perhaps the most common example of this in aircraft structure is the corrosion which occurs at

fastener holes in aluminium or magnesium alloy skin when steel bolts or rivets are used (DS++).

Cadmium is used as a protective coating and to provide a compatible surface between dissimilar metals in contact. Cadmium has a galvanic potential between aluminium alloys and the common alloy steels and therefore the electrochemical potentials formed by the aluminium/cadmium cell, and the cadmium/steel cell are less than the unprotected aluminium/steel cell and therefore galvanic corrosion will be less severe. In general the greater the difference in electrochemical potential between two metals in a dissimilar metal cell the greater the rate of chemical attack. The use of cadmium as a protective coating on steel fasteners therefore serves to moderate any corrosive reactions, but will not stop them completely. In practice therefore attempts are made to prevent metal contact by placing an insulating material, usually a sealant or jointing compound between the two parts before assembly. The use of a more corrosion resistant aluminium alloy tempers such as T76 or T73, is also recommended.

Some care must be taken when using the galvanic series to assess the galvanic corrosion potential of dissimilar metals, since some metals may occupy different positions in the series. This is most commonly observed with metals such as stainless steels which can exist in either a passive or active state. In the passive state most stainless steels will occupy positions towards the noble end of the galvanic series, while in the active state they will behave more anodically. This behaviour is believed to be due to the state of the protective oxide films which tend to form on stainless steels, and which resist further corrosive attack. When the oxide film is intact and effective as a protective covering the metal behaves cathodically, whereas a damaged film leaves the metal unprotected and it therefore tends to behave anodically." [2]

Figure 19 is a good illustration of galvanic corrosion around steel fastener in aluminium alloy. D Sight isolated corroded areas and the findings were later confirmed by ultrasonic inspection.

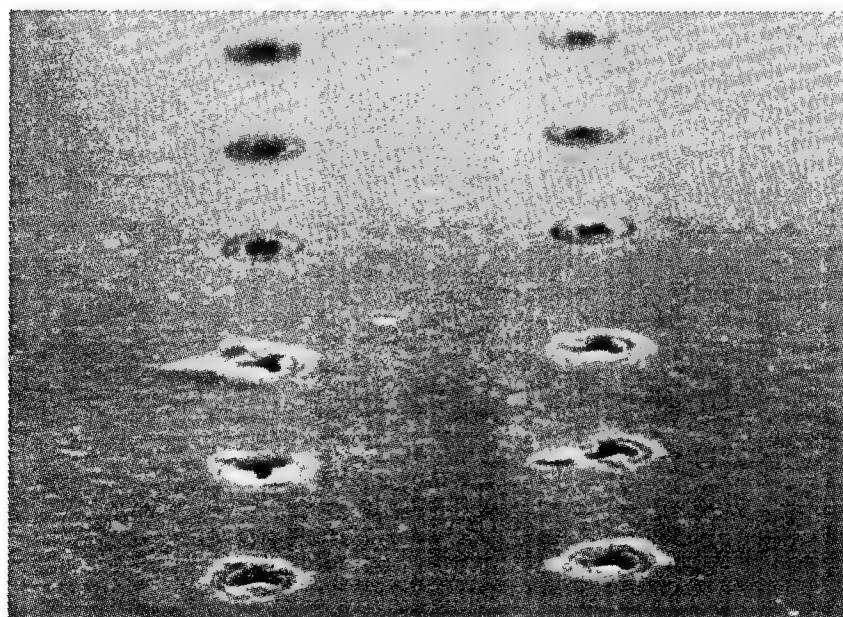


Figure 19. D Sight image of an aluminium alloy skin with two sets of fasteners. The six lower fasteners precipitated galvanic corrosion which is quite visible under D Sight.

### 4.2.3 Pitting (DS—), Crevice And Filiform Corrosion (DS++)

#### 4.2.3.1 Pitting (DS—)

"Pitting corrosion a strongly localized type of attack which leads to the formation of deep and narrow cavities. All engineering metals and alloys are susceptible, and the conditions leading to pitting vary from metal to metal, depending in part on whether the metal is normally active or passive.

For active metals uniform exposure of a large surface area to a corrosive medium would tend to cause uniform corrosion. Pitting of an active metal therefore occur as a result of local wetting, or defects in a protective coating which allow very localized exposure.

In passive metals such as certain stainless steels and aluminium alloys, which form naturally protective oxide films, pitting occurs as a result of local damage to this protective film. However, whether the metal is active or passive, pitting involves the formation of small areas which are anodic with respect to the rest of the surface, and which therefore suffer severe corrosive attack in the presence of an electrolyte.

In aircraft structures pitting corrosion may occur in many areas, but areas subject to local contamination by highly corrosive media, such as battery compartments, toilet and galley areas, are prime sites. Pitting corrosion is particularly common in aircraft structures operating in marine environments since the chloride ions promote the local dissolution of protective oxide films. Pitting in passive metals is uncommon in solutions which do not contain halide ions, since the oxide films would tend to be stable and remain protective.

Pitting occurs in two stages, initiation and growth. The initiation stage involves the period before visible pits have formed and may extend over periods of several months or several years, even for nominally constant environmental conditions. Under actual service conditions, it is likely that a transient exposure to a severe environment involving high concentrations of chloride ions or high acidity (pH) will be responsible for initiation. Once a pit has formed it can penetrate the metal at an ever increasing rate. This is because the corrosion process occurring within the pit produces conditions which favour the continued and accelerating dissolution of metal. In the pitting of a metal by an aerated sodium chloride solution, rapid dissolution of metal within the pit tends to produce an excess of positive charge in this area. This causes the migration of chloride ions into the pit to balance the positive charge, and the formation of MCl. The high concentration of chloride ions, together with the high concentration of hydrogen ions arising from hydrolysis, provides conditions which favour the continued dissolution of the metal. This buildup of high concentrations of metal, chloride and hydrogen ions in the pit is favoured by a stagnant, or only slowly moving solution, and also by the growth of the pit in the direction of gravity forces. By increasing the velocity or turbulence in a corrosive solution, or by creating conditions which oppose the formation of highly acidic conditions in the pit, the pitting action can often be stopped.

Pitting corrosion is one of the most insidious forms of corrosion because the pits are often very small and difficult to see with the naked eye, and particularly if they are hidden by general erosion products or coatings. The electrochemical conditions at the base of a pit can be such that other forms of corrosion, such as intergranular attack will occur, leading to widespread subsurface damage. In highly loaded structures the stress concentration at the base of a pit can be sufficient to cause fatigue or stress corrosion cracking to occur." [2]

Pitting corrosion will not generally be visible to D Sight, because pits are usually small and

produce sharp discontinuities on the surface without local change in surface curvature. It is only after pitting results in other forms of corrosion that D Sight might be useful inspection tool.

#### 4.2.3.2 Crevice Corrosion (DS++)

"This is a form of attack which occurs when a corrosive liquid, such as salt spray, gains access to crevices in, or between components. It is usually associated with small volumes of stagnant solution which become trapped in holes, between gasket surfaces or lap joints, under surface deposits, or in crevices under bolt or rivet heads. If there are differences in the concentration of dissolved salts or dissolved oxygen in the entrapped liquid, anodic and cathodic regions may result, and the anodic areas will be attacked. This anodic region is usually at the bottom of a crevice and a pit develops. The corrosive action at the bottom of the pit accentuates the difference in concentration of the electrolyte at that point and corrosive attack progresses more rapidly as the depth of the pit increases. Crevice corrosion has many characteristics in common with pitting. For example it is common in passive metals such as stainless steels and aluminium alloys which form protective oxide films, and it is often observed in solutions containing high concentrations of chloride ions and hydrogen ions, which promote the breakdown of these films.

In cases where the most severe corrosion damage is away from the edges of the fastener holes one can conclude that galvanic corrosion was not the major factor." [2]

Corrosion in lap joints leads to pillowing (bulging) of skins held together by fasteners or spot welds. This is a very good application of D Sight which has been demonstrated on actual aircraft (B727) as shown in Figure 20.

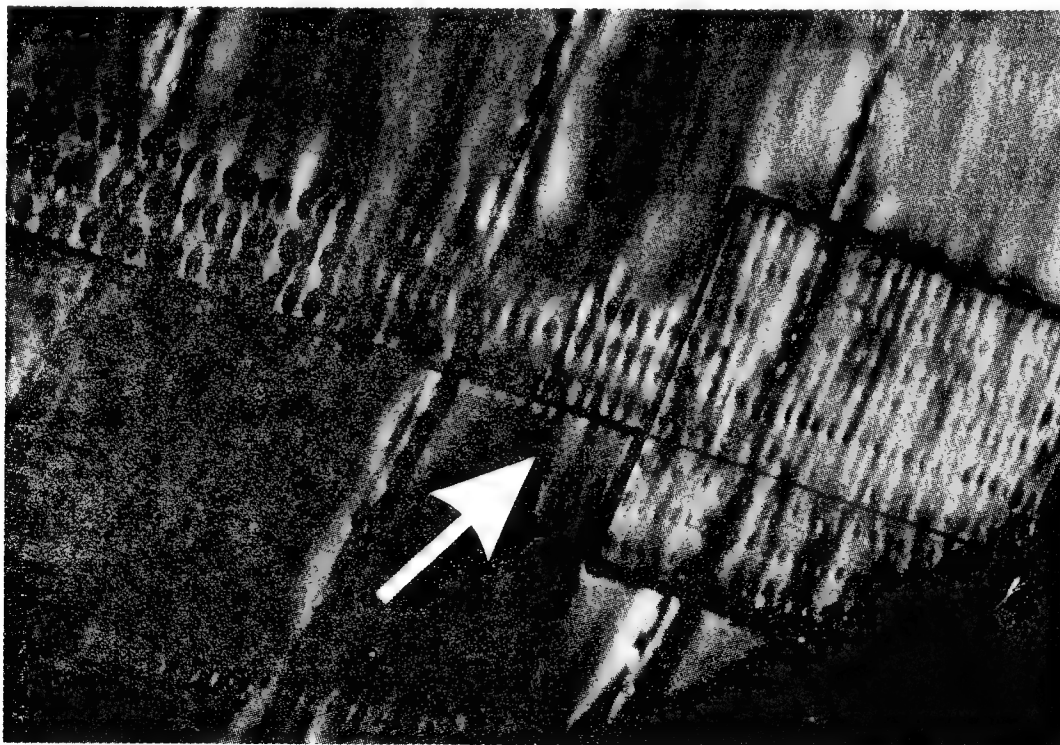


Figure 20. D Sight image of B727 lap splice showing pillowing in 8 rivet rows outside the patch. Subsequent teardown revealed extensive corrosion.

#### 4.2.3.3 Filiform Corrosion (DS++)

"Filiform corrosion is one of the less common forms of corrosion in aircraft structures and consequently is not as well understood, or as well documented as some others. It has some of the characteristics of pitting corrosion and also of intergranular corrosion. It often starts from a corrosion pit, but instead of penetrating deep into the thickness of the metal it spreads out sideways to form threadlike lines of corrosion near the surface. It is often found in clad aluminium alloys, where the initial pit will penetrate the cladding, and then will be diverted by the underlying grains to run parallel with the surface in numerous meandering filaments. It is also found under organic coatings such as paints, and it has been suggested that this may be due to the permeation of moisture through the painted surfaces under conditions of high humidity and high ambient temperatures. However it is also often found that the corrosion starts at fastener holes, where the metal is unprotected, and then extends along the surface of the sheet and beneath the paint.

This form of corrosion may become quite severe before it is detected, since it will often be hidden by either cladding or paint, and in the latter case may be indicated by blistering. Filiform corrosion has been observed in magnesium, aluminium, steel and chromium plated nickel." [2]

This is a good candidate form of corrosion for D Sight inspection as can be seen in Figure 21.

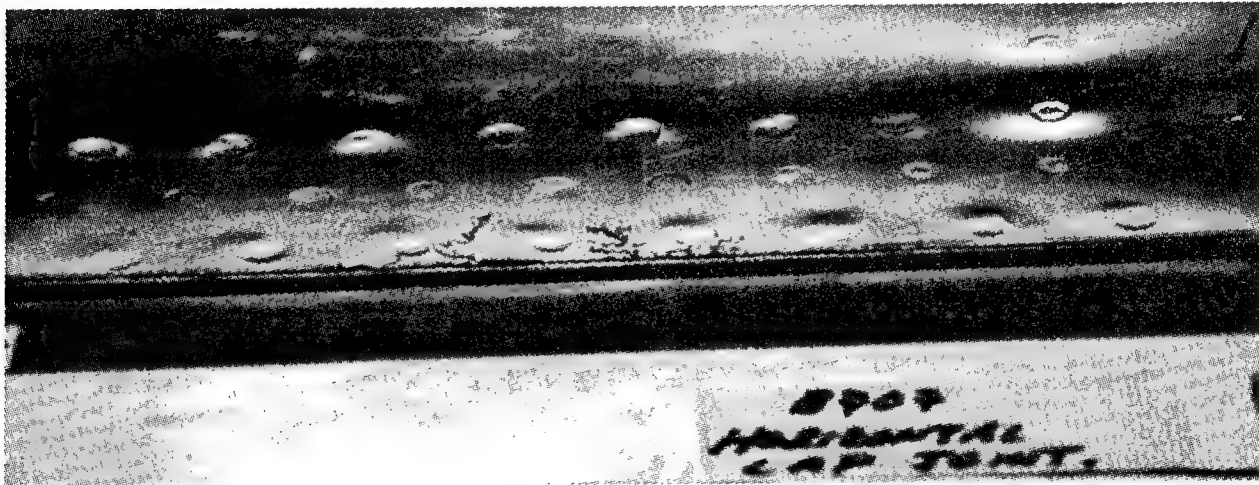


Figure 21. D Sight image. Filiform corrosion in a lap splice area.

#### 4.2.4 Intergranular Corrosion And Exfoliation Corrosion (DS++)

"Intergranular corrosion is a highly localized form of dissolution which affects the grain boundary regions in a polycrystalline metal. The corrosive attack can produce a network of corrosion or cracking on the metal surface, occasionally dislodging whole grains, or it may penetrate deeply into the metal leaving behind very little visible evidence of the damage.

In heavily rolled or extruded products where the grains are flattened and elongated in the direction of working, the presence of intergranular corrosion can lead to layering and flaking, producing a delamination effect with surface grains being pushed out by the underlying corrosion products. This is known as exfoliation corrosion, and is essentially a severe form of

intergranular corrosion occurring in the direction of grain flow. In intergranular corrosion or exfoliation the material in the grain boundary areas behaves anodically with respect to the bulk of the metal in the grain interiors. In corrosive environments dissolution of the anodic grain boundaries usually occurs at a very rapid rate while the bulk alloy is little affected. The small area of the anode with respect to the cathode area is an important factor influencing the corrosion rate. The anodic nature of the grain boundary may be due to the local segregation of impurities, or either the enrichment or depletion of the grain boundary in alloying elements. These effects may be associated with the precipitation of grain boundary phases, which may themselves behave anodically with respect to the adjacent alloy. Alloys of the 2000 (Al Cu) series may be sensitive to intergranular corrosion if they are not quenched rapidly enough after solution heat treatment. These alloys are strengthened by the precipitation of copper-aluminium, or copper magnesium aluminium phases such as  $\text{Cu Al}_2$  or  $\text{CuMgAl}_2$  during aging at room temperature (natural aging) or moderately elevated temperatures (artificial aging). However slow cooling through the range 400-260°C may lead to the formation of coarse grain boundary precipitates with substantial potential differences arising between the copper-depleted zones and adjacent material. Parts must therefore be solutioned at temperatures high enough to dissolve all precipitated phases, usually in the region of 490°C, and then quickly immersed in the quenching bath to ensure rapid cooling to room temperature. When quenching is by total immersion in water, the water must be at room temperature and cooled to maintain a temperature below 38°C during the quench. The degree of aging after quenching, which is affected by the aging temperature and the aging time, also have marked effects on intergranular corrosion. Over aging treatments such as T8 (or T851) for 2000 series alloys, or T76 (T7651) or T73 (T7351) for 7000 series alloys generally produce increased resistance to intergranular corrosion." [2]

Figure 22 shows D Sight image of heavy exfoliation around fastener caused by galvanic corrosion. Exfoliation by definition will result in surface perturbation and is therefore well suited for D Sight inspection.

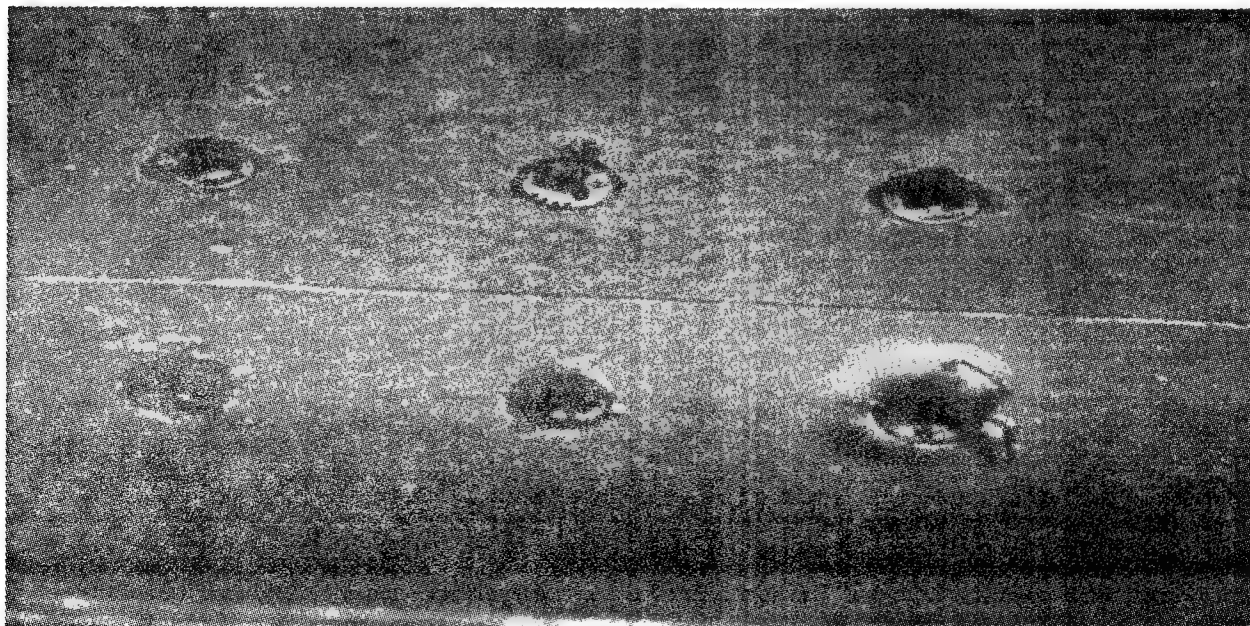


Figure 22. D Sight image showing exfoliation around a rivet head.

#### 4.2.5 Other Types of Corrosion (DS—)

Fretting corrosion, hydrogen embrittlement, corrosion fatigue and microbiological corrosion are known to appear in aircraft. However they will not be reviewed here as it is deemed highly unlikely that D Sight would be useful in detecting these types of corrosion. Extensive coverage of these types of corrosion can be found in [2].

### 5.0 CONCLUSIONS

While there are only two basic splice design concepts (lap and butt) the detailed designs found in aircraft offer a very large variety of configurations. During the specimen collection activity, it will be necessary to select the most typical for each aircraft type. Based on the data provided in the drawings, it is recommended that circular saws with 12 to 14 inch diameter be used for the specimen removal.

All aircraft in the aging category have fuselage skins made of 2024-T3 alloy with the exception of DC-9 fuselage skins which are made of 2014-T6 alloy. The stringer material is typically 7075-T6.

D Sight is best applied for inspection of external surfaces of aircraft. These inspections are carried out periodically according to corrosion related ADs and SBs and maintenance manuals. The fuselage, parts of the empennage and the control surfaces could be inspected for uniform, crevice, exfoliation and filiform corrosion using D Sight. Thicker metal gauge wing box surfaces may not produce characteristic crevice corrosion bulges necessary for D Sight indications but intergranular, exfoliation and filiform corrosion on these structures are good candidates for D Sight inspections. This project will address only crevice corrosion in fuselage lap splices. It is recommended that other areas of potential application of D Sight be investigated in Phases II and III of the project or that additional projects be formulated.

### 6.0 REFERENCES

- [1] J.P. Komorowski, D.L. Simpson and R.W. Gould, 'Enhanced Visual Technique for Rapid Inspection of Aircraft Structures', Materials Evaluation, December 1991, pp. 1486-1490.
- [2] Wallace, W., Hoepner, D.W., Kandachar, P.V., "AGARD Corrosion Handbook Vol.1, Aircraft Corrosion: Causes and Case Histories", AGARD-AG-278, 1985.
- [3] "2nd Annual International Conference on Aging Aircraft", DOT/FAA/CT-89/35, Proceedings 1989
- [4] "1991 International Conference on Aging Aircraft and Structural Airworthiness", NASA CP 3160, 1991.
- [5] "Structural Integrity of Aging Airplanes", Atluri, S.N., Sampath, S.G., Tong, P., Eds., Springer-Verlag, 1991.
- [6] Chun-Yung Niu Michael, "Airframe Structural Design, Practical Design Information on Aircraft Structures", Conmilit Press Ltd., 1988.
- [7] Hagemaiier, D.J. et al., "Aircraft Corrosion and Detection Methods", Materials Evaluation 43 (1985) 426-437.
- [8] 1989 Tri-Service Conference on Corrosion, Proceedings, Agarwala, V.S., Ed., NADC-

SIRLAB-1089.

- [9] DC9/MD-80 Corrosion Prevention and Control Document, MDC-K4606, April 1990.
- [10] Aging Airplane Corrosion Prevention and Control Program Model 727, Boeing D6-54929
- [11] Aging Airplane Corrosion Prevention and Control Program Model 737-100/200, Boeing D6-38528
- [12] Aging Airplane Corrosion Prevention and Control Program Model 747-100/200/300/SP/SR, Boeing D6-36022
- [13] Corrosion Prevention and Control Program, Model L-1011, Lockheed LR-31889
- [14] A300, Corrosion Prevention and Control Program, A300-CPCP



## APPENDIX C

Summary On-Aircraft Non-Destructive Equipment Demonstration, Tinker Air Force Base Oklahoma City, Oklahoma, May 11 - 13, 1993, Diffracto Limited.

**SUMMARY**

*ON-AIRCRAFT NON-DESTRUCTIVE  
EQUIPMENT DEMONSTRATION*

**TINKER AIRFORCE BASE  
OKLAHOMA CITY, OKLAHOMA**

by

**Dr. Frank Karpala  
Dr. Omer Hageniers  
Don Clarke**

**May 11-13, 1993**

**Diffracto Ltd.  
2835 Kew Drive  
Windsor, Ontario  
N8T 3B7**

**519-945-6373  
FAX 519-945-1467**

## **1 INTRODUCTION**

Following a successful demonstration of *D SIGHT* for Rapid Scan of lap joint corrosion on a Boeing 727 in the summer of 1992, Diffracto was invited back for an on-aircraft demonstration of the technology for several military aircraft including a C-135, an E-3, and a B-52. Appendix A includes a copy of the invitation and vendor information for the demonstration as received by Diffracto.

The demonstration was held at Tinker Airforce Base in Oklahoma City, Oklahoma (OC-ALC), over three days. The first day was spent with logistic details, receiving instructions and ground rules and unpacking and setting up equipment. The following two days were divided into three sessions: Session 1: human factors, Session 2: sensitivity and accuracy, and Session 3: multiple aircraft. Several other vendors were on-site and in some cases at the same inspection site during the demonstration. For security reasons, vendors were not permitted to take photographs during the demonstration although photographs and video were taken by ARINC personnel.

Over the course of two days, 137 images were taken of different inspection zones selected by ARINC, with no difficulty in accessing or positioning the DAIS-500 inspection unit. Although all the images were given to the evaluators from all sessions, corrosion severity was only reported for the images associated with Session 2. A copy of the reported corrosion, as entered into the ARINC computer, was given to Diffracto on-site. All inspections were performed in a timely manner and in some cases, additional areas were inspected due to the availability of time.

## **2 EQUIPMENT AND PERSONNEL**

In advance of the demonstration, Diffracto shipped the following equipment to ARINC:

- DAIS-500 inspection sensor with pole and light skirt (3.125 sq.ft inspection area)
- DAIS-40 inspection sensor (38 sq.in. inspection area)

- portable DAIS computer controller
- remote pendant
- sensor and pendant power supply
- highlighter and applicator
- 100 foot sensor cable and controller interface cables
- Laserjet III printer equipped for half-tone image printing

The equipment arrived in good shape and performed without problems during the demonstration. Because of the different sites on base, the equipment was dismantled, shipped by car or van, and then reassembled at least six times during the demonstration including the initial testing at ARINC.

Three Diffracto personnel attended the demonstration; namely, Dr. Omer Hageniers, Dr. Frank Karpala, and Don Clarke. Jerzy Komorowski, from the Institute for Aerospace Research of the National Research Council Canada, was invited by Diffracto to attend the demonstration and to assist in interpreting *D SIGHT* images for corrosion.

### **3      SESSION SUMMARY**

The order of inspection and demonstration was determined by ARINC accounting for the locations and the number of vendors on-site during the 3 day period. See Appendix A for the schedule and vendor list. Diffracto was instructed to perform inspections related to session 1 and session 3 on the first day, followed by session 2 on the second day. The session summaries below present the results in the same order.

#### **3.1    Session 1: Human Factors**

Session 1 was designed by ARINC to evaluate vendor equipment for human factor characteristics according to MIL-STD-1472D, Human Engineering Design Criteria standards. This evaluation was based on inspecting four different areas on a C-135 aircraft with tail number 61-2668. The

areas included the upper right wing, the boom pod area, an area in the upper left fuselage near the tail, and an area on the left fuselage. All areas were relatively small in size and, with the exception of the boom pod, required ladders and platforms for access. Safety harnesses were mandatory on the upper wing.

The original designated inspection area on the upper wing was abandoned due to the presence of markings by maintenance staff that would be removed by highlighter. Instead, two much larger areas were inspected while the process was video taped. Two Diffracto operators performed the inspections while two ARINC evaluators observed and recorded the activity. Other observers were present at ground floor monitoring the inspection activity on the host computer video monitor. The surface inspected was stripped of paint down to bare aluminum except that some fastener rows had been primed. The surface needed to be highlighted to make it sufficiently reflective for the *D SIGHT* equipment.

The boom pod area required the sensor to be positioned upside down but over the head of the operator from the hangar floor. Two sensor placements were made to cover the area after the surface was highlighted. The area was convex but the radius of curvature was not known.

The remaining two areas on the fuselage both needed highlighting but were not difficult to inspect. The surfaces were cylindrical in shape and the sensor was positioned in a fore-aft orientation along the lap joints. Access to the surfaces was achieved by the tall ladders already in position. Because the weight of the sensor and pendant is so low, there was no great difficulty in climbing and carrying the equipment to the top of the ladders.

Although the time for data gathering and analysis was recorded by ARINC observers, Diffracto did not independently record these times. Rather, the number of images and the time needed to acquire these images was estimated from the time stamps recorded with the image at the time of image acquisition. The data gathering time in minutes:seconds is the difference between the time stamps of the last image taken and the first image taken in the specific area described.

Inspection Area	No. of Images Acquired	Data Gathering Time
Upper Wing	21	31:52
Boom Pod	2	00:30
Fuselage - Tail	6	04:38
Fuselage - Side	4	04:26
All	33	41:26

The elapsed time for this aircraft including setup, acquisition, analysis, and breaks was just over 2 hours.

The log file for this aircraft is **61-2668.log** and the corresponding images have filenames starting with 61-2668 followed by extension numbers from 0 to 32.

### 3.2 Session 3: Multiple Aircraft

The multiple aircraft session consisted of inspections on an E-3 AWACS aircraft and a B-52 bomber. These aircraft were located in two different hangars and are reported separately.

#### 3.2.1 E-3 AWACS - Tail Number 71-1407

The designated area of the E-3 aircraft was on the upper right wing along a rivetted butt joint approximately 2 feet long. A second joint section, closer to the leading edge, was also inspected. Both joints were inspected with the DAIS-500 sensor positioned along the joint as well as perpendicular to it. The areas inspected were stripped of paint and needed to be highlighted. Because of the short amount of time needed to inspect these two small areas with the DAIS-500, both joint sections were also inspected with the DAIS-40 sensor and an optional lap joint along the lower right fuselage was inspected with the DAIS-500. The length of this lap joint was approximately 10 feet and inspections were made without highlighting since the

fuselage was painted with a light color having a glossy finish. The latter area was accessible from the hangar floor.

Inspection Area	No. of Images Acquired	Data Gathering Time
Upper Wing - Butt Joint 1	DAIS-500: 2	01:07
	DAIS-40: 11	06:48
Upper Wing - Butt Joint 2	DAIS-500: 3	01:33
	DAIS-40: 9	06:08
Fuselage - Lap Joint	DAIS-500: 7	04:22
All	32	21:50

The elapsed time to inspect the E-3 including setup, data acquisition and analysis was less than 45 minutes.

The log file for this aircraft is **71-1407.log** and the 32 images are stored with filename 71-1407 followed by extension numbers from 0 to 31

### 3.2.2 B-52 Bomber - Tail Number 61-035

The designated inspection area for the B-52 was the 7 sets of 6 fasteners between the thick upper right wing plates and the trailing edge. The fasteners were large and close together. Highlighting was needed and care had to be taken to keep the highlighter from pooling around the fasteners. Both the DAIS-500 and DAIS-40 sensors were used on the fasteners.

Sensor	No. of Images Acquired	Data Gathering Time
DAIS-500	8	10:46
DAIS-40	8	08:08
All	16	18:54

The elapsed time for the inspection of the fasteners with both sensors was about 25 minutes.

The log file for this aircraft is **61-035.log** and the 16 images are stored with filename 61-035 followed by extension numbers from 0 to 15. It should be noted that the model number for images 61-035.008 to 61-035.015 was stored incorrectly as DAIS-500 instead of DAIS-40.

### 3.3 Session 2: Sensitivity and Accuracy

The sensitivity and accuracy session consisted of two parts: inspection of 5 lap joint areas on the left fuselage of a C-135, and a small fastener area on the upper right wing of the same aircraft. The aircraft had tail number 12671 and was painted with a light colored glossy paint so that no highlighter was needed. Because of sunlight falling on the inspection areas through the hangar windows, the auxiliary skirt for the DAIS-500 was attached and used to eliminate the strong ambient light inside the inspection unit. With this skirt, the inspection could proceed normally. The data gathering times for Lap Joint Area #2 includes a seven minute gap to mount the skirt after the decision was made to use it. Each part of the sensitivity and accuracy session will be reported separately.

#### 3.3.1 Lap Joints

Each lap joint area was relatively short and as a result, each was inspected in two orientations; along the lap joint and perpendicular to it. The following table summarizes the inspection area, the number of images taken, and the time for data acquisition.

Inspection Area	No. of Images Acquired	Data Gathering Time
Area #1 Stringer 18, BHS 1100	7	02:22
Area #2 Stringer 14, BHS 1000	7	11:09

Inspection Area	No. of Images Acquired	Data Gathering Time
Area #3 Stringer 7, BHS 1020	6	03:26
Area #4 Stringer 14, BHS 640	8	04:36
Area #5 Stringer 18, BHS 1040	6	02:52
All	34	24:25

The total elapsed time for these inspections was about one and a half hours including setup, data acquisition and analysis.

The log file for this aircraft is **12671.log** and the 34 images are stored with filename 12671 followed by extension numbers from 0 to 33. This same log file also contains the fastener images to be discussed in the next section.

Prior to the inspection of the aircraft, ARINC issued instructions on the method to be used for reporting corrosion for their computer program. In addition, they allowed each vendor to select a spatial resolution for their reporting from three choices; 1/8, 1/4, and 1/2 inches. DiffRACTO chose to report on the 1/4 inch grid transparencies. Small holes, drilled every three inches along the lower portion of each lap joint, were used for the purposes of registering the position of the transparencies and any future x-ray images.

The reporting of severity level was established by ARINC in terms of percent material loss and six color bands were defined as described in Appendix A. Since DiffRACTO has not yet established a calibration procedure for corrosion in terms of material loss, it chose to report corrosion severity in three classes: white (little or no corrosion), green (moderate corrosion), and black (severe corrosion) as inferred by the amount of surface deformation caused by corrosion products below the surface and the type of joint being inspected. The categorization

of severity level was made by an experienced examiner looking at the *D SIGHT* images and studying the physical construction of the particular area being inspected.

The results of the inspections are presented in chart form in Figures 1-5. These results are transcribed from the color originals supplied to DiffRACTO by ARINC on-site. Included in the figures are the location and severity classifications determined by DiffRACTO (Note: white=white, light grey=green, dark grey=black). The grid represents 1/4 inch areas of the actual lap joint. Also included in the figures are the images from the inspections. The upper strip corresponds to the sensor positioned along the lap joint while the lower strip corresponds to the sensor positioned perpendicular to the lap joint. These images have been spatially transformed to remove the perspective normally found in the *D SIGHT* image.

### 3.3.2 Wing Fasteners

Figure 6 shows a graphic of the designated fasteners for inspection with a number for each fastener. These are found on the upper right wing on a C-135 with tail number 12671. The upper portion of the area above the joint line is 7178-T6 aluminum that is 0.170 inches thick while the lower portion is the same material but 0.250 inches thick. The orientation of these fasteners is fore (top) - aft (bottom). The table below summarizes the number of images acquired and the acquisition time for each sensor used.

Sensor	No. of Images Acquired	Data Gathering Time
DAIS-500	8	04:33
DAIS-40	14	11:18
All	22	15:51

The total elapsed time for inspection and analysis was under 45 minutes.

The log file for this aircraft is **12671.log** and the 32 images are stored with filename 12671 followed by extension numbers from 34 to 55.

As specified in Appendix A, the reporting requirements for corrosion around fasteners includes, location, orientation, and severity. At the present time, DiffRACTO does not have the experience base to report corrosion problems around fasteners to this level of precision. Instead, a full field view of an area can locate suspect fasteners by the change in the pattern around the fasteners in the *D SIGHT* image.

Based on the analysis of the images during the demonstration, the following fasteners were suspected of being corroded: 71, 64, 66, 51, 61, 45, 44, 42, 26, 25, 10, 4, and 3. Figure 7 shows a composite image of the fasteners when the DAIS-500 was oriented perpendicular to the joint. Figure 8 shows a composite image of the same fasteners when the DAIS-500 was oriented in the same direction as the joint. Figure 9 shows the same orientation with the DAIS-40 sensor. In each figure, the suspect fasteners are circled and the composite image has been formed by first removing the perspective in the original images.

Several of the fasteners were in grind out areas from previous repairs to the wing. Again, based on a lack of experience, no decision with regard to corrosion under fasteners in grind out areas was made.

#### **4 CONCLUSIONS**

The on-aircraft demonstration exercise was extremely educational and encouraging. All designated inspection areas were inspected rapidly and the areas of corrosion reported to ARINC were made with a high degree of confidence.

Three improvements to the hardware from the first demonstration in the summer of 1992 were also successful. These were the addition of a opaque skirt around the DAIS-500 sensor to eliminate ambient light; the addition of a remote pendant allowed two operators to be in close proximity to the inspection area for better communication and assistance to each other; and a

repackaging of the host computer with a hard case and fewer interconnect cables made portability, setup and use easier. Several software modifications that permit commenting and component identification from the pendant also helped tremendously.

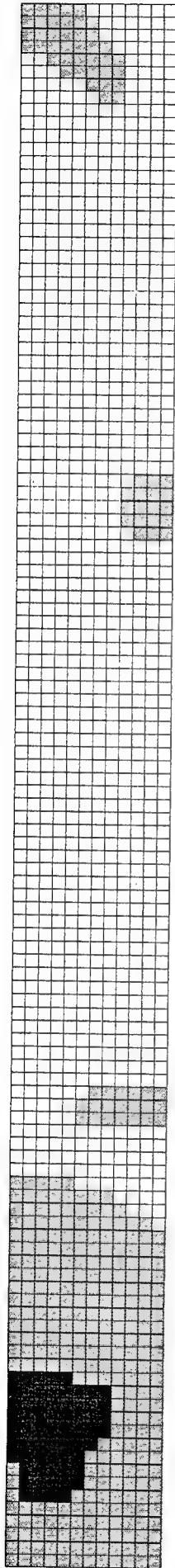
As a rapid scan vendor, Diffracto was disappointed in the size of inspection areas, in general, throughout the demonstration. Lap joints measuring 30 feet rather than 30 inches should have been included in the test. The strength of the *D SIGHT* technology for corrosion detection is rapidly finding candidate areas for further study. As of yet, it is not calibrated for measuring corrosion as a percentage of material loss. The key to *D SIGHT* for the detection of crevice or interlayer corrosion is inferring corrosion below the surface from surface curvature information produced by the corrosion products. The use of *D SIGHT* for detecting corrosion under fasteners in thick aluminum skins is not as encouraging, except in the form of exfoliation, which is easily detected.

The DAIS-500 sensor used during the demonstration was originally built and optimized for detecting impact damage on composite skins. Several modifications to the sensor could make it more sensitive and easier to find corrosion on aluminum structures. These modifications are expected to take place this year. Diffracto is encouraged by the performance of the DAIS-500 for corrosion detection despite its optimization for impact damage.

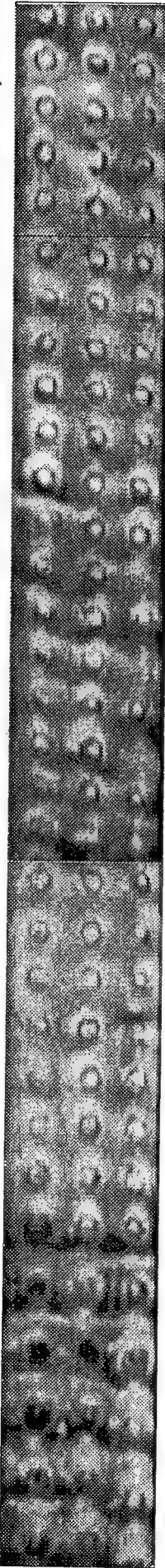
## **5 ACKNOWLEDGEMENTS**

Diffracto would like to thank Jerzy Komorowski from the Structures and Materials Laboratory, Institute for Aerospace Research, of the National Research Council Canada for participating in the on-aircraft demonstration and providing valuable expertise in interpreting *D SIGHT* images for corrosion.

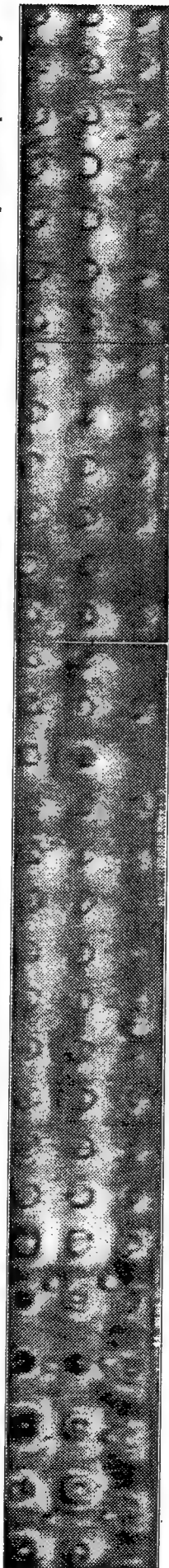
Diffracto would also like to thank Robert Rennell of ARINC for the invitation to the demonstration and his organization and running of the demonstration.



Location and Severity Classifications determined by Diffractometry

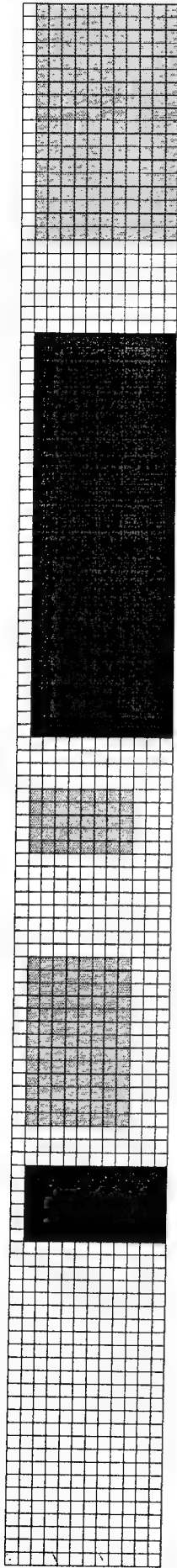


D SIGHT mosaic image with sensor positioned parallel to joint

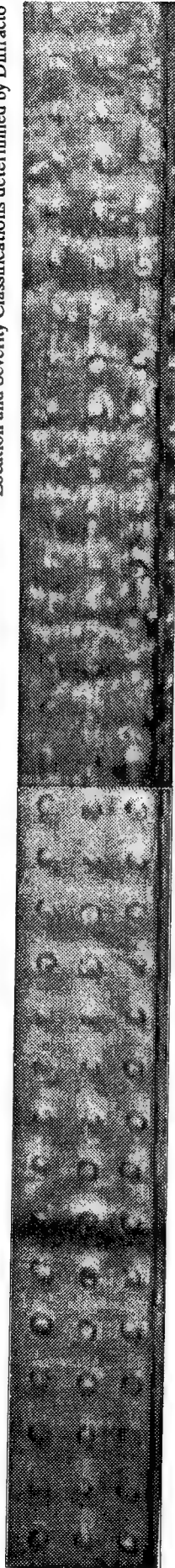


D SIGHT mosaic image with sensor positioned perpendicular to joint

Fig. 1 Area #1, Stringer 18, BHS 1100



Location and Severity Classifications determined by Diffracto

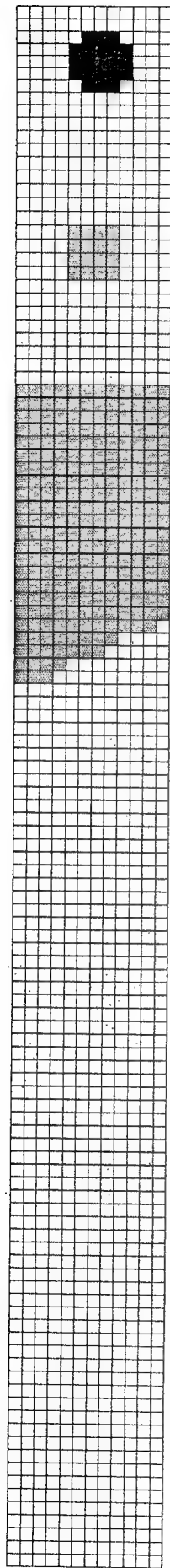


D SIGHT mosaic image with sensor positioned parallel to joint

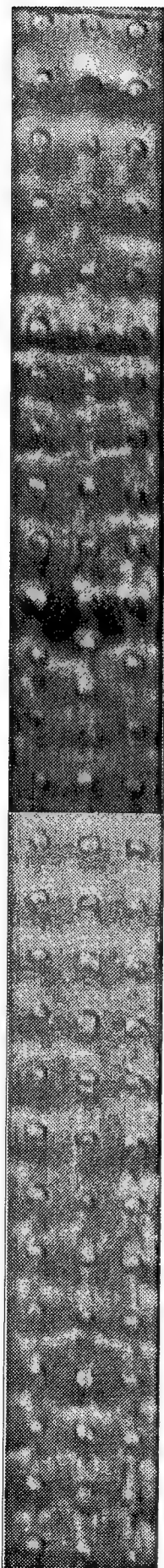


D SIGHT mosaic image with sensor positioned perpendicular to joint

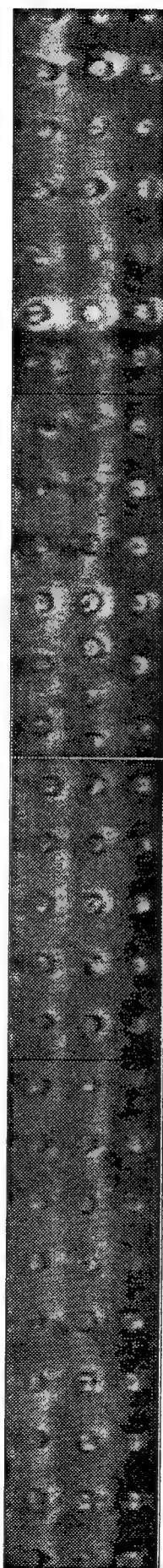
Fig. 2 Area #2, Stringer 14, BHS 1000



Location and Severity Classifications determined by Diffracto

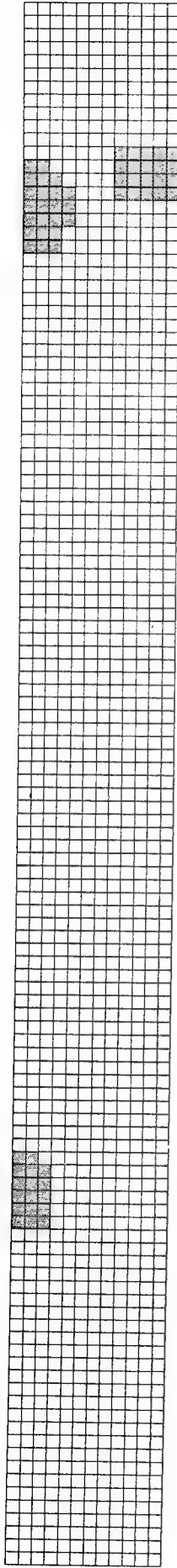


D SIGHT mosaic image with sensor positioned parallel to joint

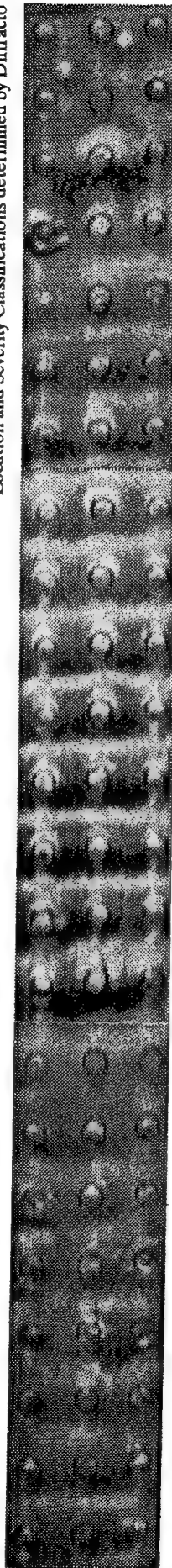


D SIGHT mosaic image with sensor positioned perpendicular to joint

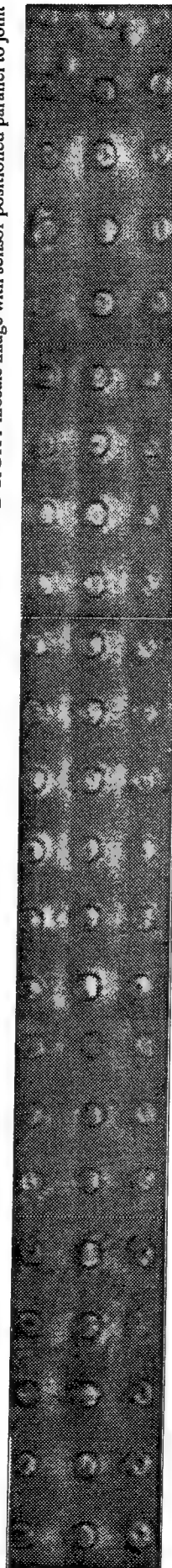
Fig. 3 Area #3, Stringer 7, BHS 1020



Location and Severity Classifications determined by Diffractometry

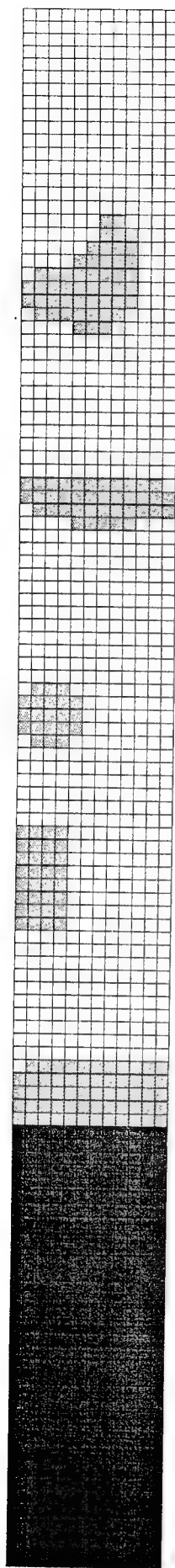


D SIGHT mosaic image with sensor positioned parallel to joint

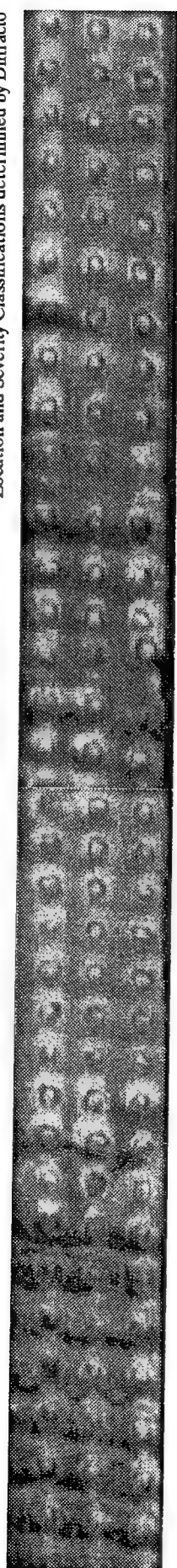


D SIGHT mosaic image with sensor positioned perpendicular to joint

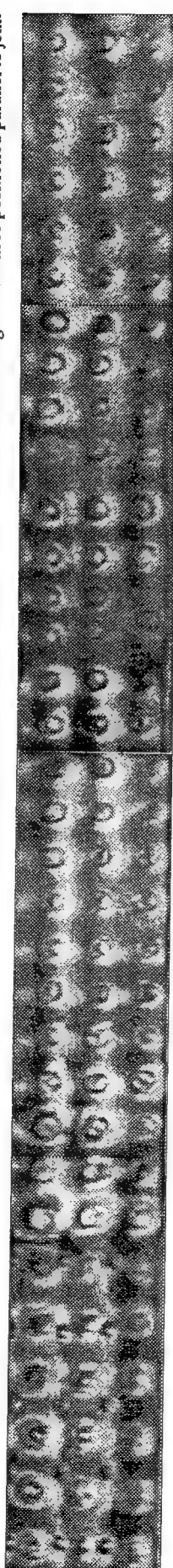
Fig. 4 Area #4, Stringer 14, BHS 640



Location and Severity Classifications determined by Diffractometry



D SIGHT mosaic image with sensor positioned parallel to joint



D SIGHT mosaic image with sensor positioned perpendicular to joint

Fig. 5 Area #5, Stringer 18, BHS 1040

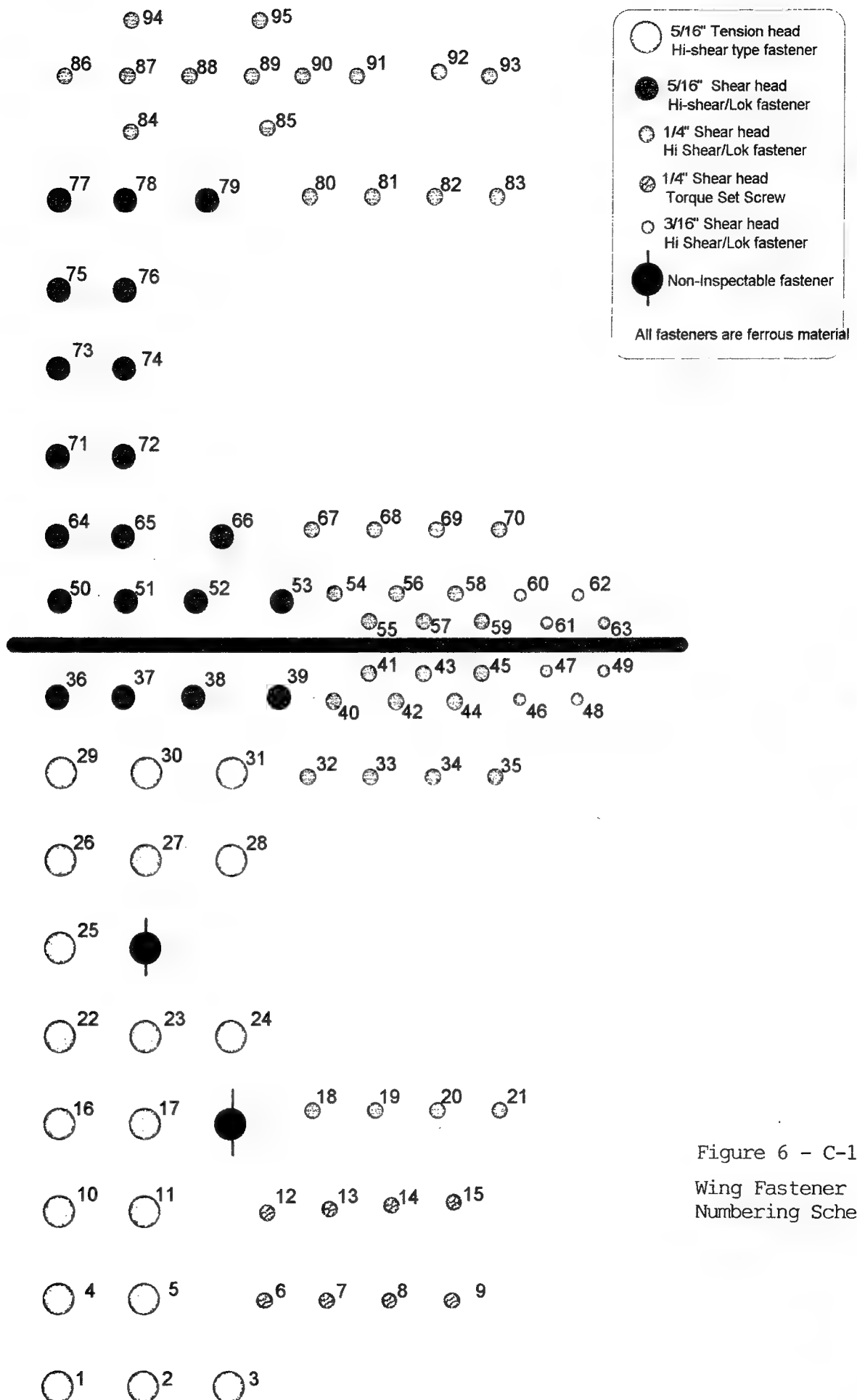


Figure 6 - C-135  
Wing Fastener Pattern  
Numbering Scheme

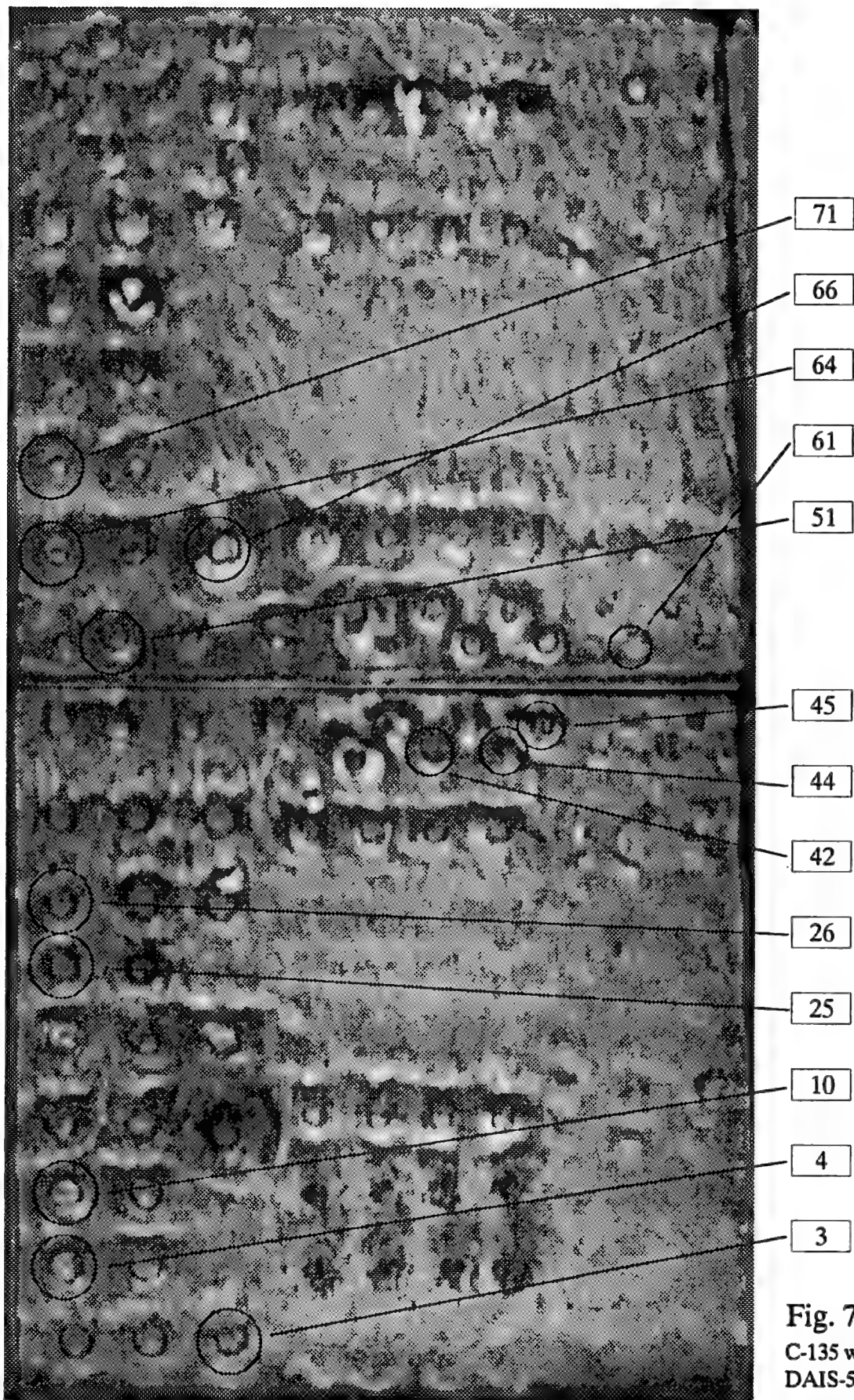
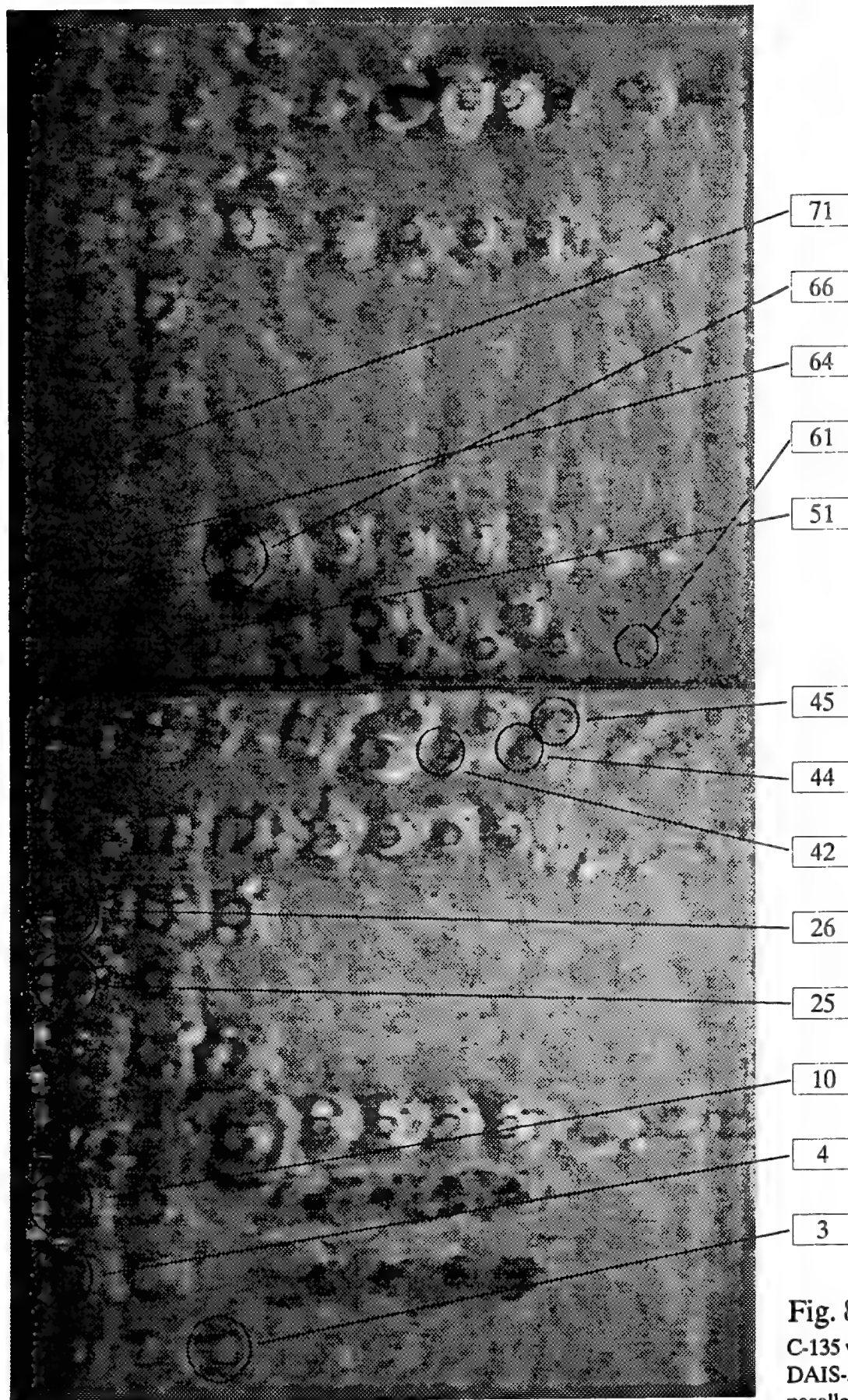
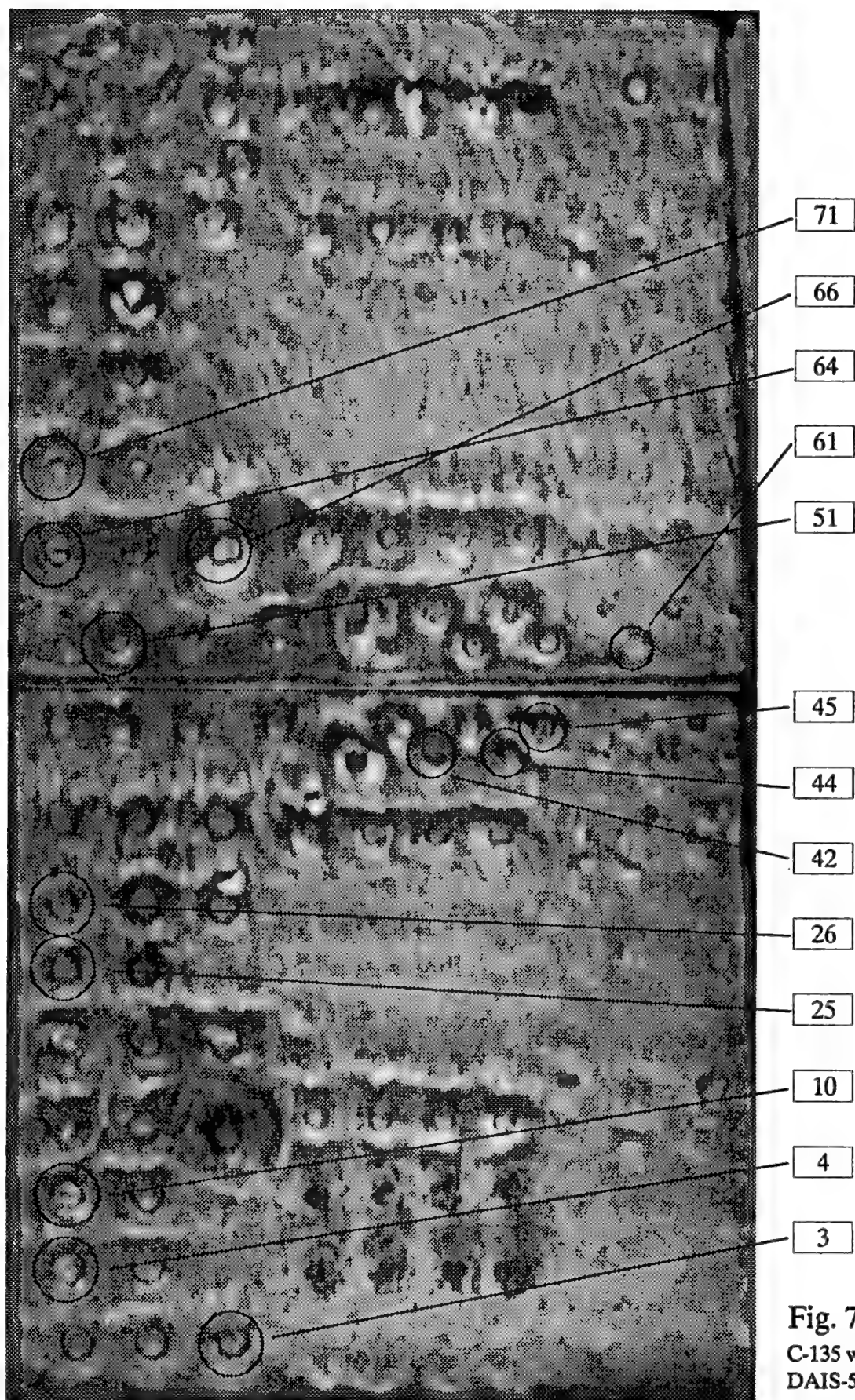


Fig. 7  
C-135 wing fasteners  
DAIS-500  
perpendicular to joint



**Fig. 8**  
C-135 wing fasteners  
DAIS-500  
parallel to joint



**Fig. 7**  
C-135 wing fasteners  
DAIS-500  
perpendicular to joint

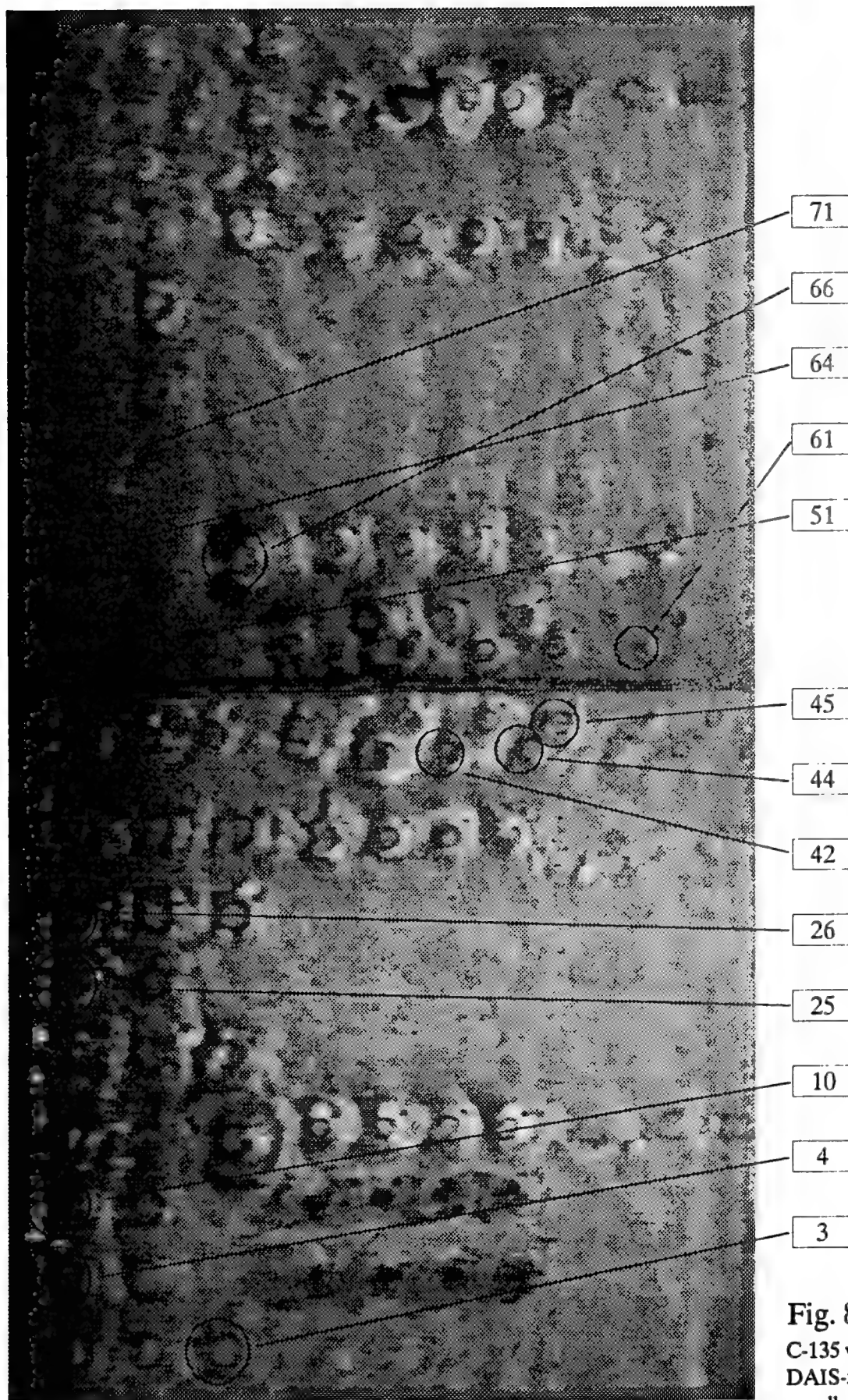


**Fig. 8**  
C-135 wing fasteners  
DAIS-500  
parallel to joint

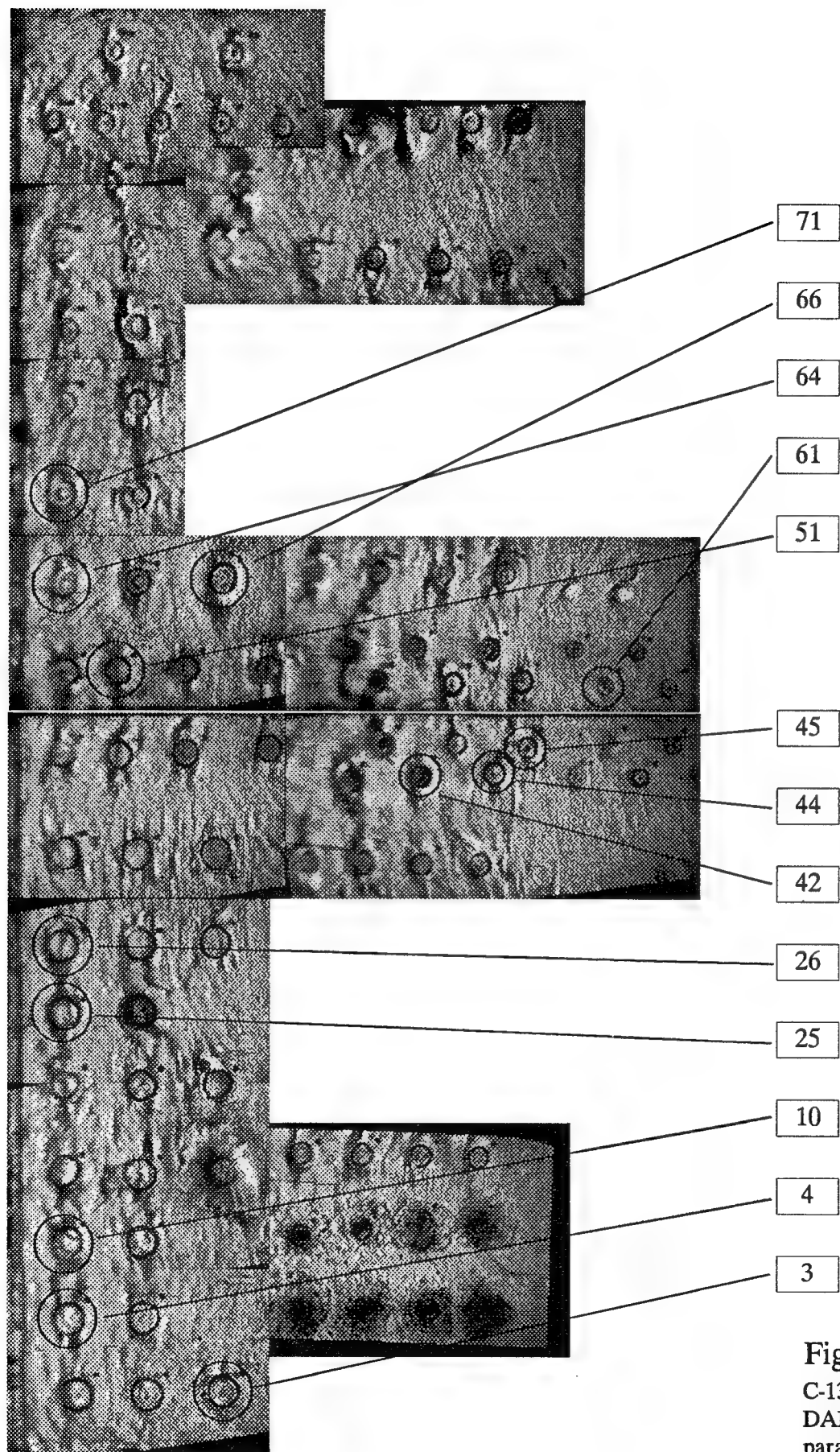


**Fig. 9**  
C-135 wing fasteners  
DAIS-40  
parallel to joint

**APPENDIX A**

# ARINC

5600 Liberty Parkway, Suite 500  
Midwest City, Oklahoma 73110

March 25, 1993  
SD/OSE/AO-93-082  
File: 05-225/P 20506

DiffRACTO Limited  
P.O. Box 441850  
Detroit, MI 48244-1850

Attention: Omer Hageniers

Subject: Non-Destructive Inspection (NDI) Equipment Demonstration

Dear Mr. Hageniers:

Last summer your company participated in the first phase of a demonstration of Non-Destructive Inspection (NDI) equipment. The demonstrations are organized by ARINC Research Corporation under contract to the Oklahoma City Air Logistic Center (OC-ALC), Tinker AFB, Oklahoma. The goal of the demonstration series is to find NDI equipment capable of detecting hidden corrosion in aircraft lap joint (multi-layer) structures and in wing fastener countersinks. The NDI equipment performance objectives were established by OC-ALC and are again provided to you as an attachment to this letter. As an added element to this demonstration your company was asked only to demonstrate the capability of your equipment to inspect large areas rapidly. A Boeing 727 (B-727) was used for this purpose.


Since the completion of the first-phase demonstration in October 1992, we have analyzed the vendor results for equipment that was demonstrated on the twelve test coupons and have also analyzed the results of your corrosion detection on the B-727. A package is enclosed which superimposes your corrosion detection results over the actual corrosion found on the B-727 lap seams (as found using other NDI techniques).

Based on your results OC-ALC and ARINC would be pleased to have you participate in the On-Aircraft demonstration phase. This demonstration will analyze the performance of your equipment in rapidly inspecting aircraft structure using C/KC-135, E-3, and B-52 aircraft at Tinker AFB, OK. The demonstration is tentatively scheduled for April 26 - May 7, 1993. A complete demonstration package will be sent to you shortly and will provide the necessary details.

Mr. Hageniers  
SD/OSE/AO-93-082  
March 25, 1993  
Page 2

We hope you decide to continue participation in this important OC-ALC project. If you have any questions please call Mr. John Alcott, 410-266-4472 or Mr. Robert Rennell, 405-739-0939.

Sincerely,

  
for Daryl Melton, Manager  
Aircraft Operations

Enclosures:

1. Demonstration Objectives Summary
2. B-727 Grid Form

## DEMONSTRATION OBJECTIVES SUMMARY

RANK	CRITERIA	DESCRIPTION	MEASURE
High	Accuracy	Corrosion is defined as greater than 1% material thickness loss as measured by metallographic procedures	No. of corroded areas detected No. of false indications detected
High	Sensitivity	Capability to measure small reductions in skin thickness	Percentage reduction in skin thickness that is detectable.
High	Versatility	Capability to detect different types of corrosion  Differentiate between good and corroded surfaces of multiple-layer lap joint.	Types or severity of corrosion detected.  Identify which layer interface(s) is corroded
Med	Portability	Ease of shipping and handling	If equipment is hand held or carried, MIL-STD-1472 Portability Criteria.
Med	Analysis Capability	How well and quickly results are presented	Real-time presentation. Clarity of display modes. Ease of corrosion location ID.
Med	Human factors	Ease of use	MIL-STD-1472 criteria.
Med	Flexibility	Detect corrosion in a variety of locations on the aircraft, under different circumstances and coupon orientations.	Detect corrosion in wing skins, fuselage lap seams, coatings, & between structural members and skin. The number of recalibrations required for different orientations /locations/circumstances.
Med	Scan Rate	Rapid/Precise	Area per unit of time
Low	Availability	Off-the-shelf and available for immediate purchase	Yes/No
Low	Cost	Purchase price.	Operational & fixed cost.

# ARINC

5600 Liberty Parkway, Suite 500  
Midwest City, Oklahoma 73110

**TO:** Diffracto

**DATE:** April 6, 1993

**FROM:** ARINC Research

**FILE:** 930412

**SUBJECT:** On-Aircraft Non-Destructive Equipment Demonstration

Dear Mr. Omer Hageniers:

Recently ARINC and the Oklahoma City Air Logistics Center extended an invitation to your company to participate in the On-Aircraft NDI Demonstration phase of this USAF hidden corrosion detection and quantification project. This invitation is based on your performance during the initial demonstration phase held in 1992.

The On-Aircraft Demonstration is scheduled April 26, 1993 through May 7, 1993 at Tinker AFB, Oklahoma. The enclosed package provides you with information on the structure of the demonstration along with necessary administrative details.

Please contact Mr. Robert Rennell, Mr. Geoff Mitchell, or Ms. Cheri Gardner at (405) 739-0939 with schedule requests or any other questions regarding the demonstration.

Sincerely,



Robert R. Rennell  
Project Coordinator

**Enclosures:**

1. Demonstration Instructions
2. Information Video
3. Chamber of Commerce Package

## **Phase 2: On-Aircraft Demonstration - Vendor Information**

### **1. Introduction**

During Phase 2 of the NDI equipment demonstration, vendors of candidate NDI equipment will demonstrate the capability of their equipment to detect hidden corrosion in an on-aircraft environment. Vendors will be grouped into three categories based on their Phase 1 performance. These categories are: Lap Joint, Wing Skin Fastener, and Rapid Scan. Phase 2 of the NDI Equipment Demonstration will consist of three sessions as follows:

Session 1:	Human Factors Session
Session 2:	Sensitivity/Accuracy Session
Session 3:	Multiple Aircraft Session

#### **1.1. Session 1: Human Factors**

The Human Factors Session will enable vendors to demonstrate the usability of their equipment in a depot maintenance line environment. MIL-STD-1472D, Human Engineering Design Criteria for Military Systems, Equipment, and Facilities will be used as guide for evaluation of the equipment. NDI equipment will be used to inspect areas on a C/KC-135 aircraft located on the OC-ALC PDM line. Vendors will operate their own equipment and will inspect several areas of the aircraft while Government and ARINC personnel observe. Equipment will be evaluated in terms of its ease of use, versatility, and other human factors criteria. Equipment will not be evaluated on sensitivity and accuracy during this session although vendors will be asked to provide equipment findings.

#### **1.2. Session 2: Sensitivity and Accuracy**

The Sensitivity and Accuracy Session will enable vendors to demonstrate equipment performance in an on-aircraft environment. Areas of a deactivated C-135 aircraft will be inspected by equipment vendors. Vendors will interpret the output of their equipment and will record their findings. The areas of inspection will be invasively inspected after the demonstration and the results of the invasive inspection will be compared with those of the equipment demonstrations. Sketches and other information are included for your review and preparation.

#### **1.3. Session 3: Multiple Aircraft Session**

During Session 3, the Multiple Aircraft Session, vendors may be asked to demonstrate the use of their equipment on a variety of aircraft to be determined including a B-52 and E-3 aircraft.

## 2. Schedule of Events

The three sessions will be conducted concurrently so that vendors may participate in all the session which are applicable to the vendor during a single trip to Oklahoma City. **Vendors should plan for two full inspection days.** Vendors need to arrive not later than 10:00 am on the day prior to their first scheduled inspection day to allow for access arrangements, and unpacking/prepositioning of equipment at OC-ALC. Please keep in mind that our access to the inspection sites is constrained by the working hours of our sponsors.

## 3. Initialization of NDI Equipment

Vendors will be allowed to initialize their NDI equipment using vendor supplied calibration coupons. Time spent in set-up and initialization will be recorded for all sessions by ARINC observers.

## 4. Security and Equipment Handling

Vendors and evaluation teams will not require security clearances to gain access to the Phase 2 site. However, visitor badges and escorts will be required by all vendor personnel while on-site a OC-ALC. **All vendors must check with the local ARINC office for instructions and making arrangements for access to the Phase 2 site. Do not proceed directly to OC-ALC.** ARINC is responsible for ensuring escorts are provided while on-site at OC-ALC. Facilities will be provided at the local ARINC office or on-site for locked storage of candidate NDI equipment over night during the demonstration. Equipment can be shipped to the local ARINC office prior to the demonstration date at the following address:

ARINC Research Corporation  
Attn: Mr. Robert Rennell  
5600 Liberty Parkway, Suite 500  
Midwest City, OK 73110-2835

Please indicate your company name on the outside any container. The local ARINC office telephone number is 405-739-0939.

All demonstrations will be performed without other vendors present. All data obtained will be treated as proprietary to the respective vendor and not releasable to any non-Government agency without vendor consent.

## 5. Post Demonstration

After the demonstrations are concluded, the evaluation team will invasively inspect the inspection areas from Session 2 and consolidate information collected in Session 1 and 3. Following the completion all demonstration data assessment and evaluation, each vendor will be provided with their equipment performance along with a copy of the evaluation criteria and invasive results.

## **Session 2: Fuselage Lap Joint Inspection - Vendor Information**

### **1. General**

Vendors will be asked to inspect selected lap joints on the fuselage of a C-135 aircraft for corrosion damage. Vendors will interpret the results output by their equipment and record these results by input to a computer program provided by ARINC at the demonstration site. The vendor will input results using the guidelines established and described below.

### **2. Inspection Objective and Rationale**

The objective of the inspection is to detect and quantify corrosion found between layers of aircraft fuselage skin lap joints without disassembly of the lap joint.

The rationale for this inspection is that corrosion damage to the fuselage skins and lap joint strength has become an aircraft life limiting problem for the C/KC-135 fleet. NDI equipment and techniques are required which can accurately detect and quantify corrosion before extensive damage has occurred to the fuselage skin.

### **3. Definitions for Use in Lap Joint Inspections**

The purpose of establishing definitions is to avoid misinterpretation of results during the vendor equipment evaluation. The same definitions will be applied for judging and comparing with the invasive inspection results. Unless otherwise specified, all measurements are to be in the English system of units.

#### **3.1 Interfaces and Surfaces at a Lap Joint (Non-Tapered Skins)**

The inspection surface,  $S$ , is defined as the outer most surface at the joint. Refer to Figure 1. All other surfaces are defined by reference to the inspection surface. For continuous sheets, an interface is defined by the physical contact of two sheets (or plates) of material which are mechanically fastened including interfaces between two sheets which are spot welded together. The identification of the surface is composed of two alpha-numeric characters. The first character indicates the interface number and the second character indicates the location of the surface relative to the inspection surface,  $S$ . The abbreviations "N" and "F" indicate near and far surface, respectively. The sheet number is defined by its position relative to the outer most sheet. The thickness of the sheet at the point of inspection is represented by the lower case letter,  $t$ .

The sheet at position  $i$  has surfaces defined as  $(i-1)F$  and  $iN$ . The original thickness of sheet  $i$ , is  $t_i$ .

If there are one or more non-continuous sheets in the inspection area, the definition of an interface becomes more complex. Sheets and surfaces will be numbered as if they were continuous in the inspection area. If more than one sheet exists at an interface (e.g. the case of two or more non-continuous sheets at the same relative position to the surface), each will be identified with a different lower case letter after the interface number.

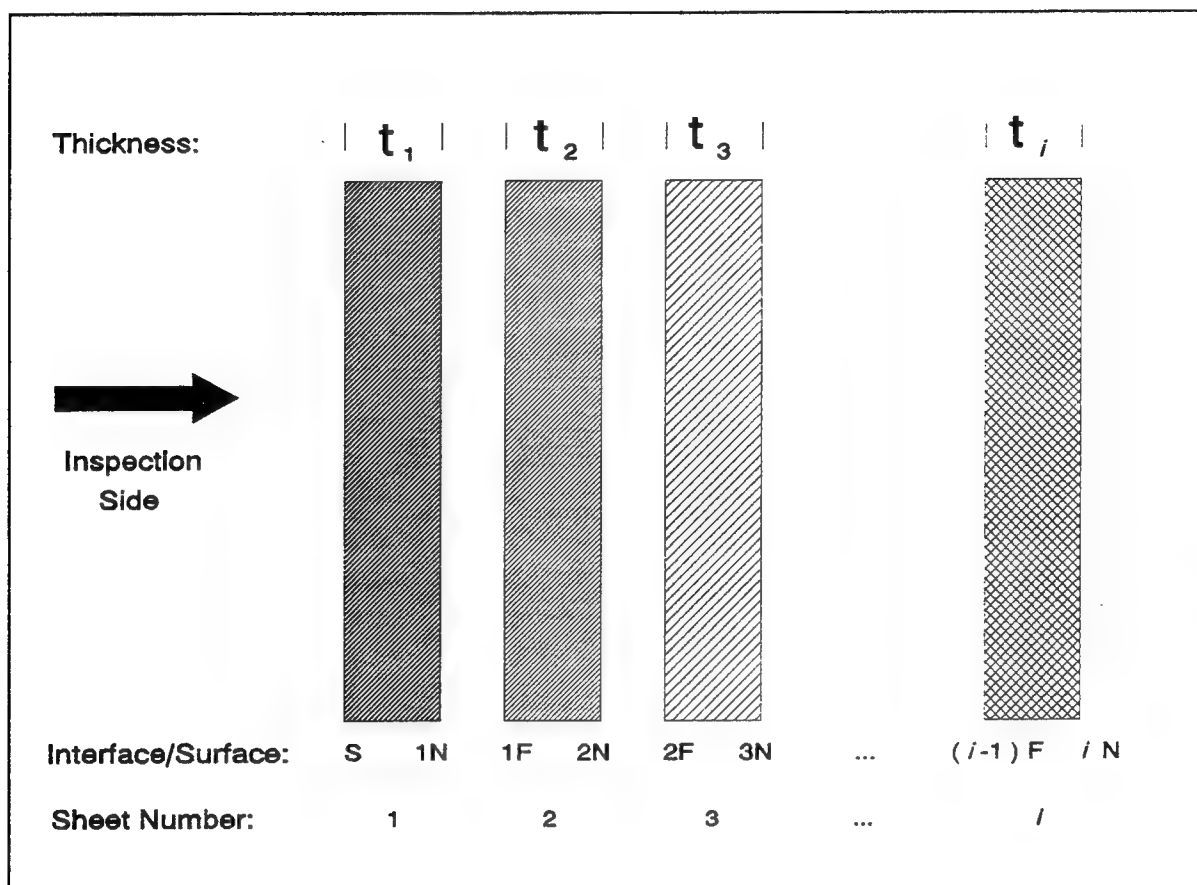


Figure 1. Lap Joint Cross Section

For example, two shims (not in contact with each other and non-continuous in the inspection area) are sandwiched between two continuous sheets. The designation of the shims would be "2a" and "2b" with surfaces as "1aF, 2aN" and "1bF, 2bN", respectively. The continuous sheets would be designated as "1" and "3" with surfaces of "S, 1N" and "2F, 3N", respectively.

### 3.2 Percent Material Loss and Average Percent Material Loss

Depending on the resolution method selected for data entry and because material loss averaging techniques will be used in evaluating the results, the following definition of

Percent Material Loss is provided. Percent material loss in a unit volume (see Figure 2) is defined by the simple ratio of volumes of material loss to the volume of original material.

The original material volume is given by,

$$V_o = x \times y \times t_2$$

The material loss volume is given by,

$$V_l = x \times y \times (t_2 - t_1)$$

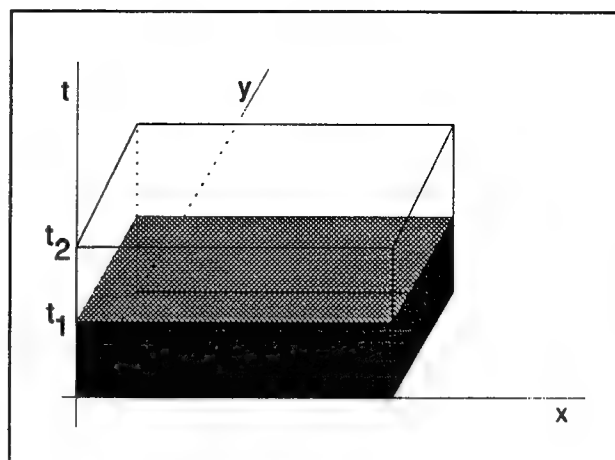


Figure 2. Unit Volume

The percent material loss is then given by,

$$PML = \frac{V_l}{V_o} \times 100$$

where  $PML$  = Percent Material Loss

For equal unit volumes, the average percent material loss is defined by the nominal average,

$$PML_{avg} = \frac{\sum_{i=1}^n PML_i}{n}$$

where

$n$  = the number of unit volumes over which average PML is based

### 3.3 Definition of PML Applied to Case of Lap Joint

Because different technologies inspect for corrosion damage differently, the vendor be allowed to choose the method to present their results. Vendors will be asked to quantify corrosion at a lap joint in terms of percent material loss in one of the following methods listed in descending order of preference.

a. Percent material loss at a single surface of an individual sheet:

This is defined as the PML using the thickness,  $t$ , of each sheet in the joint. Vendors will quantify corrosion in terms of PML at every surface of each sheet.

b. Total percent material loss of an individual sheet:

This is defined as the PML using thickness,  $t$ , of each sheet in the joint. Vendors will quantify in terms of the combined loss of both surfaces of each sheet.

c. Total percent material loss on one side of a structural lap joint:

This is defined as the PML using the combined sheet thicknesses on one side of a lap joint. Vendors will quantify in terms of material loss on all surfaces on one side of a lap joint.

d. Total percent material loss at an interface:

This is defined by the combined PML of each sheet using the combined thickness of both sheets. Vendors will quantify in terms of combined loss on both surfaces at an interface.

e. Total percent material loss of a joint:

This is defined by the PML of all sheets in a lap joint. Vendors will use the combined thickness of all sheets in the lap joint and quantify combined material loss.

#### **4. Inspection Procedure and Corrosion Quantification**

##### **4.1 Procedure**

Aircraft lap joint inspection areas previously selected by ARINC and OC-ALC personnel will be marked and identified on the aircraft. Aircraft stands and electrical extension cords will be made available.

The vendor will set-up their equipment for the first inspection area identified. Vendors will inspect the area using whatever techniques and procedures the vendor deems necessary. The vendor will be allowed to mark on the aircraft using approved erasable marking pens provided at the inspection site. The vendor will analyze the results from their equipment and transfer results to the computer program provided by ARINC for data collection before continuing to the next inspection area. ARINC will help the vendor with data entry in to the computer, but not data interpretation. The final results input for each inspection area will be saved on file and a hardcopy generated for a permanent record of the inspection.

## 4.2 Corrosion Quantification

As previously mentioned, material loss due to corrosion data will be determined by the vendor and will be recorded through the use of a computer application program. The program will be provided and is similar to "PC Paint" applications. Vendors will record the level of material loss by selecting a desired grid resolution (1/16", 1/8", 1/4" or 1/2") and painting (color coding) grid areas representing the area of interest. Vendors will be provided with assistance and as much time as necessary (within reason) to record data. The following color scheme listed in terms of percent material loss will be used:

White: 0% - 1% (considered as no corrosion)

Yellow: 2% - 5%

Red: 6% - 8%

Green: 9% - 11%

Blue: 12% - 14%

Black: 15% or greater

Crosshatched: Indeterminate (Unable to inspect)

Graph paper with 1/16" inch grids will be available as a backup to this procedure and for those vendors who need to transfer results from the aircraft fuselage to the computer.

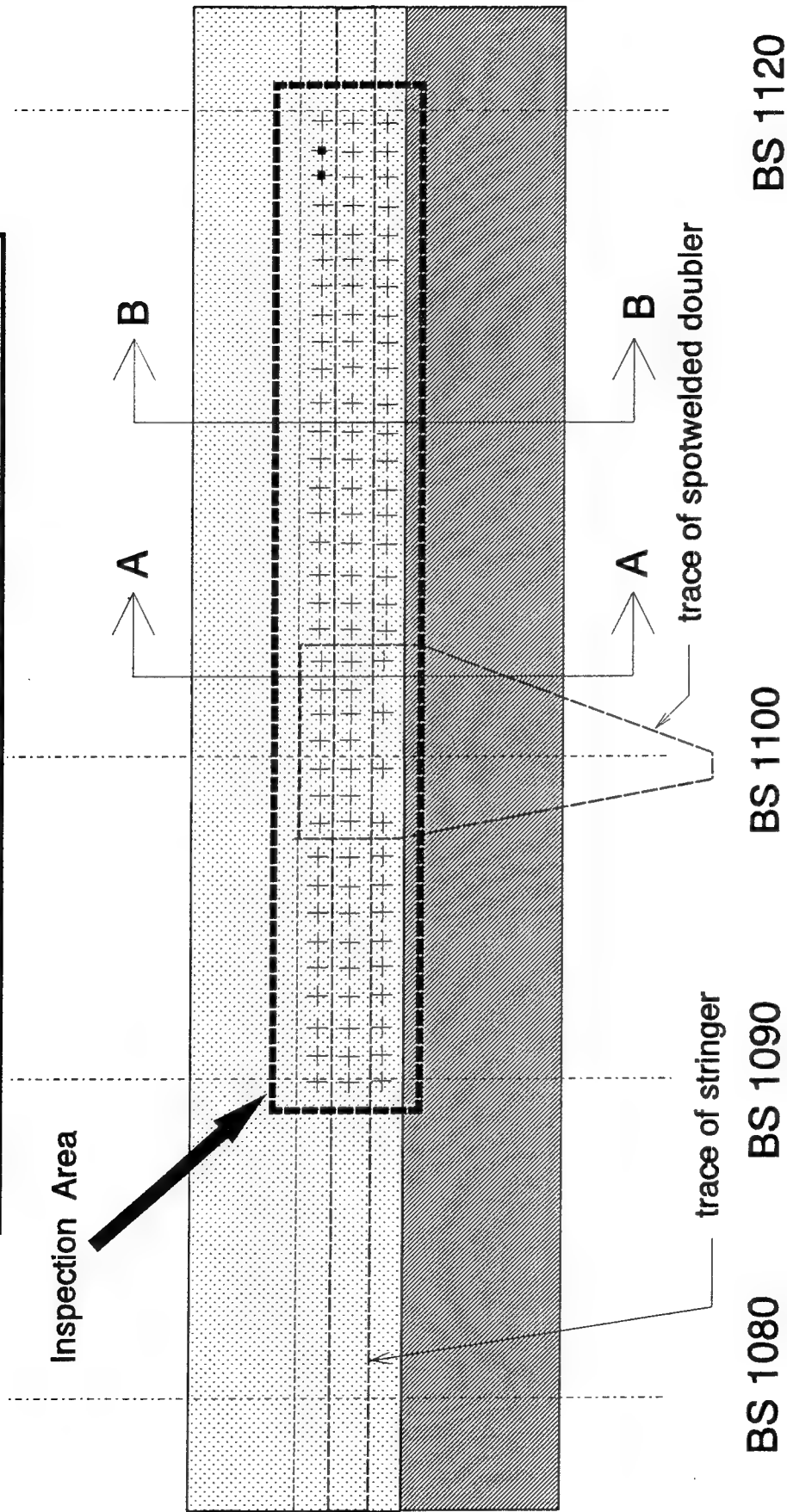
## 5. General Scoring Information

The vendor will be judged on accuracy and sensitivity for marked regions only. Crosshatched regions will not be counted against the vendors for accuracy and sensitivity assessments. Crosshatch regions will be used to ascertain equipment flexibility.

## 6. Inspection Area Descriptions

The sketches attached are intended to provide basic information regarding the aircraft structure to be inspected in Session 2. Installation drawings will be available at the demonstrations site.

Inspection Area #1 - B.S. 1080 - 1120, Stringer 18 (Left Hand Side)

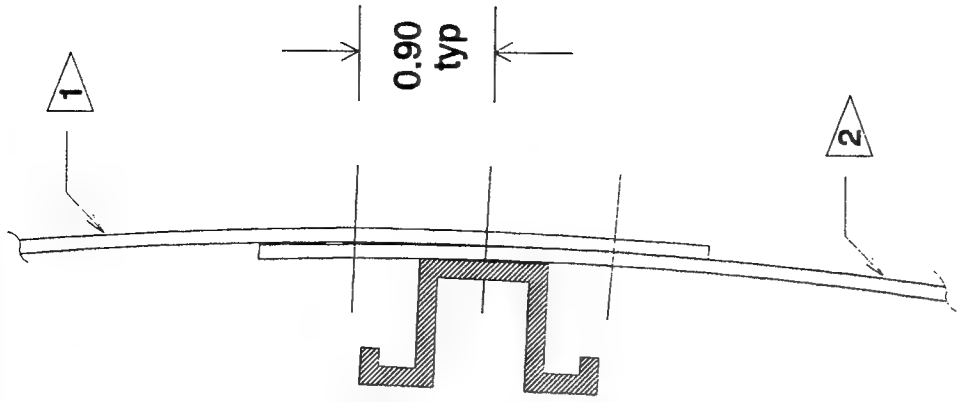


+ Aluminum rivets spaced .090 approx (typ)

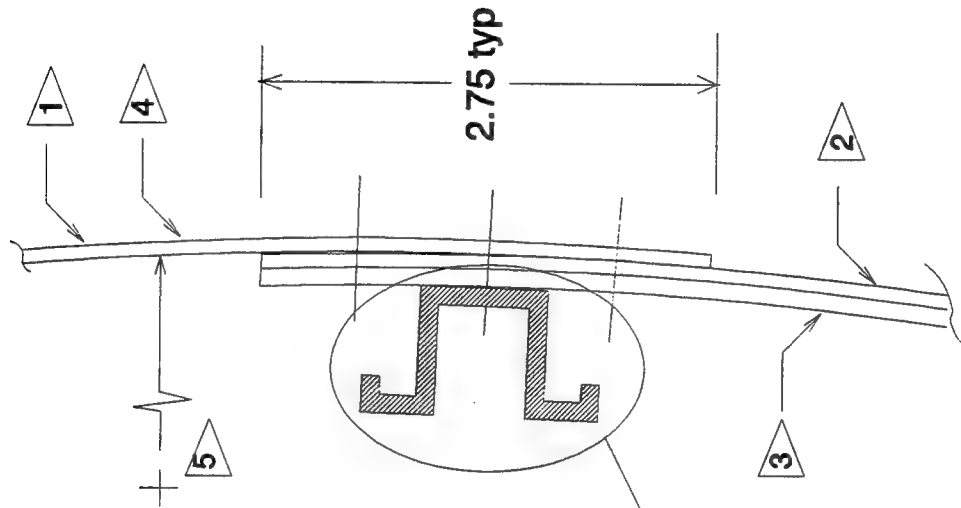
Not to Scale  
 -■- Ferrous fastener

**Inspection Area #1 - B.S. 1080 - 1120, Stringer 18 (Left Hand Side)**

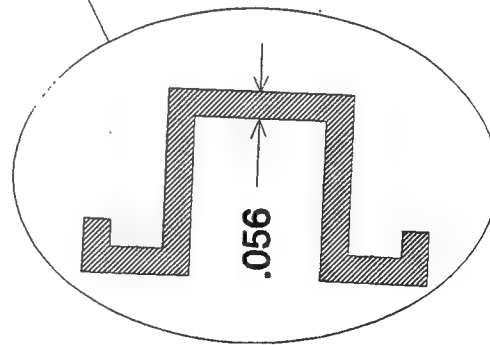
- 1 .064 Clad 2024-T3 Alum sheet
- 2 .051 Clad 2024-T4 Alum sheet
- 3 .025 Clad 2024-T3 Alum doubler
- 4 Exterior surface painted w/ TT-P-2756  
Self-Priming Topcoat (LVOC)  
Shade: Fed Std 595, Color# 16515 Grey  
Thickness: 2.3 mils (min) approx
- 5 Fuselage approx 72" Radius



**Section B-B**

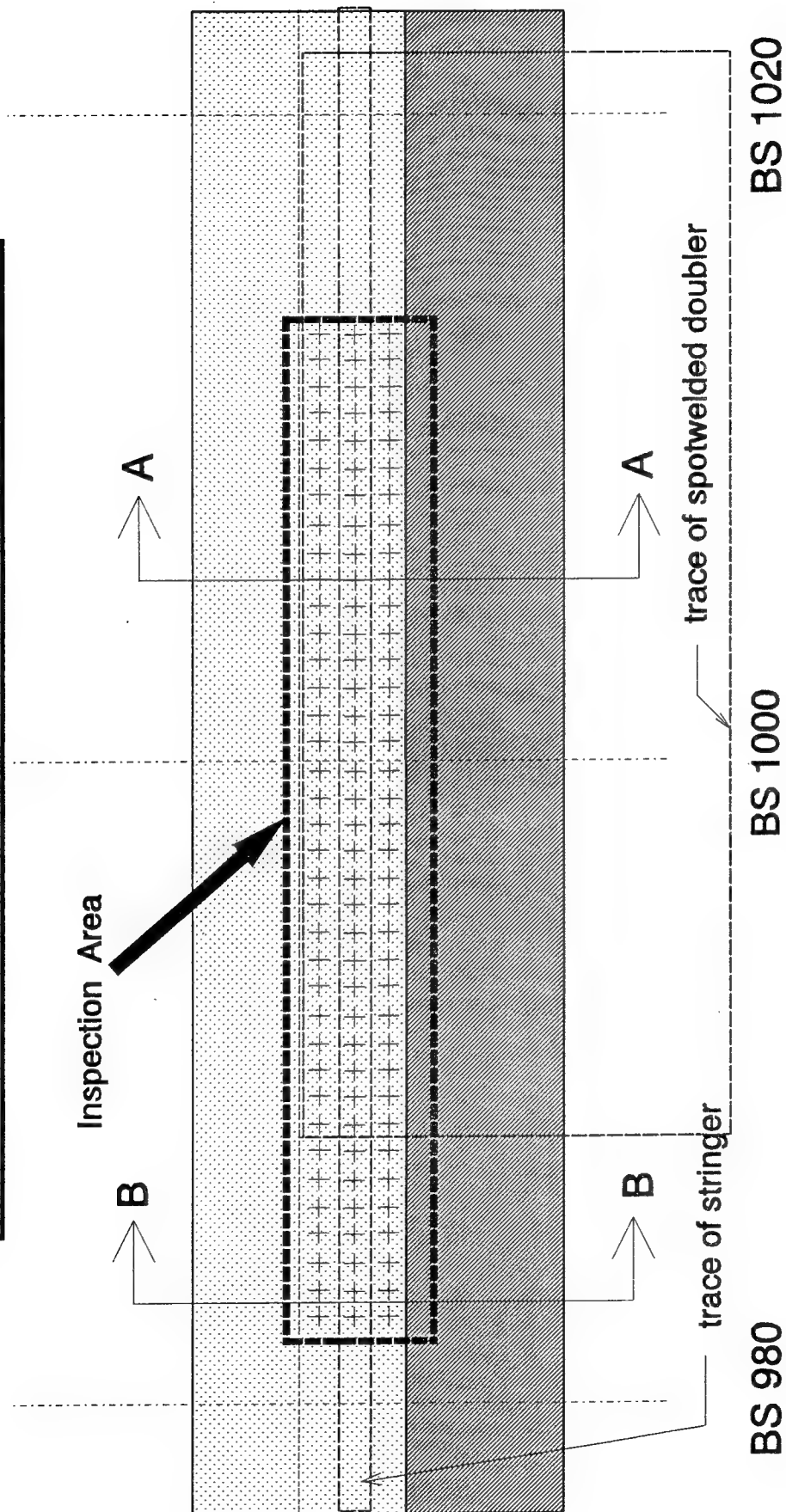


**Section A-A**



**Not to Scale**

Inspection Area #2 - B.S. 980 - 1020, Stringer 14 (Left Hand Side)

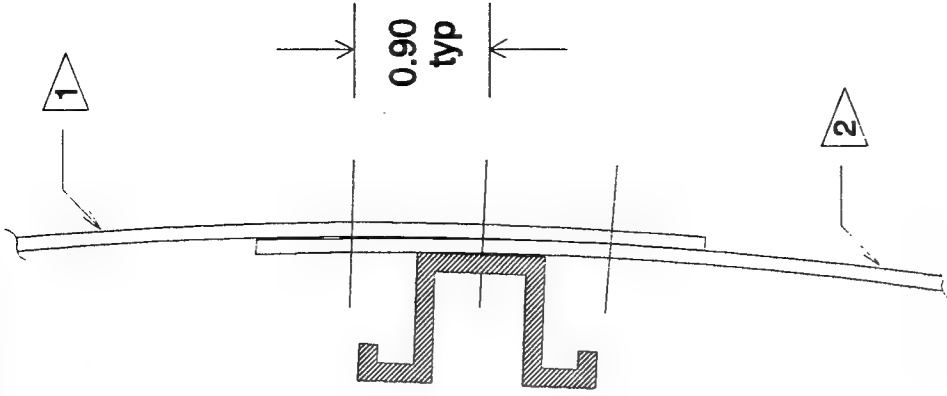


Aluminum rivets spaced .090 approx (typ)

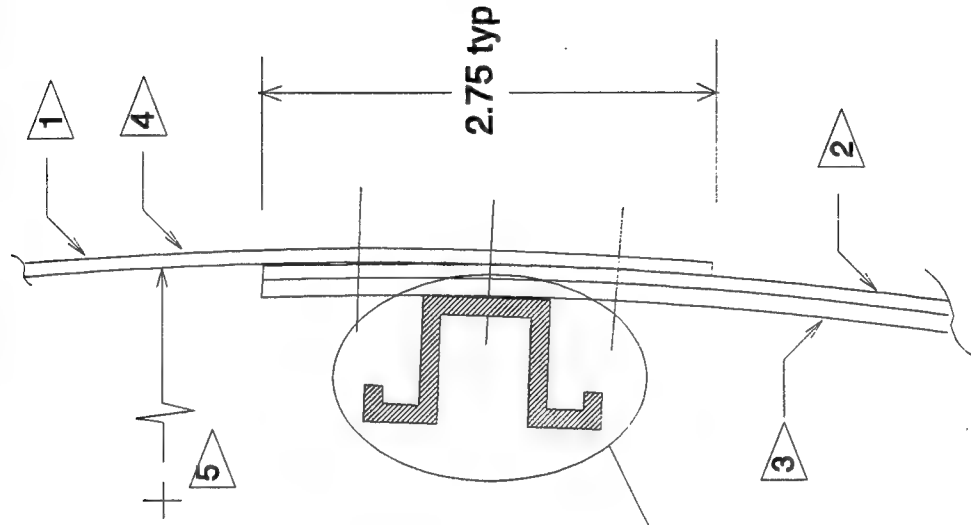
Not to Scale  
 Ferrous fastener

Inspection Area #2 - B.S. 980 - 1020, Stringer 14 (Left Hand Side)

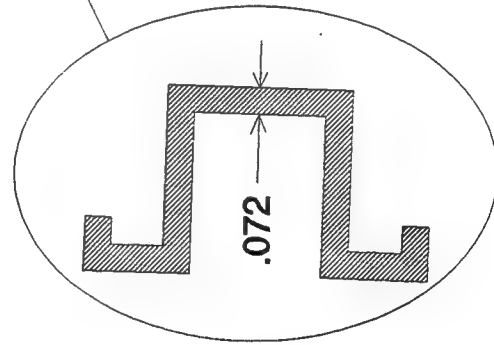
- 1 .064 Clad 2024-T3 Alum sheet
- 2 .064 Clad 2024-T3 Alum sheet
- 3 .020 Clad 2024-T3 Alum doubler
- 4 Exterior surface painted w/ TT-P-2756  
Self-Priming Topcoat (LVOC)  
Shade: Fed Std 595, Color# 16515 Grey  
Thickness: 2.3 mils (min) approx
- 5 Fuselage approx 72" Radius



Section B-B



Section A-A



Not to Scale

Inspection Area #3 - B.S. 980 - 1020, Stringer 7 (Left Hand Side)

Inspection Area

A

A

trace of stringer

BS 980

BS 1000

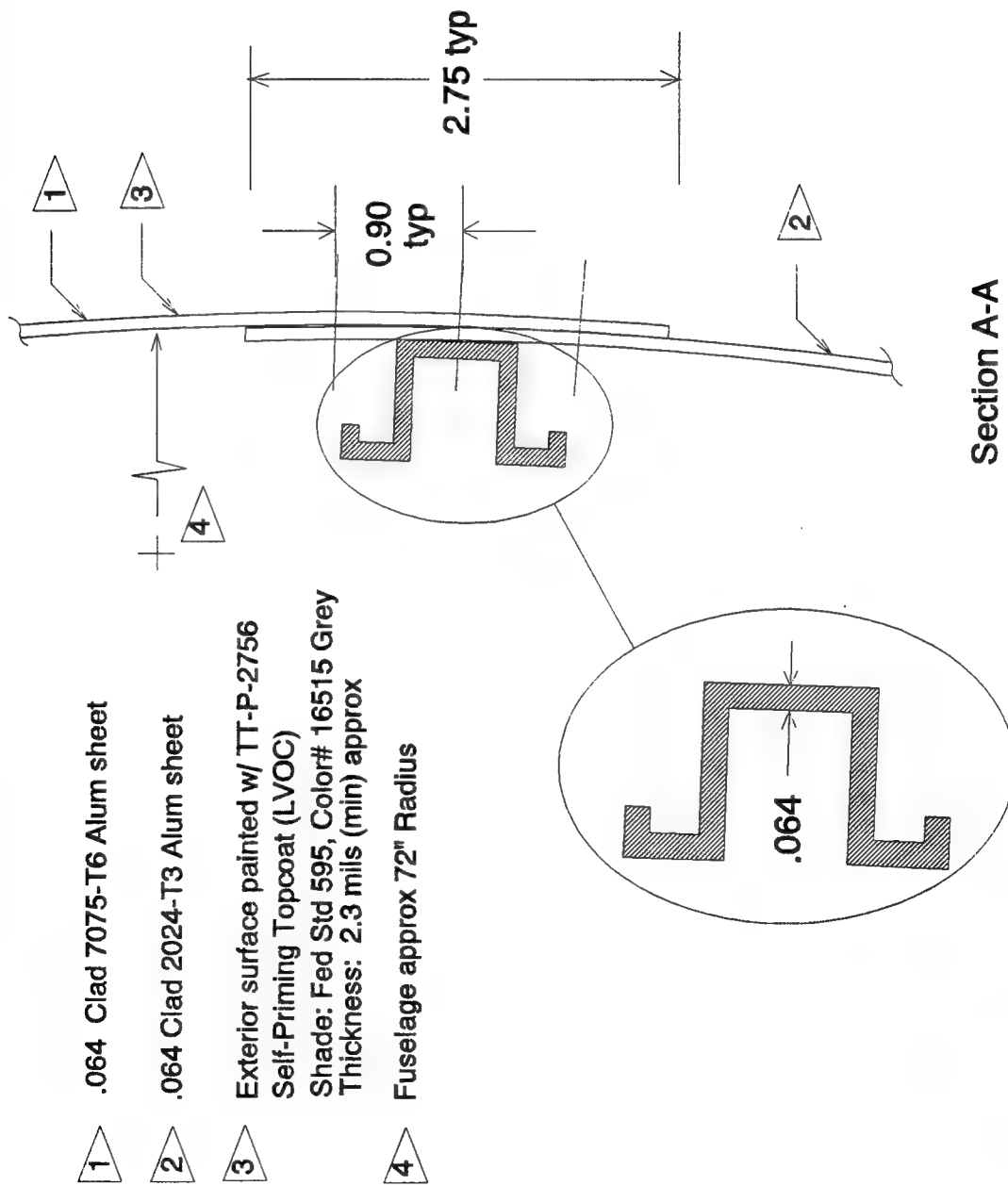
BS 1020

+ Aluminum rivets spaced .090 approx (typ)

Not to Scale

■ Ferrous fastener

Inspection Area #3 - B.S. 980 - 1020, Stringer 7 (Left Hand Side)

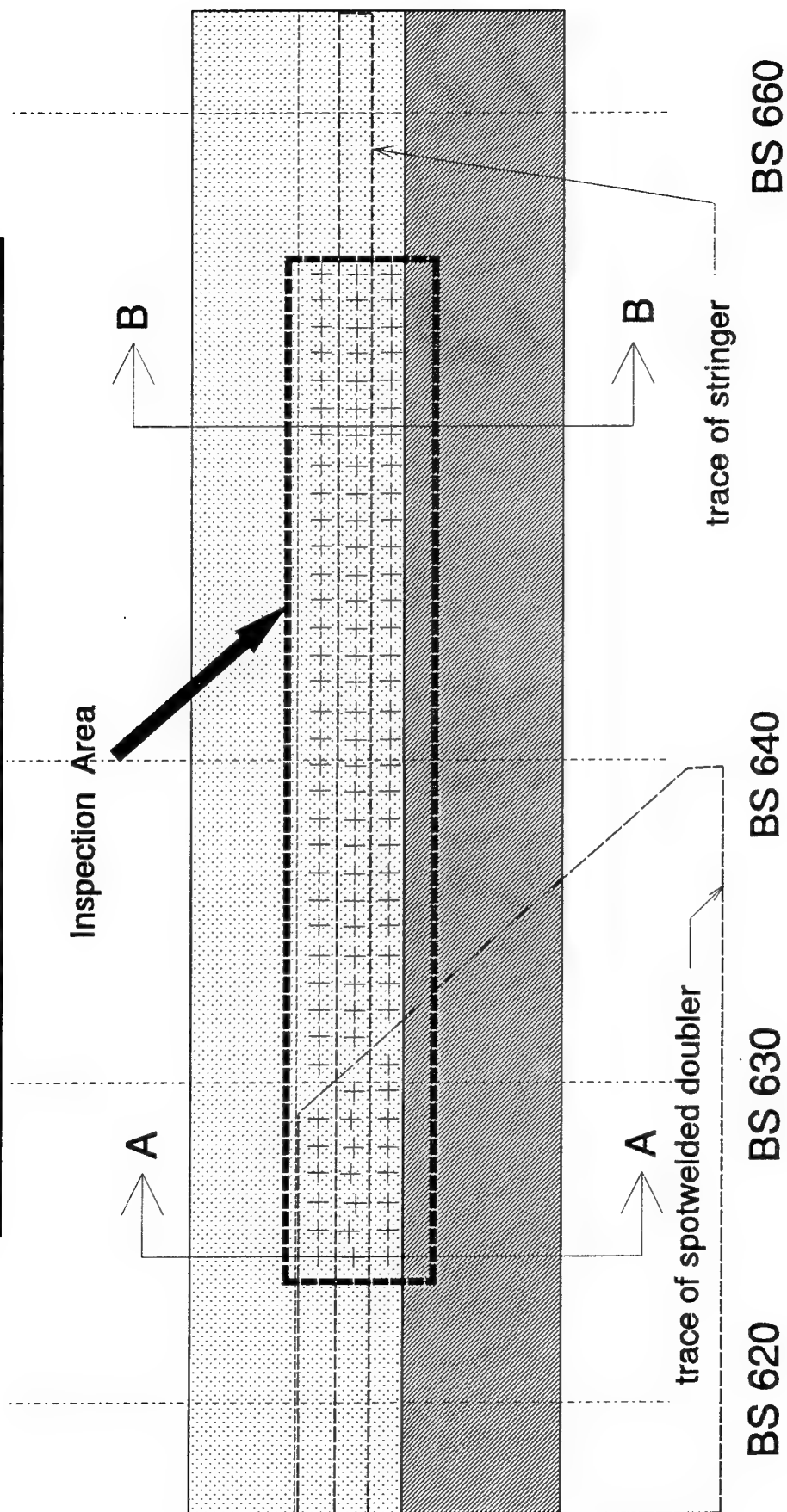


Section A-A

Not to Scale

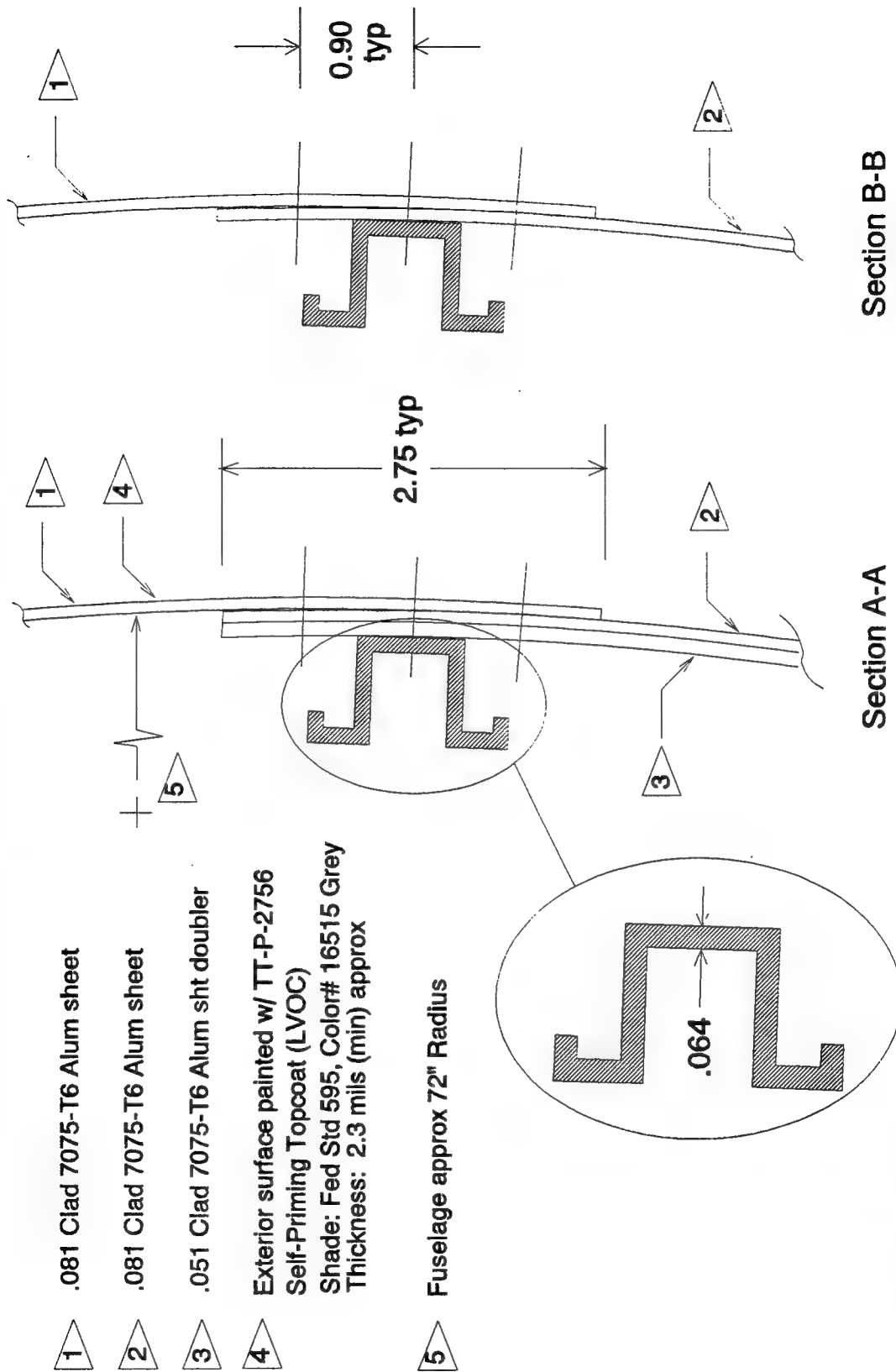
- 1 .064 Clad 7075-T6 Alum sheet
- 2 .064 Clad 2024-T3 Alum sheet
- 3 Exterior surface painted w/ TT-P-2756 Self-Priming Topcoat (LVOC)  
Shade: Fed Std 595, Color# 16515 Grey  
Thickness: 2.3 mils (min) approx
- 4 Fuselage approx 72" Radius

Inspection Area #4 - B.S. 620 - 640, Stringer 14 (Left Hand Side)



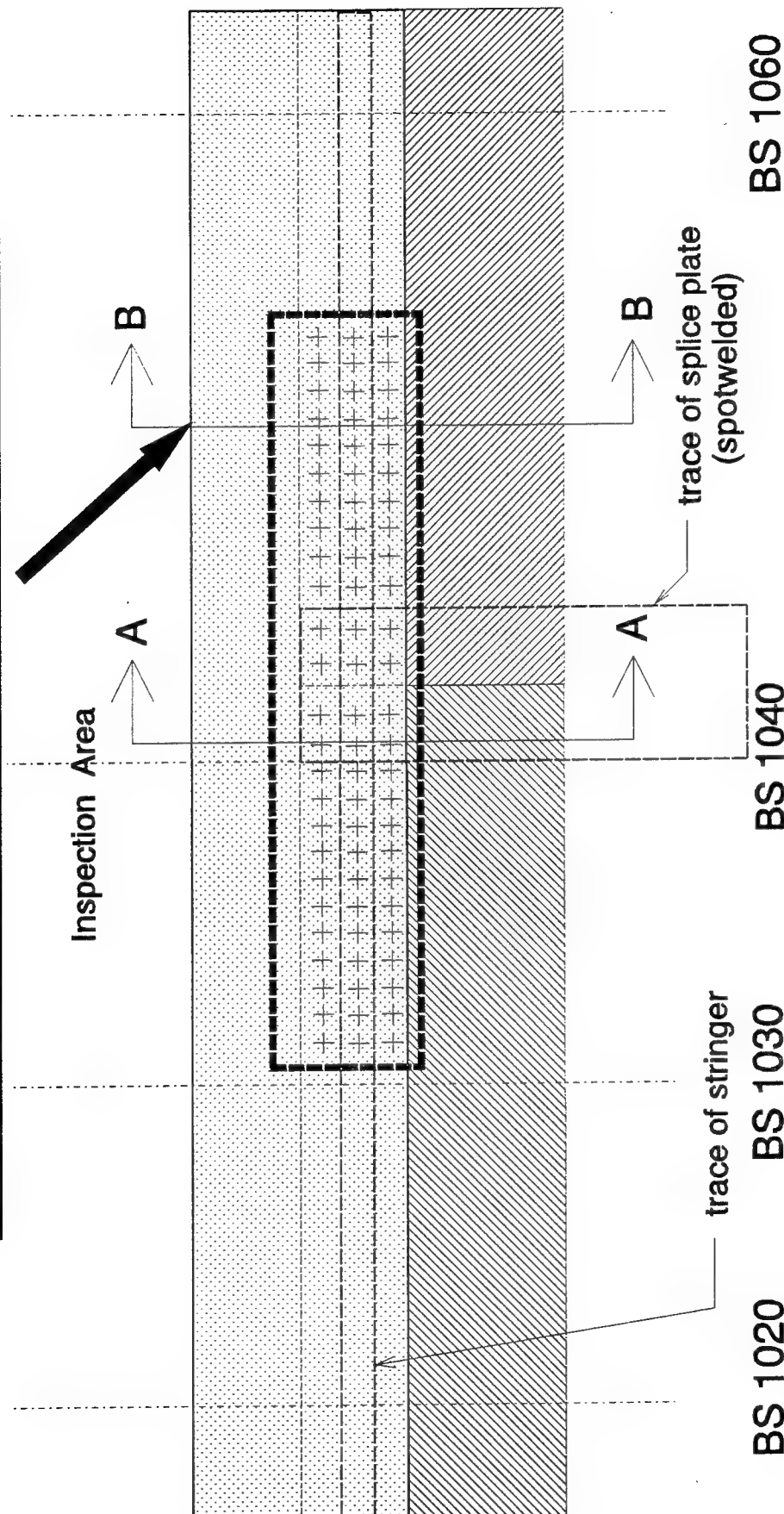
Not to Scale

Inspection Area #4 - B.S. 620 - 640, Stringer 14 (Left Hand Side)



Not to Scale

Inspection Area #5 - B.S. 1020 - 1060, Stringer 18 (Left Hand Side)



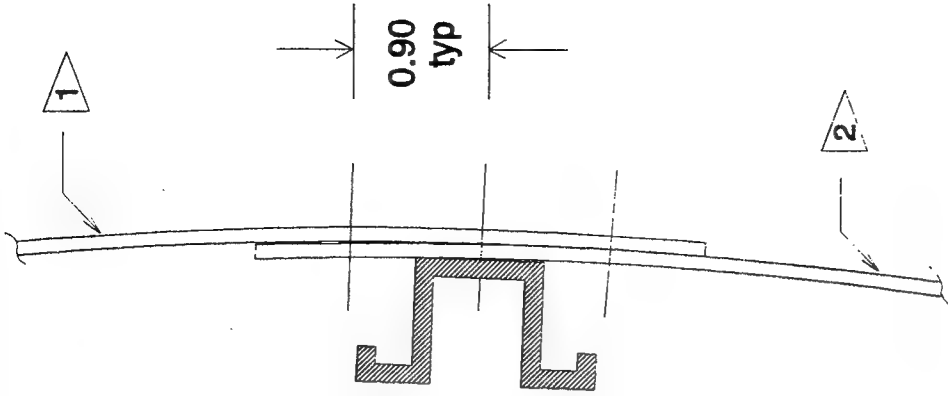
+ Aluminum rivets spaced .090 approx (typ)

Not to Scale

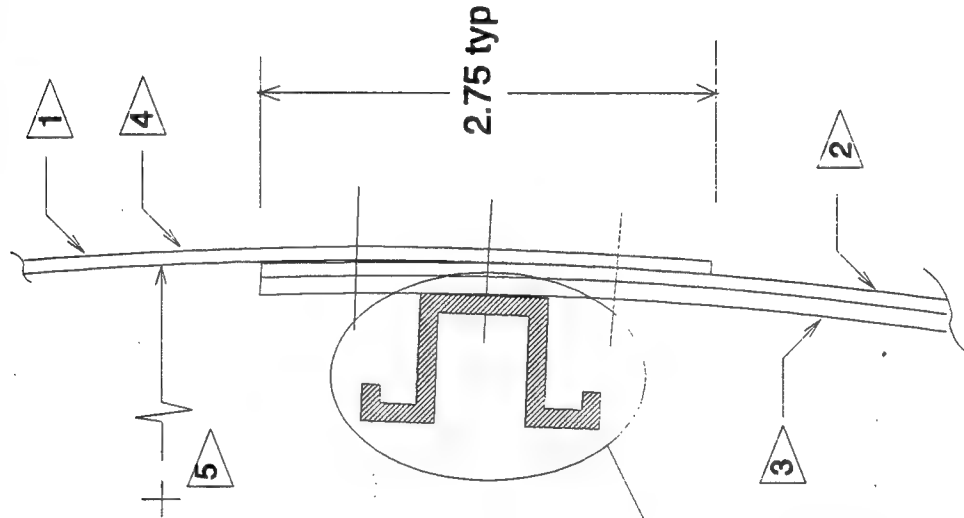
■ Ferrous fastener

**Inspection Area #5 - B.S. 1020 - 1060, Stringer 18 (Left Hand Side)**

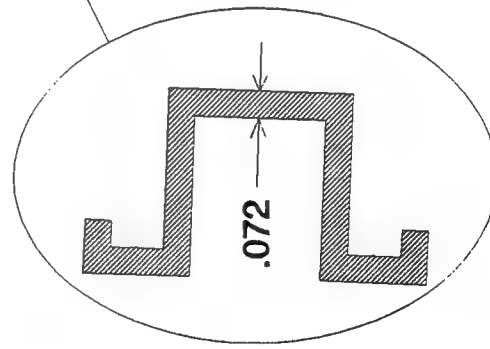
- 1 .064 Clad 2024-T3 Alum sheet
- 2 .051 Clad 2024-T4 Alum sheet
- 3 .072 Clad 2024-T6 Alum sht splice plate
- 4 Exterior surface painted w/ TT-P-2756 Self-Priming Topcoat (LVOC)  
Shade: Fed Std 595, Color# 16515 Grey  
Thickness: 2.3 mils (min) approx
- 5 Fuselage approx 72" Radius



Section B-B



Section A-A



Not to Scale

## **Session 2: Wing Skin Fastener Countersink Inspection - Vendor Information**

### **1. General**

The vendor will be asked to inspect selected fasteners installed into a section of aircraft wing skin for corrosion on the wing skin countersink surface. The vendor will interpret the results output by their equipment and record these results onto the forms provided by ARINC using the characterization guidelines established and described below.

### **2. Inspection Objective and Rationale**

The objective of the inspection is to detect and categorize corrosion found on wing skin fastener countersink surfaces without removing the fastener.

The rationale for this inspection is that corrosion and pitting initiates at the fastener to countersink interface. NDI equipment and techniques are required which can accurately detect and categorize corrosion before extensive damage has occurred to the wing skin.

### **3. Inspection and Analysis Procedure**

The vendor will perform equipment setup and calibration. The vendor will inspect the selected fasteners with their own procedures. The vendor will mark the form provided using the categorization described below.

### **4. Corrosion Categorization and Form Marking**

The vendor will mark the form provided by ARINC showing the split view of the countersink surface for each fastener inspected using the following categories. See grid form and fastener countersink cross section diagrams attached for reference. Typical photographs from the Phase I - Coupon Demonstration are also included for your general information.

1. No corrosion (defined as anomalies less than .003" inch deep (measured radially from the C/S surface).
2. Corrosion damage (pitting, innergranular, etc) which is greater than .003" deep but less than .050" deep.
3. Corrosion damage which is greater than .050 inches deep.

Each of these categories will be assigned a number by ARINC for ease of data entry. The vendor will categorize in terms of the worst corrosion found for each 90 degree segment measured circumferentially around the hole.

The vendor will have the option of marking regions by the depth down the countersink surface with the following choices (in order of descending preference):

- a. 0 - 25%, 26 - 50%, 51 - 75%, and 76 - 100% ( 4 regions per 90 degree segment).
- b. 0 - 50%, 51 - 100% ( 2 regions per 90 degree segment).
- c. 0 - 100% ( 1 region per 90 degree segment).

The vendor may leave any region blank if they are not able to inspect.

## **5. General Scoring Information**

The vendor will be judged on accuracy and sensitivity for marked regions. Blank regions will not be counted against the vendor for accuracy and sensitivity assessments. Blank regions will be used to ascertain equipment flexibility.

## **6. Inspection Area Descriptions**

The vendor will be asked to inspect a series of countersinks with installed ferrous fasteners ranging from 1/4" diameter to 3/4" diameter. The skin material type will be aluminum alloy 7178-T6. Skin thicknesses will range from .160 to .350 thick.

## **7. Special Inspection Activity**

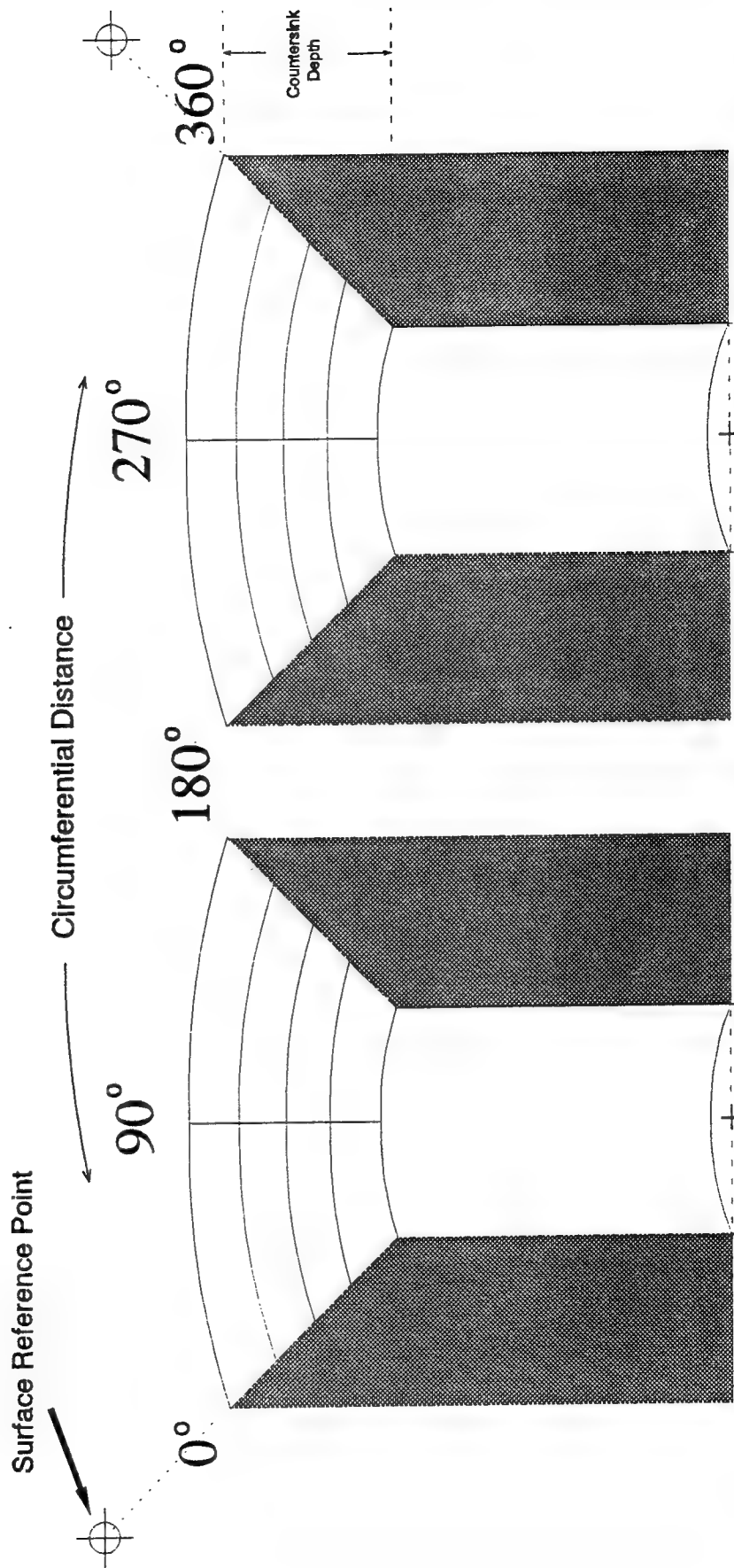
This is a non-graded activity. The vendor will be given the opportunity to categorize severe corrosion damage which extends radially into the skin (i.e. greater than .050" from the countersink surface). The vendor may use the polar graph paper provided by ARINC to describe the corrosion detected in whatever terms the vendor chooses. ARINC suggests that the vendor describe the approximate outer radial boundaries of corrosion damage and the vertical depth into the wing skin. ARINC will provide color pencils and polar graph paper. After completion of the demonstration, ARINC will provide feedback and invasive results to vendors who participated in this portion of the inspection activity.

Vendor: \_\_\_\_\_

Fastener #: \_\_\_\_\_

Date: \_\_\_\_\_

Aircraft ID: \_\_\_\_\_

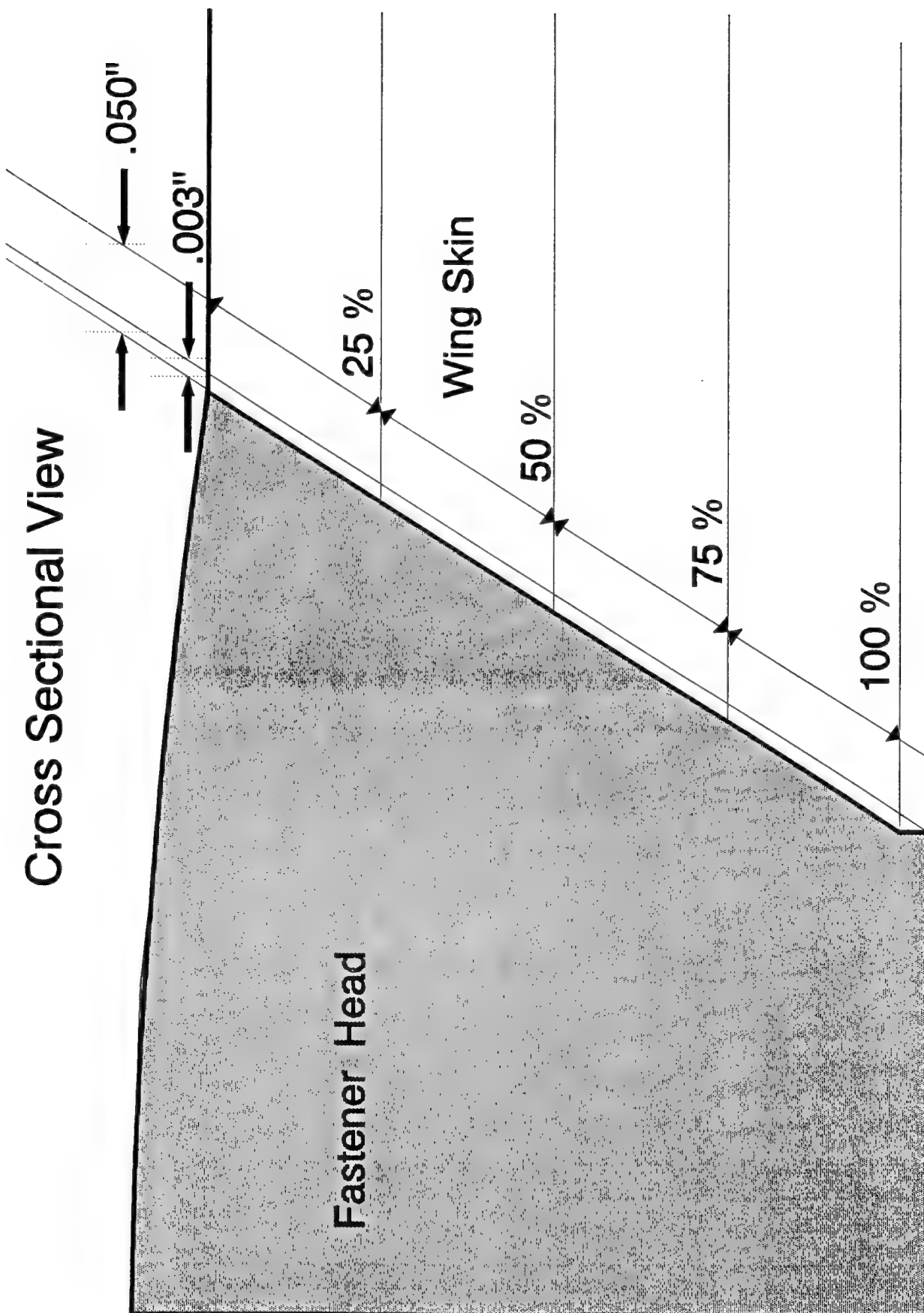


Split-View of Fastener Countersink Surface

Vendor sign: \_\_\_\_\_

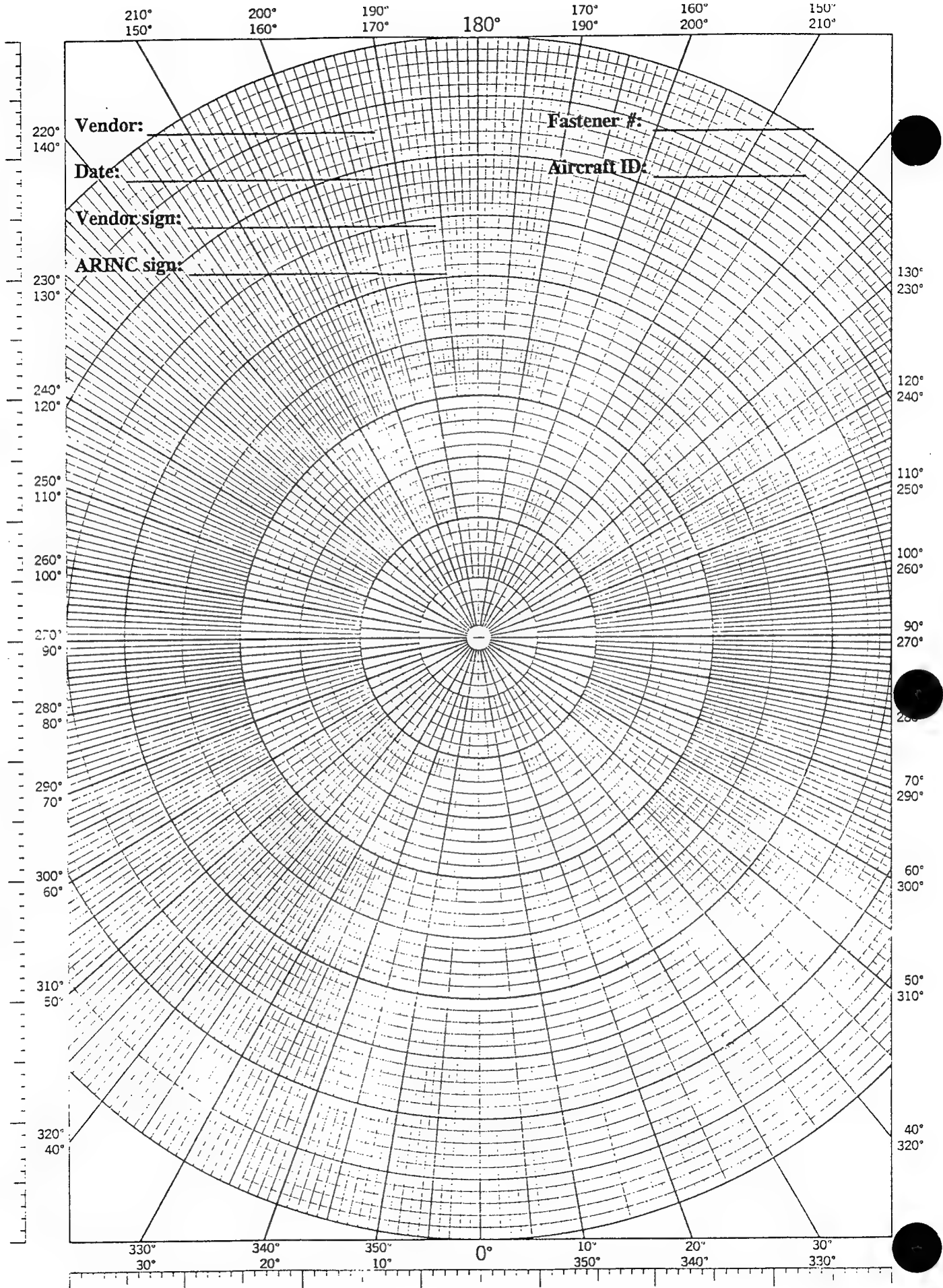
ARINC sign: \_\_\_\_\_

# Cross Sectional View

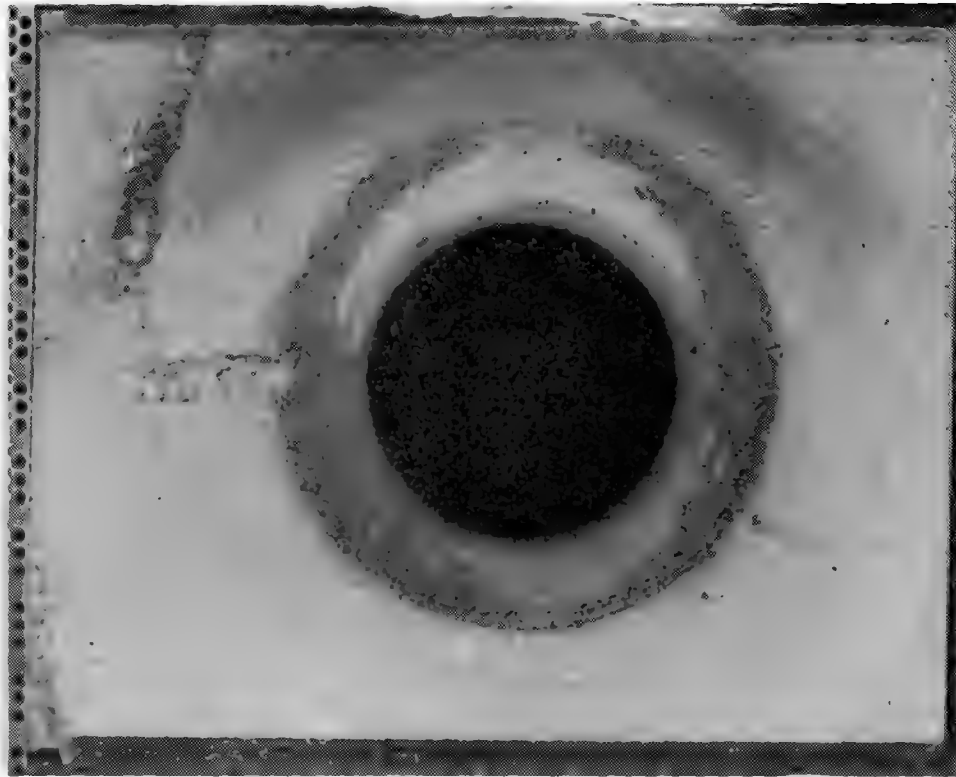


46 4410

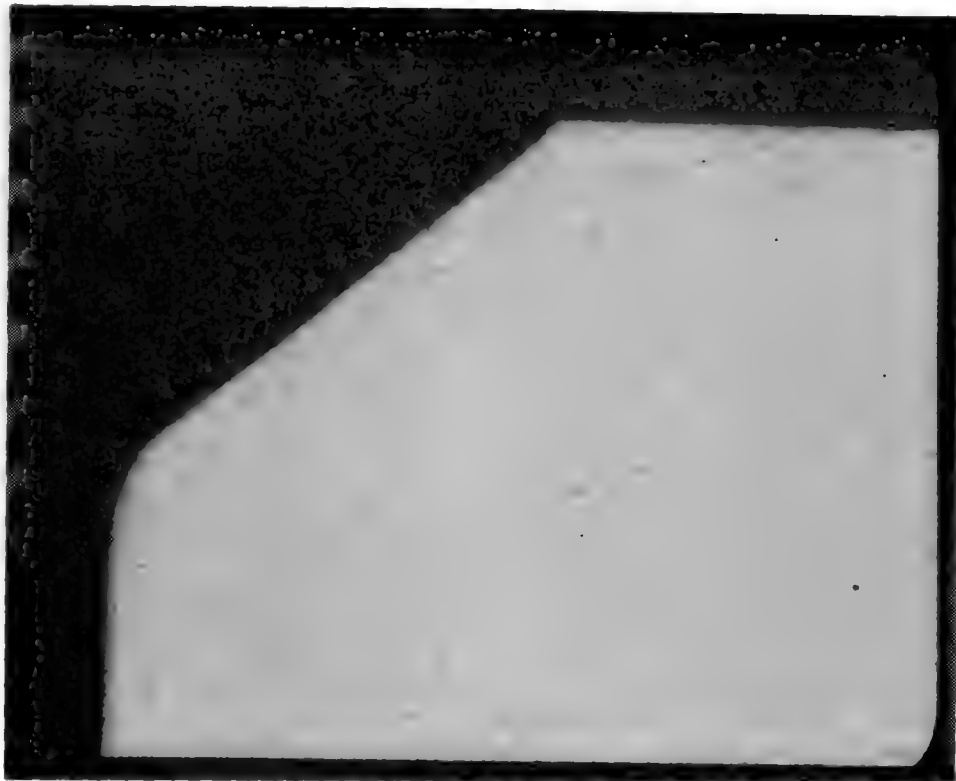
K&E POLAR CO-ORDINATE  
KILGILL & ELSSEN CO. MADE IN U.S.A.



TYPICAL FASTENER HOLE CONDITIONS

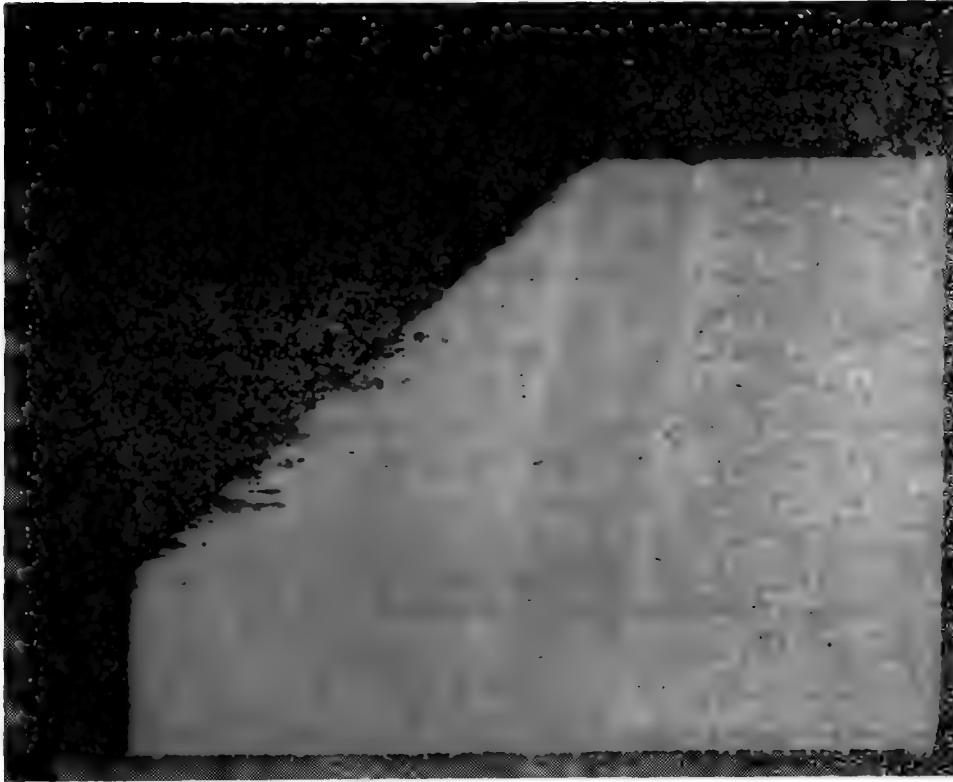


COUNTERSINK SURFACE 50X

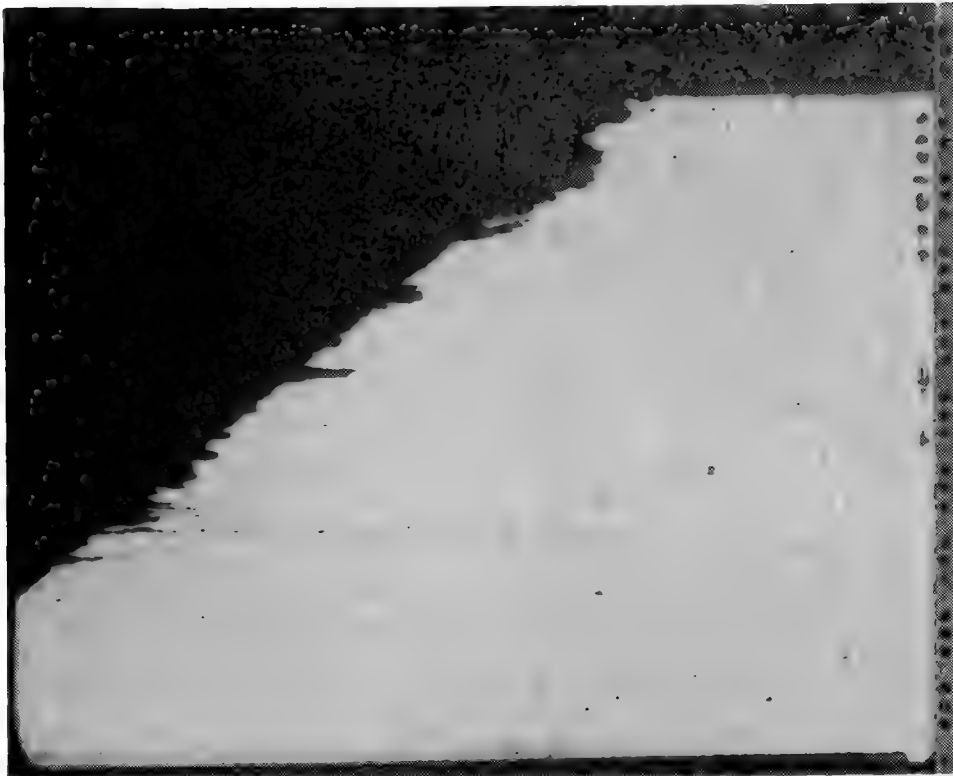


GOOD COUNTERSINK CROSS SECTION 50X

TYPICAL FASTENER HOLE CONDITIONS



CROSS SECTION WITH PITTING 50X



CROSS SECTION SHOWING PITTING AND EXFOLIATION 50X

# ON-AIRCRAFT TEST SCHEDULE

	5/10	5/11	5/12	5/13	5/14
PANAMETRICS	ARRIVE JOHN BOB	SESSION I WILLEY MATT 0800-1200	SESSION II GEOFF RICH KATHY 0800-1200		
	TRAINING JOHN BOB WILLEY MATT MIKE CHERI TOM SCOTT 1600-1800	SESSION IIIA MIKE CHERI 1300-1500 SESSION IIIB TOM SCOTT 1600-1800			
DIFFRACTO	SCOTT GEOFF RICH KATHY 0800	ARRIVE JOHN BOB	SESSION I WILLEY MATT 0800-1200 SESSION IIIA MIKE CHERI 1300-1500 SESSION IIIB TOM SCOTT 1500-1600	SESSION II GEOFF RICH KATHY 0800-1700	
WAYNE STATE		ARRIVE JOHN BOB	SESSION I WILLEY MATT 1400-1800 SESSION IIIA MIKE CHERI 0800-1000 SESSION IIIB TOM SCOTT 1100-1300	SESSION II GEOFF RICH KATHY 0800-1700	
PRI (MOD)		ARRIVE JOHN BOB	SESSION II GEOFF RICH KATHY 1300-1700	SESSION I WILLEY MATT 0800-1200 SESSION IIIA MIKE CHERI 1300-1500 SESSION IIIB TOM SCOTT 1600-1800	
BOEING				ARRIVE JOHN BOB	SESSION II GEOFF RICH KATHY 0800-1700

# ON-AIRCRAFT TEST SCHEDULE

ZTEC	5/17 ARRIVE JOHN BOB	5/18 SESSION I WILLEY MATT 0800-1200 SESSION IIIA MIKE CHERI 1300-1500 SESSION IIIB TOM SCOTT 1600-1800 ARRIVE JOHN BOB	5/19 SESSION II GEOFF RICH KATHY 0800-1200   SESSION I WILLEY MATT 0800-1200 SESSION IIIA MIKE CHERI 1300-1500 SESSION IIIB TOM SCOTT 1600-1600 ARRIVE JOHN BOB	5/20      SESSION II GEOFF RICH KATHY 0800-1700   SESSION I WILLEY MATT 0800-1200 SESSION IIIA MIKE CHERI 1300-1500 SESSION IIIB TOM SCOTT 1600-1800	5/21          SESSION II GEOFF RICH KATHY 0800-1200
BALES SCIENTIFIC					
SRL					

# ON-AIRCRAFT TEST SCHEDULE

KRAUTKRAMER/ BRANSON	5/24 ARRIVE JOHN BOB	5/25 SESSION I WILLEY MATT 0800-1200 SESSION IIIA MIKE CHERI 1300-1500 SESSION IIIB TOM SCOTT 1600-1800	5/26 SESSION II GEOFF RICH KATHY 0800-1700	5/27	5/28
FLARE TECH	ARRIVE JOHN BOB	SESSION II GEOFF RICH KATHY 0800-1200	SESSION I WILLEY MATT 0800-1200 SESSION IIIA MIKE CHERI 1300-1500 SESSION IIIB TOM SCOTT 1600-1800		
ARINC	SESSION II GEOFF RICH KATHY 0800-1700				

## APPENDIX D

Modify Impact Detection Breadboard System, Task Report 5.9, October 1993, F. Karpala and R. Reynolds, Diffracto Limited.

**Development of a *D SIGHT* Aircraft  
Inspection System - Phase 1**

**Task Report  
Task 5.9**

**MODIFY IMPACT DETECTION  
BREADBOARD SYSTEM**

**SSC File # XSD92-00184-(621)  
Contract # T8200-2-2544/01-XSD**

**by**

**Frank Karpala, PhD  
Rodger Reynolds, PEng**

**October, 1993**

**Diffracto Ltd.  
2835 Kew Drive  
Windsor, Ontario  
N8T 3B7**

**519-945-6373  
FAX 519-945-1467**

**TABLE OF CONTENTS**

LIST OF FIGURES . . . . .	iii
LIST OF TABLES . . . . .	iii
1 INTRODUCTION . . . . .	1
1.1 Purpose . . . . .	1
1.2 DAIS-500 Sensor . . . . .	2
1.3 Sensor Deficiencies . . . . .	2
1.4 Optimization Sample Set . . . . .	3
2 SENSOR OPTIMIZATION . . . . .	5
2.1 Design of Experiments . . . . .	5
2.2 Results . . . . .	8
2.3 Discussion . . . . .	11
2.4 Parameter Selection . . . . .	14
3 SENSOR DESIGN . . . . .	15
3.1 Material and Construction . . . . .	15
3.2 Controller . . . . .	17
3.3 Software . . . . .	17
4 CONCLUSIONS AND RECOMMENDATIONS . . . . .	19

**LIST OF FIGURES**

Figure 1: Sample 4743R1 imaged via the DAIS 500 configuration . . . . .	8
Figure 2: Opposing views of sample with lamp below lens . . . . .	8
Figure 3: Opposing views of sample, lamp above lens . . . . .	8
Figure 4: On axis light source . . . . .	9
Figure 5: Imaging corroded rivets at 32, 27 and 22.5 deg. grazing angle . . . . .	9
Figure 6: Effect of screen standoff set to 6, 12, 18 and 24 in. . . . .	9
Figure 7: 1.4 in. lamp below and above the lamp . . . . .	10
Figure 8: 2 in. lamp below and above the lens . . . . .	10
Figure 9: Optimized view of the sample . . . . .	10
Figure 10: Linescan image of sample 4743R1 . . . . .	11
Figure 11: Dimensionally transformed "top-down" view of image in Figure 9 . . . . .	11
Figure 12: Composite image of sample 4747L . . . . .	11
Figure 13: Profiles of the three rivet rows in order from top to bottom . . . . .	12
Figure 14: New DAIS-250C Sensor Configuration . . . . .	16

**LIST OF TABLES**

Table I: Sample Parts for Optimization . . . . .	4
--	---

## **1 INTRODUCTION**

### **1.1 Purpose**

A lightweight portable *D SIGHT* system called DAIS (*D SIGHT* Aircraft Inspection System) was designed and built for the detection of impact damage on composite skins of military aircraft under contract with the Canadian Department of National Defense (DND). Much of the hardware and software developed for impact detection will be reused and serve as the basis for further development under this contract. The hardware platform, including host controller, remote pendant, power supply, and the software interface will remain essentially fixed. The main focus in this contract is to determine the parameters of a sensor that is optimized for the detection of corrosion on aluminum skin particularly at horizontal and vertical lap joints.

The process of optimizing *D SIGHT* optical parameters involves several factors including external considerations such as weight, size, and ease of use. In this case, optimization means finding a set of parameters such as camera distance, angle, light source position and type, and retroreflector position so that the *D SIGHT* signatures of corrosion have maximum visibility (ie. sensitivity) and contrast in the image. Of particular importance to this process is the availability of corroded samples, the characterization of the corroded areas in terms of severity and physical indication, the types of structures and physical constraints on the inspection process, an understanding of the *D SIGHT* process and its configuration to enhance the physical indications, and the constraints on the geometry of the sensor.

To determine how well a given set of parameters performs in maximizing visibility and contrast, a set of experiments is planned whose output will be compared to the DAIS-500 sensor and the other optical configurations. The test configurations will be established from the perceived deficiencies in the DAIS-500 sensor and the knowledge of how to improve signature contrast from the understanding of the *D SIGHT* process. After the selection of an optimal configuration, a sensor will be built and tested on the corroded samples.

## **1.2 DAIS-500 Sensor**

The DAIS system and the DAIS-500 sensor were optimized for impact damage indications on composite skins of military aircraft. The DAIS system consists of the DAIS-500 sensor, a remote pendant, a power supply, and a host controller. In addition, cables up to 100 feet in length and other auxiliary equipment such as sensor pole and highlight applicator were incorporated.

The DAIS-500 weighs about 7 pounds and is comprised of an internal frame with an opaque cloth skin. Inside, the optical path is folded by a pair of mirrors to reduce the overall size. A CCD camera is mounted 49 inches from the surface on one side and the retroreflector is mounted 18 inches from the surface on the other side. The camera grazing angle is 32 degrees and the light source is a halogen bulb with an integral 1.4 inch reflector. The camera uses a 25 mm focal length lens and a trapezoidal field of view approximately 25 inches long with a width of 21.4 inches near the retroreflector and 14 inches near the camera is created due to the angle of the camera. This optical configuration will be the starting configuration for further refinement to detect corrosion on aluminum lap joints.

## **1.3 Sensor Deficiencies**

The DAIS-500 sensor has already been used extensively to inspect aircraft at military hangars and outdoors on tarmacs both for inspection of impact damage as well as corrosion on lap joints. From this experience, two types of deficiencies have been observed: lack of physical ruggedness of the sensor and low contrast signatures when inspecting for corrosion.

The ruggedness issue will be addressed during the discussion of the new sensor design. The lack of contrast issue is one reason for the need to modify the basic DAIS-500 configuration and is believed to be a result of a grazing angle that is too large for the type of physical indication created by a corroded lap joint. Since corrosion in lap joints and around rivets tends to manifest itself as a bulge between the rivet areas, the spatial frequency content of these areas are significantly different than impact damage that produces a localized depression over a small area.

In addition, a lap joint is a continuous narrow strip whose spatial dimensions appear distorted by the perspective and whose sensitivity appears to change across the field of view in the image. The DAIS-500 field of view is significantly wider than is required for a lap joint and the large grazing angle of the camera causes the disparity between the grazing angles at the front and back of the field of view responsible for the sensitivity change. The resolution or magnification of the DAIS-500 is also too low to easily resolve the small rivet heads. Clarity in the definition of the rivet perimeter is a useful cue to determine the level of rivet corrosion. Increased magnification would improve detection.

To address some of these problems, a number of optical arrangements will be configured to reduce or eliminate the effects caused by the differences between the physical nature of impact damage and corrosion.

#### **1.4 Optimization Sample Set**

The optimization of *D SIGHT* for corrosion relies heavily on acquiring a suitable and representative sample of corroded parts that can be used to fine tune the optical parameters. Unfortunately, the number of samples received to date containing corrosion has been minimal despite an aggressive program of field work. Many of the samples received do not show signs of corrosion under X-ray inspection but do exhibit corrosion using eddy current techniques or teardown. This means that the level of corrosion, in percentage terms, is very low (eg. ~ 1%).

Table I gives a list of the samples received to date for optimization and their known corrosion status. Included in the table is the approximate size of the sample and its surface condition. Due to their interesting features and size, samples 4746R2 and 4743R1 were used most heavily in the experiments.

**Table I: Sample Parts for Optimization**

Part ID	Aircraft	Dimension (inches)	Surface Condition	Corrosion
4739L3	B-727	11 x 17	no paint	?
4743L2	B-727	12 x 15.75	no paint	?
4743R2	B-727	13.5 x 17.5	painted	?
4746R2	B-727	13 x 31.5	painted	?
4751R2	B-727	13.5 x 17.5	painted	?
S1	B-727	29 x 73	painted	?
S2	B-727	28 x 77	painted	?
4747L	B-727	23 x 66	no paint	yes
4743R1	B-727	13.5 x 17.5	painted	yes

## **2 SENSOR OPTIMIZATION**

The essence of optimizing the performance of any system is determining the correct compromise amongst a number of conflicting requirements. Finding this compromise on a DAIS sensor is a particular challenge since it is practically impossible to improve any given aspect of the sensor's performance without detrimentally affecting a different but equally critical feature.

The overriding criterion for the design of the DAIS-500 sensor was package size. It was designed to inspect the maximum possible surface area while minimizing the sensor volume and weight.

The need to improve the sensor's sensitivity to surface bulges along a lap joint meant that it could be redesigned to inspect a smaller surface area with a long, narrow aspect ratio. Since such a configuration would result in an automatic reduction in the package size it would now be possible to beneficially increase some of the design parameters to enhance the sensor's performance.

### **2.1 Design of Experiments**

Of all the various parameters in a DAIS sensor, seven were varied to test their affect on the sensor's performance. These were:

- camera to surface distance
- retroreflective screen to surface distance
- camera grazing angle
- camera lens focal length
- camera imager aspect ratio
- light source to lens distance
- light source size

The experimental hardware used an existing lab set-up constructed of commercially available optical rails. Each major component; the camera/light source, the sample surface and the

retroreflective screen, was separately mounted. This open architecture allowed complete freedom to change any single parameter independently of the rest and judge if this improved the image's signal to noise ratio.

Inherent in any discussion of optimizing a system's performance is the assumption that there exists a solid criterion for determining whether the change in any variable is an improvement. In the case of an imaging system, such as DAIS, this suggests some form of computer based image analysis which can objectively decide if the corrosion signatures in one image are superior to those in another. However at this point in the development cycle of DAIS sensors there exists no such image analysis. Hence all results were judged subjectively by the authors and their colleagues based on their perception of which images had superior signal to noise ratios. In many case this was complicated by the natural surface waviness which seems to exist between many rivets although there is no corrosion present.

A disadvantage to the open architecture lab set-up was that it was not portable and it could accept a limited part size. For these reasons samples S1, S2 and 4747L were not thoroughly tested.

All samples benefited from highlighting with SnoFlake. When the images from multiple hardware arrangements were to be compared, the surface was highlighted once and the different set-ups recorded as quickly as possible to minimize any changes in the surface.

The first test performed used the hardware configured as a DAIS 500. Five of the samples from the first sample set received were mounted on a turntable to allow 360 deg. rotation within the camera's field of view. Although it was later discovered that none of these samples exhibited significant corrosion, they were useful in testing the effect of imaging direction. These images also showed that of this sample set, the surface of sample 4746R2 had the most distinct bulges between rivets making it the most likely candidate for further optimization testing.

Starting with the basic DAIS 500 configuration, a given hardware parameter would be changed an arbitrary amount and the resulting image visually compared to the result of the most successful previous test. In this way each new result guided the direction of successive tests.

For instance, the apparent severity of surface bulges were found to be highly sensitivity to screen to surface distance. This supplied the impetus to modify the lab hardware to allow a part to be imaged in a line-scan mode, eliminating the unavoidable changing screen to surface distance inherent in a single, planar retroreflective screen.

Ultimately a total of twenty-eight different hardware configurations were tested using sample 4746R2. The configurations tested were as follows:

camera to surface distance	tested at 37, 43, 49, 57 and 90 in.
screen to surface distance	tested at 12, 18, 24 and 36 in.
camera grazing angle	tested at 22.5 , 27 and 32 deg.
camera lens focal length	tested at 25, 50 and 100 mm
camera imager aspect ratio	tested at 3:4 and 4:3
light source to lens distance	tested on-axis and off-axis, above and below lens
light source size	tested with "point", 1.4 and 2 in. source

The resulting images suggested an optimal hardware configuration that was mocked-up as a working prototype to test for packaging limitations. Upon the receipt of samples 4743R1 and 4747L, both of which showed significant corrosion levels, most of the hardware tests were repeated to confirm the results. 4743R1 is an almost ideal specimen since it shows distinct signs of corrosion at one end with very little waviness elsewhere on its surface. As such this part will be used in all test result illustrations.

Since research to develop a model for the corrosion generated surface deformation surrounding a rivet is under consideration, contact surface profiles were taken of the three rows of rivets present in sample 4743R1. This profile data was collected using a servo-controlled linear table and a glass-scale based height indicator, essentially a medium-accuracy, uni-dimensional, coordinate measuring machine (CMM). This hardware had a measured resolution of 0.0005 mm (20  $\mu$ in.). Height measurements were taken at 0.25 mm (0.01 in.) intervals over 330 mm (13 in.). The height gage contact probe was a 1.58 mm (0.0625 in.) diameter, steel ball. Errors due to ball diameter were considered negligible. Surface noise is removed via low-pass filtering and global panel curvature is removed by subtracting a best-fit third order curve.

## 2.2 Results

Figure 1 shows the sample as imaged using the DAIS 500 configuration. (The unpainted area of the surface has been masked to produce the best possible exposure). The five rivets at the top of the part exhibit serious surface deformation around them. Early testing showed that having the camera view along the length of the lap joint gave the most readily interpretable images. Viewing the lap joint at a 45 deg. or 90 deg. angle did not improve the signal to noise and reduced the length of joint inspected with a single image.

Test images such as Figure 1 clearly indicated the need for more magnification. But this has the undesirable side effect of reducing the inspected surface area. To counteract this, it was decided early in the testing phase that it would be more efficient to mount the camera on its side. Thus the longest dimension of the camera's CCD imager would view the maximum surface length possible, making the most efficient use of the available imaging area. With this modification a 50 mm focal length lens produced an optimum image size and was used for all subsequent tests.

For efficient packaging and heat dissipation, the 1.4 in diameter reflector lamp in the DAIS 500 was located above the lens. To test the effect of lamp location the five rivets exhibiting surface deformation were centred in the field of view and imaged with

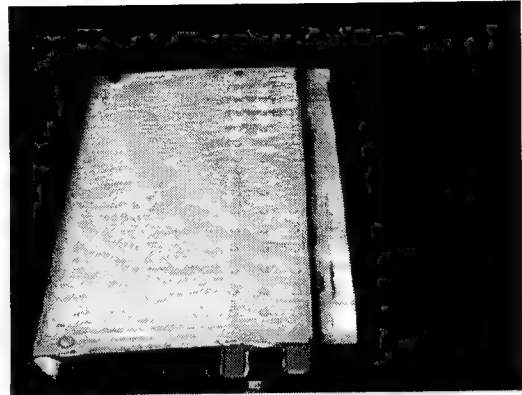


**Figure 1:** Sample 4743R1 imaged via the DAIS 500 configuration

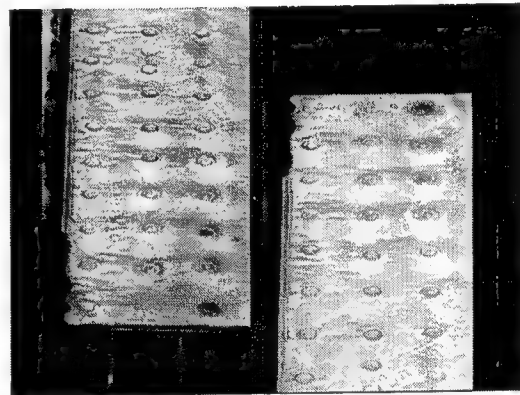


**Figure 2:** Opposing views of sample with lamp below lens

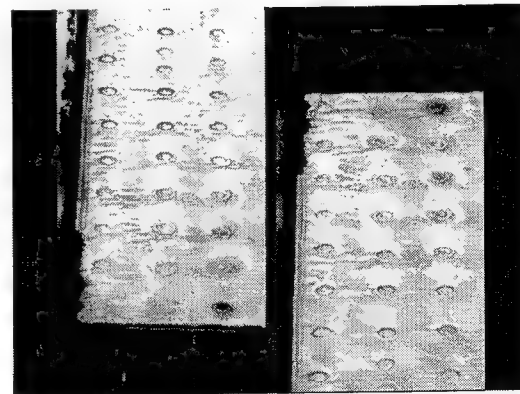


**Figure 3:** Opposing views of sample, lamp above lens

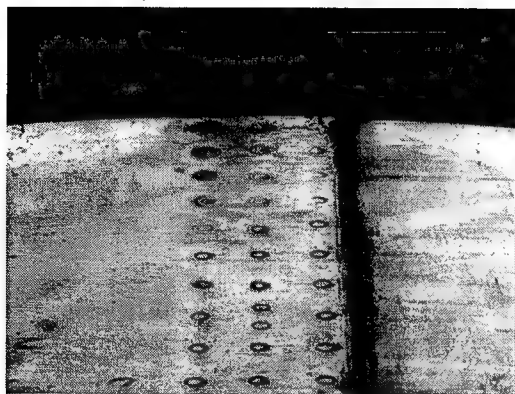


Figure 4: On axis light source

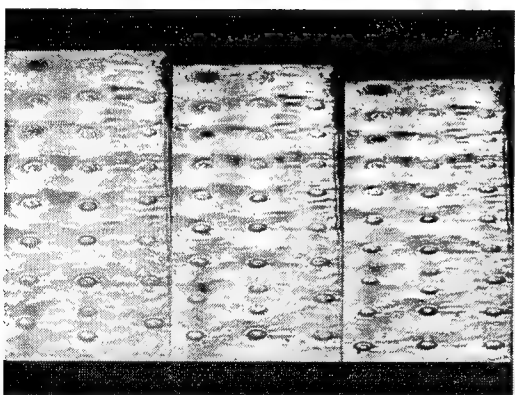


Figure 5: Imaging corroded rivets at 32, 27 and 22.5 deg. grazing angle

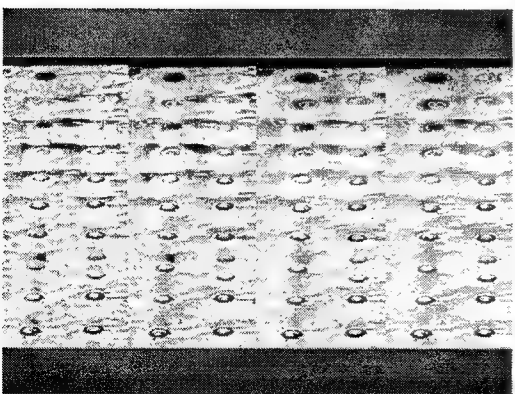
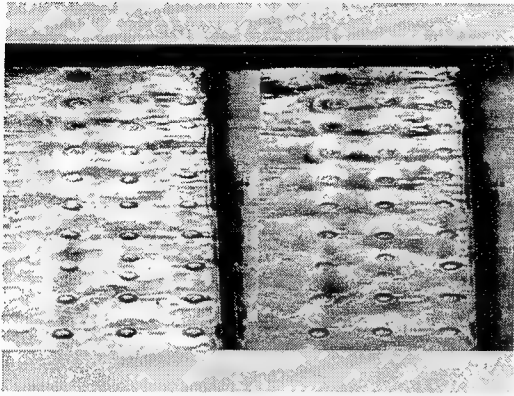


Figure 6: Effect of screen standoff set to 6, 12, 18 and 24 in.

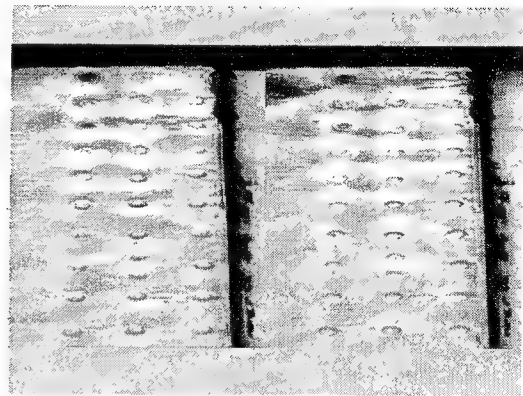
the lamp above and below the lens. In both cases the lamp is positioned as closely as possible to the lens without entering its field of view. Figure 2 shows opposing views of the rivets with the lamp below the lens while the lamp is above the lens in Figure 3. To aid in comparing the opposing views of the same part, the right view has been mirrored so that same rivet row is on the left side in both images. By using a beamsplitter the lamp can be made coincident with the optical axis of the lens. Due to the significant power losses through beamsplitter the lamp must be run at full voltage. Figure 4 illustrates an image of the surface illuminated in this manner.

Figure 5 illustrates three views of the rivets taken with the 1.4 in. reflector lamp below the lens and the camera grazing angle set to 32 deg., 27 deg. and 22.5 deg. Using a camera grazing angle of 22.5 deg. Figure 6 shows four views of the two worst rivet rows with the retroreflective screen located 6 in., 12 in., 18 in. and 24 in. from the centre of the surface. With the screen to surface distance set to 18 in. the effect of lamp size was tested next. In Figure 7 two images of the same surface region are shown with the lamp 1.4 in. diameter reflector lamp located above and below the lens. The views in Figure 8 are similar except that the lamp now has a 2 in. diameter reflector.

By mounting the camera on its side, the entire length of the sample could be imaged at once, as illustrated in Figure 9. Here, the 2 in. diameter lamp is



**Figure 7:** 1.4 in. lamp below and above the lamp



**Figure 8:** 2 in. lamp below and above the lens

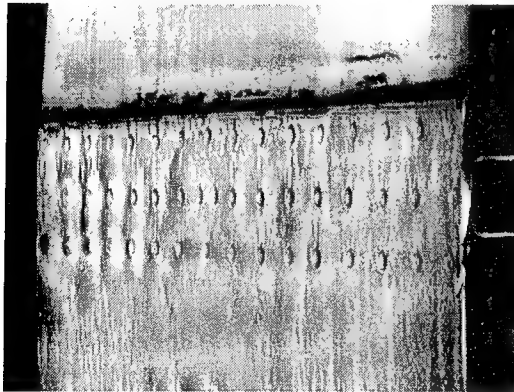


**Figure 9:** Optimized view of the sample

mounted below the lens with the camera at a 22.5 deg. grazing angle.

As with all images taken using a single flat retroreflective screen, it is impossible for the screen to surface distance to remain constant throughout the entire field of view. Two attempts were made to correct this problem. One solution was two use a segmented screen, wherein the screen is actually an array of five small flat panels which are staggered and angled to approximate the same

surface to screen distance across the entire inspected surface. Of course this approximation improves as the size of the segments are reduced and their number increased. For reasons to be outlined in the Section 2.3, this technique was tested but abandoned. The alternate solution is to build the image in memory one line at a time as the sensor is scanned over the surface. This was simulated in the lab set-up by moving the sample through the field of view as the output from a single scan line of the camera was stored sequentially on the frame buffer. The result of imaging the sample in this manner is shown in Figure 10. Compare this image to Figure 11 which is the same data shown in Figure 9 after a software dimensional transformation has created a similar "top-down" view.

Using the configuration which yielded images with the best signal to noise ratios, the entire

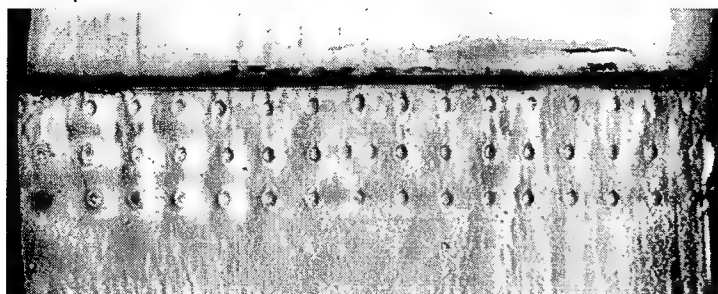


**Figure 10:** Linescan image of sample 4743R1

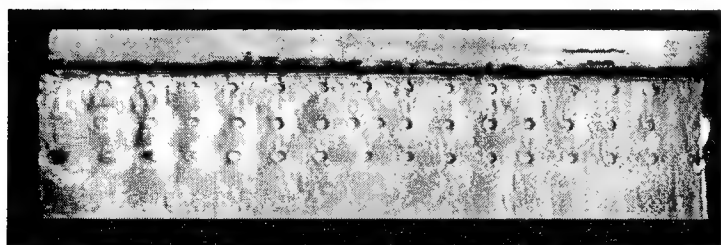


**Figure 11:** Dimensionally transformed "top-down" view of image in Figure 9

surface of sample 4747L was imaged in four sections. Figure 12 shows a composite of these images after they have been dimensionally transformed.

Finally, Figure 13 shows a line-scan image of the sample. Below this, arranged in the same order top to bottom, are dimensional profiles of the three rows of rivets.

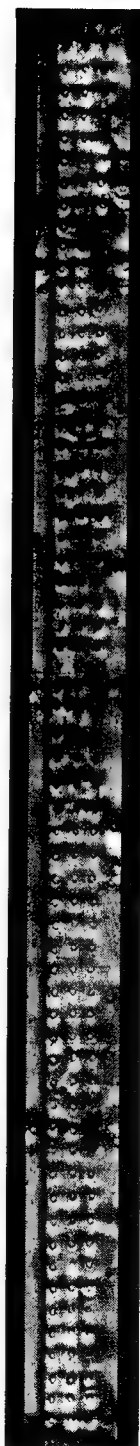


**Figure 12:** Composite image of sample 4747L

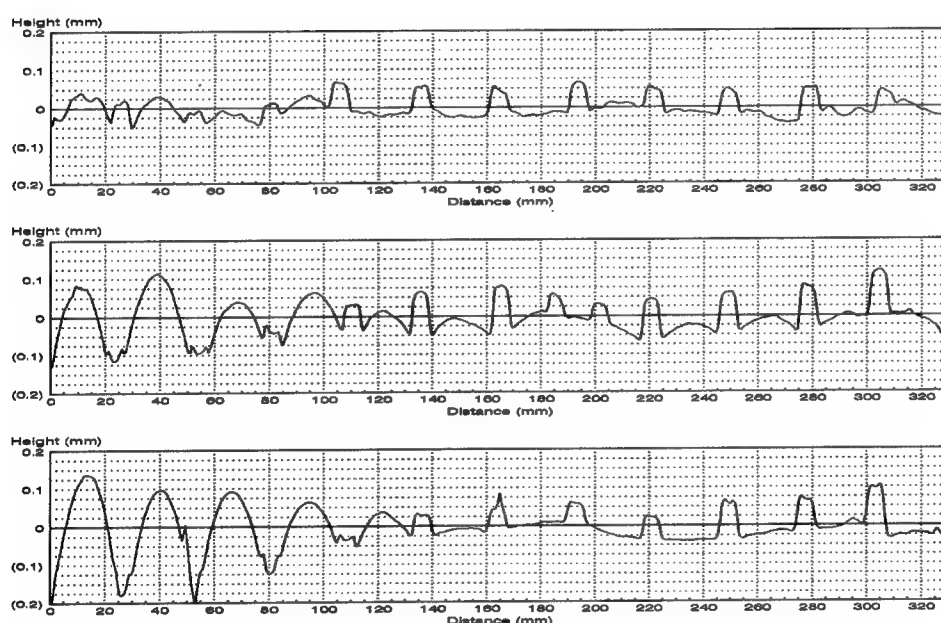
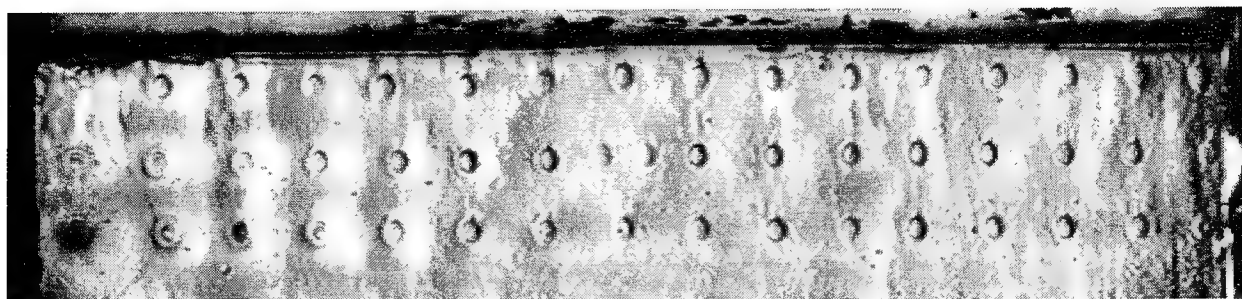


Figure 13: Profiles of the three rivet rows in order from top to bottom

## 2.3 Discussion

Perhaps the most significant innovation made during this optimization process was using the camera in a 4:3 aspect ratio. By increasing the lens focal length to 50 mm., decreasing the camera grazing angle to 22.5 deg. and mounting the camera on its side to make more efficient use of its imaging array, the magnification was improved while maintaining a reasonable length of inspected lap joint. And decreasing the camera grazing angle had the added benefit of increasing the contrast within the signatures of the surface deformations. The effect of these changes can be best seen by comparing Figure 1 to Figure 9. It was felt that further reduction

of the grazing angle would result in an unacceptable amount of magnification change along the inspected joint length.

When the decision was made to mount the lens above the lamp in the DAIS 500, it was assumed that its only effect on the resulting images would be to invert the "polarity" of the waviness signatures. However, as can be seen in Figures 7 and 8, locating the lamp beneath the lens causes a visible increase in the contrast of the surface signatures. This is likely due to the small but significant reduction in the lamp's grazing angle. The entire issue of whether the lamp should be above or below the lens or whether the signatures are too asymmetric to be readily interpretable could be resolved by mounting the lamp on-axis with the lens, see Figure 4. However this produced very subtle signatures with a serious loss of illumination power. Mounting the lamp off-axis, below the lens produced images of sample 4743R1 with the best signal to noise ratios.

The only important effect of changing the distance between the camera and the surface was a change in the field of view. Shortening this distance to reduce the package size would reduce the area inspected within one image. Increasing this distance to improve the inspected area would cause the package size and weight to grow. Hence this distance was not changed.

The size of the light source may be thought of as a hardware filter. The larger its diameter the less sensitive is the camera to high frequency surface deformations. Comparing Figures 7 and 8; the 2 in. diameter reflector lamp generated images with superior signal to noise ratios by subduing the normal surface ripples between rivets, paint runs and sags.

The parameter which most directly affects the sensor's sensitivity but over which there is the least control is the surface to retroreflective screen distance. From the aspect of design and packaging, the most convenient screen shape is a flat rectangular plane. Unfortunately at a camera grazing angle of 22.5 deg. the distance from this plane to the surface varies from 6 in. to 24 in. Referring to Figure 6, the signatures of rivet corrosion change noticeably over this range. Unfortunately a segmented screen is difficult to manufacture, only partially solves the problem and would increase the sensor's size and weight. Also, for this technique to function correctly, the light source had to be positioned above the lamp so each screen would not cast

a visible shadow on its neighbour. Since this was not the optimum location for the lamp, this technique was not considered viable. The line-scan imaging technique would require a more mechanically and optically complex sensor but would produce images with equal sensitivity and magnification across the entire field of view.

For the sake of simplicity of sensor design, the flat screen configuration was chosen. Using software transformations the changing magnification can be almost totally corrected. Similarly, any image analysis would also need to compensate for its varying sensitivity.

The profiles in Figure 13 begin just after the first rivet at the left of each row. The perception of the rivet heads "sinking" into the hills between them is a side effect of subtracting the third order curve. Generally there is a good visual correlation between the height of the bulge between rivets and its DAIS signature. Unfortunately, the largest bulges between the first and second rivets in rows 2 and 3 (0.3 mm and 0.2 mm high respectively) do not have distinct signatures. It is surmised that this is due to their proximity to the sample's edge.

## **2.4 Parameter Selection**

When optimized to produce the best images of surface deformation between rivets, the DAIS sensor used the following dimensional parameters:

camera to surface	49 in.
surface to retroreflective screen	18 in. (nominal)
camera grazing angle	22.5 deg.
camera lens	50 mm @ f11
camera aspect ratio	4:3
lamp reflector diameter	2 in.
lamp location	1.5 in. off-axis, below the lens

### **3 SENSOR DESIGN**

#### **3.1 Material and Construction**

The DAIS-500 sensor was constructed using an internal frame made from graphite composite tubing and an external cloth skin. This construction led to a lightweight sensor that was not very rugged. For the new sensor, called the DAIS-250C, a heavier but hard skin is desirable since the overall dimensions are smaller and the internal components can be attached directly to the enclosure without an internal frame.

To keep the weight down as much as possible, a thin 0.0315 inch aluminum enclosure is used and areas that need additional support are reinforced with thicker material. Two internal partitions maintain rigidity, provide attachment points for components, and act as blockers to shield the surface from stray light. As with the DAIS-500, two mirrors will be used to reduce the overall size of the sensor while maintaining a four foot optical path length from the surface to the camera. The mirror closest to the surface will be a good quality second surface mirror while the mirror closest to the camera will be a first surface mirror. A diagram of the sensor and its internal components is shown in Figure 14.

Five rigid handles are mounted to the sensor to provide positional control in all orientations. The power/signal cable is mounted high on one end to minimize interference with a highlighted surface. Four rubber feet support the sensor one inch above the surface to allow for curved surfaces. A detachable light skirt is available to reduce the influence of strong ambient light.

Internally, a CCD camera is mounted in a horizontal position on its side. This orientation maximizes the use of the aspect ratio of the camera and the perspective to create a long but narrow field of view along a lap joint. When the sensor is held horizontally on the surface with the cable on the right hand side, the top of the field of view on the video monitor will be consistent with the orientation of the inspector to the surface. The halogen light source is mounted below the camera lens approximately one inch. Since the source is only 20W heat the amount of heat dissipation is expected to be small. The size of the light source reflector is larger than in the DAIS-500. The larger size removes high frequency noise. The retroreflective

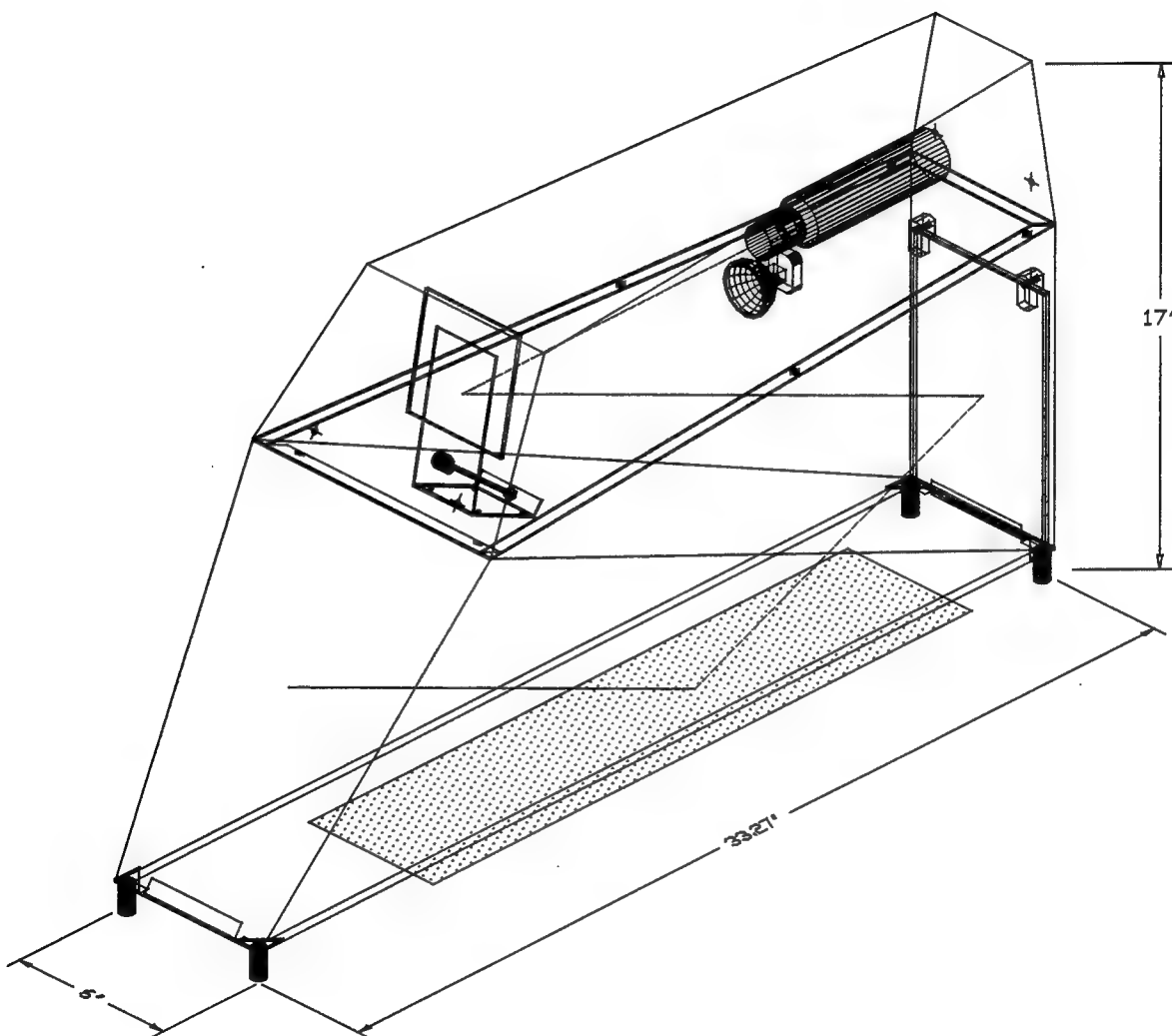


Figure 14: New DAIS-250C Sensor Configuration

material is coated so that highlighter and fingerprints will not damage its surface. Its position is 18 inches from the origin of the field of view at 55 degrees from the surface.

### **3.2 Controller**

The controller consists of three components: transportable computer (host), remote pendant, and power supply. The transportable computer is packaged in a durable case and has an integral 9 inch VGA monitor that is used for display of menus and camera video. It is a 386-33Mz computer running DOS. The computer is operated by a 101-key keyboard and although the software supports mouse operation the mouse port is unavailable due to the communication with the power supply. The computer also contains two framegrabber boards: one to allow VGA overlay on the computer monitor and the other to pipe video to the monitor in the remote pendant.

The power supply is intended to drive a total of four components: camera, light source, pendant monitor, and pendant LCD display panel. The voltage to the light source is controlled by the computer through a RS-232 control module. All camera video is also piped through the power supply to reduce the number of cables and interconnections.

The remote pendant contains a 3 inch video monitor and a touch LCD panel. The pendant is connected between the power supply and the sensor. The cable from the pendant to the sensor is about 15 feet long while the cable between the pendant and the power supply is about 100 feet long. Except for some print and view functions, most host functions are supported by the pendant.

### **3.3 Software**

The control of the sensor, video, and power supply and file management is achieved with a user friendly pull down menu system (see DAIS User's Guide). The main menu contains the following items: Files, Video, Options, Pendant, Help, and Exit.

The Files item is used to create, save, view, retrieve and print data log files as well as image files. Once a data log file is opened, all images saved will be referenced by the log file name with an automatic increment of the extension number. The data log file entry contains user supplied information about the aircraft, inspection area, operator and any comments entered by the user. When an image is optionally printed, the log file data is printed along with the image.

The Video item allows the user to control video functions such as live, freeze, and store (only when data log file is opened). In addition, auto light adjustment can be activated.

The Options item is used to set up light control parameters, user information, and the display of a grid overlay on the video. Light control can be automatic, by setting a target gray scale value, or manual, by setting a voltage value between 0-12. Automatic light control is based on the gray scale in a small window in the centre of the field of view.

The Pendant option activates the remote pendant or disables the pendant. The pendant cannot be activated from the pendant itself.

The Exit item returns to DOS or spawns to DOS temporarily.

## **4 CONCLUSIONS AND RECOMMENDATIONS**

The optimization of a sensor configuration for corrosion has been successfully completed despite the limited number of documented samples. The design takes advantage of the aspect ratio of the CCD camera, a longer focal length lens, and a lower grazing angle to achieve a field of view which is as long as the DAIS-500 sensor but much narrower yet has higher magnification. Higher overall sensitivity and lower sensitivity variation across the field of view is enhanced by the use of the lower grazing angle. A larger light source attenuates some of the high frequency noise.

The sensor enclosure is made of aluminum to improve ruggedness and the small footprint and size makes the sensor easy to handle in both horizontal and vertical orientations. To improve the ease of use of the sensor, a smaller diameter cable is recommended for future prototypes.

The sensor has been built and should be tested in field trials for ease of use and on additional documented samples for sensitivity and accuracy. From observations to date, the DAIS-250C sensor configuration is a significant improvement for the detection of corrosion from the DAIS-500 sensor.

## APPENDIX E

Task 5.11, Part 1 of 2, DAIS-250C Field Trial, AANC - Albuquerque, NM, F.  
Karpala, October 1993, Diffracto Limited.



**Development of a *D SIGHT* Aircraft  
Inspection System - Phase I**

**Task 5.11, Part 1 of 2  
DAIS-250C FIELD TRIAL  
AANC - Albuquerque, NM**

**SSC File # XSD92-00184-(621)  
Contract # T8200-2-2544/01-XSD**

**by**

**Frank Karpala, PhD**

**October, 1993**

**Diffracto Ltd.  
2835 Kew Drive  
Windsor, Ontario  
N8T 3B7**

**519-945-6373  
FAX 519-945-1467**

---

## **INTRODUCTION**

### **Purpose**

The field trip to the FAA Aging Aircraft NDI Validation Center (AANC), operated by Sandia National Labs in Albuquerque, New Mexico was originally suggested by Dave Gallela of the FAA Technical Center as part of this contract. This trip was arranged with Dennis Roach, AANC Facility Experiment Coordinator, for a three day period on Oct. 18-20, 1993 and served two purposes. First, it provided an opportunity to use the new breadboard DAIS-250C sensor for corrosion on an older aircraft that would eventually be fully characterized and second, it provided the AANC an opportunity to see a *D SIGHT* sensor in action along with a record of *D SIGHT* inspections on their aircraft. The AANC records and archives raw inspection data and inspection results in their database of all vendors who bring their equipment to the center for testing.

### **Aircraft**

The aircraft at the AANC facility is a high time B-737-222 from line number 049 with SN 19058. The aircraft was previously owned by United, Air Florida and Pan American. It has sustained 38,342 flight hours and 46,358 flights. This aircraft is located in a hangar and is complete externally with the exception of a right engine. All fairings are in place except the aft fairing on the right hand side causing certain areas of the aircraft to be unavailable for corrosion inspection. The aircraft surface is free of paint but the dirt, chemical stripping marks, and other surface blemishes required the use of highlighting during inspection.

### **Inspection Equipment**

Diffraction shipped its *D SIGHT* Aircraft Inspection System, (DAIS), equipment to the facility in advance of the visit. Included in the shipment was the DAIS host controller, remote pendant, power supply, DAIS-250C sensor, HP4 LaserJet printer, and auxiliary equipment and supplies for highlighting. All equipment was received at the facility on time and in working order.

### **Inspection Personnel**

The inspection team included Dr. Frank Karpala from Diffracto Ltd., and Mr. Jerzy Komorowski and Mr. Ron Gould from the Institute of Aerospace Research of the National Research Council Canada, NRC/IAR. Dr. Karpala and Mr. Gould operated the DAIS equipment to collect raw data while Mr. Komorowski performed the *D SIGHT* image interpretation for corrosion.

### **Observers**

Over the course of three days, a number of observers were in attendance at some point during the inspections. These observers included:

- Dennis Roach, AANC Facility Experiment Coordinator
- Craig Jones, AANC Experiment Coordinator
- Ken Harmon, ANNC Facility Owner
- Richard Shagam, AANC NDI Technical Expert
- Patrick Walter, AANC Program Manager
- Dave Gallela, FAA Technical Center
- Geoff Mitchell, ARINC
- Floyd Spencer, AANC Experimental Planner

## INSPECTION AREAS

### Service Bulletins

To maximize the comparison of the DAIS system to current techniques and inspection times, it was decided to follow two Boeing service bulletins for the inspection of fuselage horizontal and circumferential lap splices. These service bulletins are summarized below:

Number: 737-53A1039  
Date: July 19, 1972  
Revision 7: Oct. 15, 1992  
ATA System: 5330  
Subject: Fuselage - Skin Lap Joint Inspection and Repair

Number: 737-53-1076  
Date: Oct. 20, 1986  
Revision 4: Sept. 26, 1991  
ATA System: 5313 5330  
Subject: Fuselage - Circumferential Butt Splices and Bonded Doublers  
Inspection, Repair and Modification

These service bulletins call for a visual inspection of longitudinal lap splices on stringers: S4, S10, S14, S19, S20, S24, S25, S26, left and right, between body stations, BS 259.5 and BS 1016, and for circumferential lap splices: BS 259.5, BS 360, BS 540, BS 727, BS 907, and BS 1016, left and right, for corrosion. Due to the lack of proper platforms, S4 was inaccessible except for one aft section and due to the presence of fairings, part of BS 727 and BS 540 could not be inspected.

## **INSPECTION PROCEDURE**

Prior to the inspection, the following procedures were established and submitted to AANC personnel. Additional conventions were needed concerning the orientation and sequence of placements of the sensor just prior to inspection. For example, the horizontal lap splices would be performed from forward to aft while the circumferentials would be performed from top to bottom. Some of these conventions caused difficulties during analysis that were not anticipated.

### **Horizontal Lap Splices**

1. Position access stands.
2. Highlight surface as required.
3. Carry out inspection with at least 50% overlap with first sensor placement symmetrical over the initial body station. The size of the sensor field of view will result in every other placement being centered on a frame.
4. When the lap splice accessible from the access stand is complete, print and interpret results.
5. Repeat steps 1 to 4 until inspection is complete.
6. Report results of inspection.

For storage of raw data, it was decided to open log files whose names were based on the stringer number, aircraft side, and starting circumferential number in the form

XSS-BBBB

where:        X        is L or R for left or right side  
              SS        stringer number  
              BBBB    starting body station number

In most cases there were several log files for a given stringer to keep each data set compact and manageable.

### **Circumferential Lap Splices**

1. Position access stands.
2. Highlight surface as required.
3. Carry out inspection with a 50% overlap with first sensor placement symmetrical over the initial body stringer. The size of the sensor field of view will result in every other placement being centered on a stringer.
4. When the circumferential on one side is complete, print and interpret results.
5. Repeat steps 1 to 4 until inspection is complete.
6. Report results of inspection.

For storage of raw data, it was decided to open log files whose names were based on the circumferential number, aircraft side, and starting stringer number in the form

BBBBX-SS or (XBBBB-SS resulting from oversight)

where:      X      is L or R for left or right side  
             SS      starting stringer number  
             BBBB body station number

In most cases there were two log files for a given circumferential, one for each side.

## INSPECTION DATA

The following tables summarize the log files used and the number of images/placements made for each. Also included is the total time for each inspection.

### Horizontal Lap Splices

Left Side			Right Side		
Log File	Images	Time (min)	Log File	Images	Time (min)
L26-2595	31	11:19	R24-2595	13	4:28
L19-2595	21	5:40	R26-360	18	5:00
L25-747	28	7:10	R19-2595	23	5:42
L20-767	27	7:48	R25-747	29	8:25
L14-360	23	11:09	R20-767	22	7:29
L10-360	22	7:41	R14-360	22	7:28
L10-540	21	4:29	R10-360	23	5:18
L14-2595	10	3:07	R10-540	20	3:47
L10-2595	10	3:37	R14-2595	9	3:42
L14-727	32	16:52	R10-2595	11	3:07
L10-727	31	9:42	R14-727	33	10:56
			R10-727	33	9:44
			R4-1016	34	23:40

These log files contain 256 images for the left side, 290 for the right side, for a total of 546 images requiring 135 MB of disk storage. A sample of the images is shown in Appendix A.

**Circumferential Lap Splices**

Left Side			Right Side		
Log File	Images	Time (min)	Log File	Images	Time (min)
2595L-4	24	12:19	2595R-4	25	7:28
			360R-5	26	8:30
540L-4	12	3:25	540R-6	11	2:00
L727-4	13	4:32	R747-4 *	13	5:47
L907-4	27	15:41	R907-4	25	9:49
L1016-4	24	7:41	R1016-4	25	9:51

The log file R747-4 on the right side was miss named and should have been R727-4. There are 100 images on the left side and 125 images on the right side, for a total of 225 images requiring 55 MB of disk storage. A sample of the images taken is shown in Appendix B.

**Data Disposition**

Due to the disk capacity limitations of the DAIS computer, it was necessary to unload the images periodically onto two 150 MB Bernoulli disks supplied by AANC. Some of the image and log files on the DAIS computer were then deleted. Before the deletion, two copies of the images were printed, 6 to a page, for analysis and documentation for AANC. Data log files were also printed and deleted as needed.

In total, 195 MB of images and log files were transferred to the Bernoulli disks from the corrosion inspection as well as an additional 40 MB from other inspection activities such as crack detection not reported here.

## **INSPECTION ANALYSIS AND RESULTS**

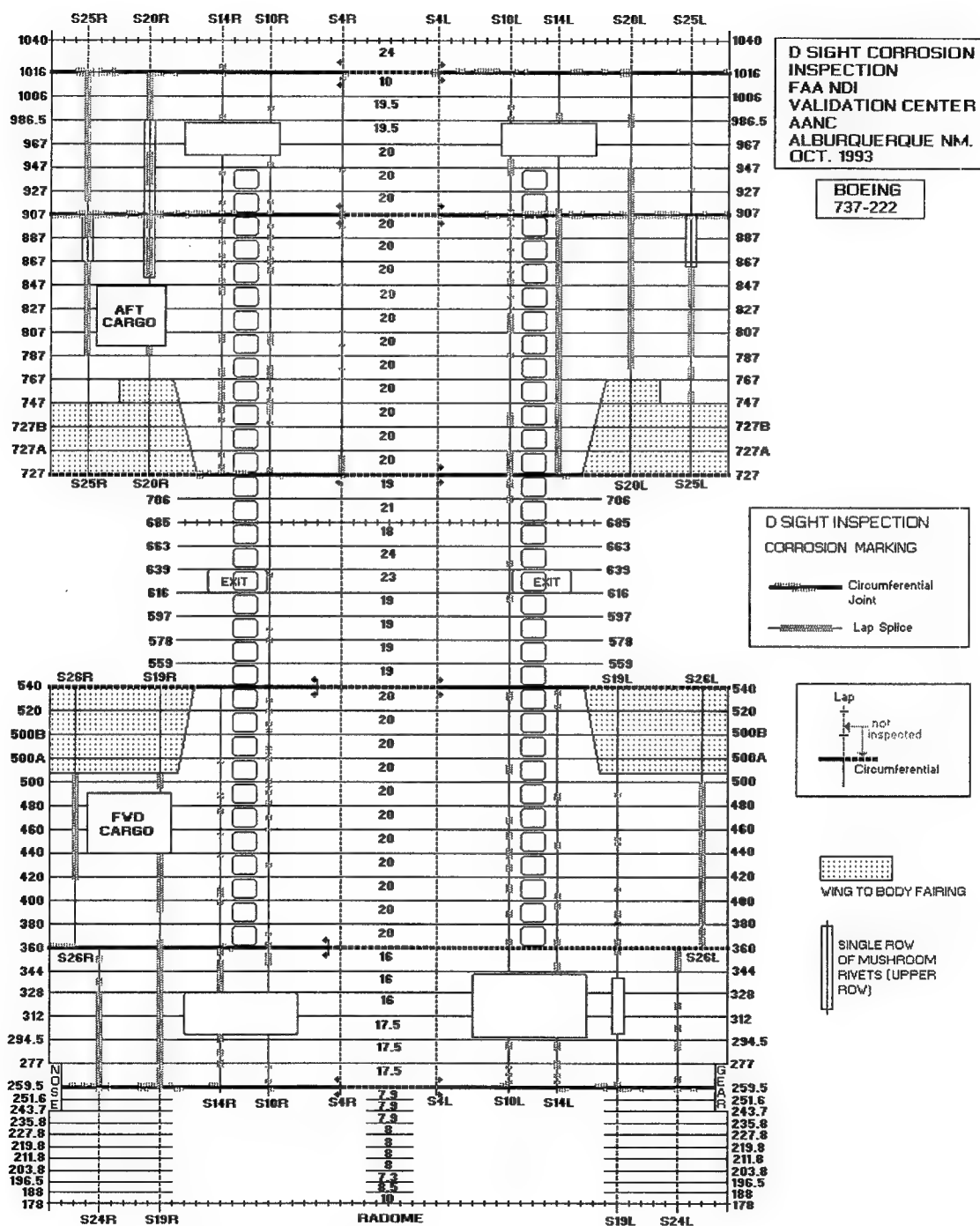
The analysis of the *D SIGHT* images for corrosion was performed solely by Jerzy Komorowski for consistency of interpretation. As he discovered, one of the time consuming parts of the analysis was determining exactly which body station or stringer was present in the image. The task of interpreting the signatures for corrosion was much easier than the task of determining which part of the surface was being inspected. This difficulty was made even worse for the inspections on the right hand side of the aircraft since the sequence of images taken during the inspection was right to left yet the images were printed in a left to right sequence. This problem was not anticipated until it was too late and should be resolved with a proper inspection procedure and sensor modification.

Each image analyzed was marked with a pen for corrosion and body station identification. A copy of these pages was made and given to AANC. Once the series of images were analyzed for a given log file, the detected corrosion was transferred to a surface map of the aircraft showing the critical body stations and stringers. No distinction was made between severity levels, although it was clear that lap splices near the belly of the aircraft were much worse than areas further up the aircraft both in severity and extent.

Most of the analysis was performed at the facility and during evening hours outside the hangar for horizontal lap splices. However, most of the circumferential image analysis was completed only after returning home. These results will be mailed to AANC to complete their records.

Indications of corrosion in the *D SIGHT* image were determined by the level of brightness found around each rivet and the overall pattern of brightness activity in a local area. As surface bulges increase in curvature, the *D SIGHT* signature around the rivet increases in brightness. Generally, a region of rivets are affected and the pattern found in the image is clearly seen. In addition, excessive corrosion causing the metal around the rivet to pull through is detected by the clarity of the rivet head in the image. Corrosion is also indicated by the rivet head and the region around the rivet appearing dark but this condition should not be confused with rivets of a different type from that used in the original manufacturing process such as button heads.

The resulting corrosion map for this aircraft, as determined by *D SIGHT*, is presented in the in the following turtle diagram for horizontal and circumferential lap splices.



## **SENSOR PERFORMANCE**

### **Sensitivity**

The sensitivity of the optimized DAIS-250C sensor could not be verified during this test since the aircraft has not yet been characterized. Images, stored during this test, can be re-analyzed for severity and location when this information becomes available in the future. However, corrosion indications were found in most areas of the aircraft and in proportion to expected conditions. For example, the lower fuselage horizontal lap splices had significantly great corrosion indications and severity than the upper fuselage. Corrosion severity was not determined or recorded specifically although the *D SIGHT* signatures do support a greater degree of corrosion in the lower fuselage areas.

### **Speed of Inspection**

The speed of inspection should consider all of the following items:

- platform set up
- highlighting
- sensor placement
- data storage
- data retrieval/printout
- image analysis
- corrosion mapping and marking

During this test only accurate times are known for highlighting, sensor placement, and data storage since each image is time stamped. The table below summarizes the time taken for inspection of horizontal lap splices and circumferential lap splices during this test.

Lap Splice	Placements	Time (hr:min:sec)	Scan Time (sec/placement)	Inspection Rate (feet/min)
Horizontal Right Side	290	1:38:46	20.7	
Horizontal Left Side	256	1:28:24	20.4	
<b>Total Horizontal</b>	<b>546</b>	<b>3:07:10</b>	<b>20.6</b>	<b>2.5</b>
Circumferential Right Side	125	0:43:25	26.2	
Circumferential Left Side	100	0:43:38	20.8	
<b>Total Circumferential</b>	<b>225</b>	<b>1:27:03</b>	<b>23.2</b>	<b>2.4</b>
<b>Total Lap Splices</b>	<b>771</b>	<b>4:34:13</b>	<b>21.3</b>	<b>2.5</b>

Due to the lack of access to stringer 4 and fairing interference, right and left, it is estimated that only 80% of the horizontal lap splices were inspected and 84% of the circumferentials. Assuming a similar rate of inspection, it is estimated that the total times for horizontal and circumferential lap inspection would be 3:53:58 and 1:43:38, respectively, resulting in a combined inspection time of 5:37:36. These times suggest that the total time required to gather raw data to satisfy both 737 service bulletins is just over 11 man-hours. It is important to note that the rate of inspection is affected by the decision to overlap each placement by 50%. This decision was taken to ensure there was complete coverage for this experimental test.

The data retrieval and interpretation time is unknown precisely since it was performed on and off site without strict control. Also, because of some of the difficulties described in the next section, this interpretation time was longer than it should have been. A conservative estimate is 25 hours resulting in an combined estimated time of inspection of 36 man-hours.

Despite the over sampling and extra thorough data interpretation, this combined inspection time,

complete with documentation, is only 13% of the 278 man-hours of visual inspection estimated in the service bulletins, a saving of 242 man-hours. In addition, only a small fraction (14% or 5:30 hrs) of this inspection time is spent on site with the aircraft resulting in less interference with other maintenance personnel.

### **Inspection Procedure**

The inspection procedure defined prior to the inspection resulted in a number of problems. These problems are associated with the direction and placement of the sensor along the lap splices and the orientation and sequence of the resulting images during interpretation and surface registration.

The inspection sequence was initially set to be from forward to aft along the horizontal lap splices and from top to bottom on circumferential lap splices. The top of the image corresponds to "top" on a horizontal lap splice when the sensor is held with the connecting cable to the right of the inspector. By moving, forward to aft, with this orientation of the sensor on the left hand side of the aircraft, the sensor is pushed into the cable which is not very desirable. However, the image sequence is quite natural with the right side of one image corresponding naturally to the left side of the next image in a left-to-right, top-to-bottom presentation.

On the right hand side of the aircraft, a forward to aft movement of the sensor with "top" remaining upward causes a problem. Even though the sensor cable is now being pulled along, the presentation of the resulting images in a left-to-right, top-to-bottom order causes local inflections in the image presentation. This order caused a number of problems in determining the body stations in the image since the image sequence did not "flow" naturally in the standard left-to-right, top-to-bottom presentation. A significant amount of time was wasted just making sense of the image progression along the lap splices on the right side of the aircraft. For stringer number 4, an aft to forward direction was chosen for sensor movement and the resulting image presentation was again quite natural. It was concluded that future inspections should be counterclockwise around the aircraft relative to a top view and that the sensor should be modified to invert "top" so that the cable is pulled during inspection rather than pushed.

The circumferential inspections were initially set to be from top-to-bottom before any problems were

recognized. This orientation causes the top of the image to be in the forward direction on the left hand side of the aircraft and in the aft direction on the right hand side of the aircraft. Due to the curvature of the surface and the need to keep ambient light from overhead lights out of the sensor, it was decided to keep the cable connection end positioned upward and the sensor held firmly to the surface at the connector end. This up direction for the sensor creates some difficulty in handling the sensor due to the cable position and in generating image sequences that follow a natural progression. By inverting the camera, as proposed for horizontal lap splices, two problems are solved. The cable will be in a down direction which is desirable but the inspection should be started from the bottom of the fuselage and progress upward in order for the image sequence to be natural. This bottom-to-top inspection sequence has the added benefit that excess highlighter will not drip inside the sensor because the direction of sensor movement is in the opposite direction from gravity. To solve the ambient light problem, it may be necessary to add additional skirt material at the two ends of the sensor as well as longer feet or repositioned feet to prevent the sensor from rocking on the surface.

### **Hardware & Software Operation**

The DAIS-250C sensor worked as expected and did not create problems with the exception of circumferential inspection due to the placement of the sensor feet. The foam skirt around the perimeter of the sensor could also be longer for these circumferential inspections. It was found that the field of view dropped from 560 mm (22 in.) to about 330 mm (13 in.) for circumferential placements. To keep the field of view long, it would be necessary to lengthen the retroreflector vertically inside the sensor. However, because of the extreme curvature, the sensitivity change across the field of view would be even more dramatic than currently exists and this is not recommended.

The placement and number of handles were found to be acceptable and the weight of the sensor did not create much difficulty or discomfort for the inspector. Over 750 placements of the sensor were executed in all orientations but most were below the shoulder of the inspector.

During the final hours of inspection, the remote pendant was accidentally dropped from about 4.5 m (15 ft) to the hangar floor when too much strain was placed on the velcro strap fixed to a hand rail. The pendant handle and case were bent but the pendant continued to operate normally. Only the small video monitor appeared to suffer some electrical problem but this cleared up upon return

of the unit to Diffracto after connections were checked over.

The software, both in the pendant and host, worked as expected. The log file system designed for DAIS including the filename convention for image files will create some difficulty for the AANC database since they expect each filename to uniquely define a location on the aircraft. The convention used with DAIS was to uniquely define the start location of an inspection with filename extensions automatically incremented by one. Over 750 images will have to be renamed by AANC to enter the images into their database. The identification and recording of body station numbers given any image is currently difficult especially when sensor placement errors are made. The only way to enter this information is through the optional comment field. However, commenting slows the speed of inspection and was not used during this test. By far, the most time consuming aspect of analysis is identifying the body station in a given image. Reducing this time will allow the inspector to analyze the image for corrosion much more efficiently.

Due to the expected number of images, it was decided to by-pass the one image per page printing facility in DAIS and use an external utility that would print six images per page on the HP4 LaserJet printer. Even with this print utility, a significant number of pages were printed. The capability of this utility should be incorporated into DAIS software so that multiple images per page can be printed along with the associated log file enter and comment. Only filenames were printed under each image using the utility.

One major shortcoming of the DAIS system is the inability to record inspection results either on the image or in a summary form after the images are analyzed. Some serious thought should be given to this problem so that the DAIS system is more than just a system to acquire raw data. The circumferential lap splices make this task more difficult since the butt splice has two sides that could be corroded.

## CONCLUSIONS AND RECOMMENDATIONS

The field trip to AANC with the new DAIS-250C corrosion sensor was very successful for what was learned or the advantages discovered, namely;

- the sensor weight, size, and sensitivity was judged acceptable for a two man crew and the inspection task
- the inspection rate was found to be considerably faster than other visual inspection procedures
- the raw data captured formed a permanent record and could be analyzed off site by an experienced inspector unlike other visual inspection techniques
- the shortcomings associated with the inspection procedure both physically and for analysis purposes were learned and noted
- the need for additional aids to improve the registration of images to the surface were recognized and experienced
- the need for computer tools to help report corrosion results were recognized
- the need to improve the printing capability of the DAIS system was reinforced by the large volume of data gathered
- the need to find a tape/disk backup/storage device as part of the DAIS system became evident based on the amount of data gathered for one aircraft inspection

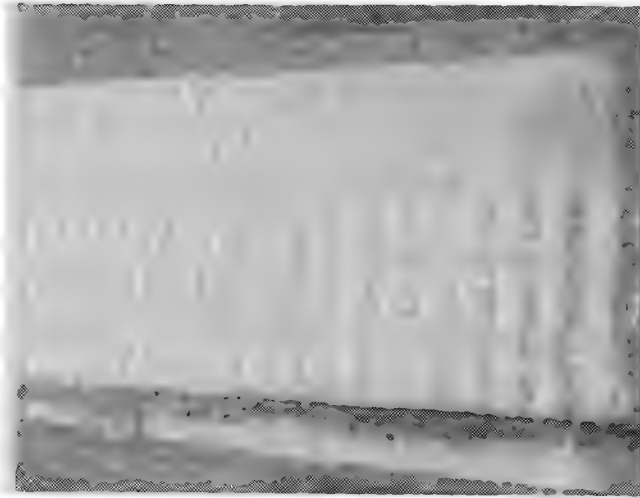
Based on this experience, the DAIS-250C sensor should be modified by rotating the camera 180

degrees so that the cable is pulled rather than pushed during inspection. Software improvements should be made to the print function and new software should be introduced to have the ability to record corrosion results through the computer. A search for a tape storage device, or alternatively, a hardware compression/decompression board should also be undertaken and procured.

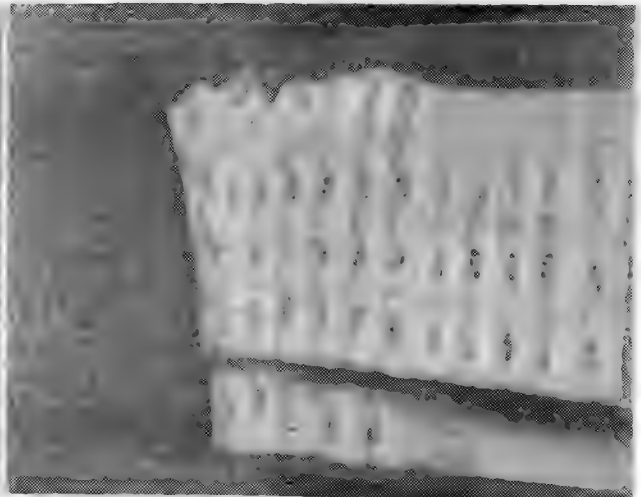
The analysis of *D SIGHT* images for corrosion should be documented fully along with the theory of why *D SIGHT* is effective for corrosion detection so that others can be trained to identify and interpret corrosion signatures.

## **APPENDIX A**

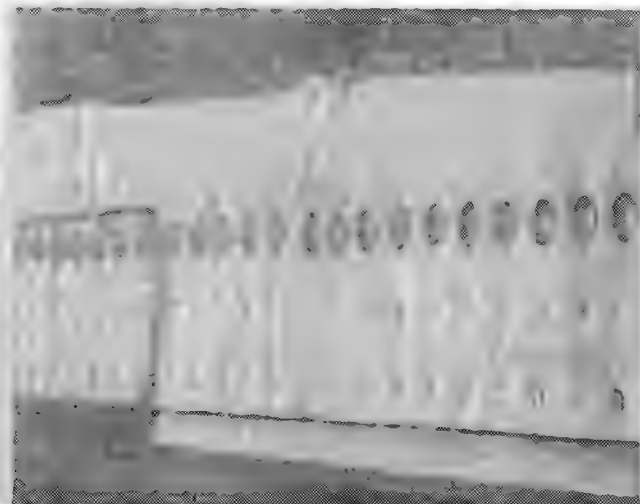
### **SAMPLE IMAGES OF HORIZONTAL LAP SPLICES**



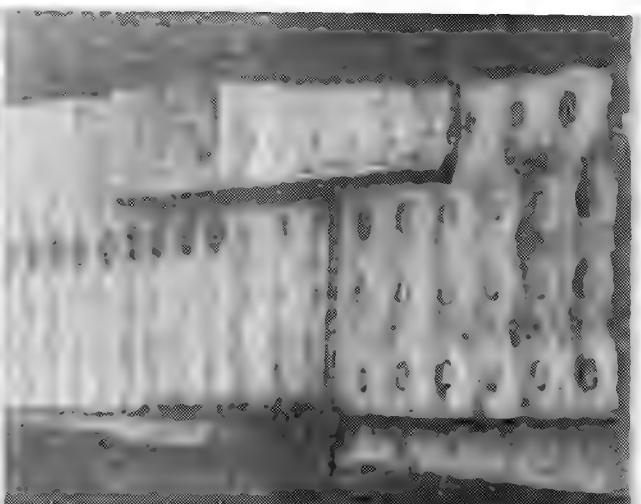
R19-2595.014



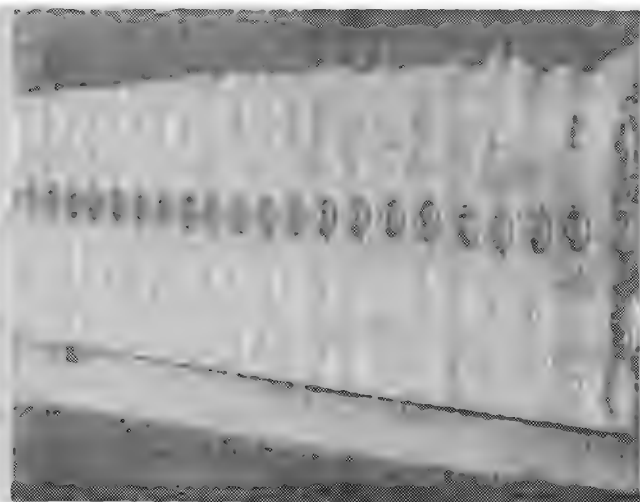
R19-2595.020



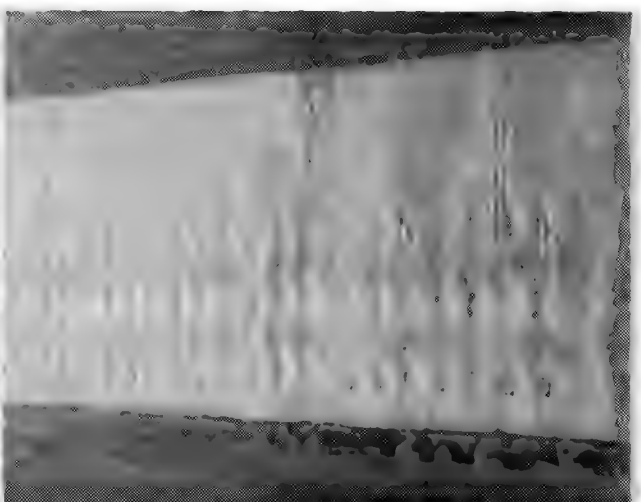
L25-747.013



R25-747.012



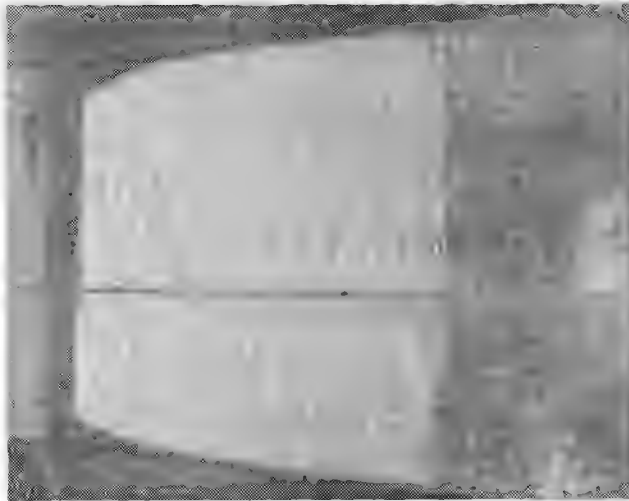
R20-767.013



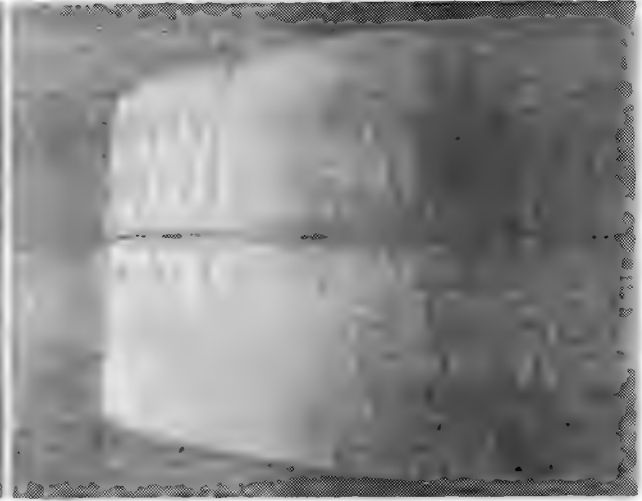
L26-2595.019

## **APPENDIX B**

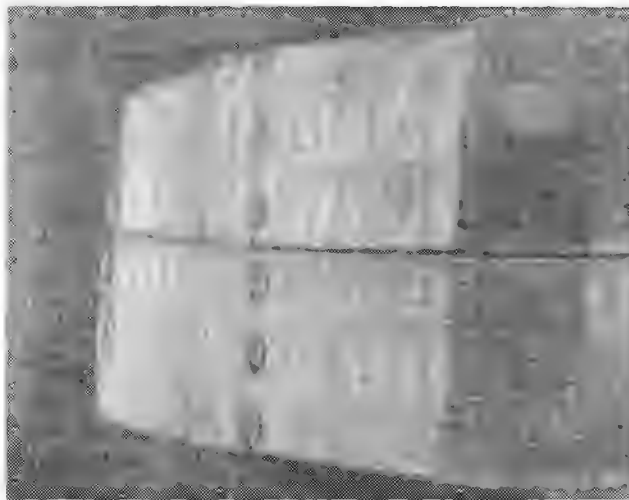
### **SAMPLE IMAGES OF CIRCUMFERENTIAL LAP SPLICES**



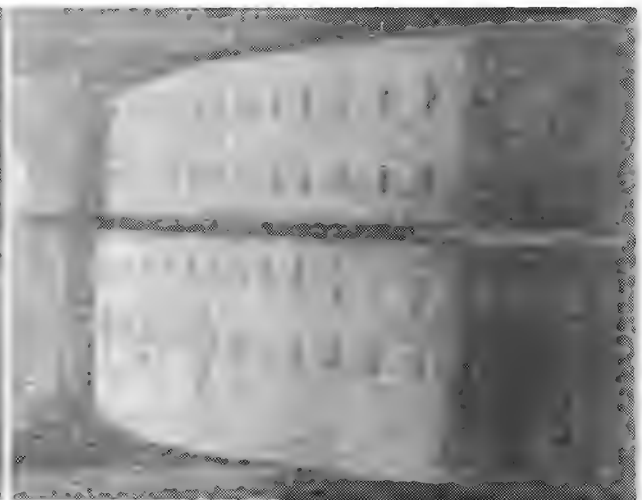
R747-4.003



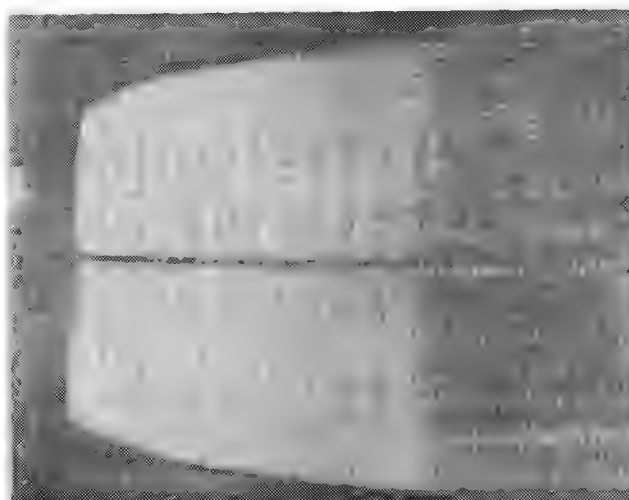
R907-4.007



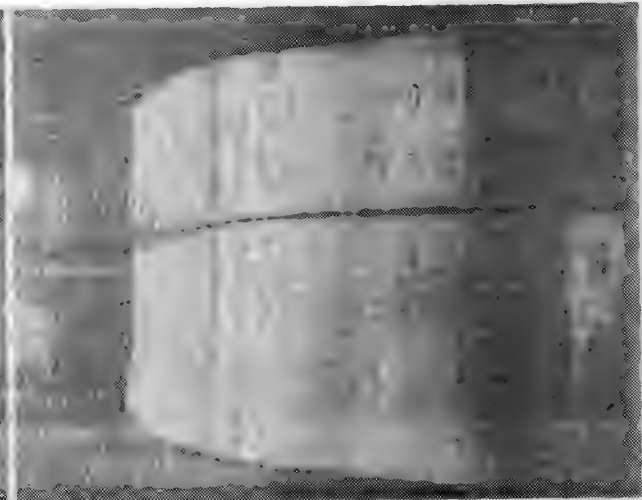
R907-4.016



L727-4.008



L907-4.005



L907-4.007

## APPENDIX F

Task 5.11, Part 2 of 2, DAIS-250C Field Trial, Air Canada, Winnipeg,  
Manitoba, by J. P. Komorowski, Don Clarke, and F. Karpala, January 1994.

**Development of a *D SIGHT* Aircraft  
Inspection System - Phase I**

**Task 5.11, Part 2 of 2  
DAIS-250C FIELD TRIAL  
Air Canada, Winnipeg, Manitoba**

**SSC File # XSD92-00184-(621)  
Contract # T8200-2-2544/01-XSD**

**by**

**Jerzy Komorowski  
Don Clarke  
Frank Karpala, PhD**

**January, 1994**

**DiffRACTO Ltd.  
2835 Kew Drive  
Windsor, Ontario  
N8T 3B7**

**519-945-6373  
FAX 519-945-1467**

---

## **INTRODUCTION**

The following trip reports were filed by two of the participants to the Air Canada maintenance facilities in Winnipeg, Manitoba. The purpose of the field trip was to inspect a DC-9 for lap splice corrosion with the new DAIS-250C sensor to test its sensitivity, ease of use, and acceptability by NDI personnel.

## **REPORT - JERZY KOMOROWSKI**

Air Canada Maintenance Base Winnipeg, Man.  
January 11-12, 1994.

### **Participants:**

Jerzy P. Komorowski, Ronald W. Gould - IAR-NRC  
Don Clarke - Diffracto Ltd.  
Bill Miller - Transport Canada

Air Canada contact: David Brooks, General Foreman Aircraft Maintenance (204) 941-2030.

January 11th. at 7:30 am the participants were met at the Air Canada Maintenance base by Mr. D. Brooks. An office was provided for our use and we received a brief introduction to the facility and staff. We were escorted around the Air Canada DC-9-32 (AC 747) which was undergoing a D2 check. The aircraft was chemically stripped of all exterior paint. Most of the aircraft was accessible for inspection from temporary scaffolding. The *D SIGHT* Aircraft Inspection System (DAIS) 250C was on site. It was unpacked and set up for inspection within 15 minutes. A short discussion was held with the Air Canada staff including Mr. D. Brooks, B. Copeland (DC-9 day shift foreman) and B. Dillon (NDT Dorval). The areas for inspection were agreed upon and work began soon after. The surface condition of a stripped aircraft required the use of highlighting fluid. All prior DAIS inspections were carried out using kerosene based highlighter. Since this raised environmental and safety concerns at some of the locations visited in the past, a new highlighter fluid was used. This is an environmentally preferred dielectric solvent, called ELECTRON, which leaves no residue and

evaporates within a short period of time. This fluid was suggested as a candidate highlighter by USAF personnel during the visit to MacLellan AFB. This was our first opportunity to use Electron and it proved to be an excellent replacement for kerosene based highlighters.

Inspections were carried out on sections of longeron 1, 7R, 11R, 15R, 18R, 23L, 26L, 26R and 30. Portions of circumferential splices were also inspected: 1078, 803 and 588. Air Canada personnel were given the opportunity to operate the DAIS equipment. The inspections attracted significant interest from the Air Canada staff and management (Mr. G. Hirose - Chief Engineer, Mr. R. Elvidge - Heavy Maintenance Manager, Mr. J.F. Lavis - Chief Inspector Aircraft). While the DAIS work continued some of the participants were collecting comments from the observers.

Preliminary analysis of the results did not reveal any areas of significant corrosion. Several sections along inspected stringers appear to contain a low level of corrosion. The strongest indication of corrosion was from the short section of stringer 18R. This observation was reinforced after the discussion with Air Canada personnel which revealed that:

- (i) it is unlikely that this area was opened during maintenance and resealed
- (ii) excessive amounts of sealant are not typical on DC-9 lap splices

Excessive application of sealant is one cause other than corrosion for pillowing detected by *D SIGHT*.

The areas inspected and suspected to contain corrosion are shown on Figure 1. It would be desirable to verify *D SIGHT* findings with low frequency eddy current techniques. A negative result from the eddy current test would confirm that the corrosion level is low, however the area should be monitored more frequently in the future. Depending on the availability of funding a specimen of stringer 18 lap splice could be subjected to accelerated corrosion testing thus allowing us to 'calibrate' the on-aircraft finding.

Mr. Elvidge expressed two concerns: the lack of *D SIGHT* calibration standards and the need for the equipment to meet explosion proof standards. The second concern will be addressed in a production version of the DAIS equipment the first relates to the very high sensitivity of *D SIGHT* to corrosion which was not appreciated at the beginning of the current project. It was then envisaged that

*D SIGHT* equipment will only isolate possible corrosion areas for subsequent inspection by 'accepted' but slower NDI methods (i.e. eddy current). This strategy of *D SIGHT* use will have to be re-evaluated. The high sensitivity to corrosion of *D SIGHT* is very encouraging as it offers early warning to the operator of possible future problem areas. An early corrosion area should be subjected to *D SIGHT* inspections more frequently and followed up by accepted NDI methods only if significant changes from previous *D SIGHT* inspections are observed. This approach has an added advantage of allowing better scheduling of preventive maintenance. A combined accelerated corrosion testing and modelling of lap splice corrosion will provide calibration images which could be used by DAIS inspectors.

An Air Canada A320 (AC 223) was undergoing a C check in an area adjacent to the DC-9. Small sections of a lap splice under the belly and the lower surface of a left wing flap were inspected with DAIS. This was aimed at demonstrating the ability to perform an inspection of a painted aircraft surface without highlighter and to inspect composite surfaces (typically for impact damage). No defects were found in the inspected areas as was expected given the age of the A320. Noted were smooth splice surfaces resulting from the automated riveting process. Several Air Canada employees noted that *D SIGHT* inspections of new aircraft would be advantageous for warranty inspections. Possible discrepancies could be easily recorded and monitored, observations documented and conveyed to the manufacturer. Comparing aircraft of the same type could also help spot potential problems. One such area are undocumented repairs in composites prior to delivery from the OEM which seem to cause difficulty during ultrasonic inspections.

The second day, January 12, the DAIS equipment was moved to the second Air Canada hangar where two Continental aircraft (an MD-80 and a B-727) were undergoing maintenance. The participants obtained permission to inspect a portion of the B-727 (N27783) skin from BS1010 to BS1183 between stringers 26 left and right. This portion of the skin will be removed and replaced. The IAR-NRC participants arranged for the scrapped skin to be shipped to NRC for subsequent investigation and comparison with the *D SIGHT* images. The inspected area was subjected to previous maintenance work and some sections were observed to contain new sealant. All locations which were suspected to be corroded are marked in Figure 2.

The B-727 aircraft was jacked up for maintenance work. This required the DAIS 250C head to be held overhead for the inspection. The participants who took turns in order to gain experience in all

aspects of DAIS inspection have agreed that at 11 lb. the head is still heavy. The lighter cable used in subsequent breadboard systems should also help alleviate the strain on the person holding the inspection head.

At the conclusion of day two, a short debriefing session was held in the office of Mr. D. Brooks, Mr. J.F. Lavis, Mr. B.Dillon of Air Canada as well as all trip participants attending. The results of the inspections were discussed as well as potential benefits to Air Canada which could be realized from *D SIGHT* equipment deployment. It is difficult for any operator to justify a purchase of equipment which is not recommended by the OEM or approved by a certification agency. An operator may request from such an agency approval for alternate means of compliance and this could be a possible route for *D SIGHT* to become an approved NDI method. It is encouraging that in the words of a senior Air Canada staff member : "*D SIGHT* equipment would pay for it self in the first year". It was agreed that given the proximity of IAR-NRC (Ottawa) to the Dorval, Que. Air Canada base, further *D SIGHT* evaluations could be arranged in the future to further explore the possible applications of the new technology.

The participants thanked Air Canada for hosting the DAIS field evaluation, and for creating an environment which was conducive to fruitful exchanges between the visitors and Air Canada staff engaged in aircraft maintenance and inspection.



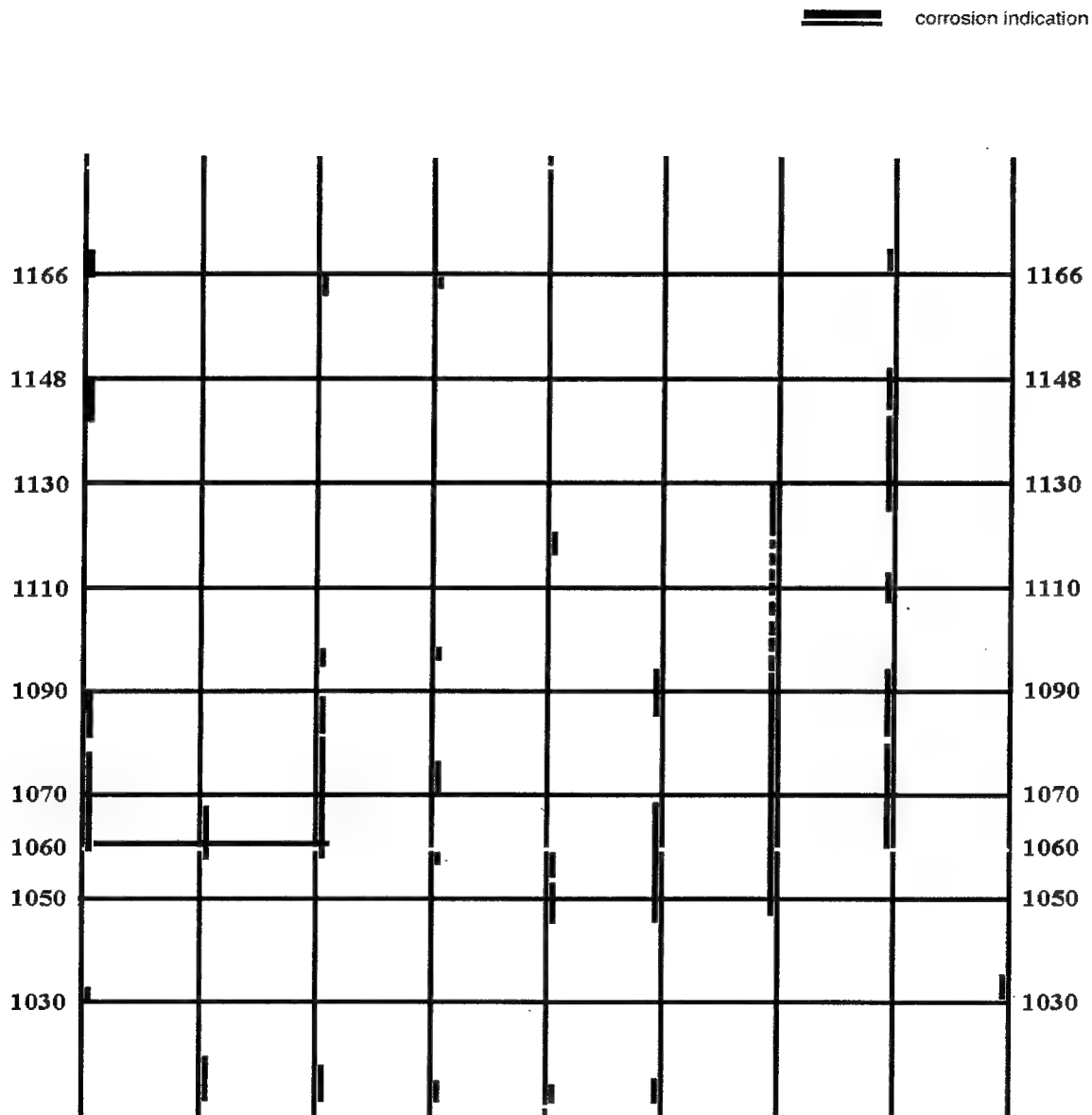


**Figure 2:** Results of *D SIGHT* inspection of B-727 between stringers 26 left and right

**REPORT - DON CLARKE**

Visit to Air Canada Maintenance Facility, Winnipeg, Manitoba

Jan 11 - 12 / 94

Attendees: Jerzy Komorowski - NRC  
Ron Gould - NRC  
Bill Miller - Transport Canada  
Don Clarke - Diffracto Ltd.

The overall impression that the Air Canada people formed, seemed to be very positive. Much interest was shown by NDI, engineering and management alike, and those that operated the system, commented upon it's ease of operation. They also thought that the interpretation of the images, could be easily learned in a couple of days of practice. They felt that the inspection technique, was very sensitive, and could help them to zero in on the areas that needed inspection by the more conventional eddy-current method. The chief inspector of the A320/B727 fleet, Mr. J.F. Lavis, stated that he thought the unit could pay for itself within a year, if it was sold for around \$50K.

Originally we were to inspect a DC-9 only, but it was arranged with the help of Dave Brooks, the general foreman, to have a quick look at a new A320, just to show how *D SIGHT* can be used on composite panels with just as much ease as aluminum skins. We were also given a great opportunity to document an older Continental Airlines B727 that was being serviced under contract by the Air Canada facility. This aircraft was having a couple of belly panels changed due to severe corrosion, and the panel we carefully inspected before removal will be shipped to NRC where we can correlate our results with the actual amount of corrosion present.

Here is a brief, unordered list of things to consider when making the next version of the DAIS unit. Some of these notes were suggestions by Air Canada (AC), and some are observations by myself:

- Image display on any computer, for ease of later engineering discussions. (AC)
- A selection of preset WOI's for illumination control differences between circumferential and lap joints.

- The cables always seem to be getting tangled.
- Disappointment was expressed that the equipment did not have a threshold one could set for automatic go/no-go decision of corrosion level.  
(AC)
- There was talk that new planes could be mapped completely, for later comparison purposes, though no one knew how this could actually work in practice. Auto position detection and/or prompting for the next position, and some database manipulation program seems to be necessary for this type of work. (AC)
- "ELECTRON" highlighter seemed to work well and was readily accepted as a safe fluid by Air Canada. It did have a narrow tolerance to the amount that was applied (runs easily or is too dry) but the lack of any odour was great.
- Something is needed to help you align the sensor to the next inspection zone. Either a monitor for the person holding the head, or some extension rods on it's sides, visible while in the normal holding posture.
- It was recommended that the unit be housed in a single enclosure; a 'flight kit' that could be easily transported and set up at a remote facility.  
(AC)
- All demo's in hangars should have their own equipment cart as it took us quite a while to find a suitable one.
- The sensor head is still too heavy for extended overhead inspection (almost the exclusive mode for this trip).
- The unit and it's inspection procedures are easily integrated into the work environment (flexible, small army of mechanics).
- All equipment for Air Canada must have APPELTON power connectors. The use of a line regulating transformer seems to be an unavoidable necessity.

## CONCLUSIONS

The results of the field trip, as reported by Jerzy and Don, and supplemented by private communication with Bill Miller, from Transport Canada, indicates a very successful demonstration of the new DAIS-250C sensor. The response of the Air Canada NDI personnel was very favourable to the use of *D SIGHT* and the DAIS equipment. Receipt of the scrapped skin from the B-727 will be very valuable to the correlation of the inspection images with physical evidence. This contribution by Air Canada is greatly appreciated.

Each field trip results in learning something new about the inspection environment, equipment shortcomings, inspection procedure, and the reaction of NDI technicians and management to the equipment. The findings of this field trip will be used along with the findings of the field trip to AANC in Albuquerque, NM to recommend changes to the hardware, software, and inspection procedure for the prototype system.

## APPENDIX G

DAIS Applications, D Sight Aircraft Inspection System for Corrosion  
Inspection, Version 1.0, November 1993, Diffracto Limited.

## **DAIS APPLICATIONS**

### ***D SIGHT* Aircraft Inspection System for Corrosion Inspection**

Diffraction Limited  
2835 Kew Drive  
Windsor, Ontario, Canada  
N8T 3B7

US: (313) 965-0140  
Canada: (519) 945-6373

© Copyright 1993 Diffraction Ltd.

*D SIGHT* is a trademark of Diffraction Limited

VERSION 1.0  
NOVEMBER 1993

Copyright (1993) Omer L. Hageniers, President; Diffraction Limited, Owner.  
Reprinted with permission.

## TABLE OF CONTENTS

LIST OF FIGURES . . . . .	iii
1 INTRODUCTION . . . . .	1-1
2 SENSOR DESCRIPTION AND SPECIFICATIONS . . . . .	2-1
2.1 Description . . . . .	2-1
2.2 Specifications . . . . .	2-2
2.3 Maintenance . . . . .	2-3
3 CORROSION DETECTION THEORY . . . . .	3-1
3.1 <i>D SIGHT</i> Principles . . . . .	3-1
3.2 Corrosion and Physical Indications . . . . .	3-1
4 SURFACE PREPARATION . . . . .	4-1
4.1 Purpose . . . . .	4-1
4.2 Highlighters and Their Properties . . . . .	4-2
4.3 Application Procedure . . . . .	4-2
5 INSPECTION PROCEDURE . . . . .	5-1
6 INTERPRETING IMAGE SIGNATURES . . . . .	6-1
6.1 <i>D SIGHT</i> and Surface Geometry . . . . .	6-1
6.2 Key Signature Features . . . . .	6-3
7 APPENDIX . . . . .	7-1

## LIST OF FIGURES

Figure 1: DAIS-250C Sensor Configuration . . . . .	2-1
Figure 2: Surface profile of horizontal lap splice . . . . .	3-2
Figure 3: Surface Deflection as a function of Material Loss . . . . .	3-3
Figure 4: Painted lap splice without highlighting . . . . .	4-1
Figure 5: Same lap splice, highlighted . . . . .	4-1
Figure 6: Unpainted lap splice without highlighting . . . . .	4-2
Figure 7: Same lap splice, highlighted . . . . .	4-2
Figure 8: Uneven application of highlighting fluid . . . . .	4-3
Figure 9: Application of too little highlighter . . . . .	4-3
Figure 10: Too much highlighter on a horizontal surface . . . . .	4-4
Figure 11: Too much highlighter on a vertical surface . . . . .	4-4
Figure 12: Highlighter streaks across the sensor's view . . . . .	4-4
Figure 13: Highlighter streaks along the sensor's view . . . . .	4-4
Figure 14: Small highlighter runs from rivet heads . . . . .	4-5
Figure 15: Orientation of sensor and <i>D SIGHT</i> image . . . . .	5-1
Figure 16: <i>D SIGHT</i> signatures when viewed across depression row . . . . .	6-2
Figure 17: <i>D SIGHT</i> signatures when viewed along depression row . . . . .	6-2
Figure 18: Lap splice corrosion signatures . . . . .	6-3
Figure 19: Circumferential lap splice corrosion . . . . .	6-3
Figure 20: Weak signatures of corrosion . . . . .	6-4
Figure 21: Lap splice corrosion on bare aluminum . . . . .	6-4
Figure 22: Two types of corrosion signatures . . . . .	6-4
Figure 23: Severe corrosion signatures and uncorroded area . . . . .	6-4

## 1 INTRODUCTION

The purpose of this application manual is to provide the user with information and guidelines to successfully inspect aircraft for lap splice corrosion using the *D SIGHT* Aircraft Inspection System (DAIS) and the DAIS-250C corrosion sensor. The detection of corrosion is based on the principal that corrosion products occupy a significantly greater volume of the surface than the original metal. As a result, the metal surrounding rivet fasteners becomes distorted or pillows with increasing levels of corrosion forming distinct local curvature changes. By detecting the presence and level of pillowing as corrosion indications, the presence and level of corrosion can be inferred.

The DAIS-250C corrosion sensor, using *D SIGHT*, produces a full field visually enhanced view of pillow curvatures in real time. This enhancement is achieved by Diffracto's patented two pass illumination of a reflective surface using a light source at a low grazing angle and a retroreflective screen. When the local curvatures on the surface are viewed or imaged from the principal light source, the light returned by the retroreflective screen and reflected off the surface creates distinct gray scale signatures at the surface in proportion to the amount of local surface curvature. This optical arrangement is extremely sensitive to subtle surface curvatures caused by pillowing and reveals the presence of sub-surface corrosion even at very low corrosion levels as distinct image signatures.

The operation of the corrosion sensor is controlled from the DAIS computer system. A host controller, remote pendant, laser printer, and power supply form the basic system components. These components and their operation are fully described in the DAIS User's Guide. Depending on the application, different sensors are available to connect to this basic system including the DAIS-500 sensor for impact damage inspection on composite surfaces. For lap splice corrosion applications, the DAIS-250C was specifically designed and configured to maximize sensitivity to corrosion indications while providing a lightweight sensor with a footprint that takes advantage of the long but narrow lap splice geometry on aircraft. All sensors in the DAIS family use *D SIGHT* technology to visually enhance local surface curvature and may be used for other applications but possibly at reduced sensitivity or resolution.

This manual explains how to operate the DAIS-250C sensor, what physical indications of corrosion are detected for the presence of corrosion and why they occur, why the DAIS corrosion sensor is sensitive to these corrosion indications, how to visually interpret the sensor data, and how to inspect large areas of aircraft for corrosion rapidly and effectively. Included in the manual are a description of the corrosion sensor specifications and sensor maintenance, a section on effective highlighting of non-reflective surfaces, and a section describing a procedure for efficient inspection of aircraft lap splices.

## 2 SENSOR DESCRIPTION AND SPECIFICATIONS

### 2.1 Description

The DAIS-250C sensor is designed with a thin aluminum skin enclosure to be rugged but lightweight at the same time. Sensor weight is 5 kg. (11 lbs.). Areas that need additional structural support are reinforced with thicker material. Two internal partitions maintain rigidity, provide attachment points for components, and act as blockers to shield the surface from stray light from the internal light source. Two mirrors are used to reduce the overall size of the sensor while maintaining a 1.2 m. (4 ft.) optical path length from the surface to the camera. A schematic diagram of the sensor and its internal components is shown in Figure 1.

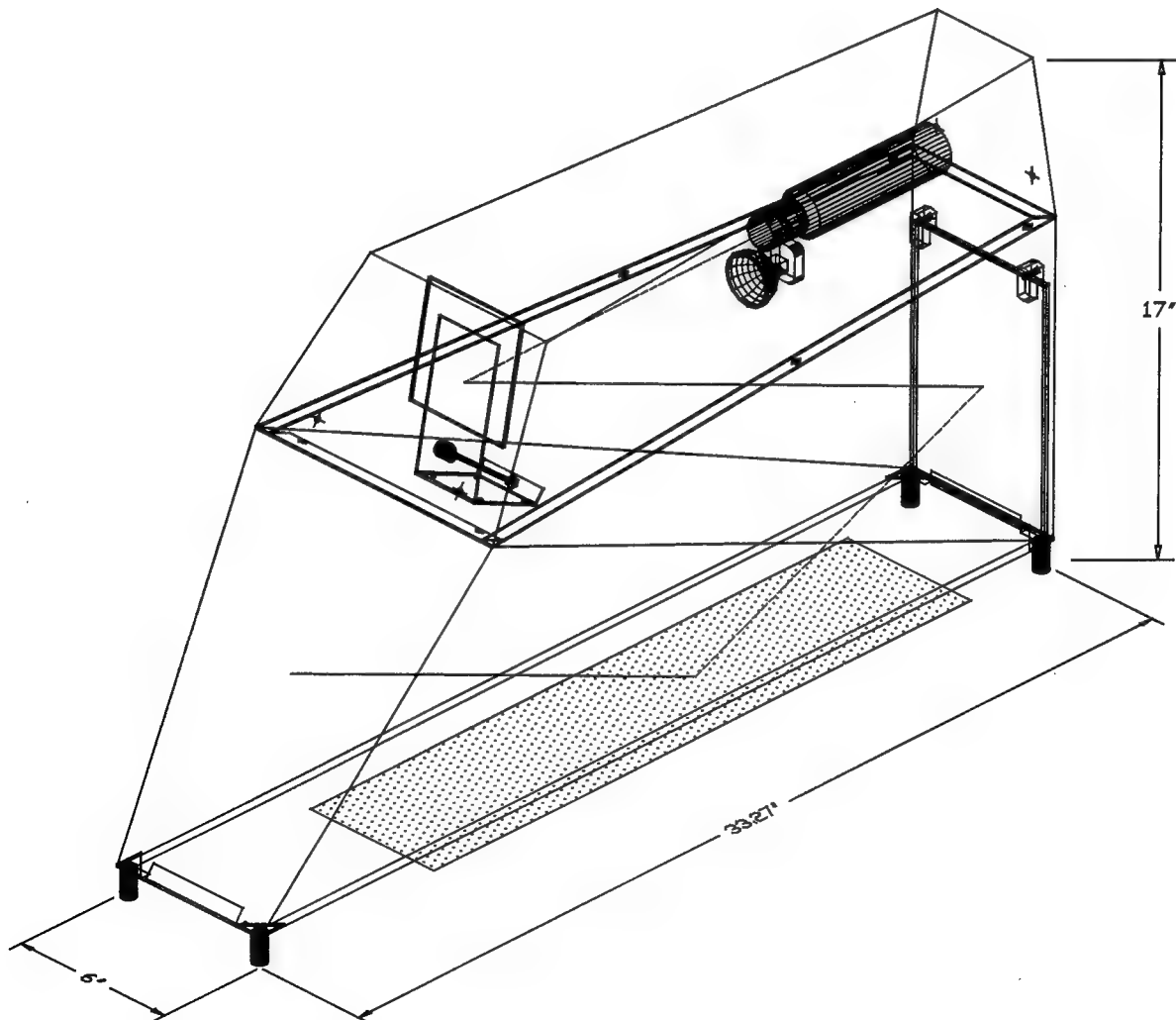


Figure 1: DAIS-250C Sensor Configuration

Internally, a CCD camera is mounted in a horizontal position on its side. This orientation maximizes the use of the aspect ratio of the camera and the 22.5 degree perspective angle to create a long but narrow field of view along a lap splice. The inspection area is approximately 130 mm (5.1 in.) wide and 540 mm (21 in.) long. When the sensor is held horizontally on the surface with its cable to the left of the inspector, the field of view displayed on the video monitor will be consistent with the inspector's orientation to the surface. The halogen light source is mounted below the camera lens. Since the source is a 20 watt bulb, the amount of heat dissipated is small and the partition protects the inspector from accidental contact. The size of the light source reflector is 50 mm. (2 in.) and helps remove high frequency noise in the image from surface textures. The retroreflective material is coated so that highlighter and other contaminants will not damage its surface. Its position is 467 mm. (18 in.) from the origin of the field of view at 55 degrees from the surface.

The sensor is equipped with five rigid handles to provide positional control in all orientations. The power/signal cable is mounted high up on the narrow end of the sensor to minimize interference with highlighted surfaces. Four rubber feet support the sensor 25 mm. (1 in.) above the surface to allow for inspection of curved surfaces. A flexible skirt around the entire lower perimeter is provided to reduce the influence of strong ambient light entering the inspection area.

The top of the sensor is removable for cleaning and servicing the internal components. Six screws hold the cover to the lower base section. Access to the screws is from the open end of the sensor.

## 2.2 Specifications

### Physical Specifications

Size	851 L x 152 W x 432 H mm. (widest point 254 mm.) 33.5 L x 6 W x 17 H in. (widest point 10 in.)
Weight	5 kg. (11 lbs)

### Optical Specifications

Camera to surface distance	1.2 m.	(49 in.)
Surface to retroreflector	457 mm.	(18 in.)
Camera grazing angle	22.5 deg.	
Camera lens	50 mm.	@ f8
Camera aspect ratio	4:3	(along lap:across lap)
Lamp type	20 W, Halogen,	50 mm. (2 in.) reflector
Lamp location	38 mm. (1.5 in.)	below lens axis
Field of view	130 mm. x 540 mm.	(5.1 in. x 21 in.)
Mirrors	2 (regular 3 mm. thick)	

## Electrical Specifications

Camera	CCD solid state, 512 x 480 pixels, 12 VDC
Lamp	20 W, 12 VDC, 2000 hr. life or greater

## Shipping Case

durable, lockable	114.3 cm W x 40.6 cm H x 63.5 cm D 45" W x 16" H x 25" D
-------------------	---

### 2.3 Maintenance

During regular use, the components that may require occasional cleaning are the large mirror attached to the inside wall holding the sensor connector and the retroreflective screen on the opposite wall. Both these components are accessible without removing the sensor cover. These components are most susceptible to fingerprints and contamination by highlighter especially when used up-side-down. Clean both surfaces with a damp soft cloth and mild detergent and wipe dry. Do not flood the surfaces or else the components may be permanently damaged. **Make sure the sensor is turned off and disconnected before cleaning any internal component.**

If a small fuzzy area is visible in the image and does not change position with sensor movement, it is likely that the small mirror in front of the camera is dusty or dirty. It is best to clean this mirror with the sensor cover off. Before removing the cover, **make sure the sensor is turned off and disconnected.** The cover is removed by loosening 6 allen screws from the bottom opening. These screws are located along the side flanges inside the sensor. After removing the screws, make sure the cover is pulled straight off the base or the small mirror could be damaged. Clean the small mirror in the same manner as the large mirror but be careful not to twist it. Attach the cover by gently placing it straight over the base and screwing it to the base from the bottom opening. Be careful not to let the cover shift while replacing the screws.

### 3 CORROSION DETECTION THEORY

#### 3.1 *D SIGHT* Principles

The *D SIGHT* technology in each DAIS sensor uses a CCD camera, a white light source mounted slightly below the camera lens, and a retroreflective screen. The retroreflective screen is a critical optical element in *D SIGHT* that returns light falling on its surface in the same direction as the incident light. The light returned by the retroreflector is slightly dispersed due to the physical and optical characteristics of the micro-beads but returns most of the light along the incident direction toward the light source.

When the inspected surface is illuminated by the light source, local curvature variations on this surface act to focus or disperse the light onto the retroreflective screen. The pattern or primary image formed on the retroreflector is unique for that surface and defines a distinct distribution of directional light just in the right position for backlighting the surface. By viewing the surface slightly off-axis from the primary light source and because the light returned is slightly dispersed by the retroreflector, the unique pattern from the retroreflector is seen through the surface near the local curvature distortions as bright and dark gray scale variations. Higher curvature variations which focus or de-focus the light more intensely will have greater image contrast so that the degree of surface deformation can be inferred from the contrast in the *D SIGHT* image. To operate properly, the surface must be reflective. When it is not, a thin liquid film must be applied to increase reflectivity. The procedure to do this is explained in chapter 4.

Because *D SIGHT* is an optical technology in the visible spectrum, it can only detect surface distortions at the upper most layer of the surface. Any subsurface disturbance of the upper most layer causing a physical deformation will be detectable by *D SIGHT*. It is this type of physical indication that makes *D SIGHT* very sensitive to corrosion in lap splices.

#### 3.2 Corrosion and Physical Indications

The oxidation of aluminum and its alloys can result from chemical reactions involving a liquid phase where an electrically conducting solution is present or from a metal/gas or metal/vapor reaction where non-metals lead to a formation of a film or scale on the metal. Uniform, crevice, intergranular, exfoliation, and filiform types of corrosion are the most common forms found on aircraft and are the best candidates for detection by *D SIGHT*.

Corrosion products may appear visibly on the surface of the metal as white or gray powdery deposits or may be hidden at the interface between two metal layers. One property of aluminum oxide that enhances detection at an interface is its volume increase as it transforms from metal to oxide. Table I below summarizes the properties of three different oxides of aluminum.

Table I: Selected Properties of Aluminum and its Oxides [1]

	Formula	Molecular Weight	Density (gms/cc)	Molecular Weight Ratio	Molecular Volume Ratio
Pure Aluminum	Al	26.98	2.702	1	1
Aluminum Oxide	Al <sub>2</sub> O <sub>3</sub>	101.96	3.965	3.779	2.575
Aluminum Oxide Monohydrate	Al <sub>2</sub> O <sub>3</sub> ·H <sub>2</sub> O	119.96	3.014	4.446	3.986
Aluminum Oxide Trihydrate	Al <sub>2</sub> O <sub>3</sub> ·3H <sub>2</sub> O	155.96	2.420	5.780	6.454

Because the volume ratio between aluminum and its oxides is relatively large, the oxidation products force the material to pillow or deflect between rivet fasteners. The metal deflection between rivets caused by the interlayer forces during oxidation is detectable by *D SIGHT* since the curvature induced in the surrounding area is precisely the type of indication *D SIGHT* is most sensitive to even for deflections as small as 0.025 mm (0.001 in.). Corrosion levels that are sufficiently high enough to cause the material around the rivet to pull through create a relatively simple indication for *D SIGHT* to detect.

The use of the amount of pillowing or surface height deflection as an indicator of corrosion presence and level is supported by surface traces of corroded and non-corroded areas on actual specimens. Figure 2 shows a two dimensional physical profile of a horizontal lap splice from a B-727. The figure clearly indicates that the surface pillowing or bulging between the rivets on the left side increases to a much higher degree than on the right side or along the bottom row of rivets. Eddy current scans between

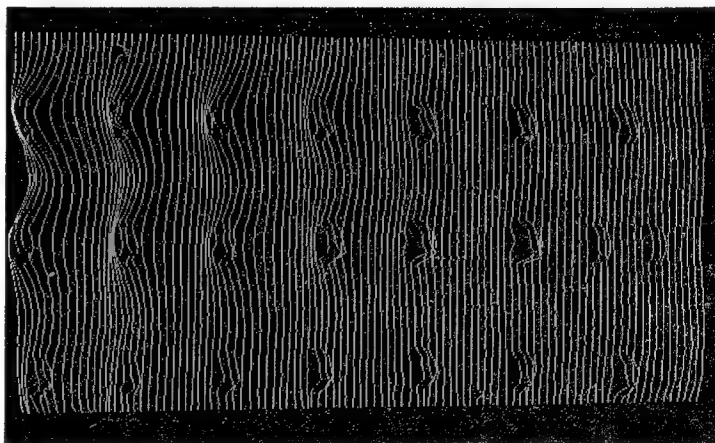


Figure 2: Surface profile of horizontal lap splice

the rivet rows indicate that the percent material loss in the areas of increased surface height reaches 25 percent in the top row and up to 15 percent in the second row. Such evidence supports the notion that the physical deformation of the upper surface has a direct relationship

[1] Krishnakumar Shankar, National Research Council Canada, Institute for Aerospace Research, Ottawa, Ont., private communication

to the presence and level of corrosion found below the surface. A *D SIGHT* image of this specimen is shown and discussed in chapter 6.

From chemical analysis [1], Aluminum Oxide Trihydrate is the primary corrosion product found in aircraft lap splices and can represent 70-100 percent of the corrosion material with a level greater than 90 percent being typical. Theoretical modelling of the corrosion process for a square pattern of rivets indicates that the maximum deflection of the surface occurs in the center between the rivets and the amount of deflection is independent of material thickness. The amount of deflection is mostly dependent on the composition of the corrosion product. Figure 3 shows the expected deflection of the surface as a percentage of the initial material thickness in relationship to the percent material loss for two common oxides present in aircraft lap splices. Using the graph, a 1.25 mm (0.050 in.) skin with a 5 percent material loss would cause a peak surface deflection of 16.7 percent or 0.21 mm (0.008 in.) over a standard 25 mm (1 in.) rivet configuration when the entire corrosion product was composed of aluminum oxide trihydrate.

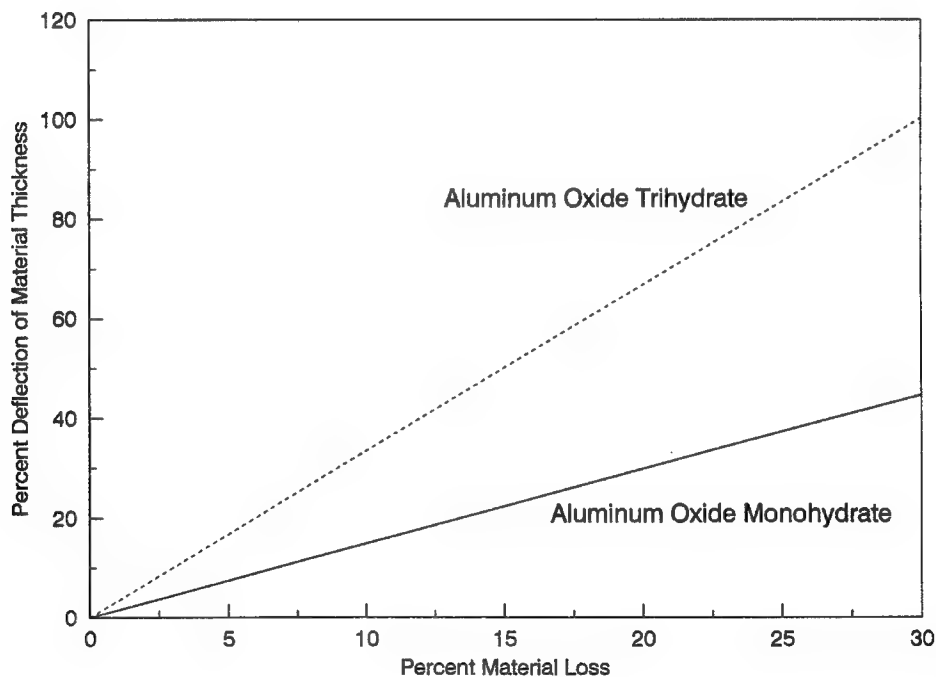


**Figure 3:** Surface Deflection as a function of Material Loss

## 4 SURFACE PREPARATION

### 4.1 Purpose

To form *D SIGHT* images, a DAIS sensor depends on light reflecting twice from the aircraft's surface. Once, as the light rays travel from the source to the screen and a second time as the light retroreflects from the screen back towards the camera. For maximum sensitivity, the inspected surface must have a mirror-like finish similar to that produced by high-gloss paint.

Giving all surfaces a consistent yet temporary reflective finish is best accomplished through highlighting. This is a process whereby a thin liquid film is evenly applied to fill in the surface's microscopic roughness making it reflective without introducing a second liquid surface that may mask the underlying surface variations. For example, Figure 4 shows a DAIS captured view of a section of horizontal lap splice cut from a decommissioned aircraft. From the seam upwards the surface has a white, low gloss paint finish while below the seam the surface is bare aluminum. Although a slight amount of surface deformation is detected around the rivets on the left hand side, the image signatures are very low contrast and ill defined. Overall, the reflectivity of this surface is poor and uneven. Figure 5 illustrates the effect of highlighting this surface. All surface variations, including the "pillowing" around the left most rivets can now be seen clearly as bright white areas.



**Figure 4:** Painted lap splice without highlighting

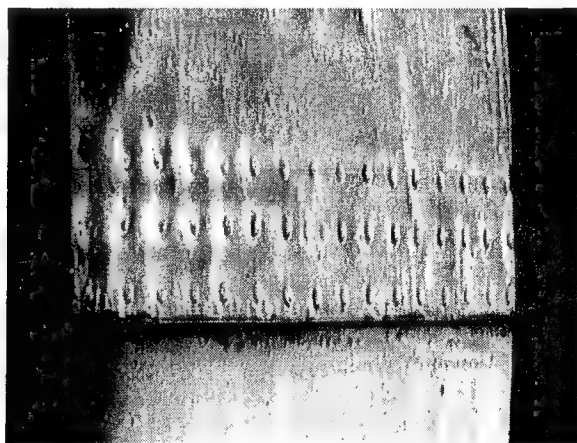


**Figure 5:** Same lap splice, highlighted

Although the bare aluminum skin of an aircraft may appear quite reflective it may still benefit from highlighting. Compare the DAIS image of a bare lap splice in Figure 6 to an image of the same splice after highlighting in Figure 7. The use of a highlighting film produces a distinct improvement in the clarity of the surface variations by increasing image contrast. In general the use of a highlighter is recommended for all aircraft surfaces, even those on which it may not appear essential, simply to avoid the effects of dirt or the occasional dull areas. When image contrast does not improve with highlighting, its use is probably not warranted.

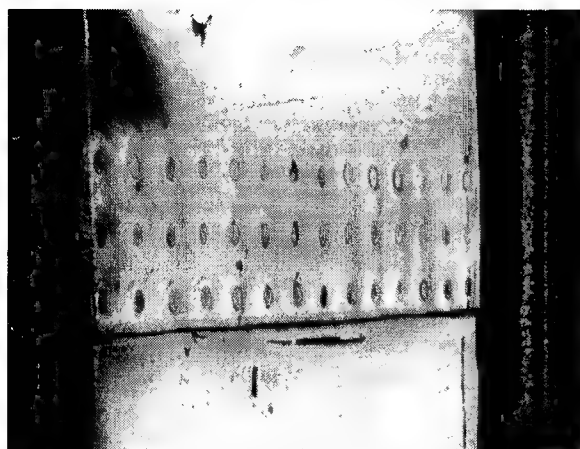


**Figure 6:** Unpainted lap splice without highlighting

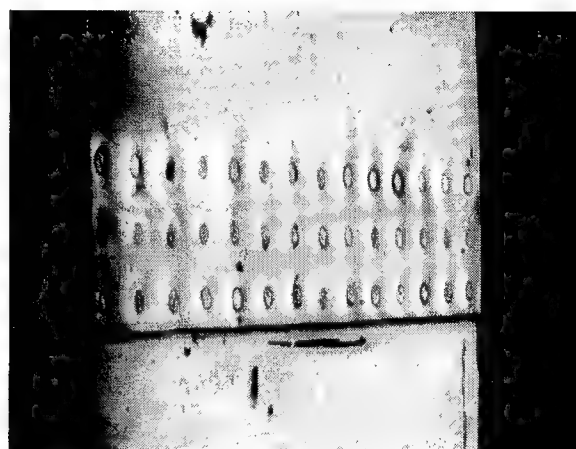


**Figure 7:** Same lap splice, highlighted

## 4.2 Highlighters and Their Properties

The important properties of a highlighting fluid are surface tension, viscosity and evaporation rate. The best fluids have a low surface tension so that they wet a surface well with no evidence of beading. They are low in viscosity so that any application streaks quickly settle out to an even film but they evaporate slowly enough to allow a useable length of inspection time. Highlighting fluids are typically combinations of components, such as a 10:1 mix of mineral spirits and baby oil, blended in proportions that yield optimal properties. Two commercially available highlighters are recommended for aircraft. SNO-FLAKE®, from Parker-Amchem Products Inc. is a kerosene based fluid while Chemlite 215®, from Chemfil Ltd. is water soluble. SNO-FLAKE is the superior highlighter, with better wettability and settling rates than Chemlite. However, its kerosene base can be objectionable for some environments and materials and its residue is not as easily rinsed off as Chemlite. Although Chemlite has the lower evaporation rate, an application of SNO-FLAKE lasts for up to 10 minutes, more than enough time to perform a DAIS inspection. (The M.S.D.S. sheets for both these fluids are included in the Appendix).

## 4.3 Application Procedure

Preparation of a surface for DAIS inspection begins by pouring onto the sponge applicator a volume of highlighting fluid sufficient to thoroughly soak it without dripping (approx. 30 ml. or 1 oz.). Wipe the surface to be inspected with the applicator. Only highlight as much surface as can be inspected with about ten DAIS images or sensor placements. If too large an area is highlighted it is likely that the film will evaporate before the entire surface is imaged so it must be re-highlighted.

The first pass application serves not only to coat the entire surface but also to clean it of any obvious dirt or oil smudges. In fact, an advantage to using SNO-FLAKE for highlighting aircraft is that its kerosene base acts as a solvent. The need for a clean surface may require that some pressure be applied to "scrub" the surface. If the inspected surface has already been cleaned, the water soluble Chemlite fluid may be used.

Make sure the entire surface area to be inspected is coated. As seen in Figure 8, dry regions will show as zones of low reflectivity with poor contrast. If too little highlighter is applied to the surface, the resulting images will be less than optimal. As seen in Figure 9, the effect is that pillowing signatures around rivets, although visible, are somewhat subdued in intensity. The result from an application of too much highlighter is dependent on the orientation of the surface. On the horizontal surface shown in Figure 10 the fluid tends to puddle and hide the surface. On the vertical surface in Figure 11 too much highlighter causes runs. In both cases the DAIS sensor is imaging variations in the surface of the fluid film, not the underlying aircraft surface.

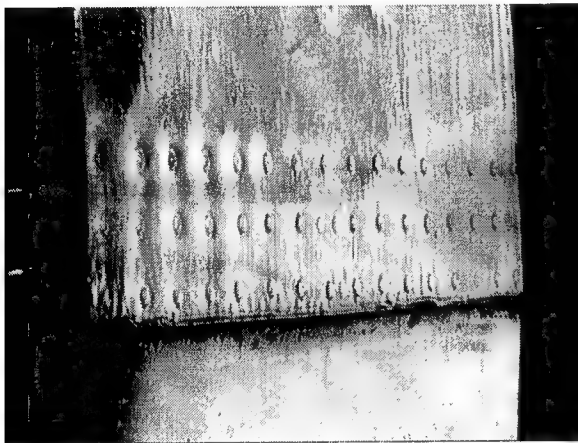


**Figure 8:** Uneven application of highlighting fluid

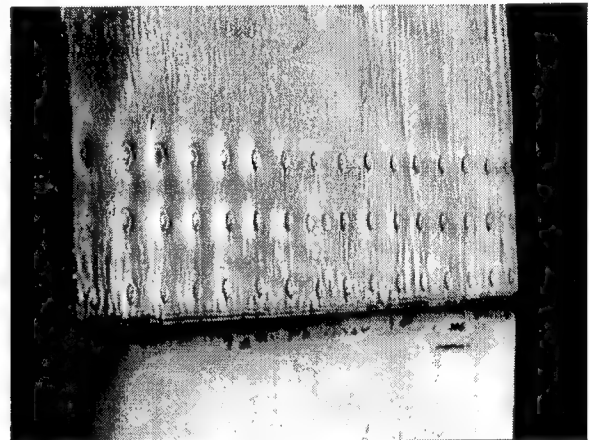


**Figure 9:** Application of too little highlighter

If there is too little fluid, add more to the surface directly from the bottle and spread it over the surface. If there is too much fluid, use the applicator to spread the highlighter over a larger area.

Having cleaned the surface of interest allow it to stand briefly. Add about 3 ml. more fluid to the applicator sponge and give the surface an additional light coat. This final step is to produce an evenly distributed, ripple free film. Using light pressure, draw the applicator sponge smoothly over the surface using parallel strokes, much as if one were painting the surface. Although the sponge applicator tends to leave few streaks, every attempt should be made so that the finishing highlighting strokes are in a direction parallel to the field of view of the DAIS sensor. For example, since a DAIS sensor images along a lap splice, highlighting streaks should be made parallel to the splice. The effect of highlighting streaks is illustrated in Figure 12 and

Figure 13. The fluid in both illustrations has been applied with a paper towel to produce streaks far more severe than those produced by the sponge applicator. When the streaks travel across the sensor's field of view, as in Figure 12, they produce a distinct pattern of background noise which can disguise legitimate surface variations. When similar streaks are oriented to run along the sensor's view, as in Figure 13, they are much less objectionable.

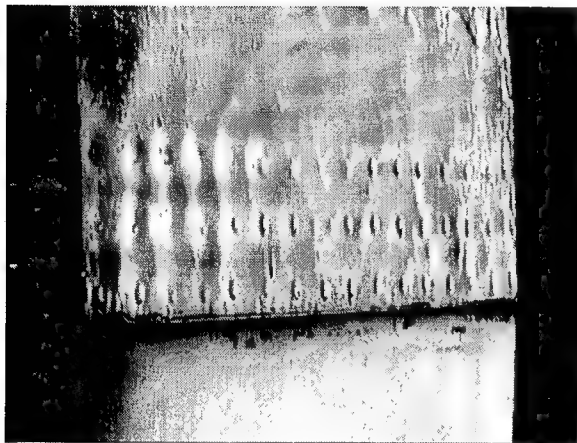


**Figure 10:** Too much highlighter on a horizontal surface

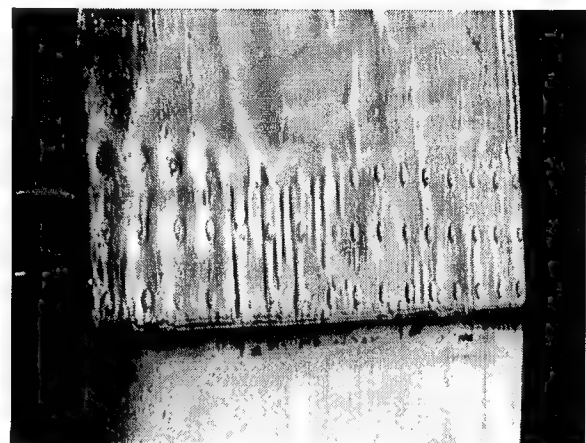


**Figure 11:** Too much highlighter on a vertical surface

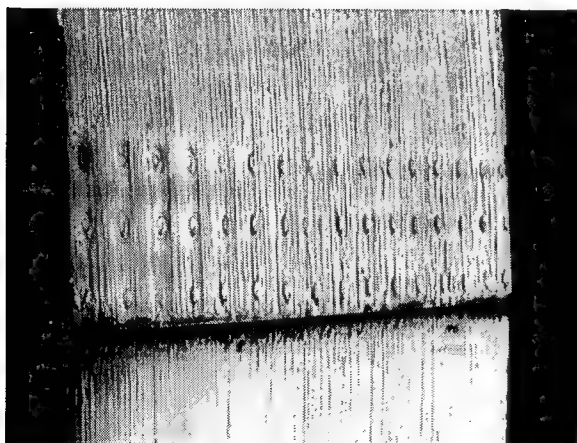


**Figure 12:** Highlighter streaks across the sensor's view

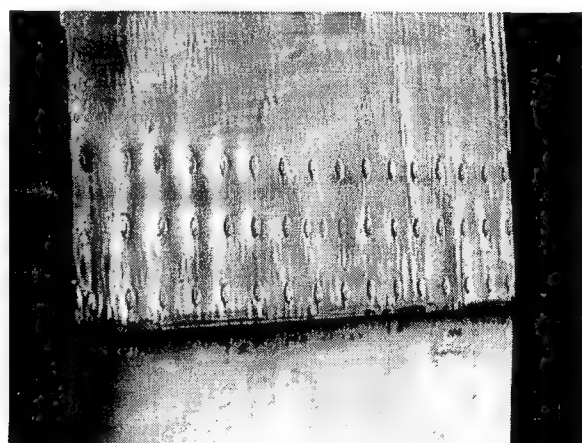


**Figure 13:** Highlighter streaks along the sensor's view

Experience with highlighting vertical surfaces has shown that even with the best possible application of highlighter there will be some unavoidable streaks due to the presence of rivet heads. As shown in Figure 14, even with a careful application the fluid tends to collect and run from some rivet heads, especially those with button heads. These surface runs must be recognized and tolerated during image analysis. Another potential hazard of applying too much highlighter to vertical surfaces is the potential for contaminating the optical components inside the upturned DAIS sensor.

When collecting DAIS images, both the sensor feet and skirt leave small but noticeable marks in the highlighting film. To minimize the effect of these contact points, lift and place the sensor between imaging locations. Do not slide the sensor across the surface as this tends to pool highlighter at the leading edge and reduce the amount of highlighter where it is needed. For similar reasons do not touch the highlighted surface with fingers or gloves until after the surface image has been acquired.

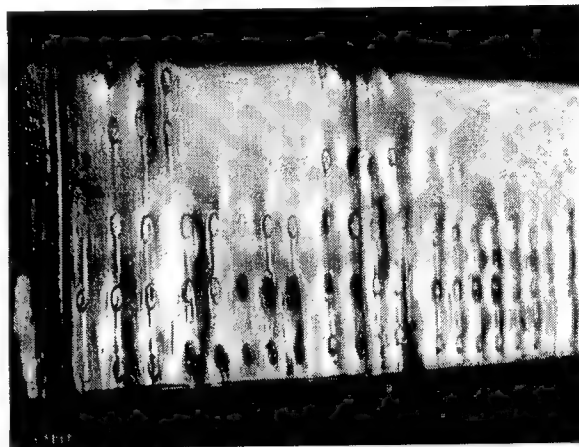


**Figure 14:** Small highlighter runs from rivet heads

As the entire aircraft is inspected, the amount of dirt and contamination which collects on the applicator sponge can become quite significant. If the sponge becomes too dirty it will degrade the quality of the highlighting films it applies. Typically one sponge can highlight one aircraft but if the surfaces in the DAIS images begin to appear to be "noisy" due to surface contaminants replace the sponge before proceeding.

When the inspection task is completed, any rags or towels which have been soaked in highlighting fluid should be disposed of in containers designed for combustible refuse. If the aircraft must be cleaned of SNO-FLAKE, a commercial degreaser is required to remove the remaining oil residue while Chemlite can be rinsed off with cold water.

In conclusion, the preparation of a surface for DAIS inspection can be summarized in three words:

**Clean**  
**Coat**  
**Distribute**

## 5 INSPECTION PROCEDURE

The inspection of horizontal and circumferential lap splices will be more efficient and effective if a number of guidelines are followed. These guidelines were derived from experience gained during inspections carried out in hangars and maintenance facilities. They relate to the sequence of placements of the sensor along lap splices and the sequence of sensor placements around the aircraft.

Whenever the surface requires highlighting, it is always preferable to start the aircraft inspection from the bottom of the aircraft and proceed to the top. Since gravity causes highlighter to drip downward, any highlighter applied at a higher elevation will make its way down to the current inspection elevation as runs. By starting at the bottom and working upward, the residual highlighter will not run into the current inspection location. This practice is especially true for circumferential lap splice inspection since the entire length of lap splice will be highlighted at some point during the inspection.

The DAIS-250C has a particular optical arrangement inside the sensor that must be understood so that the top and bottom of the *D SIGHT* image is known in relationship with the orientation of the sensor. When holding the sensor right side up in front of you with the cable connection level and to your left and the sensor opening away from you, the left side of the *D SIGHT* image will correspond to the connector side of the sensor, top will be up, right will be at the wider end of the sensor and bottom will be down as shown in Figure 15.

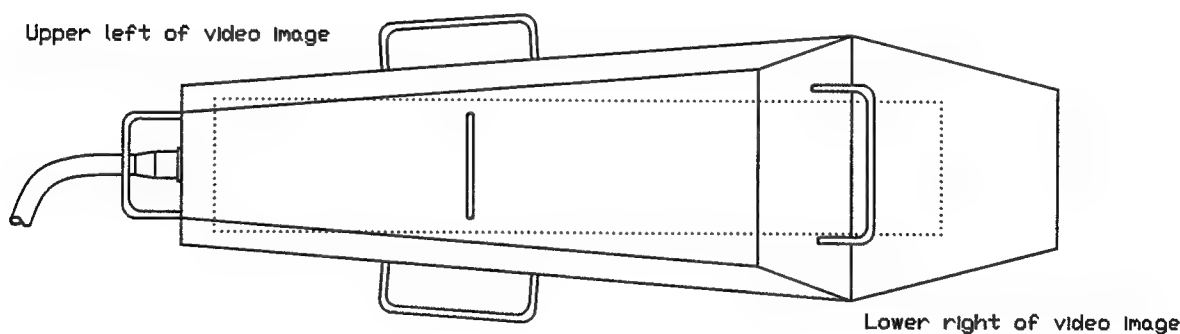


Figure 15: Orientation of sensor and *D SIGHT* image

This relationship between the orientation of the image and the orientation of the sensor placement during inspection is important so that confusion does not arise about which way is up when the surface is being compared with the image or when finding key features in the image relative to the surface. In addition, since left to right is standard for reading and general presentation, it is preferable to make sensor placements from left to right on horizontal lap splices with the connector end to the left (ie. away from the direction of subsequent placements). This sequence is counter clockwise around the aircraft relative to a top view of the aircraft. As a result, on the left side of the aircraft, inspection proceeds from fore to aft, while on the right side, the inspection is from aft to fore keeping the connector end on the left hand side of the inspector. One benefit of this procedure is that the cable is dragged along with the inspection rather than being pushed.

Circumferential inspection on the left or right side of the aircraft, should start sensor placements at the belly and proceed upward to the top of the aircraft with the connector end of the sensor in the down position. The top of the image on the left side of the aircraft will be in the fore direction while on the right side of the aircraft it will be in the aft direction.

Sensor placements can be coordinated effectively with surface features such as build stations or stringers if a 50% overlap placement strategy is used. Using the markings on the side of the sensor, place the sensor with the center mark directly over a build station. The next placement will have the center mark exactly between two build stations and the two end markings should be approximately located on a build station each. Although this strategy has significant overlap and may not be appropriate for all aircraft, there is no danger of missing part of the surface and more than one view of a particular surface area is captured for analysis purposes. For circumferential inspections, each stringer position is an appropriate location for the center of the sensor. Using this strategy, the rate of inspection can be expected to be about 0.75 meters/min (2.5 ft/min) or approximately 20 seconds per sensor placement.

To summarize, use the following guidelines during inspections:

- when highlighting, inspect from bottom to top of aircraft on both horizontal and circumferential lap splices
- move sensor counter clockwise around the aircraft
- keep connector end of sensor away from the direction of movement along the lap splice
- overlap sensor placements by using build stations and stringers as reference points with respect to the sensor

## 6 INTERPRETING IMAGE SIGNATURES

### 6.1 *D SIGHT* and Surface Geometry

In the most general case, a *D SIGHT* image consists of two superimposed images depending on the surface characteristics or features present. Features or objects that do not permit light to reflect to the retroreflective screen, such as rivets, dirt, dull areas and edges of irregular hardware, are imaged as if they were front illuminated only, as in standard photography. Continuous, slowly varying, reflective surfaces which permit the light to reflect onto the retroreflector and back again, have intensity variations that are dependent on the local curvature of the surface. The nature, size, orientation and contrast of these intensity variations determine the extent of the surface deformation and corrosion.

To appreciate and understand the true *D SIGHT* image effect without the complexity of extraneous features such as rivets, consider Figure 16. Presented are 5 artificial depressions to simulate corrosion of increasing amount (size) from top to bottom in the *D SIGHT* image ranging in size from 0.08-0.17 mm (0.3-6.8 mils) deep on 25 mm (1 in.) centers. Although size is referred to by height, optically it is the curvature and the degree to which the depressions focus or de-focus light onto the retroreflector that is most important. Higher local curvature on the surface causes the light to focus more intensely so that the intensity pattern on the retroreflector has greater light concentration. When this pattern is retroreflected back through the surface and a camera is positioned slightly off axis from the primary light source to view the returning light, two types of signatures can be produced depending on the depth (curvature) of the depression. When the depth is low, a dark-bright *D SIGHT* signature is created to the right of the physical depression marked by the cross-hair position. The bright area is simply the concentrated light on the retroreflector being reflected through non-distorted surface as a result of the off-axis view. The contrast in this signature increases until the depth is sufficient to cause some of the retroreflected light to be reflected to the left of the physical depression on the downward slope creating a bright-dark-bright signature. The downward slope on the left side of the actual depression reflects the concentrated light on the retroreflector into the lens. As the depression becomes more severe, the bright zone to the left of the depression increases in intensity. Areas away from the local depressions image as one shade of gray.

Two additional observations can be made in Figure 16. The *D SIGHT* signatures of the shallow depressions show a dark-to-bright intensity variation, left to right, on the right of the physical depression. This polarity indicates that the local curvature is concave even when the depression becomes severe enough to produce a bright zone to the left of the depression as well. A bright-to-dark polarity would indicate a convex curvature.

Secondly, the dark-bright signature is physically displaced to the right from the actual physical depression shown by the cross-hairs. The displacement is a result of the off-axis light source position with respect to the lens. The orientation of the bright-to-dark transition is also a function of the light source position relative to the camera lens and defines the orientation of

maximum sensitivity. In the DAIS-250C sensor, there is a greater sensitivity to non-symmetric surface deformations perpendicular to the optical axis or viewing direction. For example, trough-like depressions along the viewing direction (left-to-right in image) will not image with the same amount of contrast as if the identical troughs were perpendicular (top-to-bottom in image) to the viewing direction. This preferential sensitivity is important for certain applications exhibiting trough-like physical indications but is irrelevant when the physical indications are symmetric.

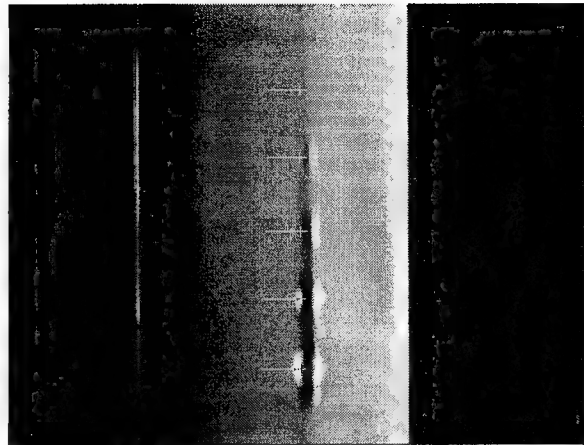


Figure 16: *D SIGHT* signatures when viewed across depression row

The displacement of the *D SIGHT* signatures to the right of the physical depression can begin to interfere or mix with the signature of the next neighboring depression. When the same set of depressions is imaged along the depression row with the shallow depression on the left as in Figure 17, signature mixing can be observed because the displacement is approximately the same as the depression spacing. Because of this, there may be some ambiguity as to the exact depression creating the signature.

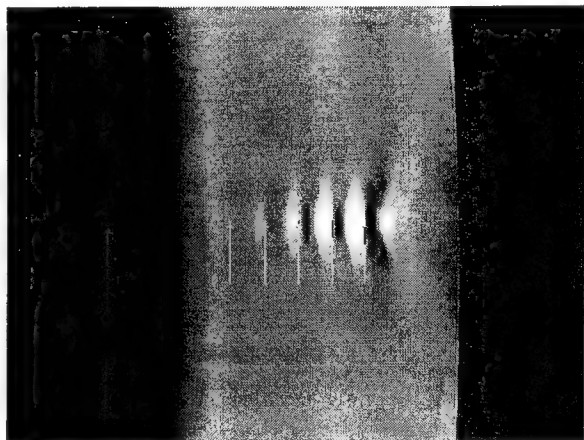


Figure 17: *D SIGHT* signatures when viewed along depression row

Physical corrosion indications generally have a symmetric geometric shape with the rivet located in a depression while the maximum deflection occurs centrally between a set of four rivets and has a convex curvature. Curvatures in the immediate vicinity of a rivet are typically higher than the curvatures between the rivets. Rivets, themselves, do not obey the requirement of a slowly varying surface to *D SIGHT* properly. Rather, they are features with abrupt surface changes that are imaged with essentially frontal illumination except for the top most flat area. Their presence is important for defining the characteristic physical corrosion indication, but they disrupt the signatures of the surrounding surface. The next section discusses corrosion signatures of actual lap splices and identifies key signature features to look for in images of horizontal lap splices and vertical butt splices.

## 6.2 Key Signature Features

The presence of corrosion in lap splices around rivets causes a physical pillowing or bulging of the surrounding surface while the clamping force of the rivet prevents the surface from bulging to the same extent in the vicinity of the rivet. As a result, the rivet area forms a local depression in the surface. The key *D SIGHT* signature that indicates the presence of this depression at a moderate to high corrosion level is the occurrence of a dark-to-bright gray scale variation to the immediate right of the rivet with a bright zone immediately to the left of the rivet. Figure 18 shows these signatures for the specimen that was physically profiled in Figure 2. The dark and bright area to the right of the rivet corresponds to the physical indication of a depression while the bright zone to the left of the rivet indicates a severe depression (corrosion). The greater the contrast in this signature (ie. greater bright-dark-to-bright gray scale disparity), the greater is the physical depression. Corrosion severity increases with increased signature contrast. Notice that signature contrast increases over four rivets from right to left in the top row as the corrosion level increases. Similar signatures are found on circumferential butt splices even though the underlying surface is cylindrical in shape as shown in Figure 19.

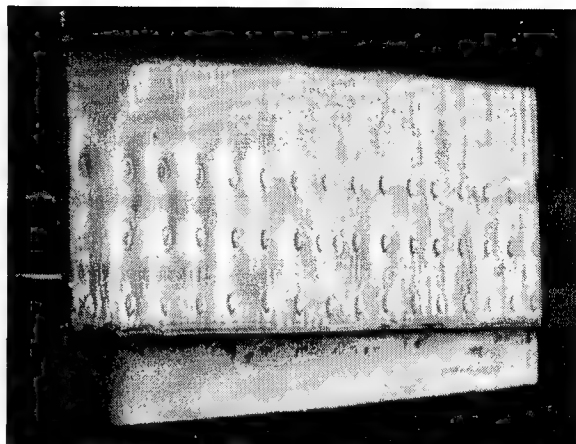


Figure 18: Lap splice corrosion signatures

Rivets on the right hand side of the lap splice show no major depression at the rivets. Referring to the horizontal splice in Figure 18, the horizontal region between the top and middle rivet row in the corroded area shows less signature contrast due to the weaker curvature variations away from the rivets even though the level of corrosion may be the same. This region will always have weaker signatures than along the actual rivet row. A key signature feature indicating less severe corrosion is the presence of vertical wave signatures without distinct bright areas around each rivet, as shown in Figure 20. The bright areas around the set of rivets to the right are less distinct than around the left-most, center row rivets even though there is a prominent wave signature pattern. This condition also may result from the rivet head not being reflective, causing a disruption in the formation of the depression's signature.

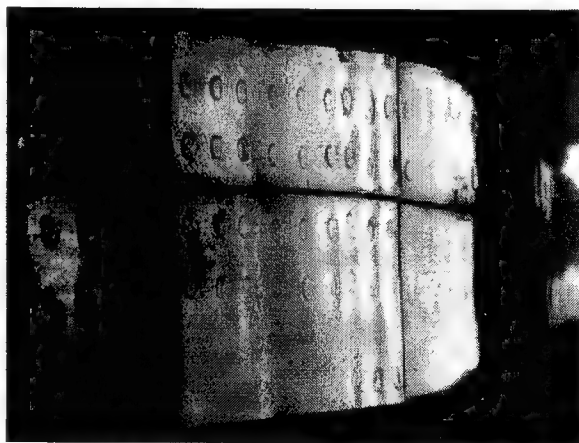
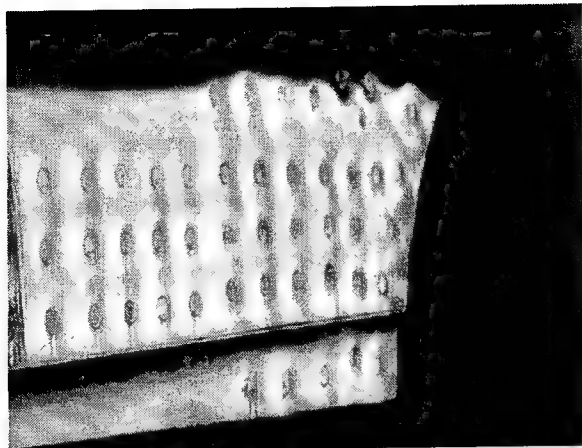
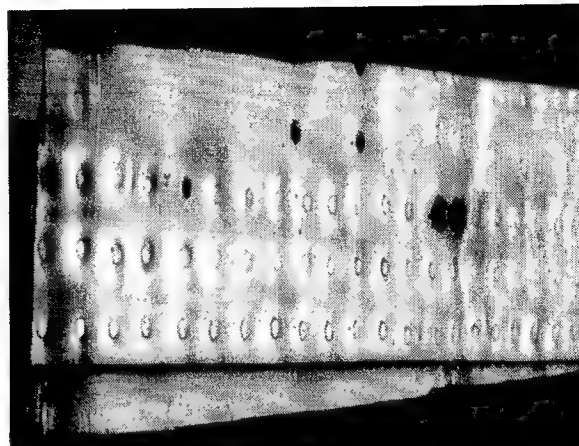


Figure 19: Circumferential lap splice corrosion



**Figure 20:** Weak signatures of corrosion



**Figure 21:** Lap splice corrosion on bare aluminum

Figure 21 is an example of a bare aluminum lap splice with corrosion predominately on the left side. The center row of rivets exhibit strong signature indications of corrosion. The edges of some rivets appear recessed to a point that they are no longer visible in the image. Such a condition is another key signature feature of corrosion. The fourth rivet from the left hand side of the middle row is recessed so deeply that the dark part of the signature is in fact in line with the rivet. Note that the fifth rivet from the left hand side in the top row is missing altogether.

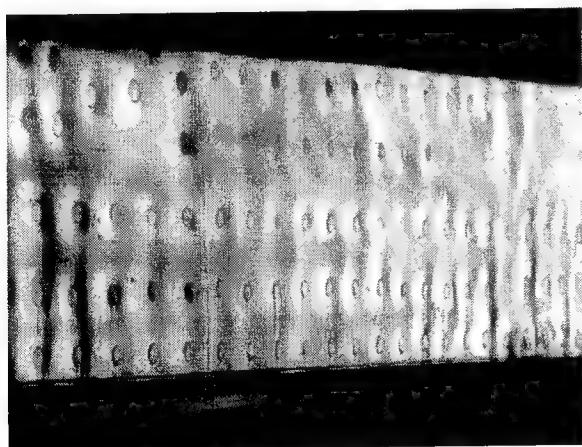


**Figure 22:** Two types of corrosion signatures

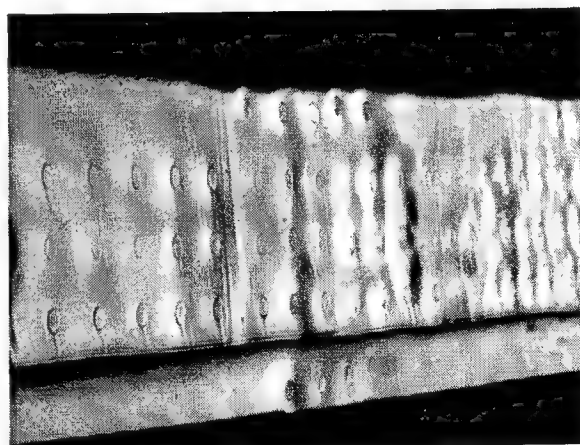


**Figure 23:** Severe corrosion signatures and uncorroded area

Figure 22 and Figure 23 are two more examples of lap splice corrosion. Figure 22 shows both types of corrosion signatures; bright areas around rivets to the right and wave signatures on the left. Figure 23 has no corrosion on the left side with two columns of rivets exhibiting corrosion followed by an area with significant corrosion signatures. The extreme right side of the image also indicates signatures of corrosion.

To summarize, the following key features in *D SIGHT* images are indicative of corrosion in lap splices:

- dark-to-bright gray scale variations to the right of a rivet indicating a physical depression at the rivet with a bright zone immediately to the left of the rivet. The higher the contrast, the higher the level of corrosion (bright area is noticeably whiter than the surrounding surface)
- dark-to-bright gray scale variation to the right of a rivet column with no significant bright area at the rivets indicates a lower level of corrosion
- rivet heads that are recessed significantly causing a dark halo around the rivet (sometimes the head is dark as well)
- a pattern of similar *D SIGHT* signatures around several rivets in an area

7 APPENDIX

MSDS sheets for SNO-FLAKE and CHEMLITE

## MATERIAL SAFETY DATA SHEET

### I. Product Identification & Use

Product Identifier: *Sno-Flake Hi Lite Compound*  
Product Use:  
WHIMIS Class:

Manufacturer: *Amchem Products, Inc.*  
*300 Brookside Avenue*  
*Ambler, PA*  
*19002*  
*(215) 628-1000*

### II. Hazardous Ingredients

Material	% Range	CAS number	LD50 m9/k9 (species/route)	LC50 m9/m3 (species/time)
kerosene	90 - 100			

### III. Physical Data

a. Physical State: *liquid*  
b. Freezing Pt. (°C/°F):  
c. Boiling Pt. (°C/°F): *>350 F*  
d. Coef. Water/Oil Dist.:  
e. Water Solubility (%):  
f. Vapour Density(air=1):  
g. Vapour Pressure(mmHG):  
h. Odor Threshold(ppm):  
i. Volatility(% by vol.):  
j. Odor/Appearance: *clear water-white liquid, kerosene odor*  
k. PH:  
l. Evap. Rate:  
m. Spec. Gravity(H<sub>2</sub>O=1): *0.81 ± 0.01*

### IV. Fire and Explosion Data

a. Flammability Yes\_\_ No\_\_ If yes, under which condition?  
b. Means of extinction: *Carbon dioxide, dry chemical, fire fighters should wear self-contained breathing apparatus*  
c. Flashpoint (°C/°F) & Method: *146 F; TCC*  
d. Auto-ignition temp. (°C/°F):  
e. Flammability limit (% of vol.): upper: lower:  
f. Hazardous combustion products:  
g. Sensitivity to impact:  
h. Sensitivity to static discharge:

### V. Reactivity Data

a. Chemical stability Yes X No\_\_ If no, under which conditions?  
b. Incompatibility with other substances Yes X No\_\_ If yes, which ones? *Strong oxidizing agents*  
c. Conditions of reactivity: *Avoid extreme temperatures*  
d. Hazardous decomposition products: *Oxides of carbon*  
e. Hazardous polymerization: *Will not occur*

## VI. Toxicological Properties

- a. Route of entry: Skin contact \_\_\_ Skin absorption \_\_\_ Eye contact \_\_\_ Inhalation \_\_\_ Ingestion \_\_\_
- b. Effects of acute exposure to product: Skin & eye: *May irritate*  
Inhalation: *Inhalation of large amounts of vapor may cause nausea and vomiting*  
Ingestion: *May irritate mucous membranes and intestines. May also cause nausea, palpitation or convulsions.*
- c. Effects of chronic exposure:  
d. Exposure limits:  
e. Irritancy of product:  
f. Sensitization to product:  
g. Carcinogenicity:  
h. Reproductive Toxicity:  
i. Teratogenicity:  
j. Mutagenicity:  
i. Synergistic products:
- 

## VII. First Aid Procedures

- a. Ingestion: *Dilute by giving several glasses of water or milk. Call a doctor.*  
b. Eye Contact: *Flush immediately with copious amounts of water for at least 15 min. Call a doctor.*  
c. Skin Contact: *Wash with soap and water and rinse thoroughly.*  
d. Inhalation: *Remove from contaminated area to fresh air.*
- 

## VIII. Spill or Leak Procedures

- a. Steps to be taken for spill or leak: *Transfer unspilled material to a clean steel container. Take up spilled material with rags or sawdust.*  
b. Waste disposal methods: *Carefully evaporate. Burn the rags or sawdust after evaporation.*
- 

## IX. Special Protection Information

- a. Respiratory protection requirements: *Fume mask - NIOSH approved*  
b. Ventilation requirements: *Local exhaust*  
c. Protective gloves required: *Vinyl*  
d. Eye protection required: *Safety goggles*
- 

## X. Special Precautions

- a. Precautionary label required? If yes, please attach. *No. Amchem Warning Statement 94*  
b. Precautions to be taken in handling and storage: *Store in a cool place away from open flames or sparking equipment.*  
c. Special shipping information:
-

# MATERIAL SAFETY DATA SHEET

## I. Product Identification & Use

Product Identifier: *Chemlite 215*  
Product Use: *Highlighter*  
WHIMIS Class: *B. 3;D. 2(B) (contains combustible & toxic material)*

Manufacturer: *PPG Chemfil Corporation*  
*1330 Piedmont*  
*Troy, MI*  
*48083*  
*(313) 564-5500*

## II. Hazardous Ingredients

Material	% Range	CAS number	LD50 m9/k9 (species/route)	LC50 m9/m3 (species/time)
<i>petroleum distillate</i>	<i>60 - 100</i>	<i>64742-80-9</i>	<i>not available</i>	<i>not available</i>
<i>alkylolamide alcohol</i>	<i>1 - 5</i>	<i>93-83-4</i>	<i>not available</i>	<i>not available</i>

## III. Physical Data

a. Physical State:	<i>liquid</i>	h. Odor Threshold(ppm):	<i>not available</i>
b. Freezing Pt. (°C/°F):	<i>not applicable</i>	i. Volatility(% by vol.):	<i>95</i>
c. Boiling Pt. (°C/°F):	<i>470 F</i>	j. Odor/Appearance:	<i>lt. yellow, slight odor</i>
d. Coef. Water/Oil Dist.:	<i>not available</i>	k. PH:	<i>not applicable</i>
e. Water Solubility (%):	<i>nil</i>	l. Evap. Rate:	<i>&lt; 0.1</i>
f. Vapour Density(air=1):	<i>not available</i>	m. Spec. Gravity(H <sub>2</sub> O=1):	<i>0.81 ± 0.01</i>
g. Vapour Pressure(mmHG):	<i>&lt; 0.1</i>		

## IV. Fire and Explosion Data

a. Flammability Yes\_\_ No X If yes, under which condition?

b. Means of extinction: *Carbon dioxide, dry chemical, fire fighters should wear self-contained breathing apparatus*

c. Flashpoint (°C/°F) & Method: *>200 F*

d. Auto-ignition temp. (°C/°F): *150 F*

e. Flammability limit (% of vol.): upper: *5.0* lower: *0.7*

f. Hazardous combustion products: *none known*

g. Sensitivity to impact: *not available*

h. Sensitivity to static discharge: *not available*

## V. Reactivity Data

a. Chemical stability Yes X No\_\_ If no, under which conditions?

b. Incompatibility with other substances Yes X No\_\_ If yes, which ones? *Avoid contact with strong oxidizing agents, flame.*

c. Conditions of reactivity: *Avoid extreme temperatures*

d. Hazardous decomposition products: *Thermal decomposition may produce oxides of carbon*

## VI. Toxicological Properties

- a. Route of entry: Skin contact X Skin absorption    Eye contact X Inhalation X Ingestion X
- b. Effects of acute exposure to product: Skin & eye: *Irritant*  
Inhalation: *Mists/vapours may cause irritation*  
Ingestion: *Gastro irritation*
- c. Effects of chronic exposure: *None known*
- d. Exposure limits: *TLV 5 m9/m3 for mineral oil mist*
- e. Irritancy of product: *irritant*
- f. Sensitization to product: *not available*
- g. Carcinogenicity: *not available*
- h. Reproductive Toxicity: *not available*
- i. Teratogenicity: *not available*
- j. Mutagenicity: *not available*
- i. Synergistic products: *not available*
- 

## VII. First Aid Procedures

- a. Ingestion: *Do not induce vomiting, get medical attention*
- b. Eye Contact: *Flush with plenty of water for 15 min., see physician*
- c. Skin Contact: *Wash thoroughly with soap and water*
- d. Inhalation: *Remove to fresh air*
- 

## VIII. Spill or Leak Procedures

- a. Steps to be taken for spill or leak: *Contain spill. Absorb onto inert material. Shovel up and place in chemical disposal area.*
- b. Waste disposal methods: *In accordance with all governmental regulations.*
- 

## IX. Special Protection Information

- a. Respiratory protection requirements: *If spraying, approved mist respirator*
- b. Ventilation requirements: *Good general room ventilation*
- c. Protective gloves required: *Chemical resistant*
- d. Eye protection required: *Safety glasses*
- 

## X. Special Precautions

- a. Precautionary label required? If yes, please attach. *No*
- b. Precautions to be taken in handling and storage: *Keep containers sealed when not in use. Store in cool dry place, away from extreme heat and oxidizers.*
- c. Special shipping information: *Not regulated under T.D.G. Act.*
- 

*Information presented herein has been compiled from sources considered to be dependable and is offered in good faith, but without guarantee. No warranty is expressed or implied as to the suitability of the product for any particular use in operations not under our direct control. Liability is limited to the net purchase price of the product. No warranty, expressed or implied, nor statement or recommendation not contained herein, shall apply unless covered by agreement signed by an authorized officer of Chemfil Canada Limited.*

## APPENDIX H

NRC-CNRC Chemical Characterization of Corrosion Products in Fuselage Lap Joints, LTR-ST-1952, November 1993, S. Krishnakumar, J.P. Komorowski, I. Sproule.



National Research  
Council Canada

Conseil national  
de recherches Canada

Unclassified  
Limited

Institute for  
Aerospace Research

Institut de  
recherche aérospatiale

---

# **NRC-CMRC**

---

## ***Chemical Characterization of Corrosion Products in Fuselage Lap Joints***

LTR-ST-1952

S. Krishnakumar, J.P. Komorowski, I. Sproule

November 1993

Pages: 20

**REPORT  
RAPPORT**

Report  
Rapport LTR-ST-1952

Fig.  
Diag. 20

**STRUCTURES AND MATERIALS  
LABORATORY  
LABORATOIRE DES  
STRUCTURES ET DES  
MATÉRIAUX**

Date November, 1993

Unclassified  
Limited

For  
Pour Diffrauto Ltd / Transport Canada / Federal Aviation

Reference JGJ-02 SSC File #XSD92-00189-(621) Contract #T8200-2-2544101-XSD  
Référence

**LTR-ST-1952**

**CHEMICAL CHARACTERIZATION OF CORROSION  
PRODUCTS IN FUSELAGE LAP JOINTS**

Submitted by  
Présenté par W. Wallace  
Laboratory Head/Chef de laboratoire

S. Krishnakumar  
J.P. Komorowski  
Author  
Auteur I. Sproule\*  
\* Chemical Characterization Group  
Institute for Microstructural Sciences

Approved  
Approuvé G.F. Marsters  
Director General

THIS REPORT MAY NOT BE PUBLISHED WHOLLY  
OR IN PART WITHOUT THE WRITTEN CONSENT  
OF THE INSTITUTE FOR AEROSPACE RESEARCH

CE RAPPORT NE DOIT PAS ÊTRE REPRODUIT, NI EN  
ENTIER PARTIE SANS UNE AUTORISATION ÉCRITE  
DE L'INSTITUT DE RECHERCHE AÉROSPATIALE

# **CHEMICAL CHARACTERIZATION OF CORROSION PRODUCTS IN FUSELAGE LAP JOINTS**

**by**

**S. KRISHNAKUMAR<sup>1</sup>, J.P. KOMOROWSKI<sup>1</sup> and I. SPROULE<sup>2</sup>**

**<sup>1</sup>Structures, Materials and Propulsion Laboratory  
Institute for Aerospace Research**

**<sup>2</sup>Chemical Characterization Group  
Institute for Microstructural Sciences**

**National Research Council of Canada**

**November 1993**

## ABSTRACT

Samples of corrosion product obtained from aircraft skin specimens subjected to accelerated corrosion testing by exposure to an acidified salt fog environment in the laboratory were chemically analyzed and compared with corrosion samples extracted from fuselage lap joints in decommissioned Boeing 727 transport aircraft. Three methods were used for the characterization of the corrosion products: X-ray Diffraction (XRD), X-ray Photo-electron Spectroscopy (XPS) and Auger Electron Spectroscopy (AES). All three methods showed that the artificially created corrosion products were very similar in composition and phase to those occurring naturally in aging aircraft. XPS and AES identified the corrosion product to be almost entirely composed of the trihydrate form of aluminum oxide. X-ray diffraction identified the presence of aluminum oxide trihydrate in both amorphous and crystalline forms, but also indicated the presence of some crystalline aluminum oxide monohydrate in both the laboratory and the aircraft corrosion samples.

## TABLE OF CONTENTS

ABSTRACT	
TABLE OF CONTENTS .....	i
LIST OF FIGURES .....	ii
1.0 INTRODUCTION .....	1
2.0 ACCELERATED CORROSION APPLICATION .....	4
3.0 X-RAY PHOTOELECTRON SPECTROSCOPY .....	5
4.0 AUGER ELECTRON SPECTROSCOPY .....	7
5.0 X-RAY DIFFRACTION ANALYSIS .....	8
6.0 DISCUSSION .....	11
7.0 CONCLUSION .....	14
ACKNOWLEDGEMENTS .....	15
REFERENCES .....	16
TABLES .....	17
FIGURES .....	20

## LIST OF FIGURES

- Figure 1. XPS Survey of  $\text{Al}_2\text{O}_3$  Standard.
- Figure 2. Oxygen Peak in XPS Spectrum of  $\text{Al}_2\text{O}_3$  Standard.
- Figure 3. Aluminum Peak in XPS Spectrum of  $\text{Al}_2\text{O}_3$  Standard.
- Figure 4. Carbon Peak in XPS Spectrum of  $\text{Al}_2\text{O}_3$  Standard.
- Figure 5. XPS Survey of  $\text{Al}(\text{OH})_3$  Standard.
- Figure 6. Oxygen Peak in XPS Spectrum of  $\text{Al}(\text{OH})_3$  Standard.
- Figure 7. Aluminum Peak in XPS Spectrum of  $\text{Al}(\text{OH})_3$  Standard.
- Figure 8. Carbon Peak in XPS Spectrum of  $\text{Al}(\text{OH})_3$  Standard.
- Figure 9. XPS Survey of Aircraft Corrosion Sample.
- Figure 10. Oxygen Peak in XPS Spectrum of Aircraft Corrosion Sample.
- Figure 11. Aluminum Peak in XPS Spectrum of Aircraft Corrosion Sample.
- Figure 12. Carbon Peak in XPS Spectrum of Aircraft Corrosion Sample.
- Figure 13. XPS Survey of Laboratory Corrosion Sample.
- Figure 14. Oxygen Peak in XPS Spectrum of Laboratory Corrosion Sample.
- Figure 15. Aluminum Peak in XPS Spectrum of Laboratory Corrosion Sample.
- Figure 16. Carbon Peak in XPS Spectrum of Laboratory Corrosion Sample.
- Figure 17. Auger Electron Spectrum of Aircraft Corrosion Sample.
- Figure 18. XRD Spectrum of Aircraft Corrosion Sample.
- Figure 19. XRD Spectrum of Laboratory Sample with Aircraft Sample Peaks.
- Figure 20. XRD Spectrum of Laboratory Corrosion Sample.

## 1.0 INTRODUCTION

The problem of corrosion in aging aircraft has been the subject of increased investigation by designers, airframe manufacturers, end users and researchers alike since its disastrous consequences were highlighted by the Aloha incident in the late eighties. Of particular concern is the detection of corrosion in fuselage longitudinal and circumferential joints, which requires many hours of painstaking inspection by skilled personnel at frequent intervals during the service life of the aircraft. The Structures, Materials and Propulsion Laboratory of the Institute for Aerospace Research at NRC has an ongoing project in collaboration with Federal Aviation Authority of the United States, Transportation Development Centre of Transport Canada and Diffraction for evaluation of D-Sight[1] as an enhanced visual inspection technique for detection of corrosion in aircraft lap splice joints. As part of this work, an accelerated corrosion testing programme was begun in the summer of 1993 to induce corrosion to various stages of advancement in laboratory specimens of fuselage lap and butt splices. The majority of these specimens were obtained from scrapped fuselage sections of decommissioned transport aircraft, mostly Boeing 727 and some DC-9. Some laboratory manufactured coupons and lap splice replicates were also tested in the early stages to optimize the test set-up and the corrosion application environment for efficient duplication of corrosion.

The application of D-Sight to detecting corrosion in lap joints is based on the observation that corrosion produces surface deformations commonly known as "pillowing" in between the fasteners of the joints in the aircraft skin. These deformations are most likely the result of

accumulation of corrosion products between the outer and inner elements of the joint, although they can also arise from extreme cases of exfoliation or inter-granular corrosion. Many forms of corrosion yield soluble compounds which get washed away without leaving any noticeable build up of corrosion products on the affected surfaces. In fact, accelerated corrosion tests using the EXCO solution (ASTM standard G34) in the laboratory produced severe thickness loss in a very short period of time without any accumulation of corrosion products on the specimen. However, in aircraft skin splice joints, where corrosion is mainly caused by the infiltration and retention of moisture in the crevices, there is usually an accumulation of insoluble products, which gives rise to the pillowing effect so familiar to aircraft inspectors. This was confirmed by opening and inspecting several fuselage lap and butt joints from decommissioned Boeing 727 and DC-9 aircraft. The inspection revealed a white flaky substance wedged in between the outer and inner skins. Artificially induced corrosion in the laboratory, in which the specimens were subjected to continuous exposure to slightly acidified salt fog environment, also produced a white flaky deposit similar in appearance to the aircraft corrosion product. The present efforts were aimed at identification of these white flaky products of corrosion, so that their similarity in terms of chemical characteristics could be ascertained.

The results of chemical characterization tests conducted on corrosion product samples obtained from aging aircraft lap sections as well as samples produced in the laboratory are presented here. The techniques of X-Ray Photoelectron Spectroscopy (XPS) and Auger Electron Spectroscopy (AES) were employed for determining the chemical state and concentration of individual element species in the samples and hence the chemical nature of the corrosion

## 1.0 INTRODUCTION

The problem of corrosion in aging aircraft has been the subject of increased investigation by designers, airframe manufacturers, end users and researchers alike since its disastrous consequences were highlighted by the Aloha incident in the late eighties. Of particular concern is the detection of corrosion in fuselage longitudinal and circumferential joints, which requires many hours of painstaking inspection by skilled personnel at frequent intervals during the service life of the aircraft. The Structures, Materials and Propulsion Laboratory of the Institute for Aerospace Research at NRC has an ongoing project in collaboration with Federal Aviation Authority of the United States, Transportation Development Centre of Transport Canada and Difracto for evaluation of D-Sight[1] as an enhanced visual inspection technique for detection of corrosion in aircraft lap splice joints. As part of this work, an accelerated corrosion testing programme was begun in the summer of 1993 to induce corrosion to various stages of advancement in laboratory specimens of fuselage lap and butt splices. The majority of these specimens were obtained from scrapped fuselage sections of decommissioned transport aircraft, mostly Boeing 727 and some DC-9. Some laboratory manufactured coupons and lap splice replicates were also tested in the early stages to optimize the test set-up and the corrosion application environment for efficient duplication of corrosion.

The application of D-Sight to detecting corrosion in lap joints is based on the observation that corrosion produces surface deformations commonly known as "pillowing" in between the fasteners of the joints in the aircraft skin. These deformations are most likely the result of

accumulation of corrosion products between the outer and inner elements of the joint, although they can also arise from extreme cases of exfoliation or inter-granular corrosion. Many forms of corrosion yield soluble compounds which get washed away without leaving any noticeable build up of corrosion products on the affected surfaces. In fact, accelerated corrosion tests using the EXCO solution (ASTM standard G34) in the laboratory produced severe thickness loss in a very short period of time without any accumulation of corrosion products on the specimen. However, in aircraft skin splice joints, where corrosion is mainly caused by the infiltration and retention of moisture in the crevices, there is usually an accumulation of insoluble products, which gives rise to the pillowing effect so familiar to aircraft inspectors. This was confirmed by opening and inspecting several fuselage lap and butt joints from decommissioned Boeing 727 and DC-9 aircraft. The inspection revealed a white flaky substance wedged in between the outer and inner skins. Artificially induced corrosion in the laboratory, in which the specimens were subjected to continuous exposure to slightly acidified salt fog environment, also produced a white flaky deposit similar in appearance to the aircraft corrosion product. The present efforts were aimed at identification of these white flaky products of corrosion, so that their similarity in terms of chemical characteristics could be ascertained.

The results of chemical characterization tests conducted on corrosion product samples obtained from aging aircraft lap sections as well as samples produced in the laboratory are presented here. The techniques of X-Ray Photoelectron Spectroscopy (XPS) and Auger Electron Spectroscopy (AES) were employed for determining the chemical state and concentration of individual element species in the samples and hence the chemical nature of the corrosion

products. The crystal structure of the products formed were identified using the X-Ray Diffraction (XRD) technique. The main objectives of the study are: (i) to determine the degree to which the accelerated laboratory process duplicated corrosion in aging aircraft and (ii) to develop a mathematical model using the chemical composition data that correlates the degree of corrosion inside the joint to the amount of "pillowing" deformation observed on the skin surface. Obviously, the extent of deformation will depend on the additional volume required to be accommodated within the joint, which in turn is a function of the chemical composition of the products generated by corrosion.

The normal air-formed surface film on aluminum is generally believed to consist essentially of aluminum oxide[2]. While the dissolution of aluminum in specific chemicals will produce distinctive corrosion products, such as aluminum nitrate in nitric acid, it is generally acknowledged that by far the most common corrosion product is hydrated aluminum oxide. It has been suggested that the initial corrosion product is amorphous aluminum hydroxide which ages with time to become a hydrated oxide or a mixture of oxides  $\text{Al}_2\text{O}_3 \cdot x\text{H}_2\text{O}$  [3]. In previous studies both *boehmite* ( $\alpha\text{-Al}_2\text{O}_3 \cdot \text{H}_2\text{O}$  or  $\text{AlO} \cdot \text{OH}$ ) and *bayerite* ( $\beta\text{-Al}_2\text{O}_3 \cdot 3\text{H}_2\text{O}$ , monoclinic) have been identified as the major constituents of the oxide film and corrosion product formed on aluminum[3,4]. Based on studies conducted on high-purity aluminum, Hart[5] suggests that below some critical temperature ( $60^\circ\text{--}70^\circ\text{C}$ ) the amorphous film formed at first becomes boehmite and finally converts to bayerite, while above the critical temperature only boehmite is formed on top of the initial amorphous film. Some authors state that at temperatures over  $80^\circ\text{C}$  the oxide is largely boehmite, while others maintain that the amount of boehmite is small at temperatures

below 250°C [3]. In any case there seems to be a general agreement that at temperatures below 70°C bayerite is the usual corrosion product found, especially after long aging. Based on thermodynamic considerations, Deltombe and Pourbaix[6] suggest that the form of the product progressively moves to less soluble oxides: from boehmite to bayerite to gibbsite. But, according to Godard et al.[3] the alpha phase of aluminum trihydrate ( $\alpha\text{-Al}_2\text{O}_3\cdot 3\text{H}_2\text{O}$ ), known as *gibbsite* or *hydrargillite*, has never been found in surface oxide films or aqueous corrosion products of aluminum. On the other hand, Shipko and Haag [7] reported that freshly precipitated  $\text{Al}(\text{OH})_3$  is amorphous and that it gradually ages at ordinary temperature to a gel with x-ray patterns of boehmite, then bayerite, and then finally to gibbsite.

## 2.0 ACCELERATED CORROSION APPLICATION

The ASTM Standard Method B368 - Copper-Accelerated Acetic Acid Salt Spray Testing (CASS Test) Procedure was employed for application of accelerated corrosion on the laboratory specimens. The corroding agent consisted of 5% parts by weight of sodium chloride solution with 0.25 gms/litre of copper chloride ( $\text{CuCl}_2\cdot 2\text{H}_2\text{O}$ ) dissolved in it. The acidity of the salt solution was raised to a pH between 2.8 and 3.0 by the addition of acetic acid. The specimens were exposed to continuous salt spray at a temperature of 48°C (118°F). Continuous exposures of six to seven days produced significant amounts of corrosion on unpainted aluminum aircraft skin panel surfaces. After removal from the salt spray cabinet, the specimens were gently washed under running tap water to remove the NaCl deposits and air dried before samples of the

corrosion product were extracted for chemical analysis. It may be noted that the laboratory samples used in the chemical analysis were obtained from corrosion on the outer surfaces of the panels and not from the internal surfaces of joints as much longer periods of exposure are required for producing corrosion in the interior of the lap joint specimens.

### 3.0 X-RAY PHOTOELECTRON SPECTROSCOPY

X-ray Photoelectron Spectroscopy (XPS), otherwise known as ESCA (acronym for Electron Spectroscopy for Chemical Analysis), was employed for identification of the various chemical elements in the two corrosion samples, one taken from a scrapped Boeing 727 fuselage lap section and the other artificially produced in the laboratory by continuous exposure to acidified salt fog. The XPS characterization was performed by the Chemical Characterization Group at the Institute for Microstructural Sciences. A commercially procured "pure" sample of anhydrous aluminum oxide was used to calibrate the set-up and to determine the sensitivity factors. XPS is a surface analysis technique which has a depth of penetration of only about 20 to 50 Angstroms[8]. A general XPS scan of the  $\text{Al}_2\text{O}_3$  standard is shown in Figure 1. and the narrow range scans covering the peaks of O-1s (between 520 and 540 eV), Al-2p (66-78 eV) and C-1s (276-296 eV) are shown in Figures 2,3 and 4 respectively. The areas under the peaks of the various species in the spectrum are in direct proportion to their respective concentrations in the sample being analyzed when corrected by the appropriate sensitivity factors[8]. The sensitivity factors for oxygen and aluminum were set at 0.711 and 0.150 respectively to obtain a value as

close to 2/3 (the ratio of number of aluminum atoms to the number of oxygen atoms in  $\text{Al}_2\text{O}_3$ ) for the ratio of the corrected area under the aluminum peak to that under the oxygen peak. Traces of carbon were found in all of the samples analyzed using the XPS. It is believed that this is the result of atmospheric contamination of the sample surfaces prior to introduction into the XPS analysis chamber. For samples known not to contain any carbon, the detection of traces of carbon originating from the XPS system (such as in this case) is usually ignored.

For comparison with the corrosion product samples, a commercially procured sample of  $\text{Al}(\text{OH})_3$  standard was also subjected to X-ray Photoelectron Spectroscopy. The general scan of this standard aluminum hydroxide sample<sup>1</sup> (for binding energies in the range of 0 to 1440 eV) is shown in Figure 5. The narrow range scans for oxygen, aluminum and carbon are shown in Figures 6, 7 and 8 respectively. The XPS spectra of the aircraft corrosion sample and the laboratory corrosion sample are shown in Figures 9 and 13. The peaks corresponding to oxygen, aluminum and carbon species in these samples are shown in Figures 10, 11, 12 and Figures 14, 15 and 16 respectively. The percentage concentrations of aluminum, oxygen and the carbon species in the two standards and the two corrosion samples tested are listed in Table 1. It may be noted that the concentration of carbon species is high in the corrosion specimens. In particular over sixty percent of the species detected in the sample obtained from laboratory induced corrosion is carbon. There is also a slight mismatch between the aluminum and oxygen peaks

---

<sup>1</sup>Aluminum hydroxide is chemically similar to aluminum oxide trihydrate since  $\text{Al}_2\text{O}_3 \cdot 3\text{H}_2\text{O} = 2\text{Al}(\text{OH})_3$ . In this report we have followed the convention of referring to the amorphous phase as aluminum hydroxide and the crystalline phases as aluminum oxide trihydrate.

obtained for the corrosion samples and those recorded for the standard samples, in terms of their positions and peak shapes. The reason for this mismatch is not yet clear. However, in spite of these minor anomalies, the XPS spectra yield definite conclusions regarding the composition of the corrosion samples and their similarity to each other. In Table 2 the ratios of aluminum to oxygen concentration in the two standard samples and the two corrosion samples are listed and compared to the theoretical ratios of aluminum elements to oxygen elements in  $\text{Al}_2\text{O}_3$  and  $\text{Al}_2\text{O}_3 \cdot 3\text{H}_2\text{O}$ . The relative concentrations of aluminum and oxygen in the two corrosion samples are practically identical and in close agreement with that of the  $\text{Al}(\text{OH})_3$  standard, while all three differ marginally (by the same amount) from the theoretical value of 1:3 expected for aluminum hydroxide. The excellent correlation between the experimental values for the  $\text{Al}(\text{OH})_3$  standard and the corrosion samples indicates that nearly all the material in the corrosion product is in the form of aluminum oxide trihydrate and very little, if any, is in the anhydrous form.

#### 4.0 AUGER ELECTRON SPECTROSCOPY

The Auger Electron Spectroscopy (AES), was employed for identification of the chemical constituents of another sample of corrosion product obtained from a lap joint from an old Boeing 727 aircraft. The AES was also conducted at the Institute for Microstructural Sciences. Like the XPS, Auger is also a surface analysis technique, wherein the volume analyzed is mainly confined to the top 20 to 50 Angstroms of the sample surface [8]. The Auger spectrum obtained from the aircraft corrosion sample is shown in Figure 17. The strong Auger line in the spectrum (around

510 eV energy) is that of oxygen and the smaller one (at about 1400 eV) is that of aluminum. The Auger signals of individual elements in the AES spectrum are proportional to their respective atomic concentrations in the area analyzed. The amplitudes of the oxygen and aluminum peaks are in the ratio of 1:0.34, which translates to a value of 0.254:0.746 for the relative concentration ratio of aluminum to oxygen species in the sample. This value is in good agreement with the theoretical ratio of 0.25:0.75 for aluminum to oxygen elements in the  $\text{Al}_2\text{O}_3 \cdot 3\text{H}_2\text{O}$  phase. Thus the Auger analysis confirms the findings of the XPS study on the aircraft sample. No carbon species were detected in the samples analyzed by AES.

## 5.0 X-RAY DIFFRACTION ANALYSIS

Having determined the chemical composition of the corrosion products by AES and XPS, X-Ray Diffraction (XRD) was employed in an attempt to identify qualitatively their crystal structure. The Rigaku X-Ray Diffractometer in the Structures, Materials and Propulsion Laboratory of the Institute for Aerospace Research was used to study the X-Ray Diffraction spectra of both the aircraft and laboratory corrosion samples. The samples were analyzed using a small step size of 0.2 degrees of rotation for the diffraction angle. The spectrum for the aircraft corrosion sample is shown in Figure 18. The peaks in the spectrum are clearly identifiable although there is an overall background noise which is believed to be caused by the amorphous content of the corrosion product. Comparing the peaks in the spectrum with those of the standards provided in the X-Ray Powder Data File [9], it was found that they matched well with

those documented for three different phases of aluminum oxide, namely, alpha basic aluminum oxide,  $\alpha\text{-Al}_2\text{O}_3\cdot(\text{OH})_2$  (known as **boehmite**, also called gamma alumina monohydrate), alpha aluminum oxide trihydrate,  $\alpha\text{-Al}_2\text{O}_3\cdot 3\text{H}_2\text{O}$  (also known as **gibbsite** or hydrargillite) and beta aluminum oxide trihydrate,  $\beta\text{-Al}_2\text{O}_3\cdot 3\text{H}_2\text{O}$  (also known as **bayerite**). The d values and the relative intensities of the peaks observed in the XRD spectrum of the aircraft sample are compared to those of boehmite, gibbsite and bayerite in Table 3. The match with the monohydrate phase is excellent in that the four strongest peaks of the standard boehmite spectrum are clearly identified in the sample spectrum. The three strongest peaks of the gibbsite phase also match well although the standard gibbsite spectrum indicates a much higher intensity for its first peak (at  $d = 4.83 \text{ \AA}$ ,  $2\theta = 18.4^\circ$ ). The number of peaks of the bayerite phase detected in the sample spectrum are greater than those of the gibbsite phase. However, only the first of the two strongest peaks specified for bayerite, for d-space values of  $4.73 \text{ \AA}$  ( $2\theta = \sim 18.4^\circ$ ) and  $2.22 \text{ \AA}$  ( $2\theta = 40.5^\circ$ ) respectively, is identifiable in the sample spectrum. The sample spectrum shows a rather inconspicuous peak at the second location of  $2.23 \text{ \AA}$ . Except for this, most of the peaks that are not of the monohydrate phase in the spectrum appear to match equally well with those of both  $\alpha\text{-Al}_2\text{O}_3\cdot 3\text{H}_2\text{O}$  and  $\beta\text{-Al}_2\text{O}_3\cdot 3\text{H}_2\text{O}$ .

Thus it appears that a precise identification of the trihydrate phase in the corrosion product may not be possible without further investigation, particularly due to the rather poor correlation of the peak intensities to those expected at their respective d values in the spectrum of either of the trihydrate phases. The lack of correlation in peak intensity values could be attributed to the overall background noise caused by the amorphous phase present in the

corrosion product. It may also have been caused by the co-existence of both the alpha and beta trihydrate phases simultaneously in the sample. It would require a detailed thermodynamic investigation to assess whether such co-existence is a stable phenomenon or an intermediate stage in the conversion process from bayerite to gibbsite as suggested in References 6,7. No such investigation is attempted here. The present XRD results only allow the inference that, in addition to the amorphous structure and the boehmite, some aluminum oxide trihydrate, either in the alpha phase (gibbsite) or in the beta phase (bayerite), or possibly a mixture, is present in the corrosion product sample. Although the X-ray Diffraction is employed here only for a qualitative analysis, it was noted that the area under the strongest peak of the trihydrate phase (peak 2 in Fig.18) is approximately twice as large as the area under the strongest peak of the boehmite phase (peak 1 in Fig.18). This appears to suggest that the relative concentrations of the crystalline trihydrate phase to the monohydrate phase in the sample may be roughly of the order of two is to one. This figure, however, is highly approximate and speculative. For reliable figures it is necessary to employ more sophisticated techniques, like the ratio of slopes[10], to quantify the relative concentrations of the various phases in the sample from the XRD data. Such quantitative methods require precise calibration of the set up and the spectral data and are not within the scope of the current work.

The X-ray Diffraction spectrum of the laboratory induced corrosion sample is shown in Figure 19. The peaks in this spectrum are not as readily identifiable as those in Figure 18. This is perhaps due to the greater amount of overall background noise caused by the greater fraction of the amorphous content in the laboratory sample. The spectrum in Figure 19 is that of the

laboratory corrosion sample while the peaks shown in it are those recorded from the aircraft sample spectrum. The superimposition clearly demonstrates that the laboratory sample has peaks at the same diffraction angle or d-space values as the aircraft corrosion sample, although they are not as prominent. In Figure 20 the XRD spectrum of the laboratory corrosion sample is shown with its peaks identified using the XRD analysis software. Their d-space values and relative intensities are tabulated and compared to those of the boehmite, gibbsite and bayerite standards in Table 4. The ambiguity between the alpha and beta trihydrate phases (bayerite and gibbsite) observed in the aircraft sample spectrum is seen here also. Once again the data definitely indicates the presence of one or the other (or both) of these trihydrate phases along with the monohydrate phase of aluminum oxide.

## 6.0 DISCUSSION

The quantitative analysis of the aircraft and laboratory samples using X-ray Photoelectron Spectroscopy and Auger Electron Spectroscopy determined the species concentrations of aluminum to oxygen in the corrosion products to be in the ratio of 1:3, indicating that the sample mainly consists of aluminum hydroxide  $\text{Al}(\text{OH})_3$  or aluminum oxide trihydrate  $\text{Al}_2\text{O}_3 \cdot 3\text{H}_2\text{O}$ . The XPS and the AES do not identify the structure or the phase of the sample, hence the X-Ray Diffraction technique was employed for phase analysis. The main conclusions from the analysis of the XRD spectra of the two samples were that there is a large fraction of the amorphous phase in both samples and that both contained a mixture of the monohydrate phase known as boehmite

and at least one of the two trihydrate phases, bayerite and gibbsite. It is significant that both XPS and the XRD indicated similar compositions for the laboratory sample and the aircraft corrosion sample.

The presence of the amorphous phase, which is presumably  $\text{Al}(\text{OH})_3$ , in addition to the mixture of the monohydrate and trihydrate crystalline phases, is in keeping with the findings of earlier researchers [3-7] and in accordance with the theory that the corrosion product is initially amorphous aluminum hydroxide and gradually progresses to less soluble crystalline forms with time [6]. The XRD data suggest the possibility of a part of the sample being in the gibbsite phase which is in accordance with the theory and findings of References 6 and 7 but in contradiction to the position of Ref.3 that gibbsite is never found in aluminum corrosion products. However, only further tests can provide conclusive evidence regarding the presence (or absence) of the gibbsite phase.

There appears to be some difference between the findings of the XPS and AES results and the results of the XRD spectrum analysis, in that the former identified the samples to be composed primarily of aluminum hydroxide or aluminum oxide trihydrate, while the latter detected a significant fraction of the monohydrate phase also. The difference in results maybe explained as follows. The XPS and the AES are surface analysis techniques probing only the top 20 to 50 Å of the sample surface, while the XRD receives signals from layers many tens of microns in depth. Thus the results indicate that the top region of the samples is made up of  $\text{Al}_2\text{O}_3 \cdot 3\text{H}_2\text{O}$  only while the inner layers contain a mixture of both  $\text{Al}_2\text{O}_3 \cdot 3\text{H}_2\text{O}$  and  $\text{Al}_2\text{O}(\text{OH})_2$ .

The number of oxygen atoms associated with one atom of aluminum in  $\text{Al}_2\text{O}_3 \cdot 3\text{H}_2\text{O}$  and  $\text{Al}_2\text{O}(\text{OH})_2$  are 3 and 1.5 respectively. Hence it appears reasonable that the outer surfaces of the sample, which are directly exposed to oxygen and water vapour in the atmosphere, are almost entirely composed of  $\text{Al}_2\text{O}_3 \cdot 3\text{H}_2\text{O}$ , while interior regions of the granular corrosion product particles, being deficient in oxygen and water, contain  $\text{Al}_2\text{O}(\text{OH})_2$  along with the trihydrate phase. It appears reasonable to assume that the concentration of  $\text{Al}_2\text{O}_3 \cdot 3\text{H}_2\text{O}$  would gradually decrease from 100% as we go below the surface of the particles while that of the  $\text{Al}_2\text{O}(\text{OH})_2$  increases.

Another possible cause for the difference between the XPS and the XRD results is the time lag between the performance of the two sets of analyses. The X-ray diffraction analysis was conducted about 40 to 45 days after the XPS. The laboratory samples used in the two tests were obtained from specimens which were subjected to the accelerated corrosion application at about the same time. Similarly the aircraft corrosion samples were extracted from lap joint sections which were disassembled for inspection at about the same time. Hence both the aircraft and the laboratory specimen employed in the XRD study were exposed to laboratory atmosphere and allowed to age for an additional period of about forty five days before being analyzed. It is possible that initially all four samples contained only amorphous aluminum hydroxide and that the  $\text{Al}(\text{OH})_3$  in the XPS samples got converted to the boehmite phase and subsequently to the trihydrate phase during this aging period. The Auger spectroscopy was performed even earlier than the XPS, hence this analysis may also have encountered only the amorphous aluminum hydroxide phase. Unfortunately the crystal structure of the samples in their initial condition is

not known, hence there is no experimental evidence to prove or disprove this line of reasoning at this juncture. However it is in accordance with the theory that the crystal structure of the corrosion product changes with age and that this time dependent process is influenced by temperature, moisture and other environmental conditions. One may interpolate that between the skins of the aircraft lap or butt joint, the corrosion product remains largely amorphous until the joint is disassembled and the oxide exposed to atmosphere. The oxide then passes through a brief phase of existence as Boehmite, at least in the interior regions of the corrosion particles, before it crystallizes into one or both of the two phases of Aluminum Oxide Trihydrate.

## 7.0 CONCLUSIONS

The following conclusions may be drawn based on the limited number of tests performed in this study:

- ★ The copper accelerated acetic acid salt spray method (ASTM B368) successfully duplicates the corrosion processes in the longitudinal and circumferential skin splices in aging transport aircraft. The products of corrosion generated by this accelerated laboratory method are very similar in composition and phase to those obtained by corrosion in aircraft due to natural aging.
  
- ★ The major constituents identified in the aircraft as well as the laboratory samples of the

corrosion product were aluminum hydroxide (amorphous), aluminum oxide trihydrate (crystalline) and aluminum oxide monohydrate (boehmite).

- ★ The XPS and the Auger analyses performed on relatively fresh samples showed that they were comprised almost entirely of the trihydrate form (either amorphous or crystalline) of aluminum oxide.
- ★ A small but significant fraction of the corrosion product samples investigated after a lapse of about forty five days was found to be made up of boehmite, while the remaining contained a mixture of amorphous aluminum hydroxide and crystalline states of aluminum oxide trihydrate. Resolution between the alpha (gibbsite) and the beta (bayerite) phases of the crystalline trihydrate was not possible with the available data.
- ★ The results from the present tests appear to support the theory that the corrosion product is initially amorphous aluminum hydroxide, which progressively converts to the monohydrate and then the trihydrate crystalline phases of aluminum oxide under natural aging conditions.

## ACKNOWLEDGEMENTS

The authors gratefully acknowledge the assistance rendered by Dr.S.N. Kumar of Kingston Ceramics, Kingston, Ontario in performing the X-ray Diffraction analysis and interpreting its

results. This work was carried out under the National Research Council's IAR Program 3G3 - Aerospace Structures, Structural Dynamics and Acoustics, Sub-Program 304 - Fatigue and Damage Tolerance of Structures, Project JGJ-02.

## REFERENCES

1. Komorowski, J.P., Gould, R.W. and Simpson, D.L., *Recent Progress in the Application of Diffractometer to the Inspection of Aircraft Structures*, presented at the 1992 USAF Structural Integrity Program Conference, San Antonio, Texas, December 1992.
2. H.H. Uhlig and R.W. Revie, *Corrosion and Corrosion Control*, John Wiley and Sons, New York, 1971.
3. H.P. Godard, W.B. Jepson, M.R. Bothwell and R.L. Kane, *The Corrosion of Light Metals*, John Wiley and Sons, New York, 1967.
4. U.R. Evans, *The Corrosion and Oxidation of Metals: Scientific Principles and Practical Applications*, Edward Arnold (Publishers) Ltd., London, 1960.
5. R.K. Hart, Trans. Faraday Soc., Vol.53, pp.1020, 1957.
6. E. Delmonde and M. Pourbaix, Corrosion, Vol.14, pp.496, 1958.
7. F.J. Shipko and R.M. Haag, Report KAPL-1740, General Electric Co., Knolls Atomic Power Laboratory, July 1957.
8. Czanderna, A.W. (ed.), *Methods of Surface Analysis*, Elsevier Scientific Publishing Co., Amsterdam, 1975.
9. *Index to the X-Ray Powder Data File*, ASTM Special Technical Publication 48-I, American Society for Testing Materials, 1960.
10. Monshi, A. and Messer, P.F., *Ratio of Slopes Method for Quantitative X-Ray Diffraction Analysis*, Journal of Materials Science Vol.26, pp.3623-3627, 1991.

**Table 1. Percentage Concentration of Main Species detected by XPS**

Sample	Percentage Concentration of Main Species		
	Aluminum	Oxygen	Carbon
Al <sub>2</sub> O <sub>3</sub> Standard	37.0	55.1	7.9
Al(OH) <sub>3</sub> Standard	21.3	58.1	20.6
Aircraft Corrosion Sample	17.2	46.7	36.1
Laboratory Corrosion Sample	10.9	28.7	60.4

**Table 2. Relative Concentrations of Aluminum and Oxygen in the Samples**

Sample	Measured Value	Expected Value
	Aluminum : Oxygen	Aluminum : Oxygen
Al <sub>2</sub> O <sub>3</sub> Standard	40.2 : 59.8	40 : 60
Al(OH) <sub>3</sub> Standard	26.8 : 73.2	25 : 75
Aircraft Corrosion Sample	26.9 : 73.1	
Laboratory Corrosion Sample	26.9 : 73.1	

**Table 3. Comparison of XRD Data for Aircraft Corrosion Sample**

Peak Number	Aircraft Corrosion Sample Data			Standard Data for $\alpha\text{-Al}_2\text{O}_3(\text{OH})_2$ (Boehmite)			Standard Data for $\alpha\text{-Al}_2\text{O}_3 \cdot 3\text{H}_2\text{O}$ (Gibbsite)			Standard Data for $\beta\text{-Al}_2\text{O}_3 \cdot 3\text{H}_2\text{O}$ (Bayerite)		
	d-space (Å)	Relative Intensity		hkl	d-space (Å)	Relative Intensity	hkl	d-space (Å)	Relative Intensity	hkl	d-space (Å)	Relative Intensity
1	6.31	58		020	6.110	100						
2	4.83	100					002	4.85	320	001	4.73	100
3	4.38	61					110	4.37	50	100	4.37	80
4	3.26	44		021	3.164	65				101	3.21	60
5	2.34	51		041	2.346	53	311	2.388	27	002	2.36	20
6	2.23	33					022	2.244	10	111	2.22	100
7	2.02	28					313	2.043	17	201	1.981	20
8	1.86	40		150	1.860	32						
9	1.73	23					024	1.750	16	---	1.719	70
10	1.69	23					314	1.689	13	---	1.691	10
11	1.44	27		132	1.453	16				---	1.445	20
12	1.33	18		152	1.312	15						

ESCA Survey 20 Dec 91 Angle: 45 degrees Acquisition Time: 4.67 min  
File: st211 Al2O3 standard  
Scale Factor: 51.558 kc/s Offset: 0.213 kc/s Pass Energy: 187.850 eV Aperture: 0 Al 600 M

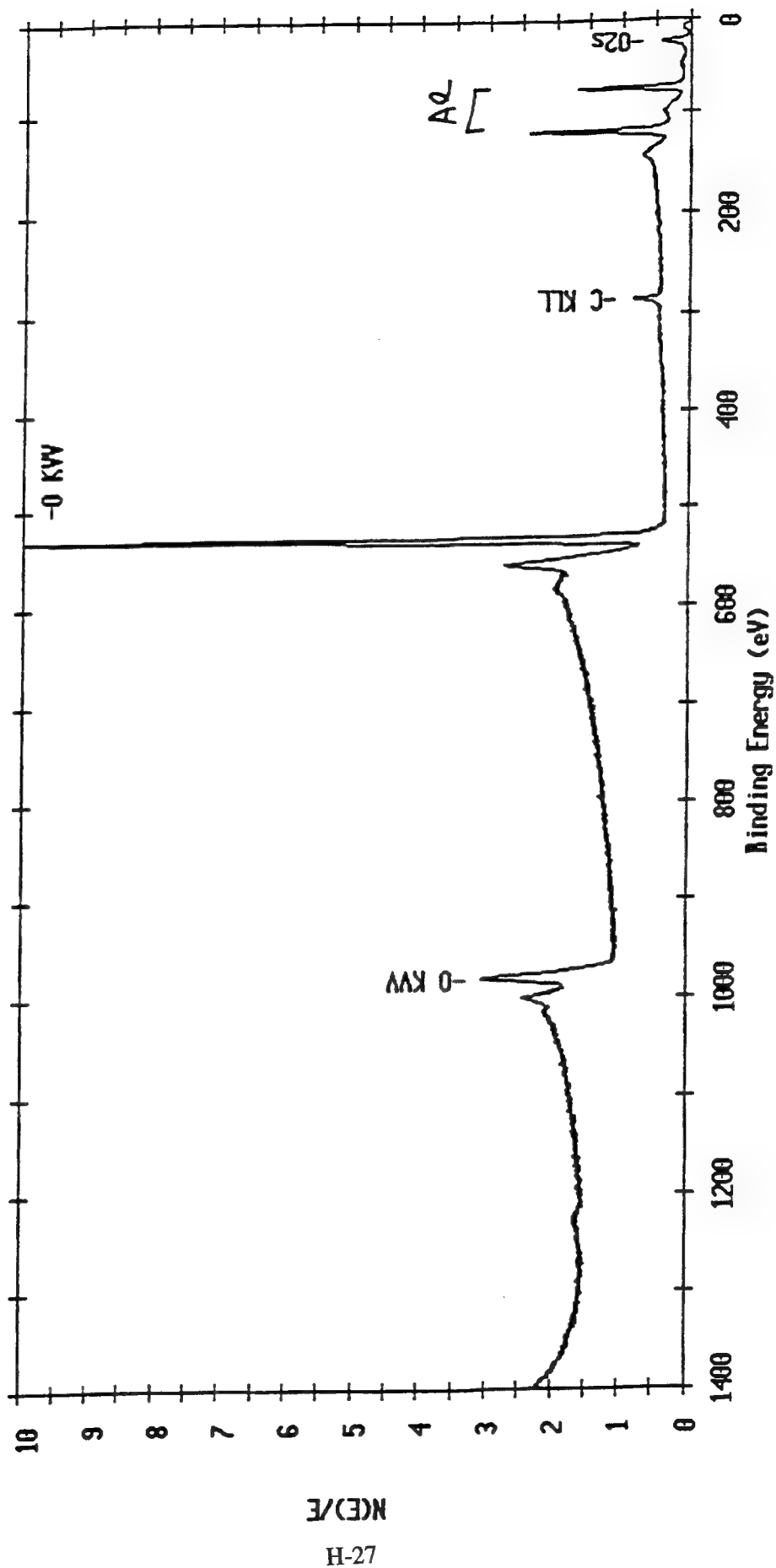


Figure 1. XPS Survey of Al<sub>2</sub>O<sub>3</sub> Standard

ESCA Multiplex 11 Aug 93 Species: 01 Region: 1 Angle: 70 degrees Acquisition Time: 3.38 min  
File: ron\_29 Al203 standard  
Scale Factor: 3.550 kc/s Offset: 0.818 kc/s Pass Energy: 29.350 eV Aperture: 3 Al 500 M

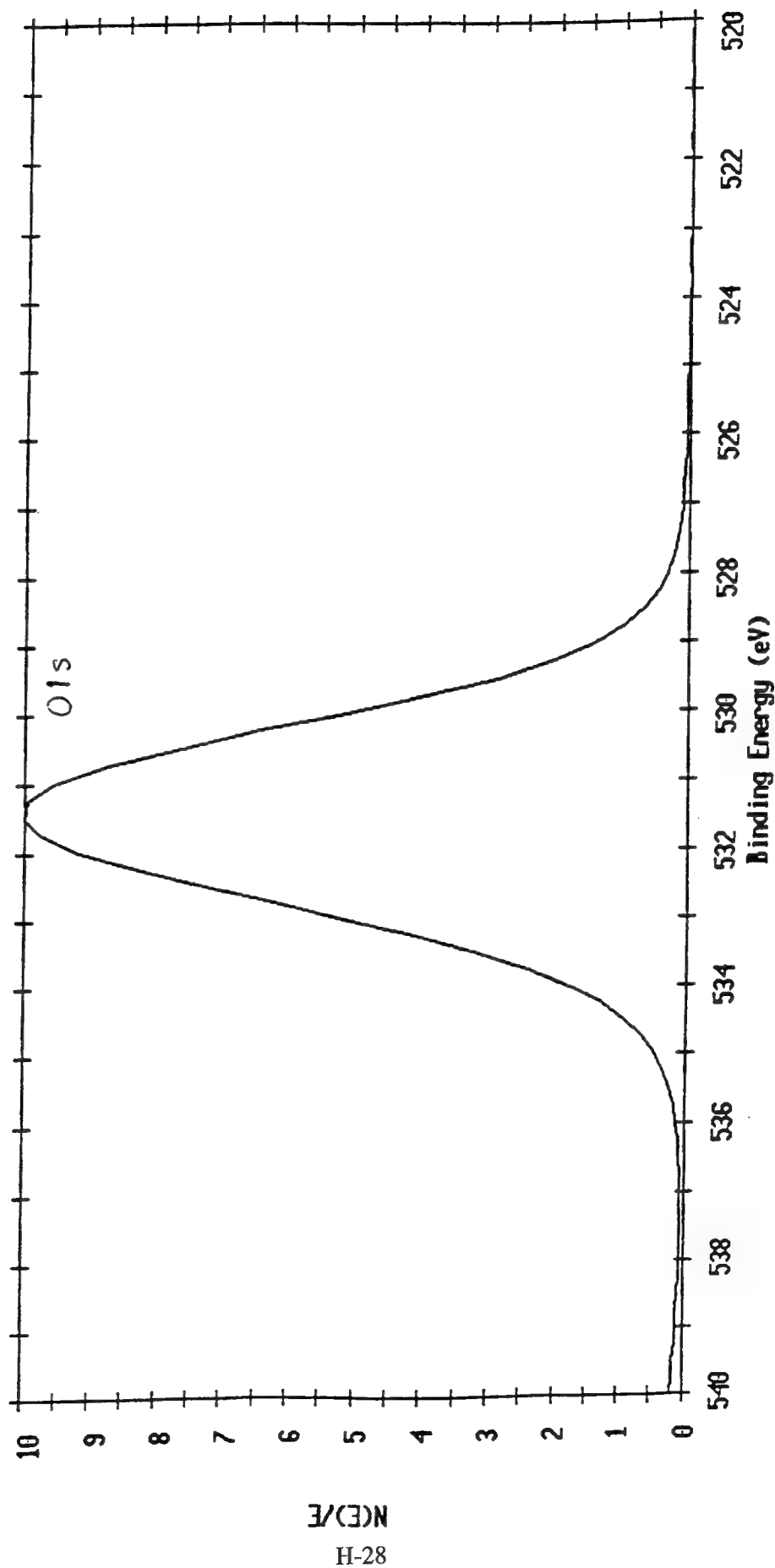


Figure 2. Oxygen Peak in XPS Spectrum of  $\text{Al}_2\text{O}_3$  Standard

**Table 4. Comparison of XRD Data for Laboratory Corrosion Sample**

Peak Number	Aircraft Corrosion Sample Data		Standard Data for $\alpha\text{-Al}_2\text{O}_3(\text{OH})_2$ (Boehmite)			Standard Data for $\alpha\text{-Al}_2\text{O}_3 \cdot 3\text{H}_2\text{O}$ (Gibbsite)			Standard Data for $\beta\text{-Al}_2\text{O}_3 \cdot 3\text{H}_2\text{O}$ (Bayerite)		
	d-space ( $\text{\AA}$ )	Relative Intensity	hkl	d-space ( $\text{\AA}$ )	Relative Intensity	hkl	d-space ( $\text{\AA}$ )	Relative Intensity	hkl	d-space ( $\text{\AA}$ )	Relative Intensity
1	6.36	58	020	6.11	100						
2	4.82	100				002	4.85	320	001	4.73	100
3	4.38	61				110	4.37	50	100	4.37	80
4	3.26	44	021	3.164	65				101	3.21	60
5	2.32	51	041	2.346	53	311	2.388	27	002	2.36	20
6	2.23	33				022	2.244	10	111	2.22	100
7	1.87	40	150	1.860	32						
8	1.72	23				024	1.750	16	---	1.719	70
9	1.44	27	132	1.453	16				---	1.445	20
10	1.31	18	152	1.312	15						

ESCA Multiplex 11 Aug 93 Species: Al1 Region: 2 Angle: 70 degrees Acquisition Time: 2.04 min  
File: ron\_29 Al2O3 standard  
Scale Factor: 0.611 kc/s Offset: 0.256 kc/s Pass Energy: 29.350 eV Aperture: 3 Al 500 W

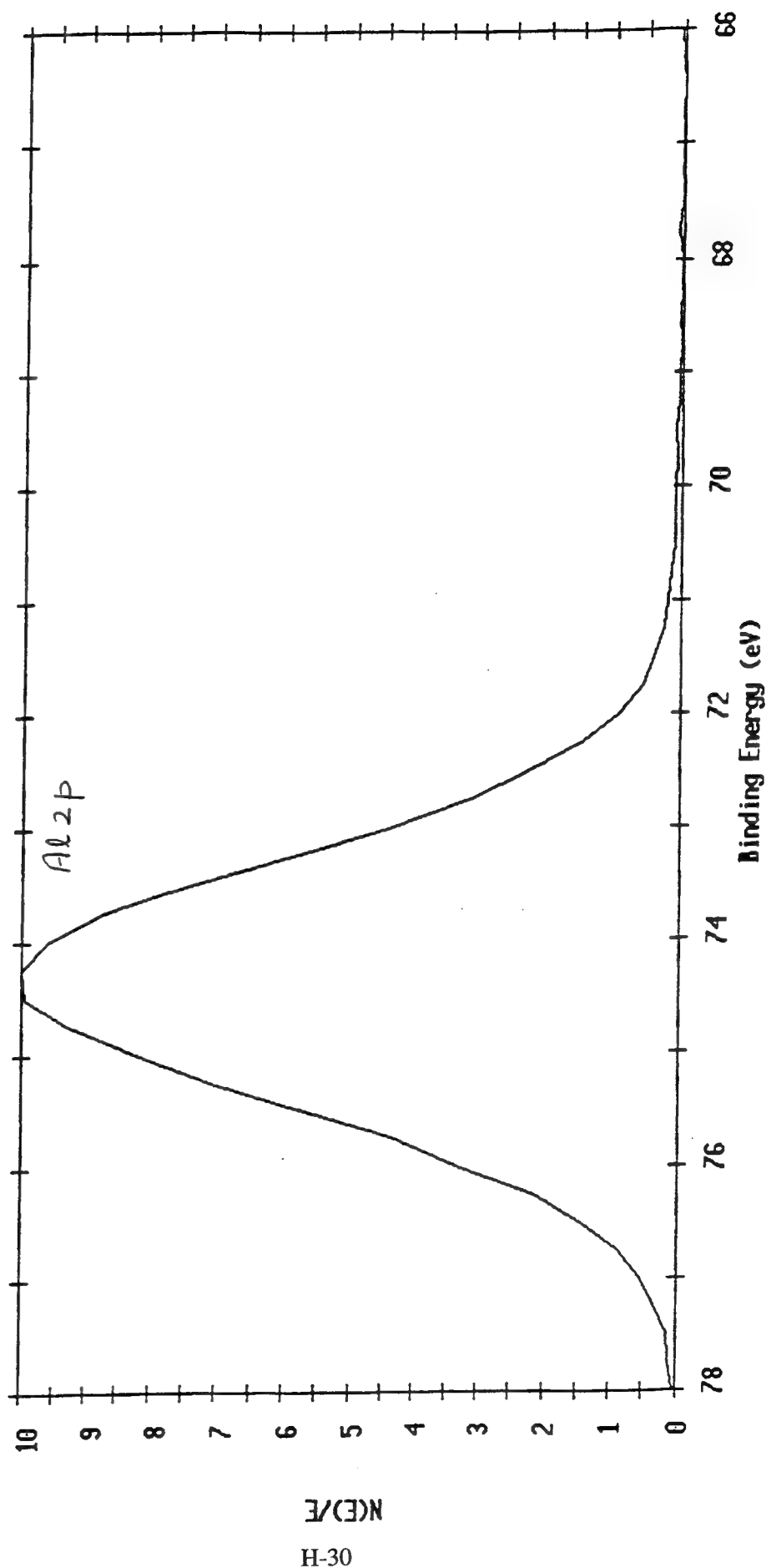


Figure 3. Aluminum Peak in XPS Spectrum of Al<sub>2</sub>O<sub>3</sub> Standard

ESCA Multiplex 11 Aug 93 Species: C1 Region: 70 degrees Acquisition Time: 3.38 min  
File: ron\_29 Al2O3 standard  
Scale Factor: 0.154 kc/s Offset: 5.871 kc/s Pass Energy: 117.400 eV Aperture: 3 Al 500 M

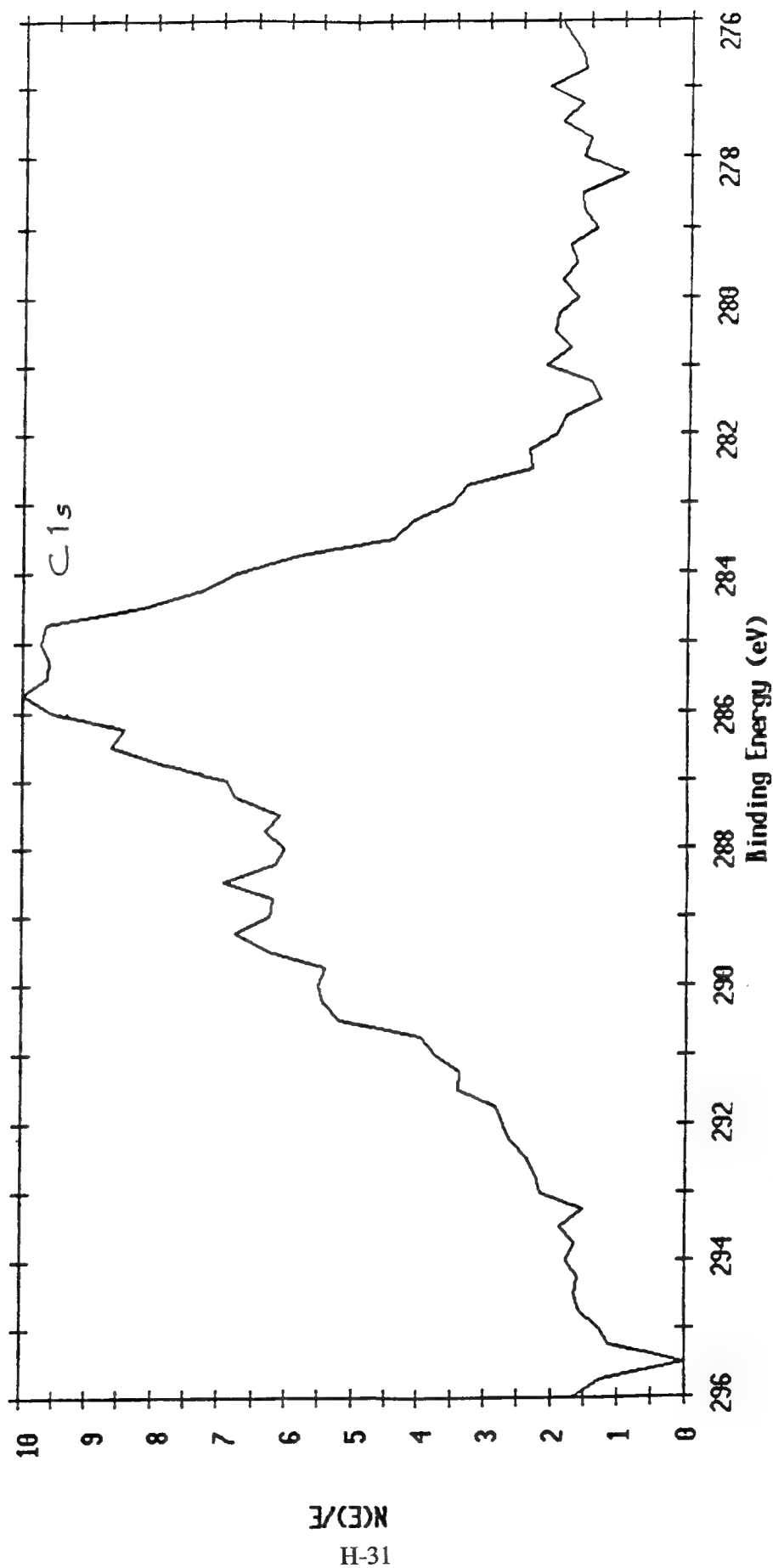


Figure 4. Carbon Peak in XPS Spectrum of  $\text{Al}_2\text{O}_3$  Standard

ESCA Survey 16 Aug 93 Angle: 70 degrees Acquisition Time: 9.34 min  
 File: ron\_32 Al(OH)<sub>3</sub> standard  
 Scale Factor: 11.841 kc/s Offset: 0.175 kc/s Pass Energy: 117.400 eV Aperture: 3 Al 500 W

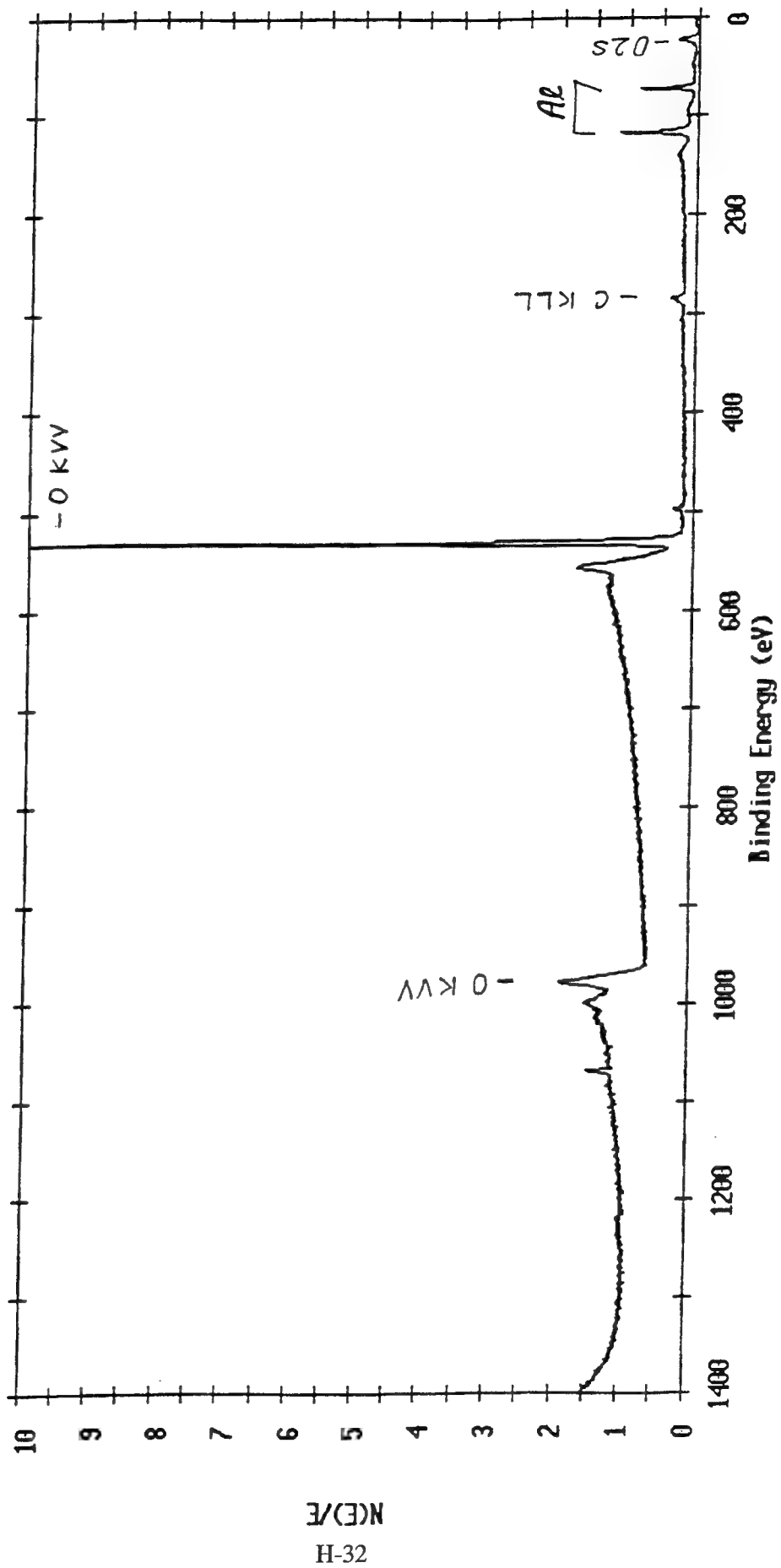


Figure 5. XPS Survey of Al(OH)<sub>3</sub> Standard

ESCA Multiplex 16 Aug 93 Species: 01 Region: 1 Angle: 70 degrees Acquisition Time: 3.38 min  
File: ron\_31 Al(OH)<sub>3</sub> standard  
Scale Factor: 2.944 kc/s Offset: 0.386 kc/s Pass Energy: 29.350 eV Aperture: 3 Al 500 M

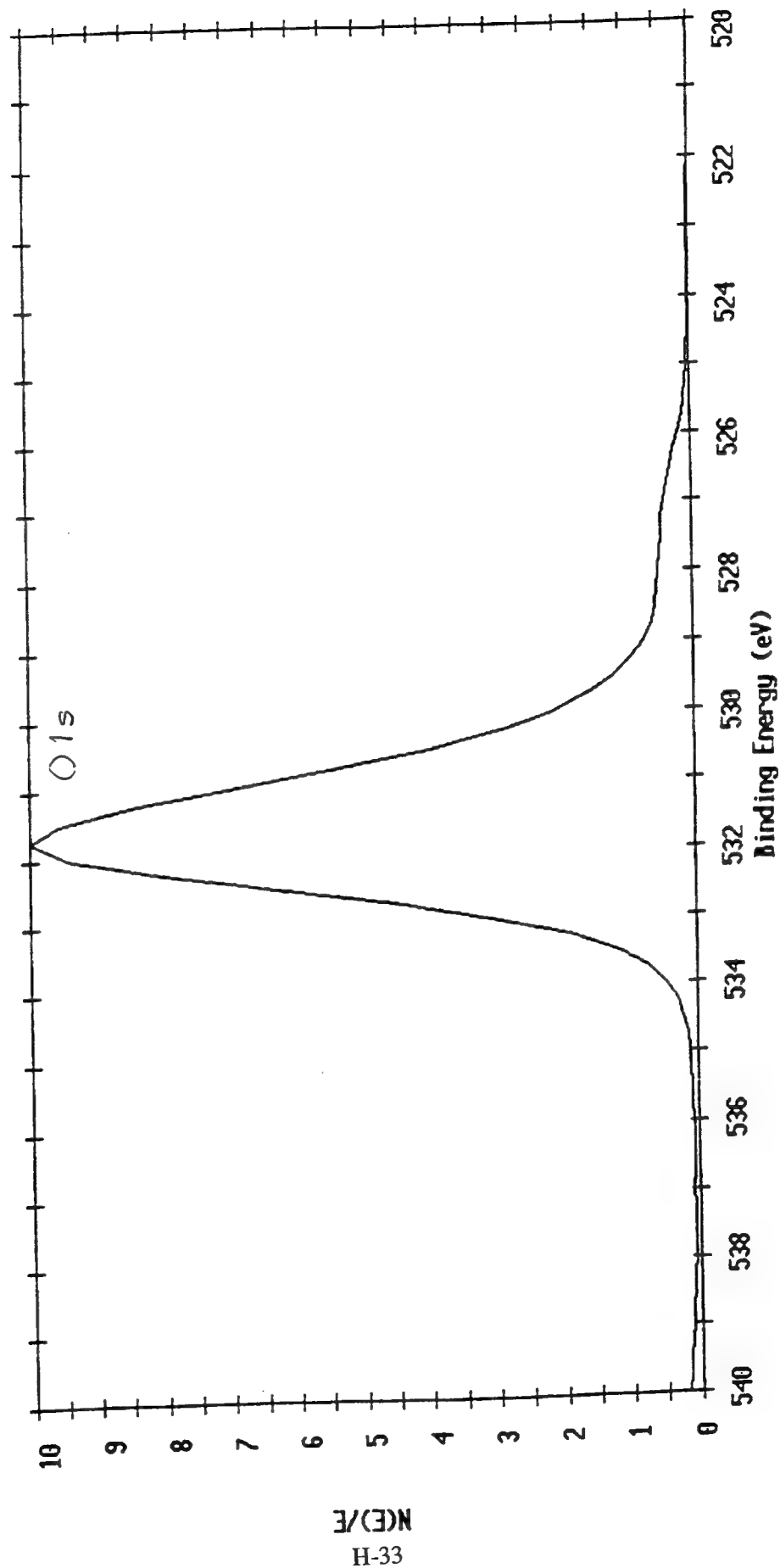


Figure 6. Oxygen Peak in XPS Spectrum of Al(OH)<sub>3</sub> Standard

ESCA Multiplex 16 Aug 93 Species: Al1 Region: 2 Angle: 70 degrees Acquisition Time: 2.04 min  
File: ron\_31 Al(OH)3 standard  
Scale Factor: 0.238 kc/s Offset: 0.166 kc/s Pass Energy: 29.350 eV Aperture: 3 Al 500 W

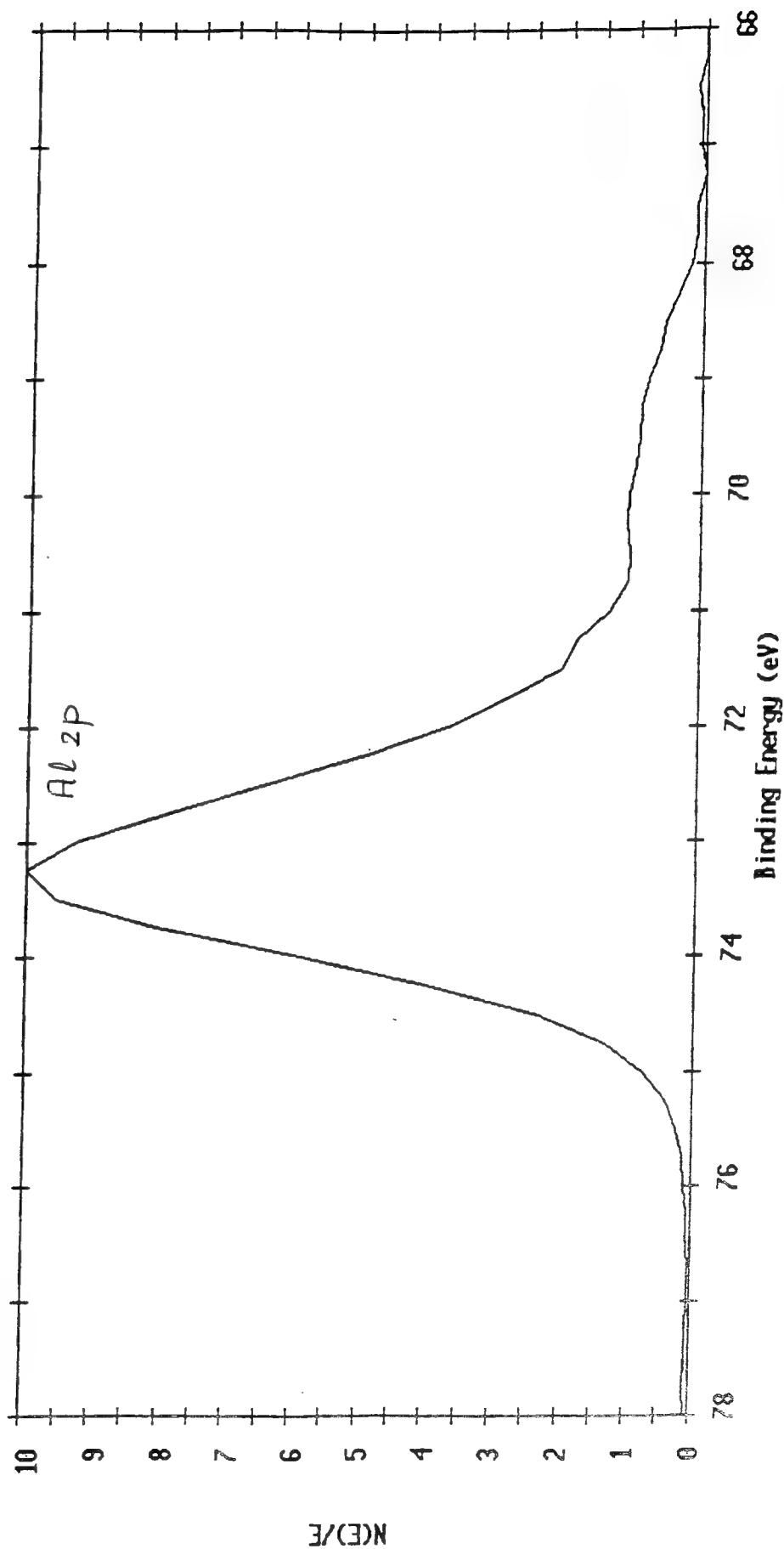


Figure 7. Aluminum Peak in XPS Spectrum of Al(OH)<sub>3</sub> Standard

ESCA Multiplex 16 Aug 93 Species: C1 Region: 70 degrees Acquisition Time: 3.38 min  
File: ron\_31 Al(OH)3 standard  
Scale Factor: 0.246 kc/s Offset: 2.102 kc/s Pass Energy: 117.400 eV Aperture: 3 Al 500 M

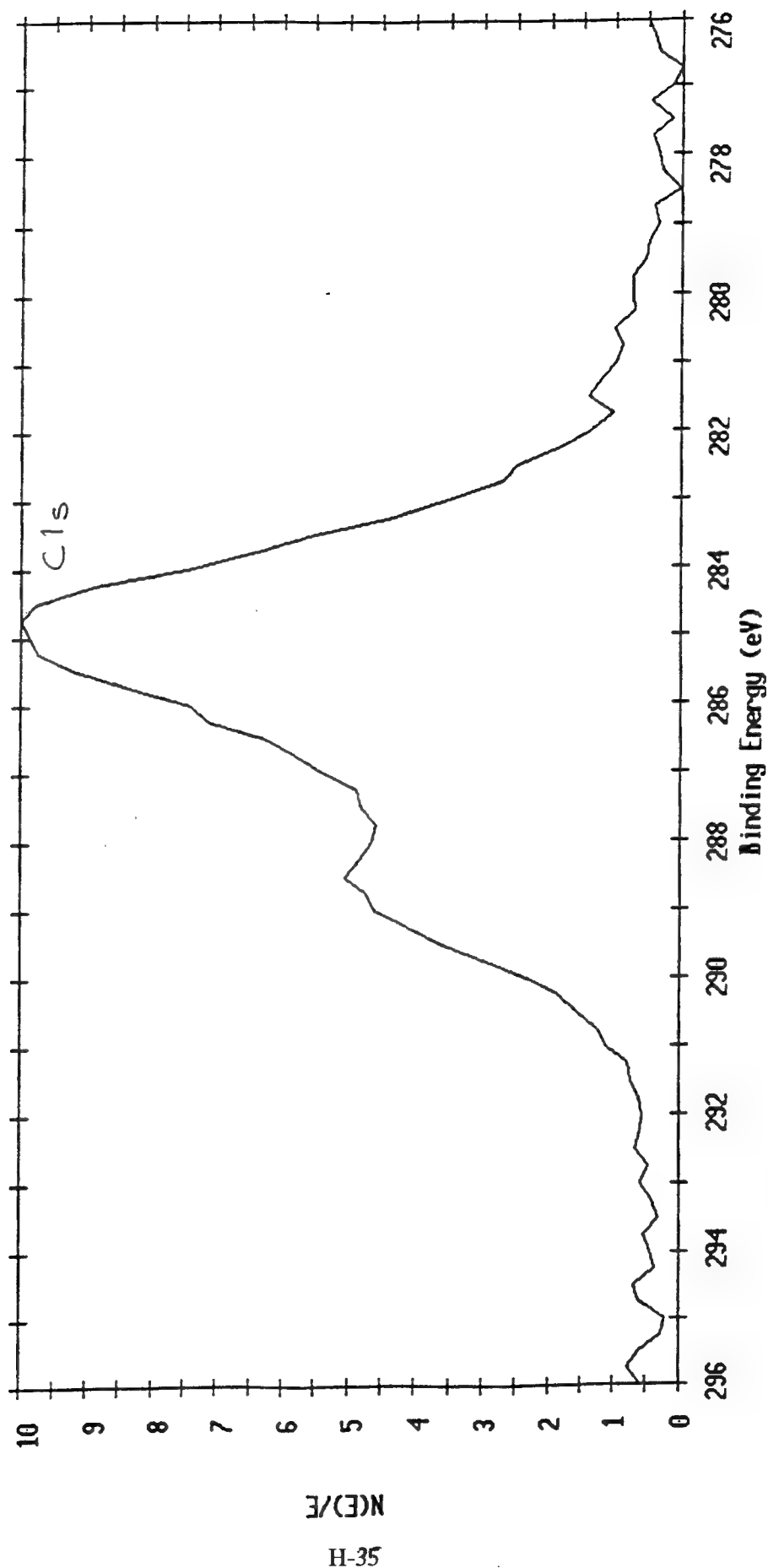


Figure 8. Carbon Peak in XPS Spectrum of Al(OH)<sub>3</sub> Standard

ESCA Survey 11 Aug 93 Angle: 70 degrees Acquisition Time: 9.34 min  
 File: ron\_25 aircraft corrosion product  
 Scale Factor: 14.240 kc/s Offset: 0.100 kc/s Pass Energy: 117.400 eV Aperture: 3 Al 500 M

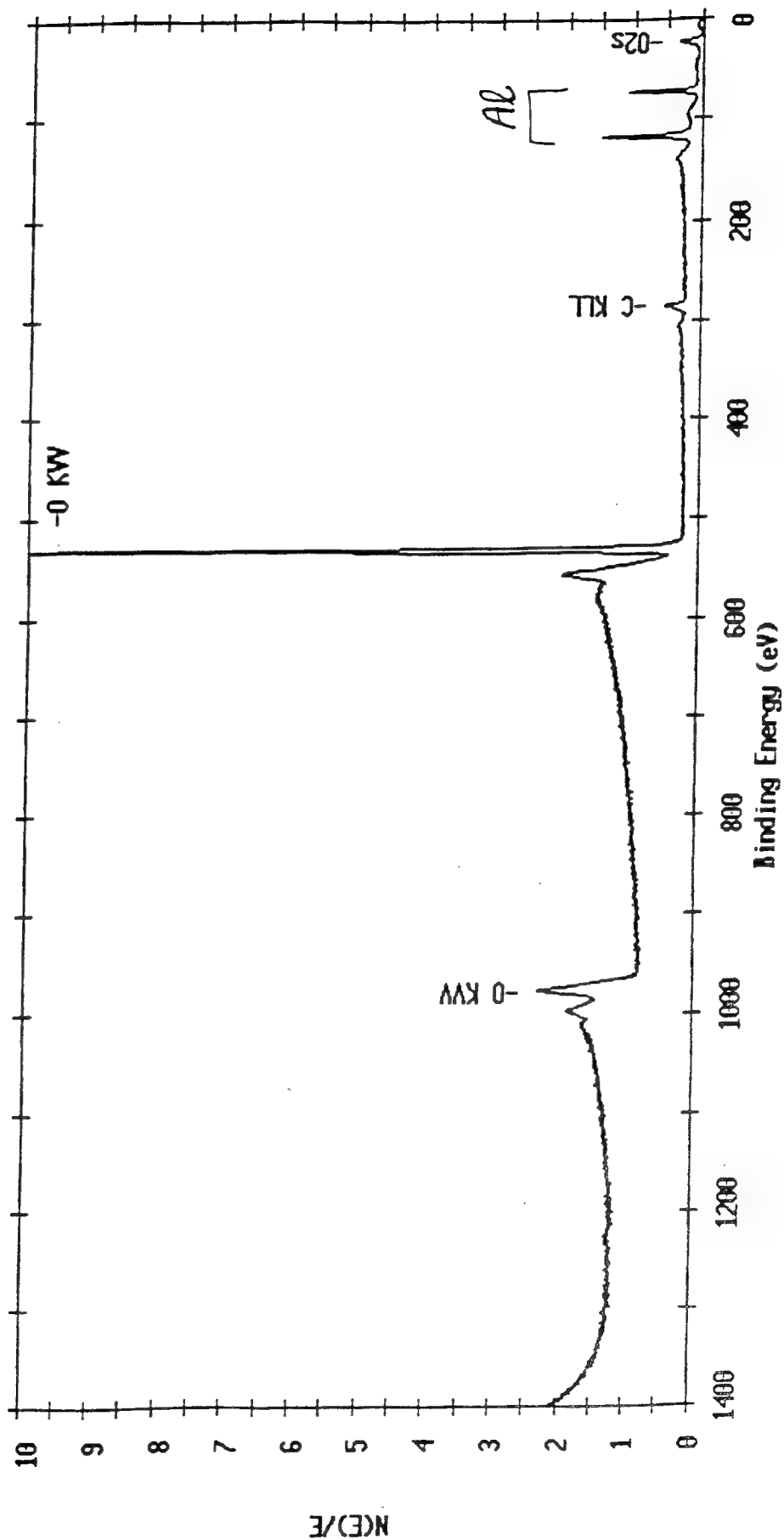


Figure 9. XPS Survey of Aircraft Corrosion Sample

ESCA Multiplex 13 Aug 93 Species: 01 Region: 1 Angle: 70 degrees Acquisition Time: 3.38 min  
File: ron\_30 aircraft corrosion product  
Scale Factor: 2.364 kc/s Offset: 0.411 kc/s Pass Energy: 29.350 eV Aperture: 3 Al 500 W

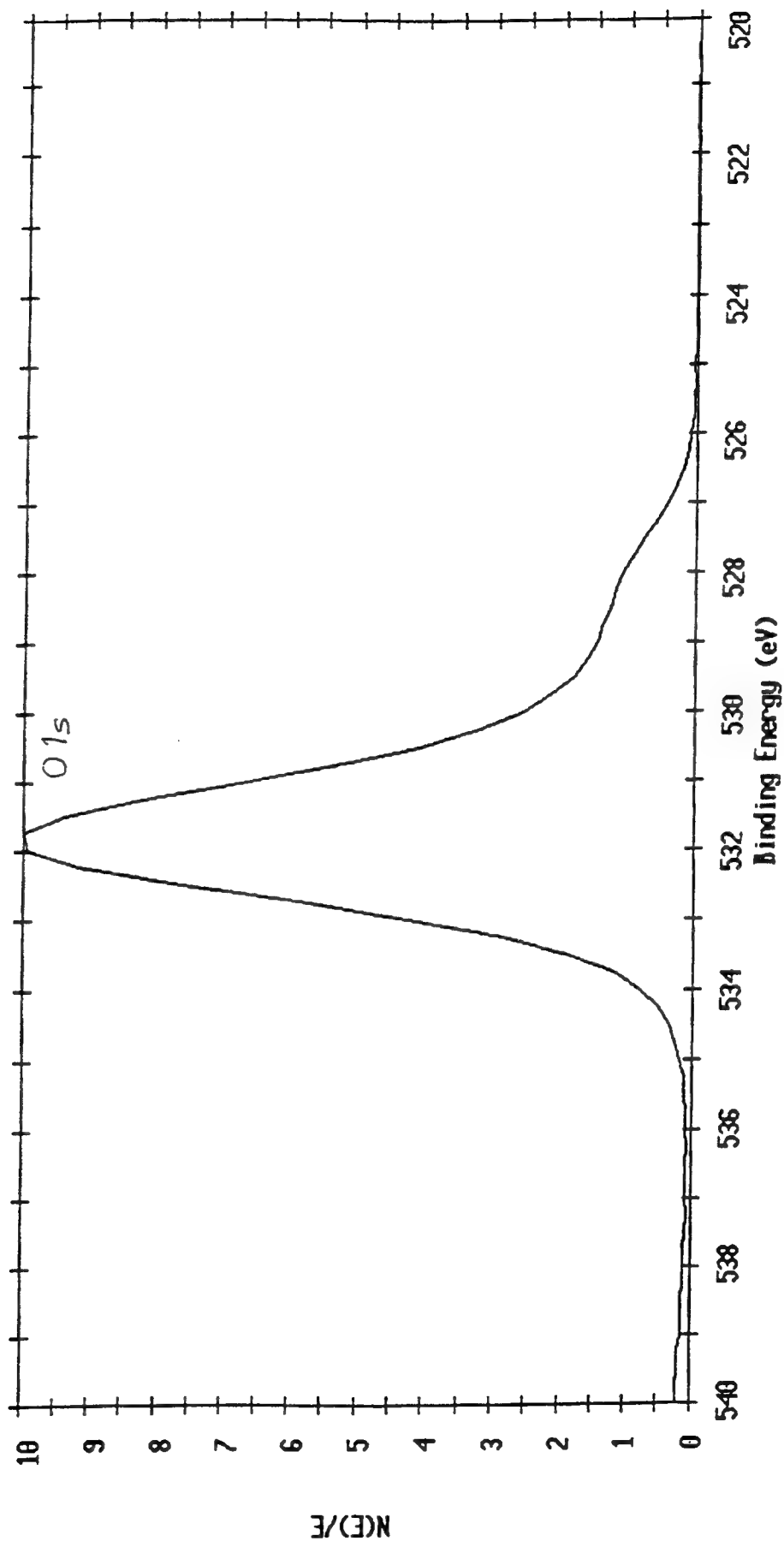


Figure 10. Oxygen Peak in XPS Spectrum of Aircraft Corrosion Sample

ESCA Multiplex 13 Aug 93 Species: Al1 Region: 2 Angle: 70 degrees Acquisition Time: 2.84 min  
File: ron\_30 aircraft corrosion product  
Scale Factor: 0.161 kc/s Offset: 0.188 kc/s Pass Energy: 29.350 eV Aperture: 3 Al 500 W

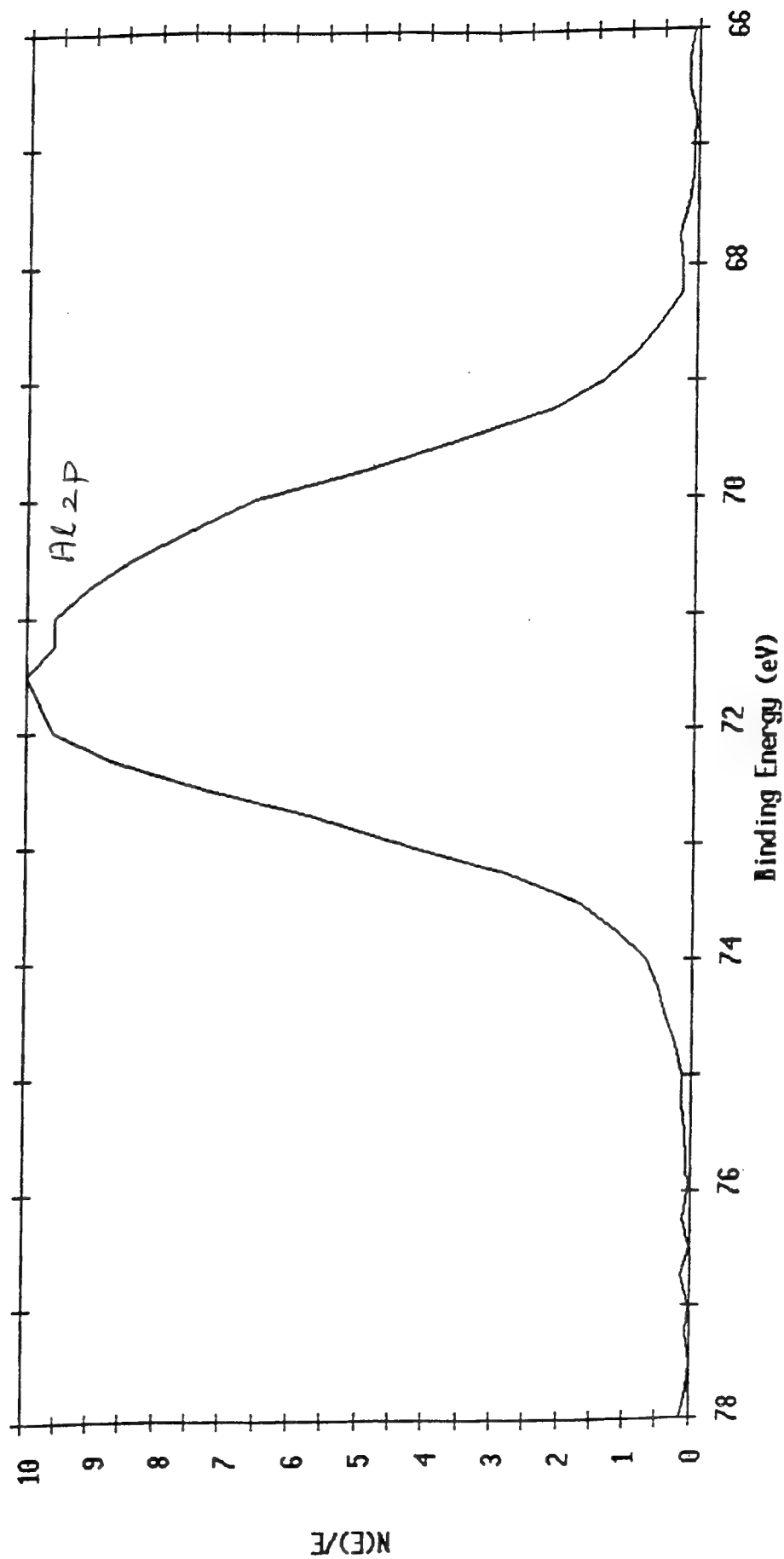


Figure 11. Aluminum Peak in XPS Spectrum of Aircraft Corrosion Sample

ESCA Multiplex 13 Aug 93 Species: C1 Region: 3 Angle: 70 degrees Acquisition Time: 3.38 min  
File: ron\_30 aircraft corrosion product  
Scale Factor: 0.493 kc/s Offset: 2.063 kc/s Pass Energy: 117.400 eV Aperture: 3 Al 500 N

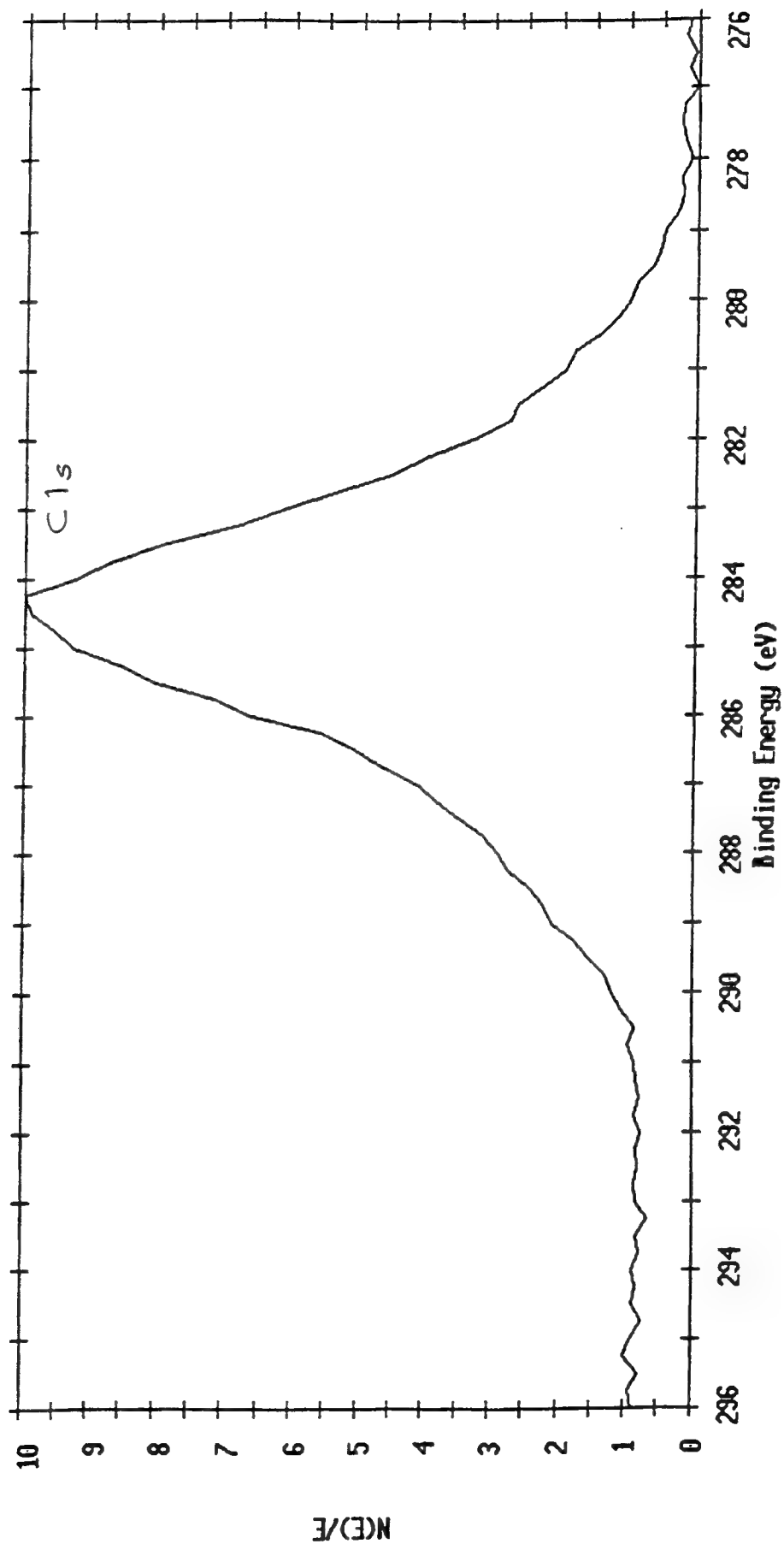


Figure 12. Carbon Peak in XPS Spectrum of Aircraft Corrosion Sample

ESCA Survey 11 Aug 93 Angle: 70 degrees Acquisition Time: 9.34 min  
File: ron\_22 Lab corrosion product  
Scale Factor: 11.148 kc/s Offset: 0.715 kc/s Pass Energy: 117.400 eV Aperture: 3 Al 500 M

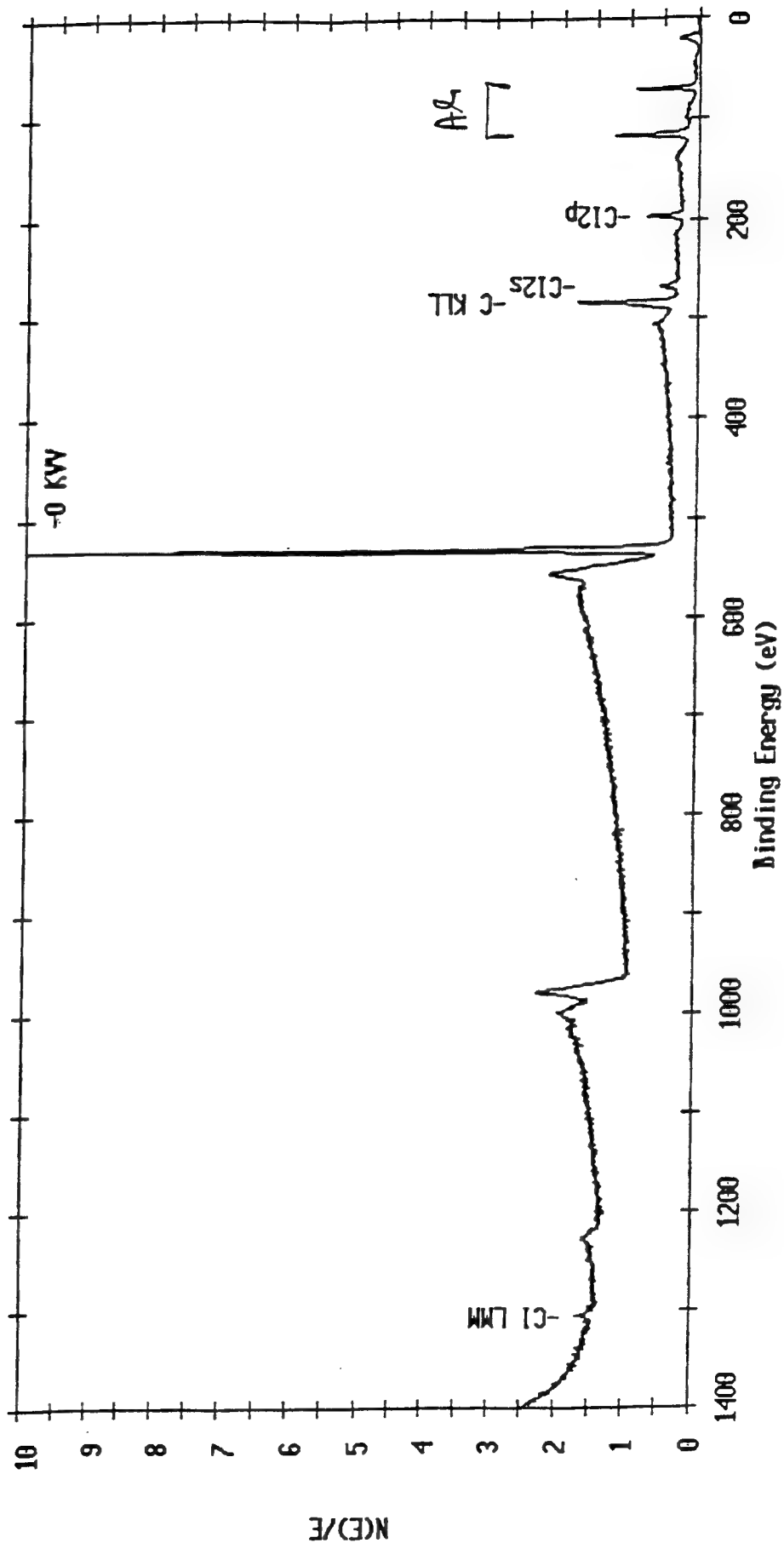


Figure 13. XPS Survey of Laboratory Corrosion Sample

ESCA Multiplex 11 Aug 93 Species: 01 Region: 1 Angle: 70 degrees Acquisition Time: 3.38 min  
File: ron\_23 Lab corrosion product  
Scale Factor: 2.483 kc/s Offset: 0.872 kc/s Pass Energy: 29.350 eV Aperture: 3 Al 500 W

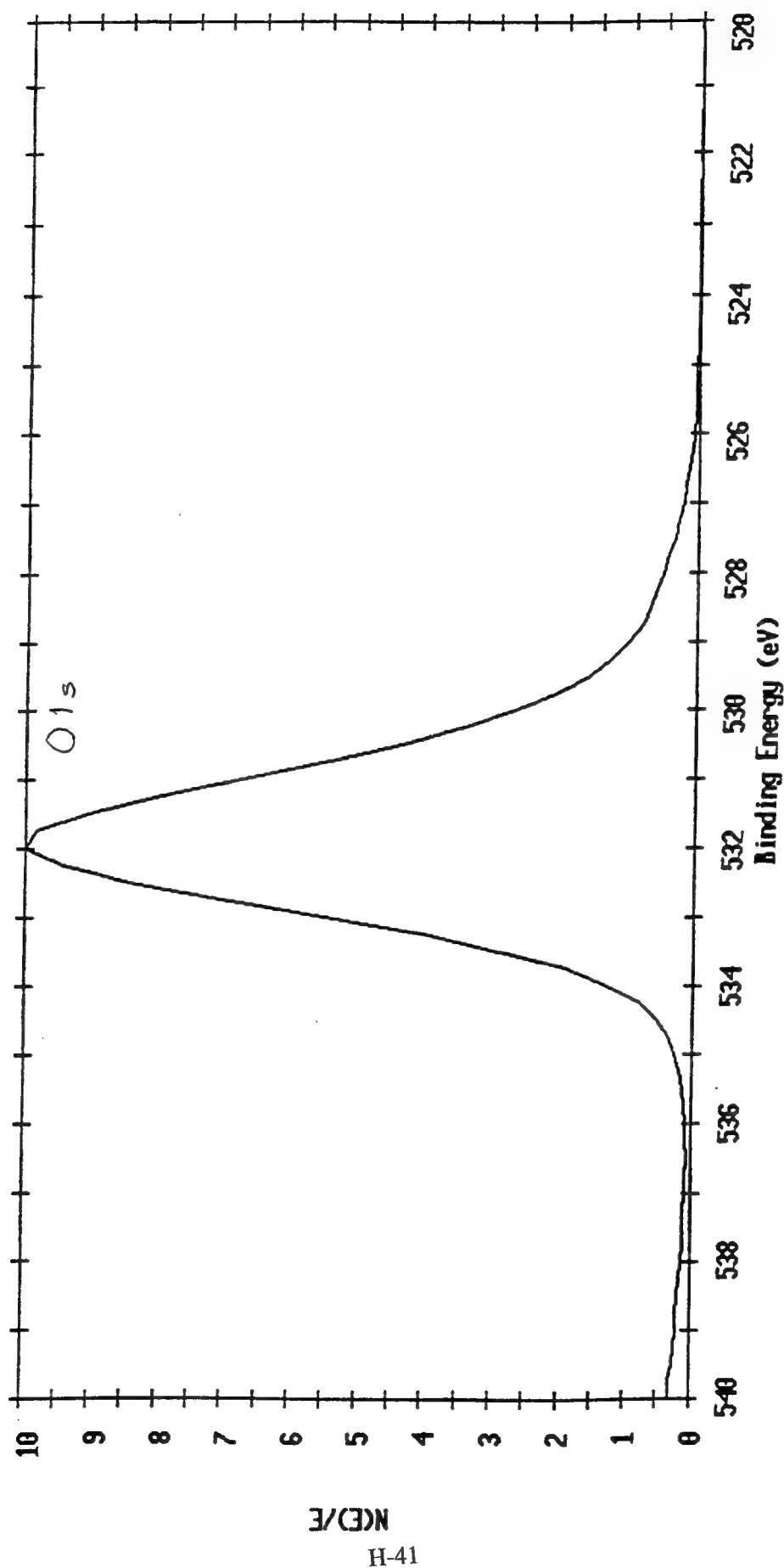


Figure 14. Oxygen Peak in XPS Spectrum of Laboratory Corrosion Sample

ESCA Multiplex 11 Aug 93 Species: Al1 Region: 2 Angle: 70 degrees Acquisition Time: 2.04 min  
File: ron\_23 Lab corrosion product  
Scale Factor: 0.211 kc/s Offset: 0.241 kc/s Pass Energy: 29.350 eV Aperture: 3 Al 500 W

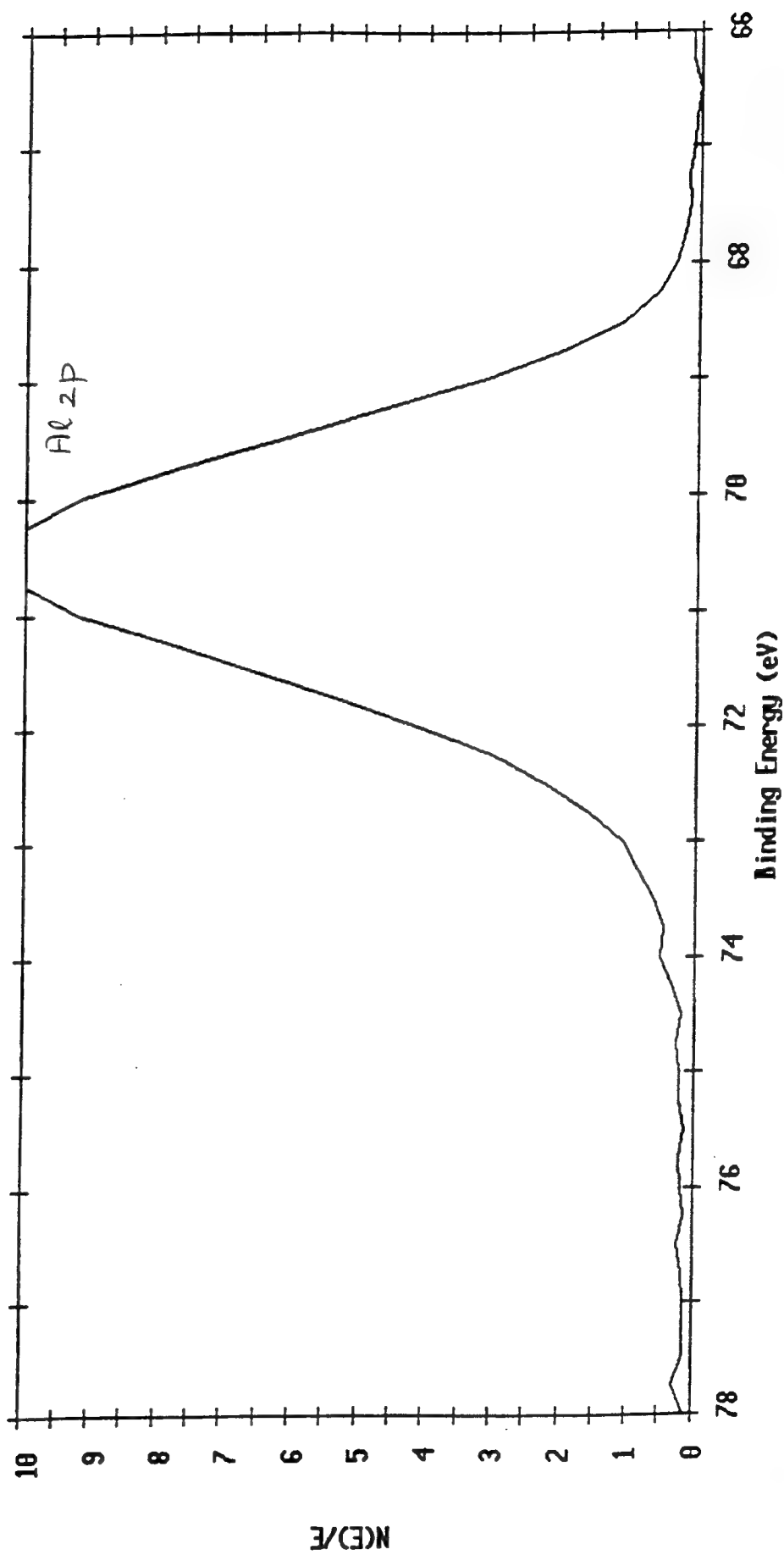


Figure 15. Aluminum Peak in XPS Spectrum of Laboratory Corrosion Sample

ESCA Multiplex 11 Aug 93 Species: C1 Region: 3 Angle: 70 degrees Acquisition Time: 3.38 min  
File: ron\_23 Lab corrosion product  
Scale Factor: 1.557 kc/s Offset: 4.107 kc/s Pass Energy: 117.400 eV Aperture: 3 Al 500 W

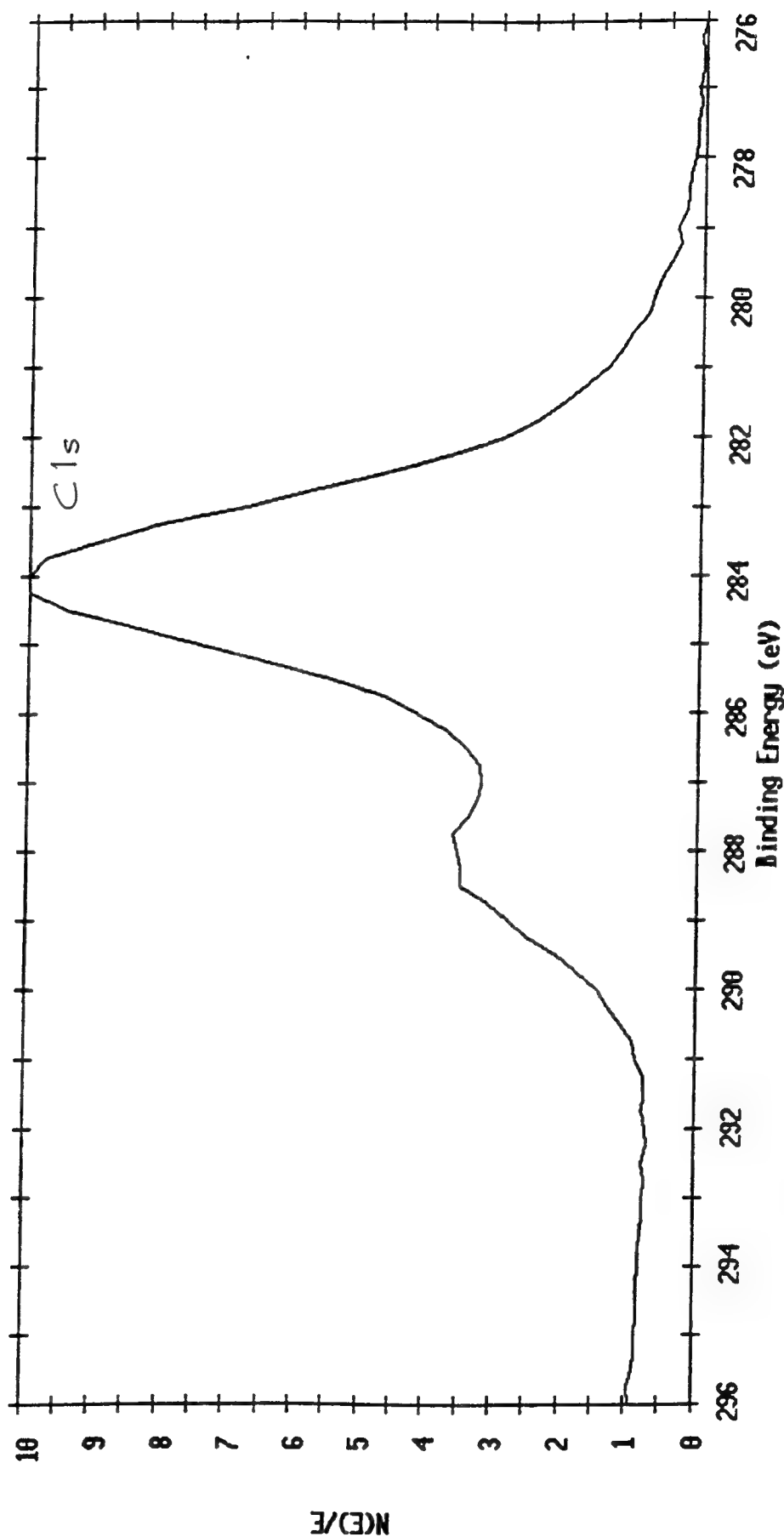


Figure 16. Carbon Peak in XPS Spectrum of Laboratory Corrosion Sample

AES Survey V/f 20 Jul 93 Area: 1 Acquisition Time: 3.00 min

File: ron\_11 N 4747

Scale Factor: 262.656 kc/s Offset: -1456.778 kc/s

Ep: 5.00 kV Ip: 0.0000 uA

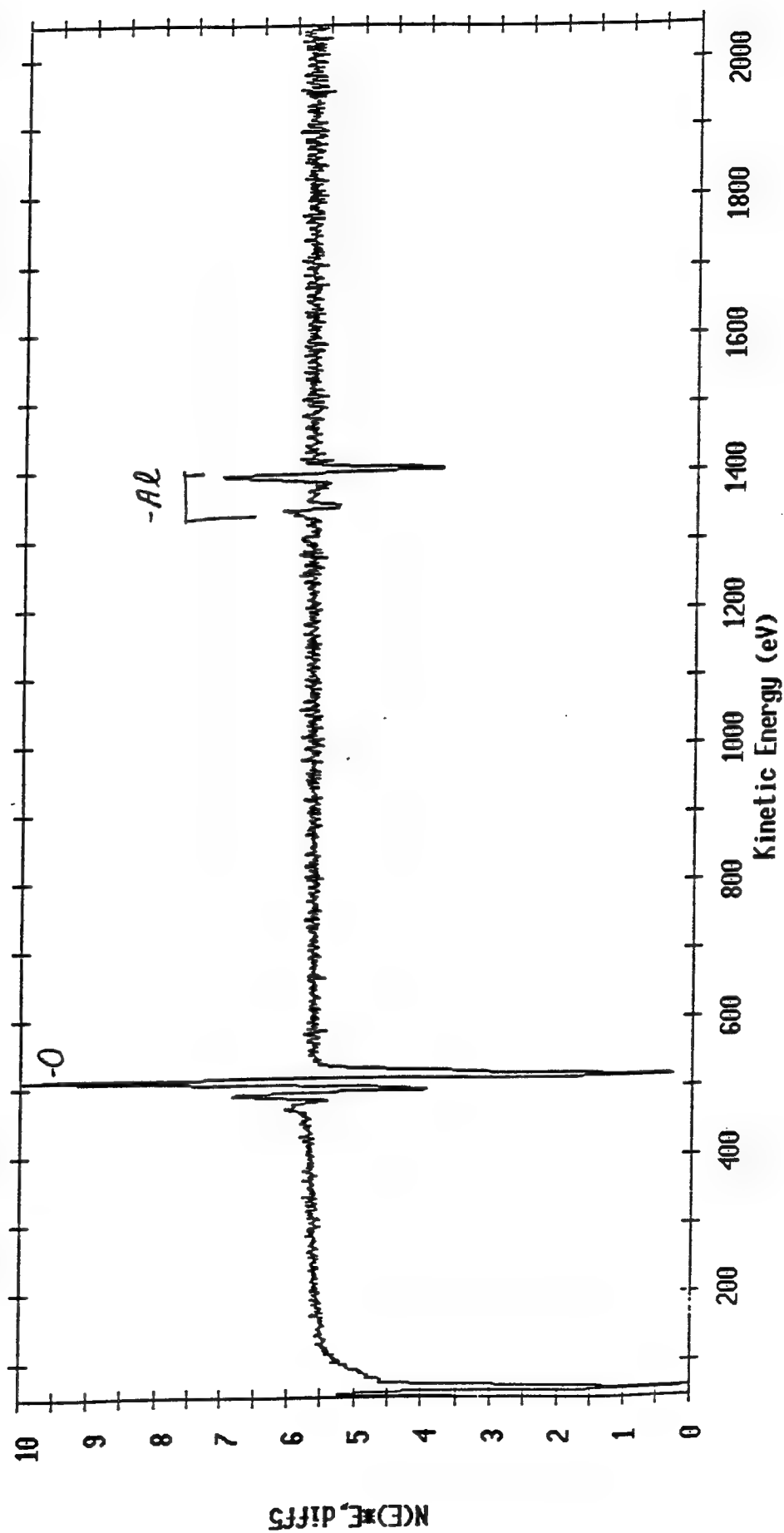


Figure 17. Auger Electron Spectrum of Aircraft Corrosion Sample

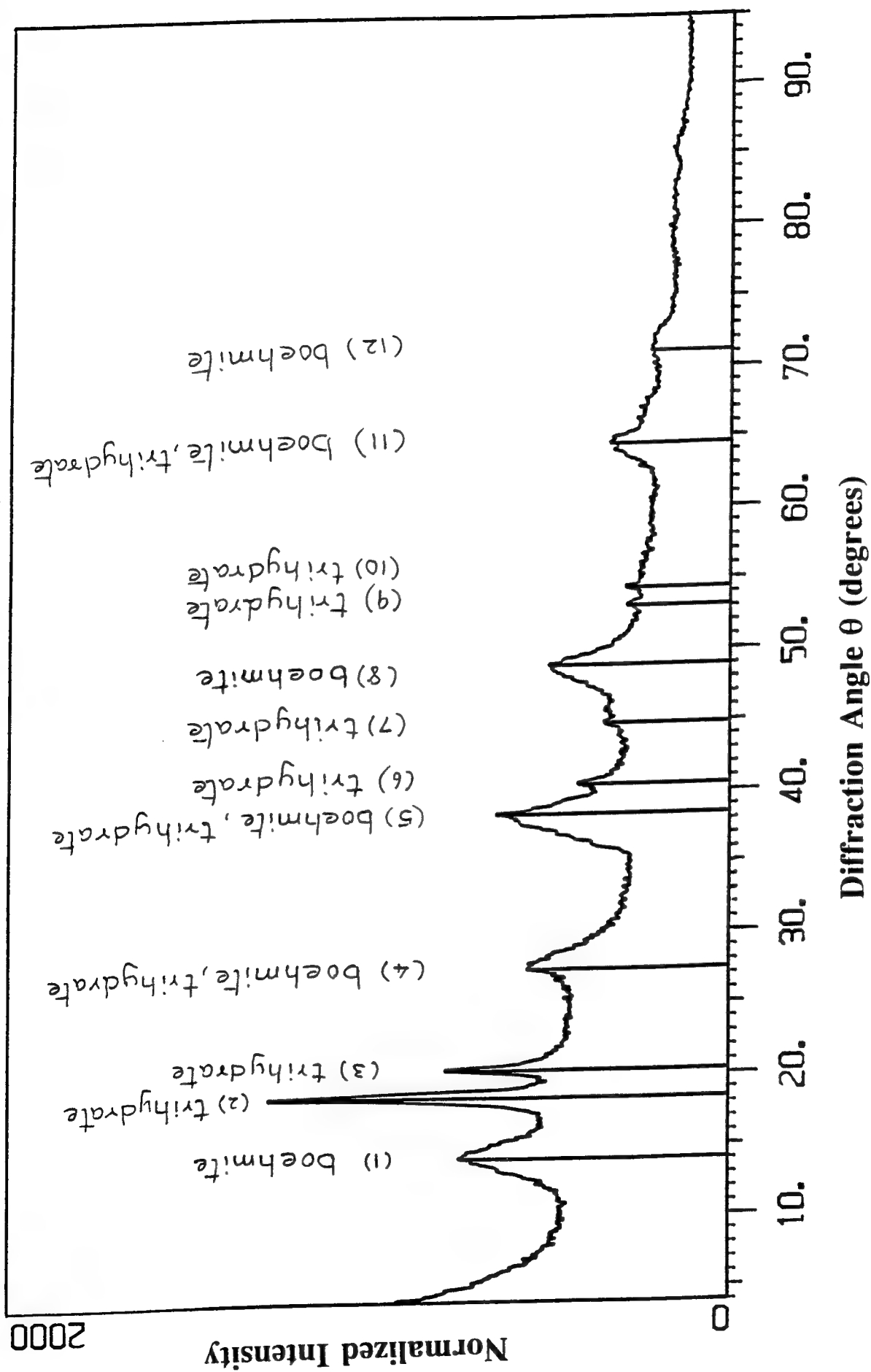


Figure 18. XRD Spectrum of Aircraft Corrosion Sample

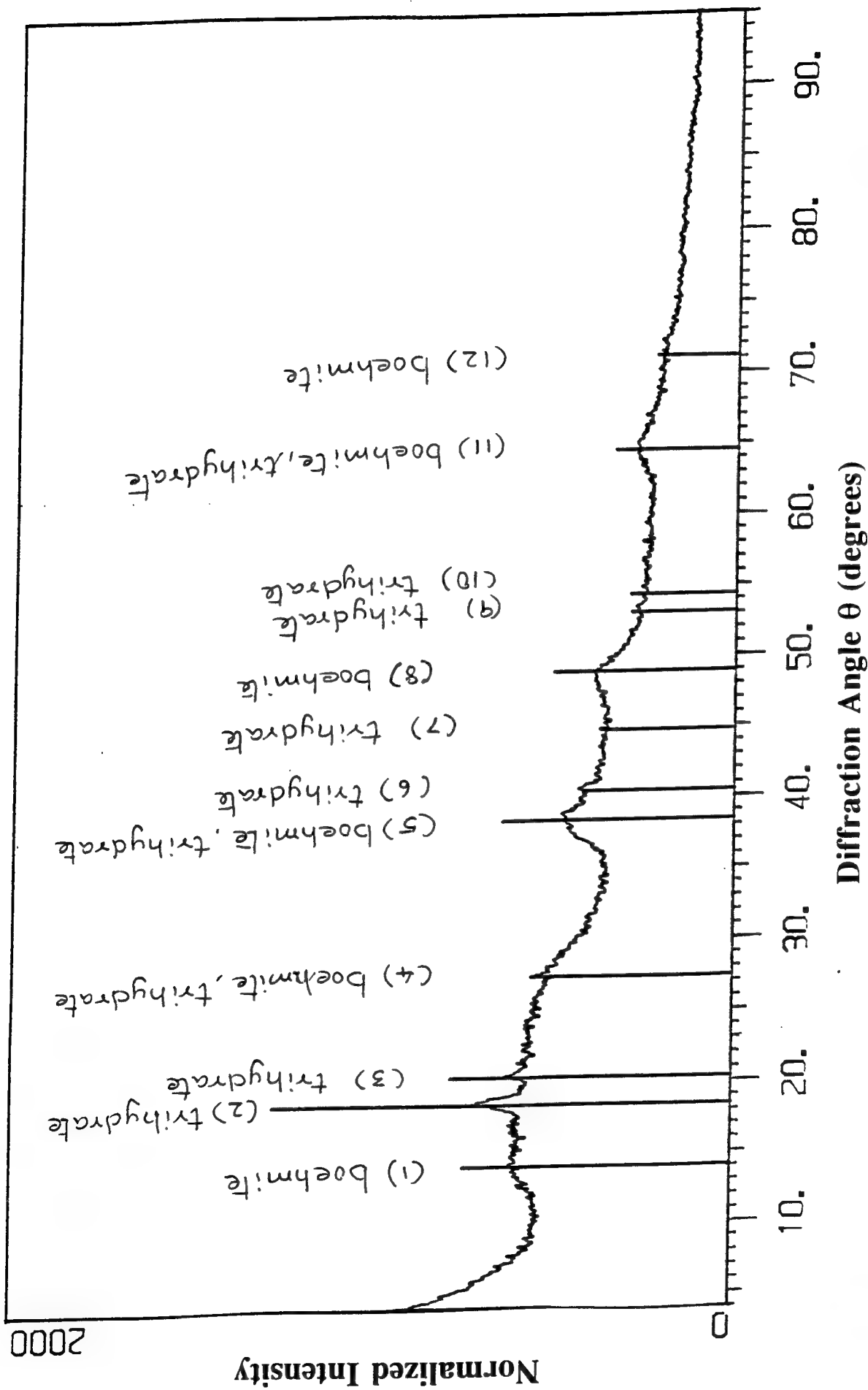


Figure 19. XRD Spectrum of Laboratory Sample with Aircraft Sample Peaks

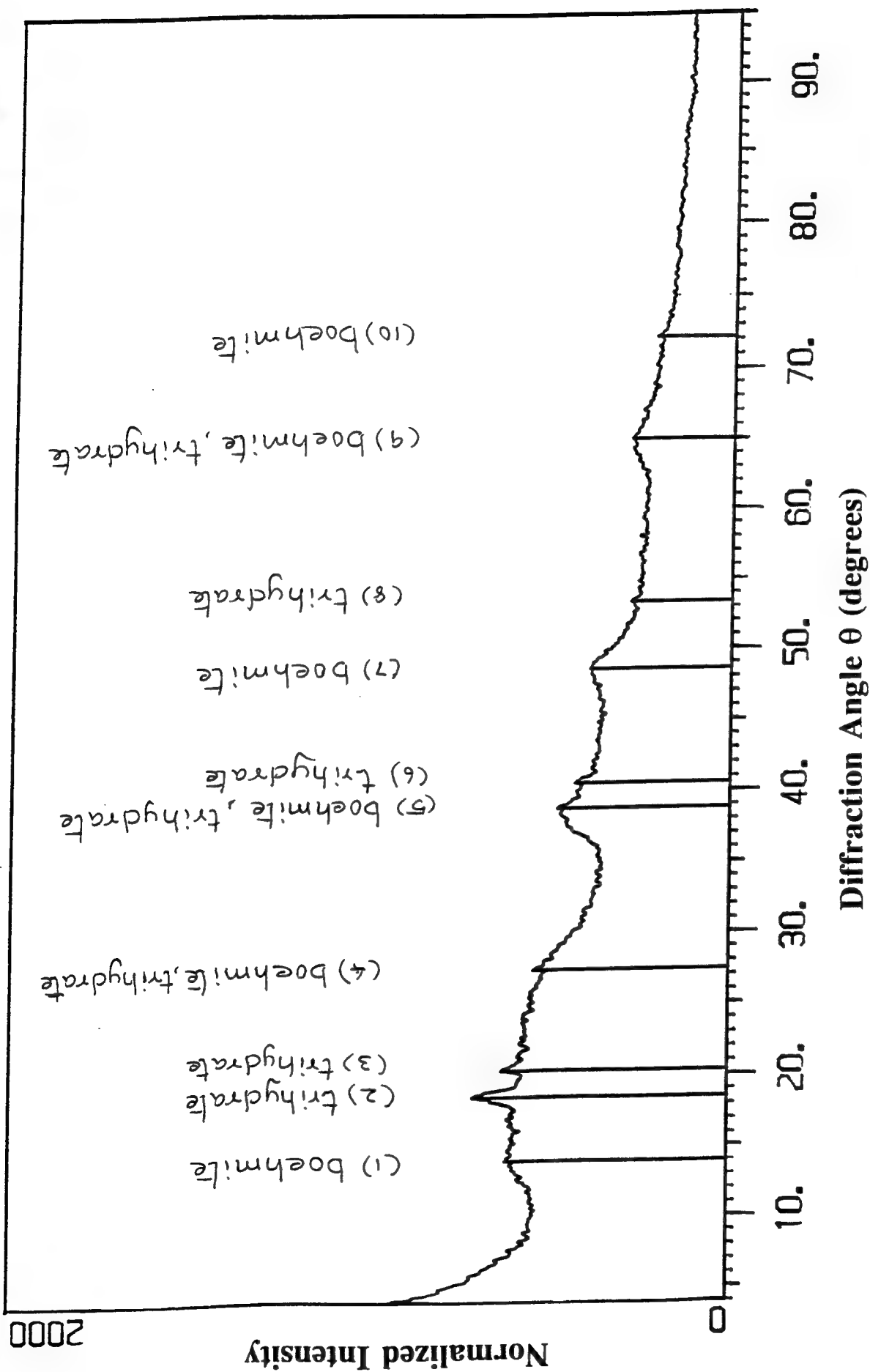


Figure 20. XRD Spectrum of Laboratory Corrosion Sample

## APPENDIX I

Application of D Sight for Corrosion Detection in Fuselage Lap and Butt Joints, January 1994, J.P. Komorowski, R.W. Gould, A. Marincak, S. Krishnakumar, NRC/IAR.

Pages: 85

**REPORT  
RAPPORT**

Report  
Rapport LTR-ST-1960

Fig.  
Diag. 7

**STRUCTURES, MATERIALS AND  
PROPULSION LABORATORY**

Date January 1994

**LABORATOIRE DES STRUCTURES,  
DES MATÉRIAUX ET DE PROPULSION**

Unclassified  
Unlimited

For  
Pour Diffraeto Ltd., Transport Canada, FAA

Reference  
Référence TRAX: JGJ02

**LTR-ST-1960**

**APPLICATION OF D SIGHT FOR CORROSION  
DETECTION IN FUSELAGE LAP AND BUTT JOINTS**

Submitted by  
Présenté par W. Wallace  
Laboratory Head/Chef de laboratoire

J.P. Komorowski  
R.W. Gould  
Author  
Auteur A. Marincak  
S. Krishnakumar

Approved  
Approuvé G.F. Marsters  
Director General

THIS REPORT MAY NOT BE PUBLISHED WHOLLY  
OR IN PART WITHOUT THE WRITTEN CONSENT  
OF THE INSTITUTE FOR AEROSPACE RESEARCH

CE RAPPORT NE DOIT PAS ÊTRE REPRODUIT, NI EN  
ENTIER PARTIE SANS UNE AUTORISATION ÉCRITE  
DE L'INSTITUT DE RECHERCHE AÉROSPATIALE

## ABSTRACT

The report details work performed under Phase I of a project aimed to develop D Sight based equipment for corrosion detection in large jet transport fuselage lap joints. D Sight is a double-pass retroreflection optical method which is very sensitive to surface perturbations as small as 10 microns. In order to demonstrate the capabilities of the breadboard D Sight Aircraft Inspection System (DAIS) over 150 fuselage sections were removed from decommissioned aircraft (B727, B737, DC9, DC10 and L1011). Several B727 and DC9 sections were subjected to accelerated corrosion at IAR. The corrosion products from the accelerated testing and from naturally corroded specimens were analyzed and found to be nearly identical.. Aluminum oxide trihydrate is the main corrosion product in lap splices. The volume of this oxide is more than six times greater than the aluminum from which it originated. Preliminary modeling of pillowing indicated that due to this large volumetric increase the pillowing is greater than the corrosion thickness loss and is thus easily detected by D Sight. Extensive inspections of collected specimens using D Sight, eddy current, x-ray, shadow moiré and tear-down methods revealed that the DAIS is more sensitive to corrosion in lap splices than eddy current. The x-ray methods used in this study were least successful. The shadow moiré method provided a quantitative assessment of pillowing in specimens subjected to corrosion in the laboratory. The inspections also revealed that the IAR/NRC specimen library contains a well balanced mix of corroded and non corroded fuselage sections. Recommendations for further work include continuation of specimen collection and accelerated corrosion, and modeling of pillowing for D Sight image simulation.

# Table of Contents

1.0 Introduction .....	1
2.0 Specimen Acquisition .....	1
3.0 Accelerated Corrosion Testing .....	15
4.0 Chemical Characterization of Corrosion Products.....	23
5.0 Inspection of Aircraft Specimens for Corrosion Caused by Aging.....	26
6.0 Inspection of Specimens Subjected to Accelerated Corrosion Testing .....	47
7.0 Comparison of D Sight Results with Other Inspection Techniques .....	68
8.0 Future Work .....	82
9.0 Conclusions .....	83
10. Acknowledgements .....	84
11. References .....	85

## 1.0 INTRODUCTION

In December 1992, the National Research Council - Institute for Aerospace Research (NRC/IAR), Transport Canada - Transportation Development Center (TC/TDC) and Federal Aviation Administration - Technical Center (FAA/TC) agreed to jointly fund a project to address the problem of corrosion detection in transport aircraft fuselage lap splices. The work was to be carried out by the Structures, Materials and Propulsion Laboratory of the IAR/NRC under collaborative agreement with Diffracto Ltd.

The Statement of Work for the project "Development of a D Sight Aircraft Inspection System - Phase I" included the following Tasks:

- 5.4 Obtain Non-Corroded Specimens
- 5.5 Accelerated Corrosion Testing
- 5.6 Pre and Post Corrosion Testing NDI
- 5.7 Obtain Corroded Specimens (CS)
- 5.8 Characterize Corrosion Damage in CS by D Sight and Tear down
- 5.10 Test Breadboard on Specimens to Verify Performance

The work carried out under tasks 5.1 to 5.3 was previously reported in Reference [1]. This report documents all work conducted at the NRC/IAR to address tasks 5.4 to 5.10. Since some tasks were combined (i.e. 5.4 and 5.7), the report does not strictly follow the task headings.

## 2.0 SPECIMEN ACQUISITION

Task 5.4 - Obtain Non-Corroded Specimens and Task 5.7 - Obtain Corroded Specimens were addressed concurrently. This approach was dictated by the availability of withdrawn from use aircraft for specimen retrieval. Five separate locations were visited during the course of the project by IAR personnel.

A search through the Canadian Institute for Scientific and Technical Information (CISTI) came up with several companies involved in the parting, scrapping and storing of retired aircraft.

The first trip made by NRC/IAR personnel was to Dynair Tech, Miami Airport, Miami, Florida, 22 to 26 February 1993. Five retired Boeing 727-200 aircraft which used to be operated by Pan American Airlines were at the time in the final stages of spare parts removal. Air driven hand tools with 3 inch in diameter abrasive cut off discs were used to remove sections of the fuselage marked by IAR personnel. Removal was performed by Dynair employees. Attempts at

renting heavier gas driven saws failed as these were still in demand following the hurricane 'Hugo' devastation (10 months earlier). This precluded retrieval of larger sections or sections attached to heavier substructure. Over the course of two days, 39 lap-splice specimens were removed and shipped to IAR. The shipment included several corroded specimens. Table 2.1 contains aircraft information and the number of specimens removed. Specimen locations on the aircraft are shown in Figures 2.1 to 2.5.

Type	Line number	Tail number	Cycles	Hours	Number of specimens
B727-200	530	N4739	49256	56784	5
B727-200	552	N4743	49527	56866	9
B727-200	562	N4746	48589	57872	9
B727-200	590	N4751	48674	56259	12
B727-200	591	N4752	48693	56965	4

**Table 2.1** Aircraft from which specimens were retrieved in Miami Airport.

The second specimen retrieval trip included two locations: 1) AirZona Inc., Kingman, Arizona, and 2) Dynair Parts, Amarillo, Texas. This trip was undertaken May 16 to 22, 1993.

Kingman, Arizona is about 2 hours by car from Las Vegas, Nevada. Through the contacts established earlier with Soundair, it was determined that three DC-9 aircraft were being scrapped. These aircraft belonged to Midway airlines and still displayed the airline colors. All aircraft were parked on the tarmac and the parting and cutting operations were conducted outdoors. One of the aircraft, 1056T, with 55,147 hours and 54,893 cycles was already completely stripped and was ready to be cut up for scrap. cursory visual and D SIGHT equipment inspections indicated only a few corroded areas. These were selected for removal along with a complete selection of longitudinal and circumferential joints. A gas driven circular saw was rented in Kingman and two AirZona mechanics alternated as the saw operators. The cutting blade diameter was not sufficiently large to cut through all of the substructure. This required the cutting to be performed both inside and outside the fuselage. The job was difficult,

Type	Line number	Tail number	Cycles	Hours	Number of specimens
DC9-14		1056T	54,893	55,147	21

**Table 2.2** DC-9 aircraft from which specimens were retrieved in Kingman.

somewhat dangerous and extremely noisy. In two days all of the NRC/IAR identified samples were removed and prepared for shipment on pallets by Yellow Freight to Ottawa (approximately 400 kg in 21 sections). The specimen locations on the aircraft are shown in Figure 2.6.

Dynair Parts is a newly formed subsidiary of Dynair Inc. (third party aircraft maintenance company). Four retired 727 aircraft were parked outside the hangar. When the NRC/IAR personnel arrived the first of the four - an ex Pan Am 727-235 (N4747, 55,644 hr., 48,655 cycles) was nearly completely stripped and the cockpit, tail and part of the upper fuselage were already cut in sections and stacked outside the hangar where the parting and cutting was continuing. A small furnace was ready for smelting the aluminum scrap into billets. Two mechanics were contracted by Dynair to cut the specimens selected by NRC/IAR. The gas driven saw used was bigger than the one available in Kingman and special blades for non ferrous metals were available. The cutting operations were thus greatly facilitated. Several significantly corroded lap splices were selected for removal. From the non-corroded splices, a selection was made so that all typical longitudinal and circumferential joints would be represented in the project's library. The 25 samples selected weighted 600 kg. The specimen locations on the aircraft are shown in Figure 2.7.

Type	Line number	Tail number	Cycles	Hours	Number of specimens
B727-200	566	N4747	48655	55,644	25

**Table 2.3** B727-200 aircraft from which specimens were retrieved in Amarillo.

The FAA TC in Atlantic City organized a workshop on Enhanced Visual and Coherent Optical Workshop (June 31, 1993). The next day Mr. Gould, who participated in the workshop selected and marked DC-10-30CF specimens for cutting with assistance from Mr. D. Galella (FAA/TC). The DC-10 has been scrapped following an accident in Boston on 23 January 1982 (N113WA, s/n47821, 6327 hours). The fuselage was incomplete and it was not possible to identify the fuselage body station locations above and below the window belt from which the specimens were retrieved. The selected specimens were removed by FAA/TC personnel and shipped to NRC/IAR. A total of 9 specimens were received for the project library.

Type	Line number	Tail number	Cycles	Hours	Number of specimens
DC10-30		N113WA		6327	9

**Table 2.4** DC10 aircraft from which specimens were retrieved in Atlantic City.

The last trip (August 30 - September 03) was to P&M Aircraft Co. Inc. in Mojave,

California. The Mojave Municipal Airport is one of the largest aircraft storage locations. The P&M Aircraft company was in the final stages of parts removal for Soundair from an L1011 which was operated by All Nippon Airways J8515, s/n 1119 and was first flown in 1976. The selection and removal of specimens was difficult due to the size of the aircraft. The desert heat and dust blowing winds were also factors. A total of 18 large sections were removed as shown in Figure 2.8 and shipped to IAR.

Type	Line number	Tail number	Cycles	Hours	Number of specimens
L1011	s/n 1119	J8515	31373	38,039	18

**Table 2.5** L1011 aircraft from which specimens were retrieved in Mojave.

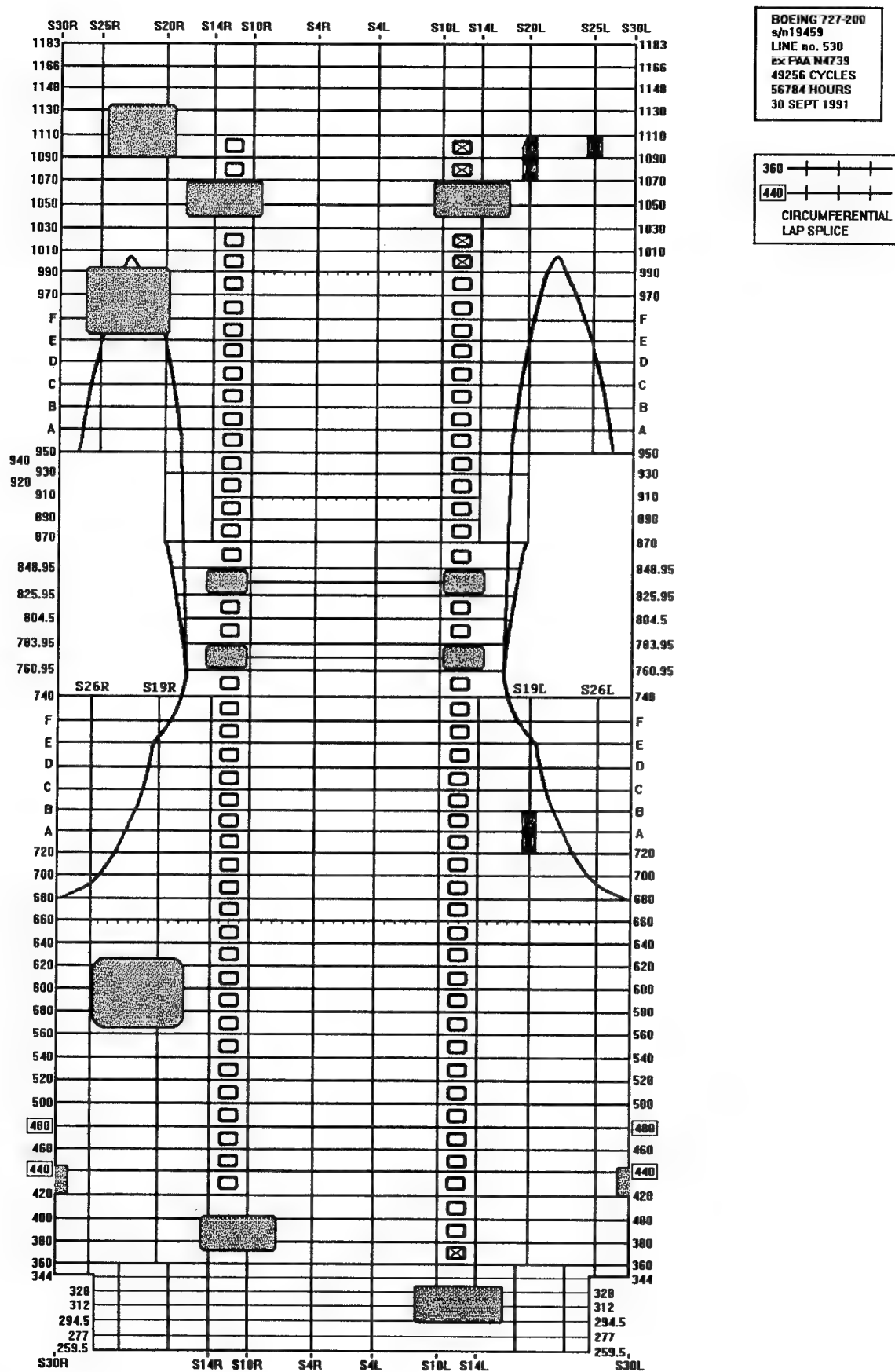
While the removal process carried out by P&M Aircraft was proceeding, two 737-200 aircraft scheduled for parts removal and scrapping were marked. It was expected that the specimens would be removed the following month (October 1993). The aircraft marked were:

Type	Line number	Tail number	Cycles	Hours	Number of specimens
B737-200	39	N4502	58912	50716	24
B737-200	56	N4507	60049	51219	26

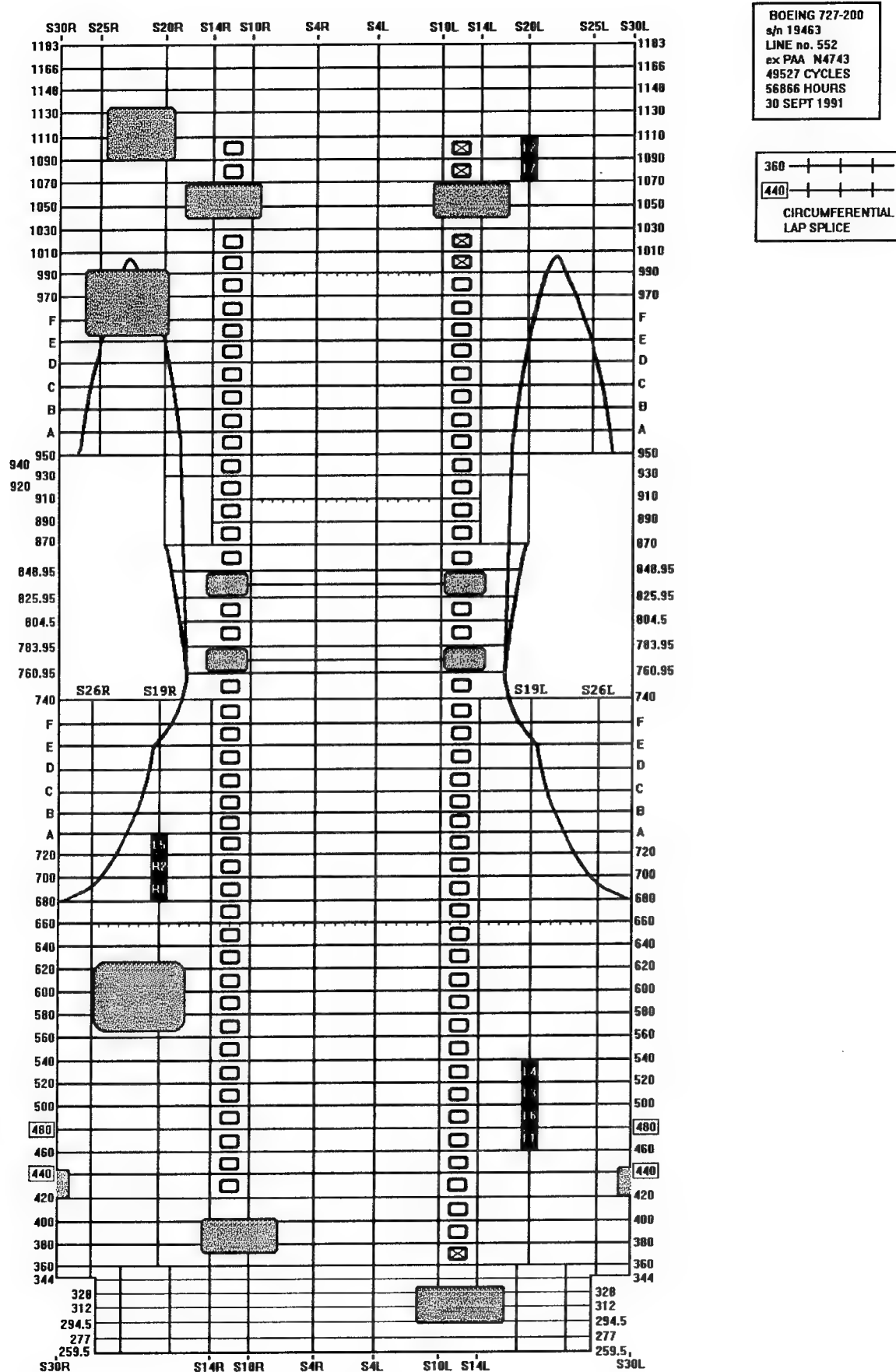
**Table 2.6** B737 aircraft from which specimens were retrieved in Mojave.

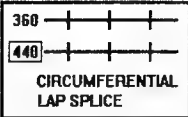
It was agreed prior to the trip that half of the sections marked would be removed and shipped to Sandia National Laboratories AANC (at their expense) to complement their specimen library. Due to circumstances beyond the control of NRC/IAR, the specimen removal process was delayed until the end of January 1994. A selection of specimens from both aircraft have now been removed and are being shipped to IAR. These will be evaluated in Phase II of the project. Specimen locations on the aircraft are shown in Figures 2.9 and 2.10.

The NRC/IAR has established connections with potential suppliers of airframe sample sections. NRC/IAR personnel have learned when to arrive at the site (timing is crucial) and what equipment to request to ensure the most efficient removal of the samples. A specimen library has been established containing nearly 150 specimens representing five typical transport aircraft types.

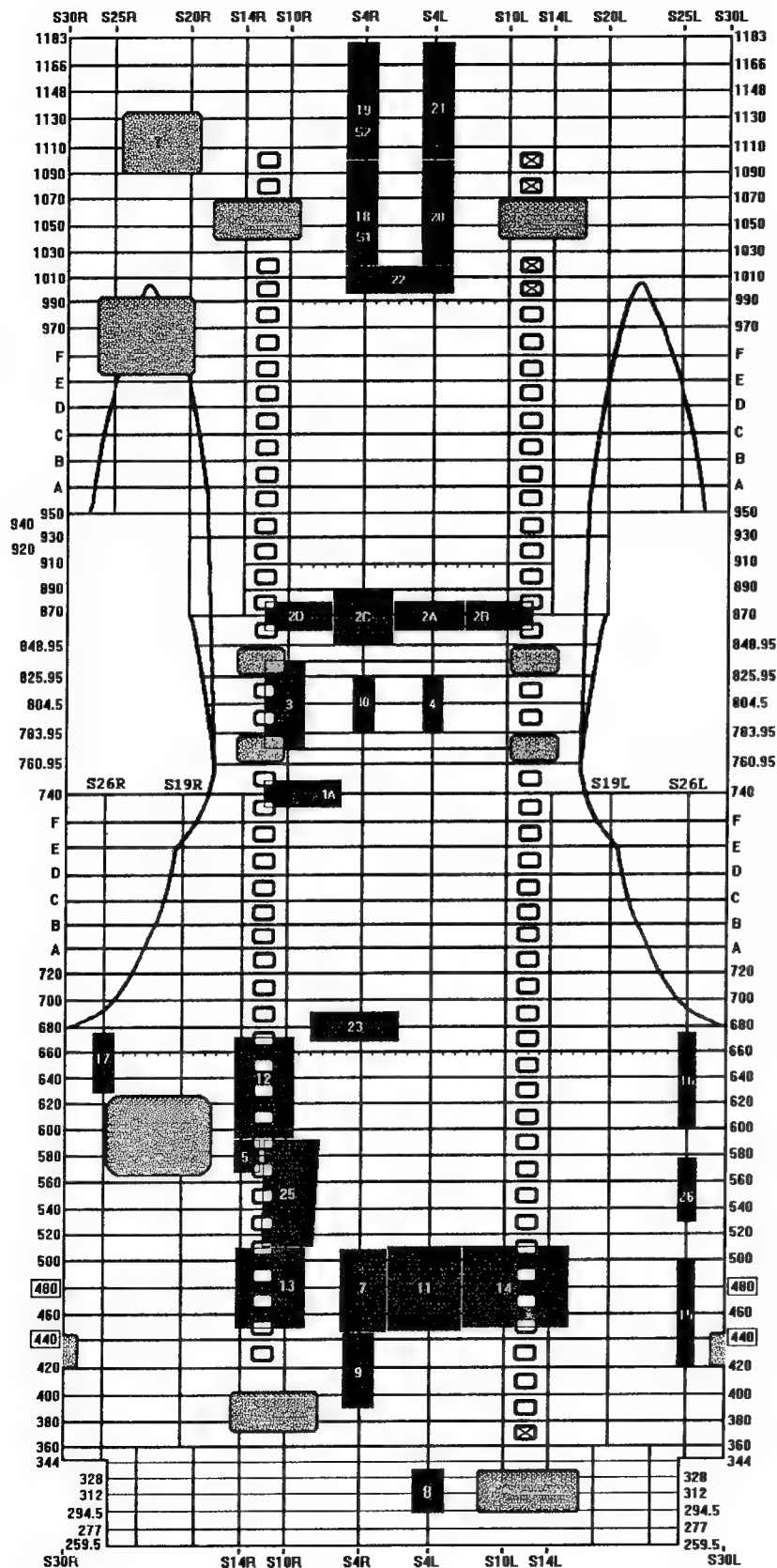


**Figure 2.1 Specimens retrieved from B727 - N4739.**

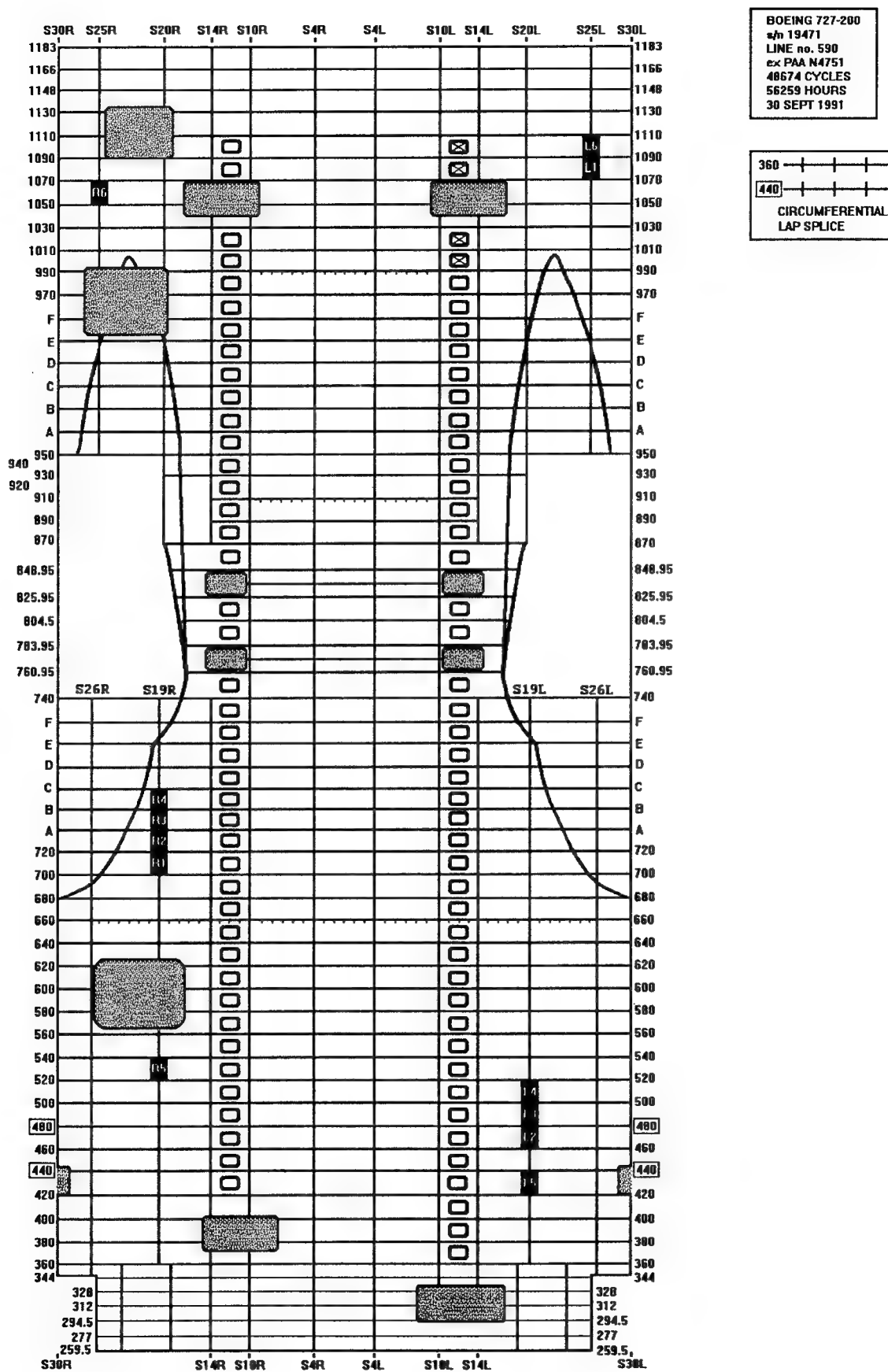




**Figure 2.3 Specimens retrieved from B727 - N4746.**



I-14



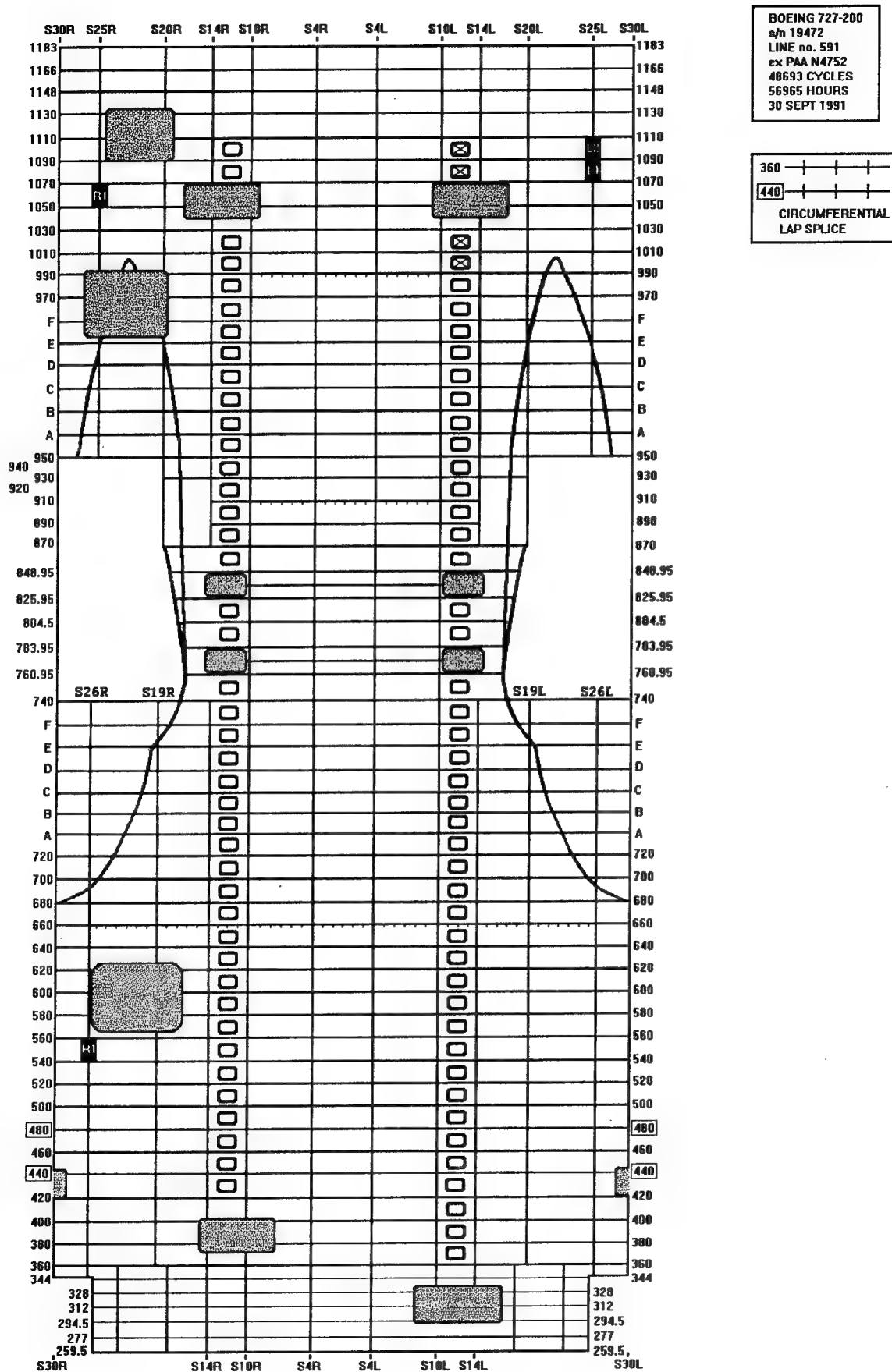
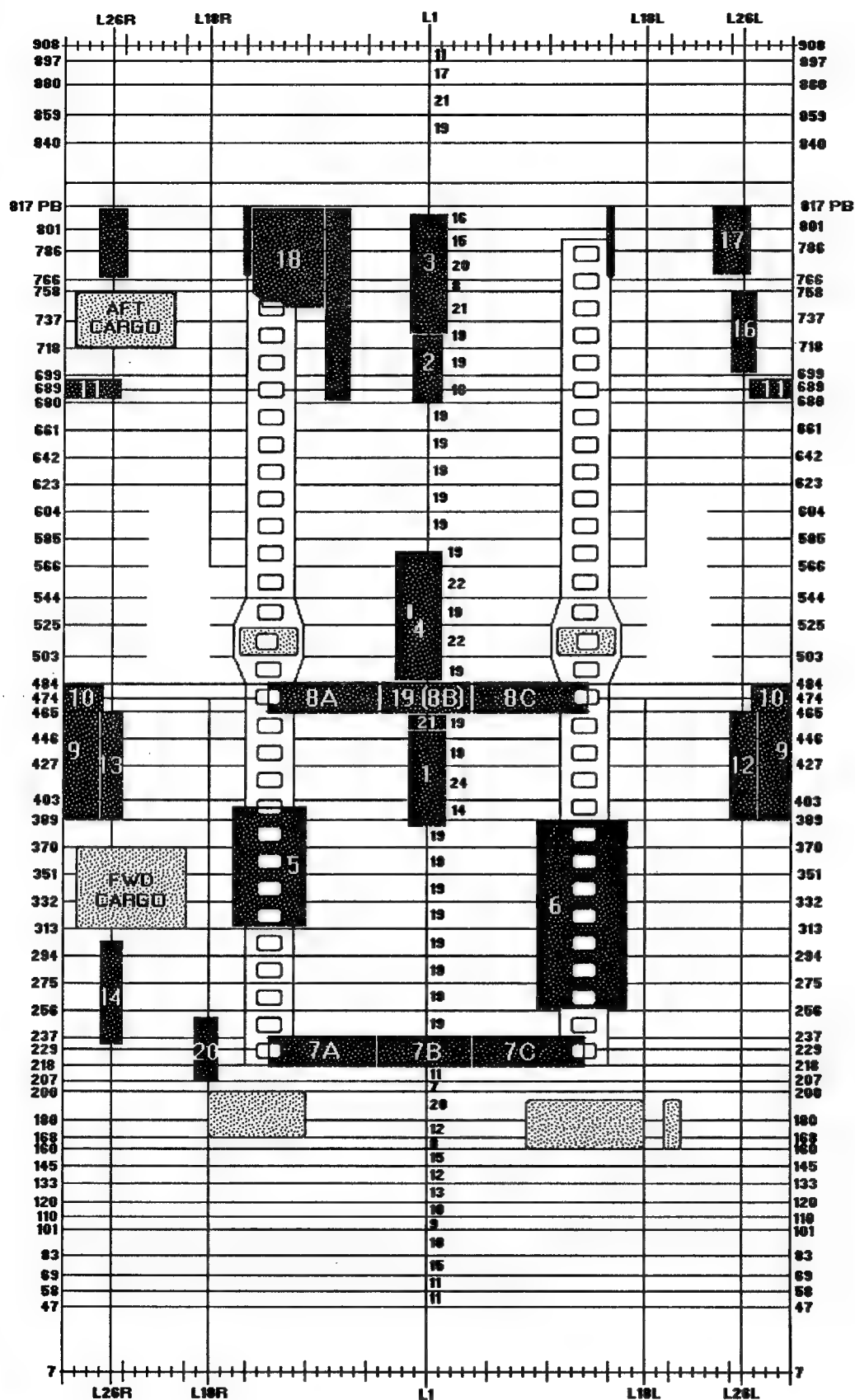
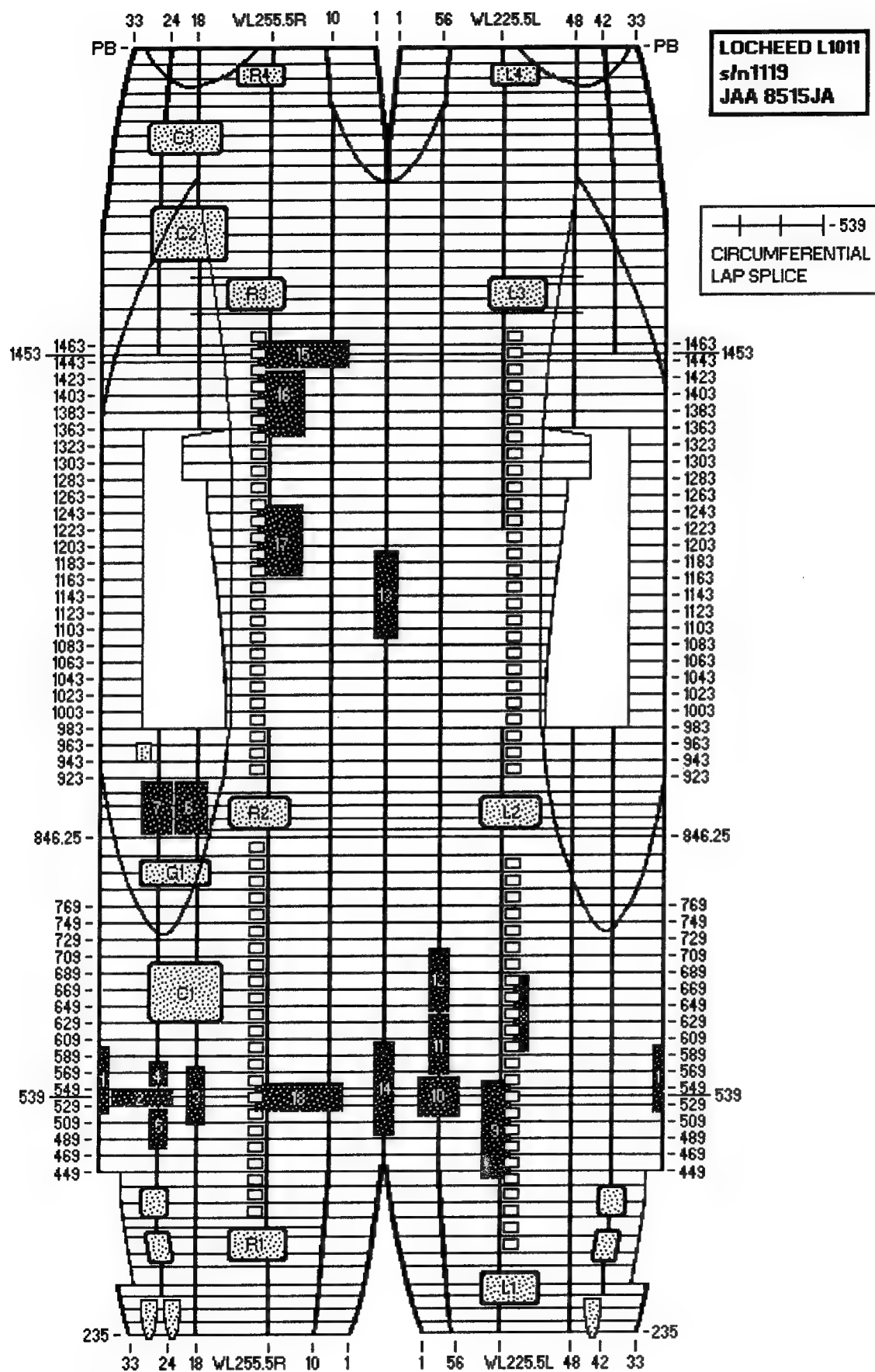


Figure 2.6 Specimens retrieved from B727 - N4752.

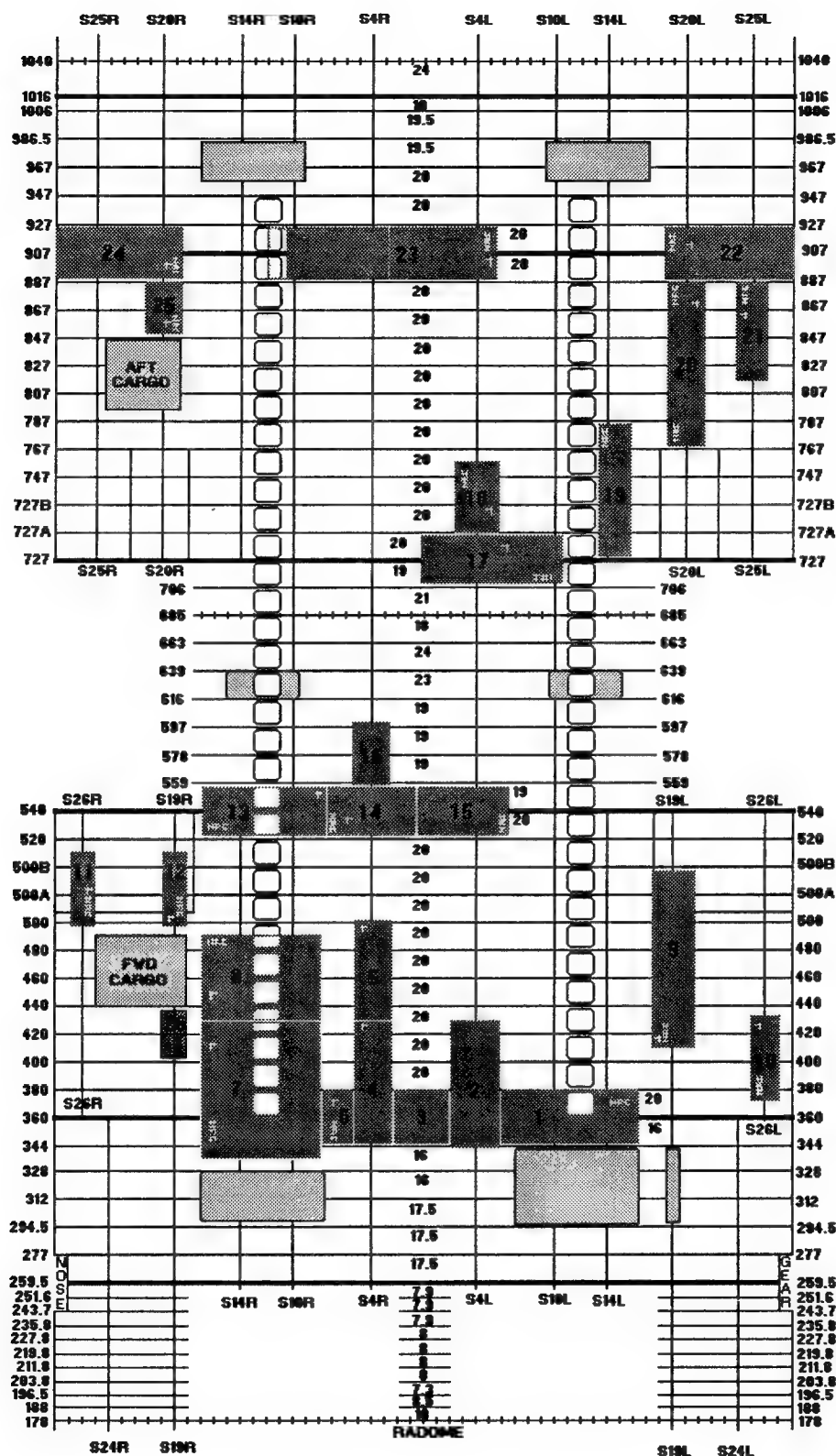


DC-9-14  
Fus# 049  
s/n 45737  
55147 hours  
54893 cycles  
Midway  
1056T

Figure 2.7 Specimens retrieved from DC9-14..



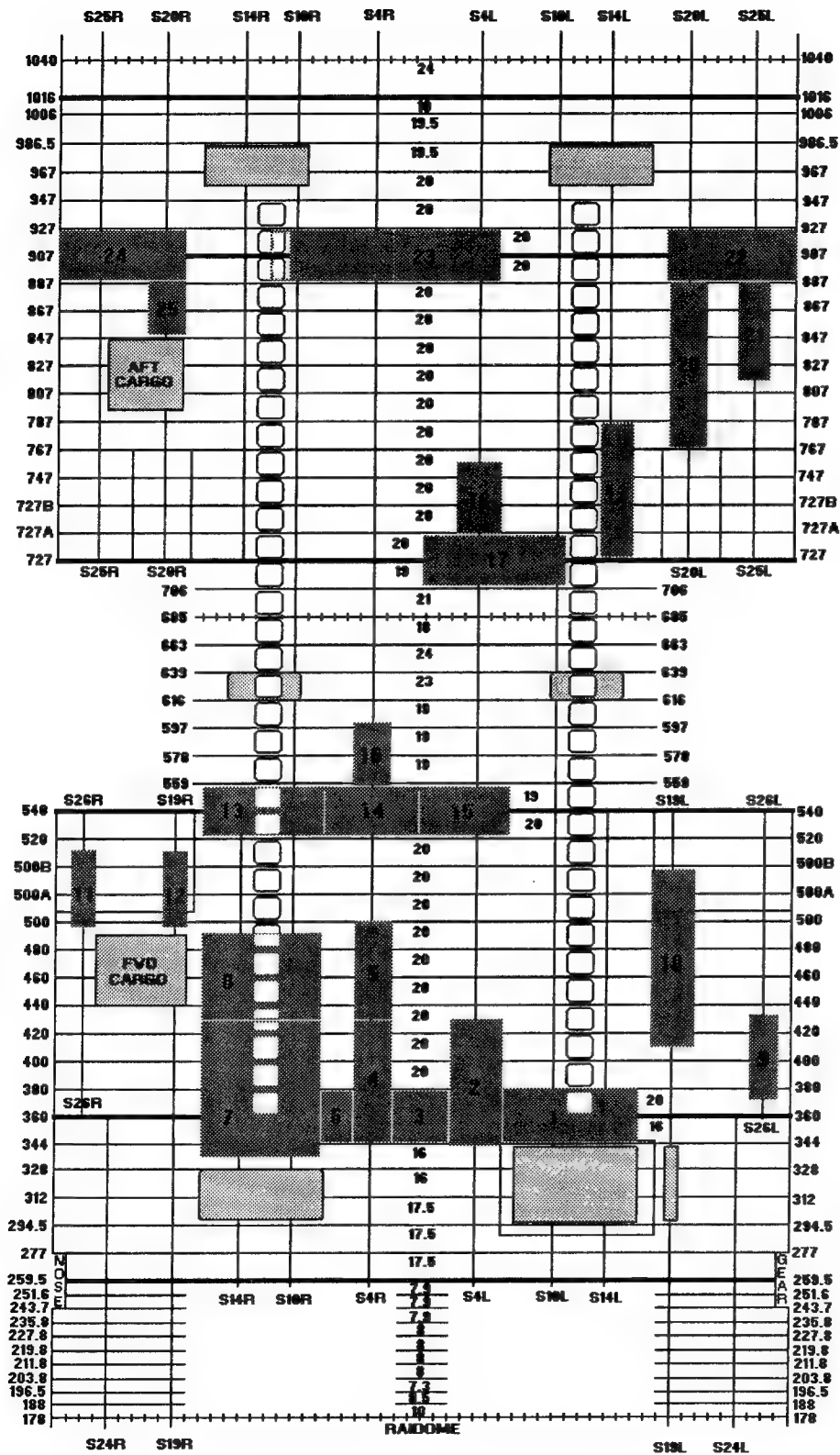
**Figure 2.8** Specimens retrieved from L1011.

**NRC-CNRC**National Research  
Council CanadaInstitute for  
Aerospace ResearchStructures, Materials  
and Propulsion  
Laboratory

Ottawa, Canada

**BOEING**  
737-200  
N4502WSECTIONS MARKED  
FOR REMOVAL

Figure 2.9 Specimens retrieved from B737-502.

**NR-CRC**

National Research  
Council Canada

Institute for  
Aerospace Research

Structures, Materials  
and Propulsion  
Laboratory

Ottawa, Canada

**BOEING**  
**737-200**  
**N4507W**



SECTIONS MARKED  
FOR REMOVAL

**Figure 2.10** Specimens retrieved from B737-507.

### 3.0 ACCELERATED CORROSION TESTING

#### 3.1 Selection of Test Method

The American Society for Testing and Materials have standardized a number of procedures for the application of accelerated corrosion for testing purposes. These mainly fall into two categories: (1) Immersion Techniques such as the EXCO Constant Immersion Test ASTM G34[2] and the Alternate Immersion Test ASTM G44[3], and (2) Salt Spray (Fog) Testing which includes ASTM B117 - Standard Salt Spray Testing Method[4], ASTM G85 - Standard Practice for Modified Salt Spray Testing[5] and ASTM B368 - Standard Method for Copper-Accelerated Acetic Acid-Salt Spray (CASS) Testing[6]. The choice of the test method depends on the specific application whose conditions are to be simulated by the test. The EXCO and the Alternate Immersion Methods are excellent for testing Exfoliation and Stress Corrosion resistance, and are known to produce corrosion within a very short time. However exploratory tests performed in the laboratory revealed that the immersion techniques are not suitable for simulating the corrosion phenomenon that occurs within fuselage lap joints. Painted and unpainted aluminum alloy panels subjected to continuous immersion in the EXCO solution in the laboratory corroded substantially within two or three days; however the corrosion was mainly in the form of pitting and erosion of material from the surface of the samples. With continued immersion the pitting and the loss of material increased but virtually no build up of corrosion products could be observed even after two or three weeks of testing. It became apparent that the chemical processes due to immersion in the EXCO solution generated soluble products which dissolved in the corrosive medium, causing significant weight loss but no accumulation of corrosion products on the specimen surfaces. This is quite uncharacteristic of the phenomenon observed in aircraft fuselage joints, wherein substantial build-up of corrosion products occurs within the splice, causing the outer skin of the joint to bulge out. Hence immersion techniques were not considered for the present purpose of simulating aging aircraft corrosion in the laboratory.

The ASTM B117 is the basic standard for application of corrosion by exposure to salt fog. It is the simplest of the salt spray techniques and is widely used. The corroding medium is salt fog generated from mildly acidic (pH of 6.5 to 7.2) sodium chloride solution with a concentration of 5 parts by weight. The specimens are exposed to continuous salt spray at a temperature of about 35°C (95°F). In ASTM G85 four modifications of the basic salt spray techniques are standardized. These mainly involve making the salt spray more acidic by the addition of acetic acid to the solution or mixing the salt spray with SO<sub>2</sub> gas and/or the use of cyclic exposure instead of continuous exposure to the corrosive medium. These variations are mainly employed when a more corrosive environment than the salt fog method of B117 is

required. In the CASS Test Method of ASTM B368, the corrosive environment is made even more severe by the addition of copper chloride to the acidified salt solution. The presence of copper, which is highly cathodic with respect to aluminum alloys, accelerates the corrosion process significantly.

Initial studies were performed on a number of plain aluminum alloy specimens using the acetic acid-salt spray testing method as per ASTM G85. The Singleton Salt Fog Test Chamber in the NRC/IAR Structures, Materials and Propulsion Laboratory was employed for this purpose. It was found that continuous exposures of up to one hundred and twenty hours produced appreciable amounts of corrosion build-up on the specimen surfaces. The product consisted of a white flaky insoluble substance similar in appearance to the residue that is observed in between the skin segments of naturally corroded fuselage lap joints disassembled for inspection. Thus at least in terms of physical characteristics, the salt spray technique appeared to simulate the process of corrosion occurring in aging aircraft lap joints<sup>1</sup>. Comparison of the results of continuous and intermittent (cyclic) exposures revealed that continuous exposure to salt spray produced much more corrosion than cyclic exposure for the same total duration. This is apparently in contrast to the results observed in immersion studies, wherein intermittent exposure to ambient atmosphere significantly increases the rate of corrosion development. Presumably the difference is due to the abundant availability of oxygen for the specimens exposed to salt spray, while those immersed in a liquid corroding medium have only a limited supply of free oxygen. Hence in the interest of reducing the test duration, continuous exposure to salt spray was chosen over cyclic application techniques. Further tests verified that the addition of copper chloride as per the ASTM Standard B368 substantially increased the rate of corrosion on the aluminum alloy samples. It was therefore concluded that the most appropriate laboratory procedure for simulating corrosion within aircraft fuselage skin splices in the shortest time frame was the ASTM Standard B368 Copper-Accelerated Acetic Acid-Salt Spray (CASS) Testing Method.

### 3.2 Optimization of Test Parameters

In an attempt to minimize the exposure time required to duplicate corrosion within the laboratory, several additional tests were conducted on plain and built-up aluminum alloy specimens for optimizing the test set up and procedure. Some of the parameters considered for optimization were: (i) exposure temperatures (ii) concentration of sodium chloride in the salt

<sup>1</sup> It was later confirmed by chemical characterization tests that even the chemical processes of corrosion in aging aircraft were simulated reasonably well by exposure to salt spray within the laboratory (see Section 4).

solution (iii) acidity of the corrosive medium (iv) positioning of specimens inside the corrosion cabinet (v) surface preparation of the faying edges of the joint in terms of removal of corrosion protection systems such as sealants, paint, the anodized layer and primer using solvents, abrading and sand-blasting (vi) the use of a wick to facilitate penetration of the corroding medium into the joint (vii) surface protection for the outer faces using additional paint, coating with wax and a combination of both.

It was found that increasing the concentration of sodium chloride in the salt mixture from 5% to 10% by weight resulted in the accumulation of too much dry salt on the specimen surfaces which tended to inhibit corrosion growth. Similarly increasing the temperature inside the salt cabinet over 50°C (122°F) also reduced the incidence of corrosion within the lap joints, probably because at higher temperatures the corrosive medium tended to evaporate before it could seep into the joint and act on the inner surfaces. Hence it was decided that the tests on the aircraft specimens would be conducted with 5% by parts of sodium chloride at an exposure temperature of about 48°C-50°C as per the ASTM B368 specifications. While earlier tests had indicated that increasing the acidity of the salt solution from a pH value of 6.5 to a pH of 3.0 considerably accelerated the development of corrosion, it was found that maintaining the pH value of the salt fog at values below 2.8 was considerably difficult and required large amounts of acid to be added to the salt mixture. It was therefore decided to conform to a pH value of 2.8 to 2.9 for the salt solution to be used in all the tests. This provided a pH value of about 3.0 for the collected salt fog, making it slightly more acidic than required by the ASTM Standard B368 which specifies a pH value in the range of 3.1 to 3.3. With regard to the positioning of specimens, an inclination of the monolithic panels by about 15° to the vertical as suggested in ASTM standards resulted in producing a greater amount of corrosion on the top surfaces of the specimens than on the bottom surfaces. However, since it was desirable to keep both surfaces of the aircraft lap and butt joint specimens as free of corrosion as possible, suspending the specimens vertically inside the salt spray cabinet was the most expedient approach. This also facilitated the deployment of a large number of specimens efficiently inside the corrosion chamber.

In one of the early studies, several lap joint specimens were manufactured in the laboratory with wicks, consisting of a woven fiber glass fabric, inserted between the two overlapping sections of the skin. The edges of the joint were left unsealed. The experimentation with wicks was motivated by previous corrosion studies using immersion techniques, wherein the use of a wick was reported to greatly enhance development of corrosion by facilitating the penetration of the corroding solution into the joint. However in the present case, the lap joint specimens with wicks were found to perform no better, and in some cases worse, than the specimens without wicks. Apparently the capillary action of the wick is helpful only when the specimen is immersed in a liquid medium and not when the corrosive medium is salt fog, as in this case. The use of wicks was therefore discontinued.

In terms of surface preparation of the inner surfaces of the joint, several possibilities were looked at. In the case of Boeing aircraft specimens, in which case the lap joints were usually bonded in addition to being rivetted together, it was found that breaking the bond, removing the epoxy and cleaning the inner surfaces was usually sufficient, since these surfaces were already stripped of all corrosion protection in preparation for good bonding. The Douglas aircraft lap joints were not bonded, but held together with fasteners and their inner surfaces were usually treated for corrosion protection. In these specimens the corrosion protection system was removed from the inner surfaces by means of abrading or grit-blasting before re-assembling.

### **3.3 Surface Treatment for Corrosion Protection**

The accelerated corrosion testing of lap joint specimens for D Sight application had two rather contradictory basic requirements: one, that of inducing the maximum amount of corrosion inside the lap joint within a short period; and the other, that of retaining the outer skin surfaces as clean and undamaged as possible. The latter was required for the application of inspection techniques: eddy current, shadow moiré and D Sight, for detecting corrosion within the lap joint. Not only did the deterioration of the outer surfaces hinder distinguishing between damage inside and damage outside from the scanned images, but it also thwarted meaningful comparisons between images obtained before and after the application of corrosion treatment. For this reason it was critical to minimize the development of corrosion on the outer surfaces. Further, the surface treatment employed for protection, at least on one side (usually the outboard surface) had to be amenable to the application of eddy current, shadow moiré as well as D Sight. One of the earliest treatments experimented with was the application of wax on the surface of the specimens. If the wax provided adequate protection against corrosion to the outer surfaces then it would have constituted a very convenient surface treatment since it could easily be applied and removed for optical and eddy current inspection of the panel surfaces. Unfortunately it was discovered that the wax tended to disperse and run down the panel surfaces even though the melting point of the wax used was much higher than the temperature in the test chamber. Hence the idea of applying wax for corrosion protection was discarded.

Most of the paints used for aircraft maintenance afford fairly good protection against corrosion, but none of them could provide total protection against continuous exposure to salt spray for prolonged periods. Moreover, unpainted surfaces were found to give the best results for eddy current inspections. So it was desirable that the paint used for corrosion protection in the test chamber be easily strippable. The epoxy paints normally used for aircraft maintenance offered very good protection, but could not be removed easily without the use of environmentally unsafe stripping agents. Enamel based paints were found to be easily

removable, but initial trials with enamel spray paints showed that they started blistering and cracking fairly quickly inside the corrosion chamber. This was due to the large fraction of propellants in the spray paint cans, which tended to evaporate quickly (in ten to twenty minutes) leaving only a thin film of paint that did not provide adequate protection. Some tests were done with exterior latex paints, but these proved to have very little resistance to continuous exposure to salt fog environment. After numerous trials, it was found that white enamel based Tremclad was the most suitable paint. When applied slowly using a paint gun, this paint took about ten to twelve hours to dry properly, but formed a moderately thick and uniform film over the specimen surface. Tremclad offered good protection, preventing corrosion from developing even after two to three weeks of exposure in the salt spray chamber. The weakest spots in the Tremclad paint were at the sharp panel edges and around the rivet holes. Tremclad could readily be removed using an environmentally acceptable paint stripper. Further, it also provided a smooth glossy finish, suitable for D Sight application. Hence, for most of the final test specimens, Tremclad was used as the corrosion protection for the outboard surfaces. At each inspection interval in between the cycles of corrosion applications (as well as at the beginning and the end), the specimens were taken out of the salt spray cabinet, dried, and stripped of their previous paint before being subjected to eddy current inspection. They were then repainted with Tremclad, allowed to dry and subjected to shadow moiré and D Sight interrogations, before being re-introduced into the corrosion chamber. The inboard surfaces of the joints, which did not need visual monitoring, retained their original chromate zinc primer, which provided sufficient protection against corrosion.

### 3.4 Test Set Up and Specifications

The accelerated corrosion application on the lap and butt joint specimens was performed using a Singleton Salt Corrosion Cabinet (SCCH Model #22). The cabinet is made of plain steel with an interior lining of inert, oven-cast, seamless PVC. It is uniformly heated by water jackets on all four sides and the bottom with a maximum temperature of about 82°C (180°F). The top is covered with a transparent high temperature Plexiglass dome. The cabinet is equipped with a humidifying (bubble) tower with a micro bubble aerator for generating humidified air. Distilled water inside the bubble tower, which is fed from a 10 gallon supply reservoir, is maintained at a constant level by a Level-matic (patented) control unit. The bubble tower is instrumented with a pressure gauge and an airflow meter. The output flow rate is controlled by regulating the pressure of the air supply into the tower. The humidified air from the bubble chamber is fed into a fog tower reservoir inside the cabinet where it is mixed with the salt solution before being dispelled through an atomizer into the dispersion tower. The latter is fitted with internal baffles to produce a homogenous mist of free falling spray without directional corrosion effects. The salt solution is brought into the fog tower from another

reservoir (36 gallon capacity) by gravity feed. The temperatures inside the bubble tower and the cabinet are monitored by automatic electronic controls with digital displays. The corrosion chamber was fitted with an exhaust condenser assembly, wherein the salt fog exhaust from the cabinet was condensed by mixing it with a continuous supply of running water and collected for disposal into a third reservoir.

The salt spray corrosion chamber could be operated in both manual and automatic modes using the Singleton precision control package. The electronic control unit could be programmed to perform a series of test cycles, each consisting of sequential applications of individual spray, purge and soak cycles of predetermined durations. The total number of test cycles applied is automatically recorded. The wet and dry bulb readings inside the cabinet could also be recorded for the entire test period on a chart indicator.

For the application of accelerated corrosion to the lap and butt joint specimens, the humidifying (bubble) tower temperature was maintained at 35°C (95°F) and the temperature inside the salt spray cabinet at 48°C (118°F). Initial studies showed that a pressure of 125 KPa (18 psi) was required to be maintained inside the bubble tower to obtain fog collection rate of over 1.0 mL per hour as recommended by the ASTM standards. However, this produced a very high rate of humidified airflow into the salt spray cabinet which could not be matched by the exhaust flow rate. The result was a pressure build-up inside the cabinet, which vented itself occasionally by lifting the Plexiglass cover unit over the chamber. Needless to say, the presence of salt fog in the air-conditioned atmosphere of the laboratory, which contained a lot of other sensitive hardware, was not at all desirable. The bubble tower pressure was therefore reduced to about 90 KPa (13 psi), which eliminated the problem, although it also decreased the fog collection rate inside the cabinet to less than 0.8 mL per hour.

As per ASTM standard B368 for Copper Accelerated Acetic Acid Salt Spray Testing (CASS Test), the salt solution was prepared with 5 parts by weight of sodium chloride dissolved in 95 parts of distilled or reagent grade water and reagent grade copper chloride ( $\text{CuCl}_2 \cdot 2\text{H}_2\text{O}$ ) added at the rate of 0.25 g/litre. The pH of the salt solution is lowered to a value of 2.8-2.9 by the addition of glacial acetic acid, which provided the atomized salt spray with a pH value between 3.1 and 3.3.

### **3.5 Specimen Preparation**

A number of constructions representing longitudinal and circumferential lap joints were prepared for accelerated corrosion testing. In general these had a nominal surface area of about 1400 cm<sup>2</sup> (1.5 ft<sup>2</sup>). A few specimens were subjected to corrosion testing in their original

unaltered condition, i.e., without disassembly and removal of corrosion protection from the inner surfaces. The majority of specimens were disassembled, their inner surfaces inspected for existing conditions, and treated on selected surfaces for removal of protective coatings before being re-assembled and introduced into the corrosion chamber. Specimens with thin skin material had their original stiffener structure included in the reconstruction.

The specimens were opened to prepare one or more surfaces of the joint for corrosion activity. The fasteners were removed as follows: first the formed tail of the aluminum rivets was drilled undersize and then chiselled off. The remaining rivet was then punched out with the specimen lying face down on a padded surface. The adhesive layer between the faces and the sealant were also removed when present. The specimens with adhesive layers were prewarmed to about 80°C to aid in separation of the skins.

One early specimen was abraded by grit blasting but even at the lowest air pressure (30 psi) the grit impact deformed the thin skins. Thereafter the specimens were abraded with a medium or ultra fine ScotchBrite disc to remove just the protective primer and/or cladding. The speed of removal was kept very low to avoid overheating the skin.

The disassembled components were relocated with and held together initially by Kleeko fasteners. Replacement rivets were then installed in the original holes. An arbour press and stacked bevelled washers were used in a sequential process to ensure adequate clamp-up. This avoided the introduction of deformations and marks from air driven hand held riveting guns. The original countersinks were adjusted when required to provide a flush fit for the head of the new rivet.

The outboard surfaces which were to be monitored during the test were brought to a uniform condition. Where the original paint system had suffered damage and degradation, it was chemically stripped and the surface repainted to a gloss white finish. Suitable original paint systems were retained but also repainted. As mentioned previously, an enamel spray paint and exterior latex paint were tried on some of the early specimens, but the final batch of specimens were painted with Tremclad using a paint gun. The inboard surfaces and exposed new fasteners were spray painted with a zinc chromate primer.

Each group of specimens were inspected by several techniques such as eddy current scans, radiographs, shadow moiré and D Sight prior to introduction into the corrosion test chamber and subsequently at defined inspection intervals. These are described in greater detail in section 5.

### 3.6 Corrosion Application

As of this time, 20 specimens including both longitudinal lap and circumferential butt joints have been subjected to accelerated corrosion testing. These specimens belong to retired Boeing 727, DC-9 and DC-10 aircraft. All the specimens were obtained from the belly section of their respective aircraft except one, specimen #47-5, which was taken from a lap joint located below the windows. Fifteen specimens were subjected to over a thousand hours of exposure to salt spray, nine of them for up to 1100 hours. The two DC-10 specimens and three butt joints from DC-9 have a total exposure time of only 695 hours. Table 3.1 lists the specimens that have

Serial number	Specimen number	Aircraft ID	Joint Type	Condition	Surface Treated	Period of Exposure
1	51L2	B727	Lap	Original		1104 hrs
2	43L6	B727	Lap	Original		1104 hrs
3	43L7R	B727	Lap	Rebuilt	1	1104 hrs
4	46L3A	B727	Lap	Rebuilt	1+2	1104 hrs
5	46L3C	B727	Lap	Rebuilt	1+2	1104 hrs
6	46L3E	B727	Lap	Rebuilt	1+2	1007 hrs
7	46L4A	B727	Lap	Rebuilt	1	1104 hrs
8	46L4C	B727	Lap	Rebuilt	2	1104 hrs
9	47-5	B727	Lap	Rebuilt	2	1007 hrs
10	56T1A	DC-9	Lap	Rebuilt	1	1007 hrs
11	56T1B	DC-9	Lap	Rebuilt	2	1007 hrs
12	56T1C	DC-9	Lap	Rebuilt	6	1007 hrs
13	56T21A	DC-9	Lap	Rebuilt	1+2	1104 hrs
14	56T10A	DC-9	Butt	Rebuilt	3+4	695 hrs
15	56T10B	DC-9	Butt	Rebuilt	5	695 hrs
16	56T10C	DC-9	Butt	Rebuilt	3+4	695 hrs
17	56T19A	DC-9	Butt	Rebuilt	3+5	1104 hrs
18	56T19D	DC-9	Butt	Rebuilt	3+4	1007 hrs
19	WA7A	DC-10	Butt	Rebuilt	3+4	695 hrs
20	WA7B	DC-10	Butt	Rebuilt	3+4	695 hrs

**Table 3.1** Aircraft Specimens Subjected to Accelerated Corrosion Testing

been tested to date and their particulars. Two of the specimens 51L2 and 43L6 were introduced into the corrosion chamber in their original condition, i.e., these were not disassembled to facilitate the corrosion of the faying edges. All the remaining specimens were disassembled and their inside surfaces treated by grit blasting to increase their sensitivity to corrosion attack. These rebuilt specimens were not resealed, which further increased their susceptibility to corrosion by facilitating the penetration of the corroding medium into the joint. The surfaces that were treated for removal of previous corrosion protection are indicated for each specimen by numeric codes in column six of the table. Code 1 denotes the inside surface of the outer skin, and Code 2 the outer surface of the inner skin of the lap joint specimens. Codes 3 and 4 respectively indicate the right and left halves of the outer skin of butt joints, while Code 5 stands for the outer surface of the doubler at the butt joint. The DC-9 lap joint has a finger doubler in between the inner and the outer skins. In the case of specimen 56T1C, neither of the skin surfaces were treated, but both the inner and outer surfaces of the intermediate finger doubler were treated for corrosion protection removal (Code 6). Not only D Sight, but other NDE techniques such as radiography, eddy current and shadow moiré, were used for monitoring the development of corrosion in the specimens subjected to accelerated testing. These methods and their results are described in Chapter 6.

One of the difficulties encountered early on was the malfunctioning of the exhaust fog condensing system, which resulted in the salt spray being released into the atmosphere inside the laboratory. The increase of humidified air pressure inside the cabinet also caused its plexiglass top cover to rise up occasionally venting the salt fog directly into the laboratory air. This caused considerable concern about salt contamination of other sensitive equipment inside the laboratory, especially expensive computer and electronic hardware. While the exhaust system was rectified eventually, for several days the running of the corrosion chamber had to be restricted to working hours during which it could be continuously monitored. The periods of shutdown during these days have been discounted, and only the hours of actual exposure to the salt spray environment taken into consideration.

#### **4.0 CHEMICAL CHARACTERIZATION OF CORROSION PRODUCTS**

Chemical Characterization tests were conducted on corrosion product samples extracted from lap joints in aging aircraft and also those produced by exposure to acidified salt fog in the laboratory. The objective of these tests was to determine precisely the chemical compositions of the two corrosion products[7], which was desirable for two reasons: one, to establish the degree of similitude between corrosion occurring naturally in aging aircraft and that produced artificially

by exposure to salt fog in the laboratory; and two, for the development of a mathematical model of the “pillowing” deformation of the outer skin caused by the accumulation of corrosion products within aging fuselage skin joints. Three methods were used for the chemical analysis of the corrosion products: x-ray diffraction (XRD), x-ray photoelectron spectroscopy (XPS) and Auger electron spectroscopy (AES).

It is generally believed that the usual product of corrosion of aluminum and aluminum alloys in a humid atmosphere is some form of hydrated aluminum oxide[8]. The opinion most favoured by researchers is that the initial product is amorphous aluminum hydroxide ( $\text{Al}(\text{OH})_3$ ) which crystallizes with time to become a hydrated oxide or a mixture of oxides. The major crystalline phases commonly identified are aluminum oxide monohydrate *Boehmite* ( $\alpha\text{-Al}_2\text{O}_3\cdot\text{H}_2\text{O}$  or  $\text{AlO}\cdot\text{OH}$ ) and aluminum oxide trihydrate, the latter existing in both alpha form as *Gibbsite* or *Hydrargillite* ( $\alpha\text{-Al}_2\text{O}_3\cdot 3\text{H}_2\text{O}$ ) and beta form as *Bayerite* ( $\beta\text{-Al}_2\text{O}_3\cdot 3\text{H}_2\text{O}$ , monoclinic) [9,10]. Based on thermodynamic considerations, Deltombe and Pourbaix[11] suggest that the form of the product progressively moves to less soluble oxides: from boehmite to bayerite to gibbsite. The studies of Hart[12] and Shipko and Haag[13] appear to support this hypothesis. The results of the chemical analysis tests described in the following sections are also in general agreement with this point of view. They indicate that the major portion of the corrosion product is either amorphous or crystalline aluminum oxide trihydrate, while a small fraction is in the monohydrate form, which appears to be an intermediate transition state. The tests were conducted partly at the Institute for Aerospace Research and partly at the Institute for Microstructural Studies of the National Research Council of Canada.

#### 4.1 X-ray Photoelectron Spectroscopy

A corrosion product sample extracted from the lap joint of an aging Boeing 727 aircraft and another sample of corrosion produced by exposure to salt spray in the laboratory were subjected to x-ray photoelectron spectroscopy. The analysis of the XPS spectra indicated the presence of aluminum, oxygen and additionally some carbon elements in both the natural and the laboratory corrosion samples. The areas under the peaks produced by the individual element species in the XPS spectrum are in direct proportion to the atomic concentrations of those elements in the sample being analyzed. The theoretical values for ratios of oxygen to aluminum concentrations in  $\text{Al}_2\text{O}_3\cdot 3\text{H}_2\text{O}$ ,  $\text{Al}_2\text{O}_3\cdot\text{H}_2\text{O}$  and  $\text{Al}_2\text{O}_3$  are respectively 75:25, 67:33 and 60:40. Calculations based on the XPS spectra of the samples analyzed showed that the atomic fractions of oxygen to aluminum in the natural and laboratory samples were of the order of 73.1:26.9 and 72.5:27.5 respectively. A similar analysis conducted on a commercially pure sample of standard aluminum oxide trihydrate yielded an atomic ratio for oxygen to aluminum of 73.0: 27.0, practically identical to the values obtained for the two corrosion samples and quite close to the

theoretically expected value for aluminum oxide trihydrate or aluminum hydroxide. Thus the results of x-ray photoelectron spectroscopy established two things: (1) that the corrosion product generated by exposure to salt spray in the laboratory is very similar in chemical composition (at least in terms of relative concentration of constituents) to the product of corrosion naturally occurring in fuselage lap joints in aging aircraft, and (2) that corrosion products in both cases consist mainly of aluminum oxide trihydrate (in the crystalline form) or aluminum hydroxide (amorphous form).

The presence of carbon, which was also noticed in the analysis of the aluminum hydroxide standard, was assumed to have resulted from contamination of the sample surfaces from ambient atmosphere. Surface contamination of samples by carbon from the atmosphere is very difficult to eliminate and it is usual to neglect the presence of such carbon. It was however noted that the amounts of carbon detected in the two corrosion samples were much higher than that detected in the hydroxide standard, which cast some suspicion regarding the reliability of the XPS results.

#### **4.2 Auger Electron Spectroscopy**

A sample of the corrosion product collected from the lap joint of the decommissioned Boeing 727 aircraft was also analyzed using the Auger electron spectroscopy. The Auger spectrum of the naturally corroded sample clearly identified the presence of oxygen and aluminum elements. No carbon was detected. A comparison of the amplitudes of the peaks of oxygen and aluminum in the AES spectrum showed that the concentrations of these elements in the sample was in the ratio of 75:25. This is again in excellent agreement with the theoretical ratio of oxygen to aluminum concentrations for aluminum oxide trihydrate and aluminum hydroxide. Thus the AES also indicated that the corrosion product in aircraft lap joints was mostly a trihydrate (either amorphous or crystalline), confirming the results of the XPS analysis.

#### **4.3 X-Ray Diffraction Analysis**

X-ray diffraction analysis is capable of identifying the crystalline phase or the phases present in the sample, unlike XPS and AES which only identify the elements constituting the sample and their relative concentrations. Further, the XPS and AES are surface analysis techniques, which probe only the layers in the top 20 to 50 Angstroms ( $1 \text{ Angstrom} = 10^{-10} \text{ m}$ ) of the sample, while the XRD analyzes samples to a depth of about 20 to 30  $\mu\text{m}$  ( $1 \mu\text{m} = 10^{-6} \text{ m}$ ). Samples of both the natural and the laboratory induced corrosion products were subjected to x-ray diffraction analysis.

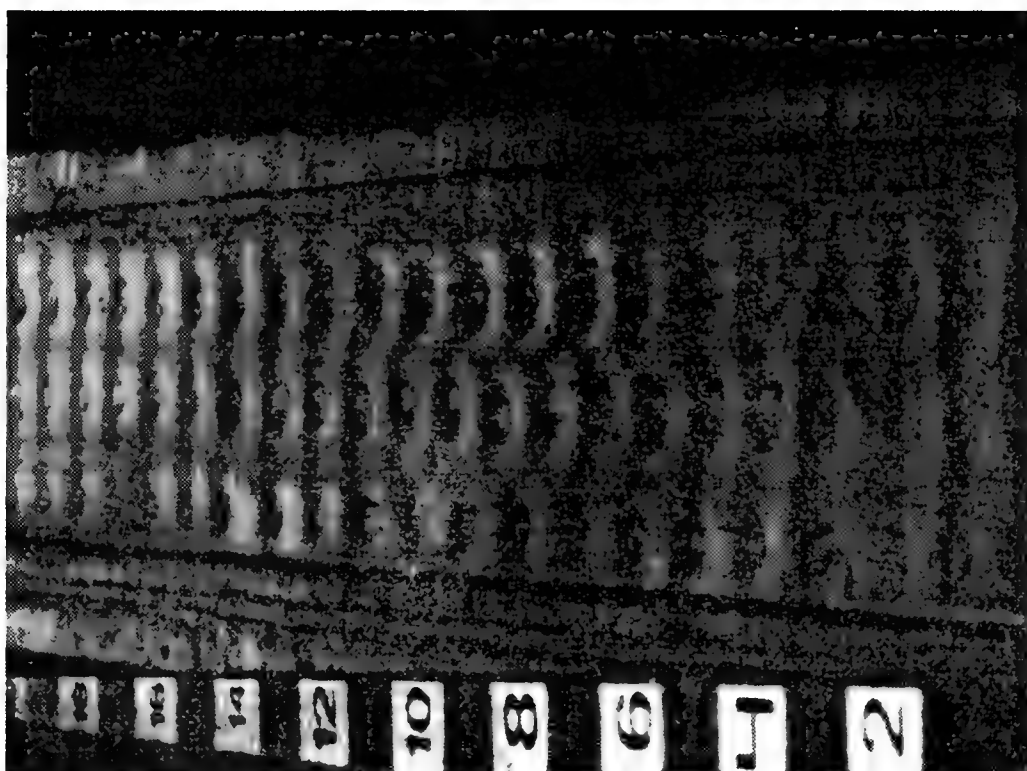
The XRD spectra of both the natural corrosion sample and the laboratory sample strongly indicated the presence of two distinct crystalline phases in addition to a substantial amount of amorphous matter. The two phases were identified as: alpha basic aluminum oxide (Boehmite) and aluminum oxide trihydrate. The amorphous matter in the sample produced a substantial amount of background noise, which tended to obscure the precise heights and locations of the peaks in the XRD spectra. This made it difficult to identify the trihydrate phase precisely, since the data appeared to match well with the peaks of both the alpha phase (Gibbsite) and the beta phase (Bayerite) of aluminum oxide trihydrate. The match with the monohydrate phase was quite definite. It was also apparent that the remaining peaks observed in both spectra belonged either to gibbsite or to bayerite or possibly, to both. The determination of which of these two trihydrates is the one actually present in the corrosion product is a matter that requires further research. Noting that XPS and AES techniques (which could not distinguish between amorphous and crystalline material) indicated the corrosion products to be primarily composed of aluminum oxide trihydrate or aluminum hydroxide, it appeared reasonable to conclude that the background noise in the XRD spectra was mainly produced by aluminum hydroxide in the amorphous phase.

The results of the present x-ray diffraction analysis could not be analyzed in any quantitative manner to obtain an estimate of the relative concentrations of the monohydrate phase (Boehmite) and the trihydrate phases (Gibbsite or Bayerite and amorphous aluminum hydroxide). However they definitely suggested that a large fraction of the corrosion product is as the trihydrate phase as suggested by the two earlier analysis. However the XPS also indicated that at least a small fraction of the samples was in the monohydrate phase. The difference between the XPS, AES results and the XRD result appears to stem from the greater depth to which the latter technique can analyze the sample. Additionally the contamination of the sample surfaces by carbon may also have significantly affected the results of the surface analysis techniques.

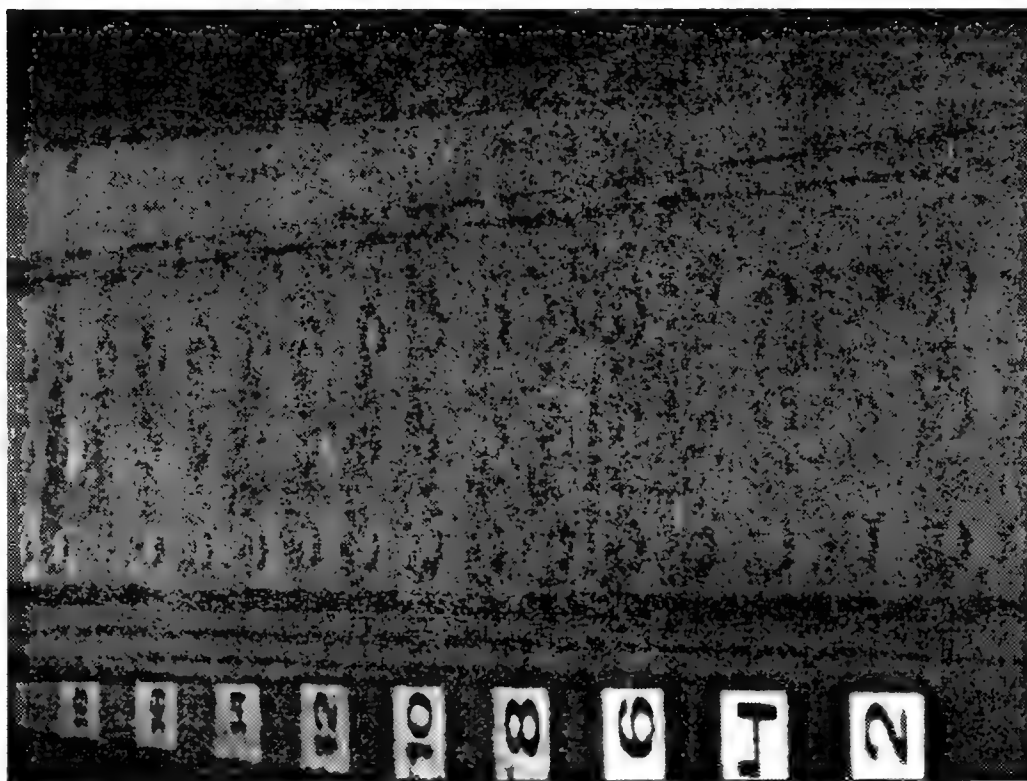
The most significant result from the x-ray diffraction analysis was the similarity of the spectra generated by the natural corrosion product and the laboratory sample, which again confirmed that exposure to acidified salt spray in the laboratory quite closely duplicated the process of corrosion in aging aircraft.

## **5.0 INSPECTION OF AIRCRAFT SPECIMENS FOR CORROSION CAUSED BY AGING**

All specimens retrieved from the aircraft were inspected with D Sight. This was carried out twice: first relatively soon after the specimens arrived at IAR using a laboratory open D Sight set up and a second time after the DAIS 250C equipment was made available to IAR by



B727-N4747 SPECIMEN 12 IMAGE 5 - showing extensive corrosion



B727-N4747 SPECIMEN 4 IMAGE 1 - showing no corrosion

**Figure 5.1** Typical DAIS 250C D Sight images.

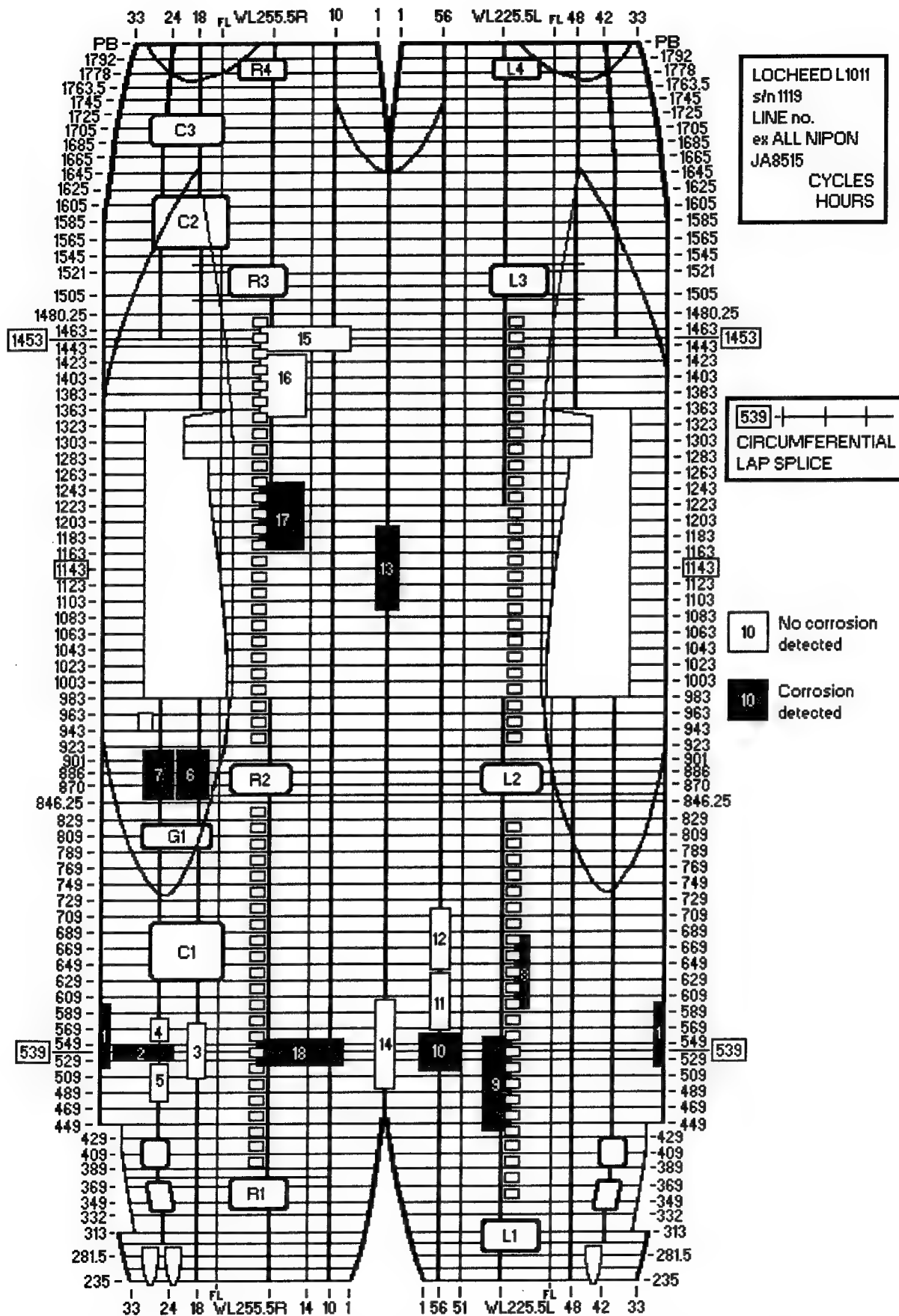
Specimen Number	Image Number	D Sight Image Comment
1	0-3	pillowing throughout
2	0	
	1	top rivet at mark 10
	2-5	
2	6-13	
3	0-7	
4	0-2	
5	0-3	
6	0	bottom row mark 14 to 16
	1	
	2-4	evidence of grinding, bottom to middle row
	5	
	6-11	pillowing and grinding along several rivets
7	0-9	pillowing bottom two rows of rivets
	10-15	pillowing and grinding
8	0-1	
	2-6	
	7-8	pillowing lower two rows of rivets
9	0-5	pillowing at several rivets in groups of 2 to 5
	6-15	
10	0	
10	1	4 top rivets on the patch
10	2 to 9	
11	0 to 7	
12	0-3	

**Table 5.1 D Sight Inspection of Specimens Retrieved from L1011**  
(continued on next page)

Specimen Number	Image Number	D Sight Image Comment
13	0	top two rows, from the edge of the specimen
	1 to 3	
	4	top two rows at 12" mark
	5	top two rows 10 to 12" mark
	6 to 10	
	11	all rivets from 12-14 mark
	12 to 13	
14	0 to 10	
15	0 to 9	
	10 to 11	
	12 to 13	
	14 to 16	
16	0 to 7	
17	0 to 2	
	3	top rivet row from 11 up
	4	there seems to be something missing from image 3
18	0 to 7	
	8	small area above 16 mark
	9 to 15	

**Table 5.1 Continued .. D Sight Inspection of Specimens Retrieved from L1011**

Diffrauto Ltd. In this report (with few exceptions) only the DAIS results are included in Appendix A. Two typical DAIS images are shown in Figure 5.1. Each image contains approximately 0.5 m of specimen length. Where more than one image was required to D Sight the specimen, a typical 50% overlap between images was used. Analysis of the D Sight images was carried out from the printed images without visual reference to the specimens. Results are reported in two forms for each airplane from which specimens were removed: i) in Tables 5.1 to 5.9 with comments noted where corrosion indications were observed and ii) in Figures 5.2 to 5.9 prepared for each aircraft in which specimens which were corroded were marked to distinguish them from the non-corroded specimens. The second method was intended as a quick summary



Specimen Number	Image Number	D Sight Image Comment and (construction of the joint)
1		(accelerated corrosion specimen)
2	0	(circumferential)
	1-3	(lap splice)
	4	bottom row mark 4-10
3	0-6	
4	0-3	
	4-6	slight indication bottom row
5	0-15	
6	0	slight indication top and bottom mark 11-16
	1	
	2-3	top and bottom not continuous
	4	top mark 6-7 3 rivets
	5-6	
	7-8	bottom row slight indications not continuous
	9-10	
	11	two top rivets at mark 10
	12-14	
	15	2 rivets mark 4
	16	
	17	5 rivets top and bottom mark 10-12
	18-24	slight but continuous indication
7A	0-5	(circumferential)
7B	0-4	(circumferential)
	5	top 2 rivets mark 12
	6-9	
7C	0	(circumferential) top rows 3 rivets mark 6-8
	1	top row 3 rivets mark 8-9
	2-6	

**Table 5.2 D Sight Inspection of Specimens Retrieved from DC-9**  
(continued on the next page).

<b>Specimen Number</b>	<b>Image Number</b>	<b>D Sight Image Comment and (construction of the joint)</b>
8A	0-5	(circumferential)
8C	0-5	(circumferential)
9	0-3	single row - pillowing
	4	single row - pilowing to mark 8
10		[accelerated corrosion specimen]
11	0-2	pillowing in all rows
	3-4	pillowing in lower part
11	0-5	(circumferential)
12	0	4 rivets bottom row mark 16-18
	1	4 rivets bottom row mark 3-6
	2	
	3-6	bottom row
13	0-7	
14	0	bottom row mark 10-14
	1	
	2-4	bottom row
	5-6	
15	0-2	top and bottom row
16	0-1	
	2-6	top row very faint signs
17	0-2	bottom row on 2 top row
	3	
	4	top row

**Table 5.2 (continued) D Sight Inspection of Specimens Retrieved from DC-9 (continued on the next page).**

<b>Specimen Number</b>	<b>Image Number</b>	<b>D Sight Image Comment and (construction of the joint)</b>
18	0-3	
	4-7	slight indication
	8	
19		[accelerated corrosion specimen]
20	0-4	slight indications on all images around many rivets
21A		3 rivets top and bottom middle of specimen [before accelerated corrosion]

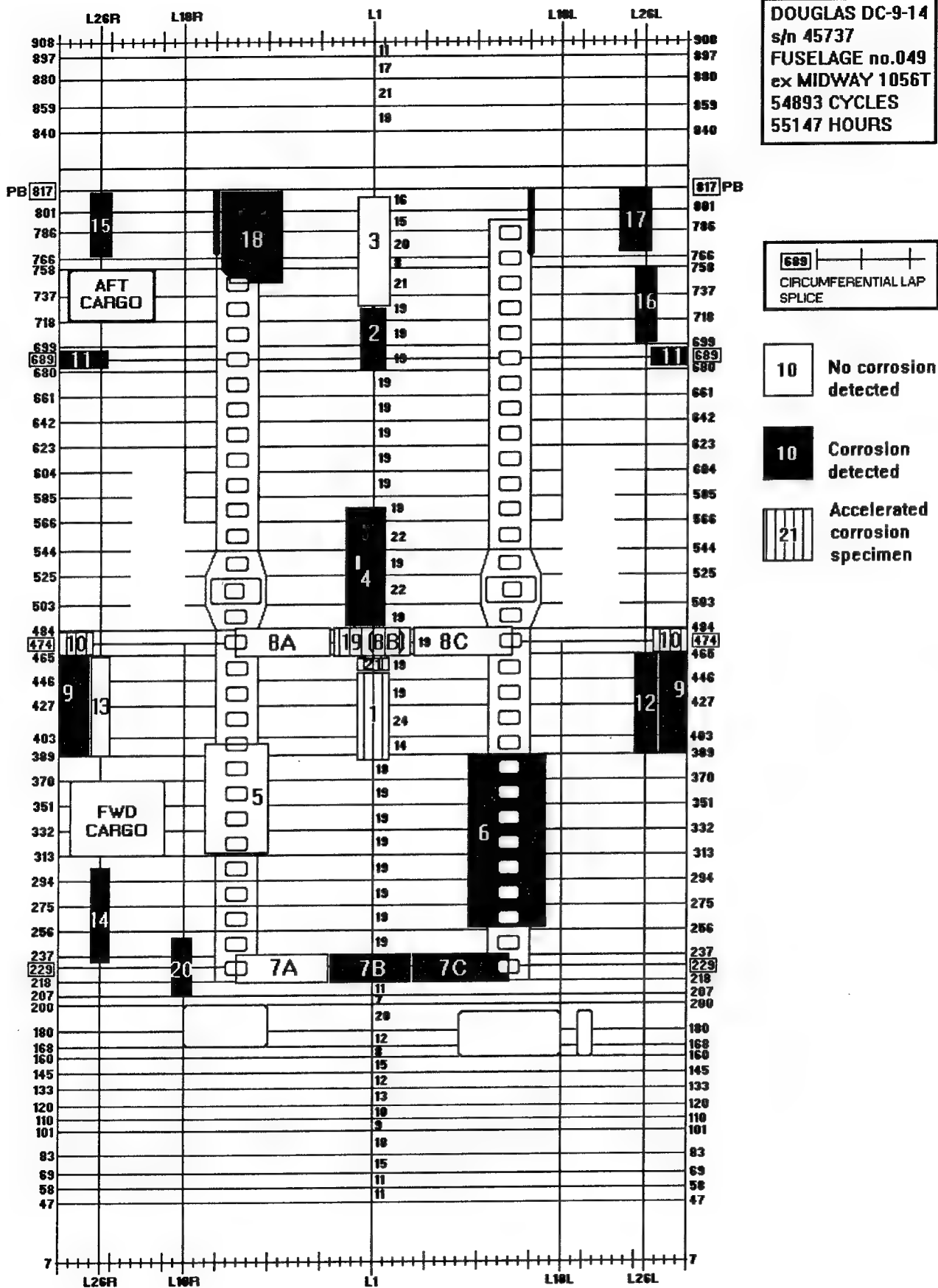
**Table 5.2** (continued) D Sight Inspection of Specimens Retrieved from DC-9

<b>Specimen Number</b>	<b>Image Number</b>	<b>D Sight Image Comment and (construction of the joint)</b>
WA1	0-3	

**Table 5.3** D Sight Inspection of Specimens Retrieved from DC-10

of findings and does not reflect the amount of corrosion found in a particular aircraft. The L1011 is a good example of this - actually very little evidence of corrosion was found but since the specimens are relatively large on the summary figure large areas seem to be affected. No summary figure is provided for the DC-10 aircraft as we were unable to identify the precise location of the specimens on the aircraft fuselage.

In the first phase of the project it was decided to report all D Sight located perturbations which could be related to corrosion. Further work on accelerated corrosion and tear down to be conducted in Phase II will attempt to establish which (if any) of these were false calls. Correlation between D Sight and other methods will be discussed in Chapter Seven.



Specimen Number	Image Number	D Sight Image Comment and (construction of the joint)
L1		top row
L2		top and middle row
L3		
L4		
L5		[teardown & neutron radiography]

**Table 5.4** D Sight Inspection of Specimens Retrieved from B727-200/N4739.

Specimen Number	Image Number	D Sight Image Comment and (construction of the joint)
L1		
L2		top and bottom row
L3		
L4		
L5		top and middle row
L6		
L7		[accelerated corrosion specimen]
R1		(at Diffracto)
R2		top and middle row

**Table 5.5** D Sight Inspection of Specimens Retrieved from B727-200/N4743.

The selection of specimens from the DC-9, L1011 and B727-200 (N4747) is fairly comprehensive and contains nearly all typical splice constructions. It should be noted that the number of sections suspected of corrosion seems to be highest in the B727-200 aircraft. This general observation is corroborated by corrosion problems reported by airlines during the survey conducted at the beginning of this phase of the project.

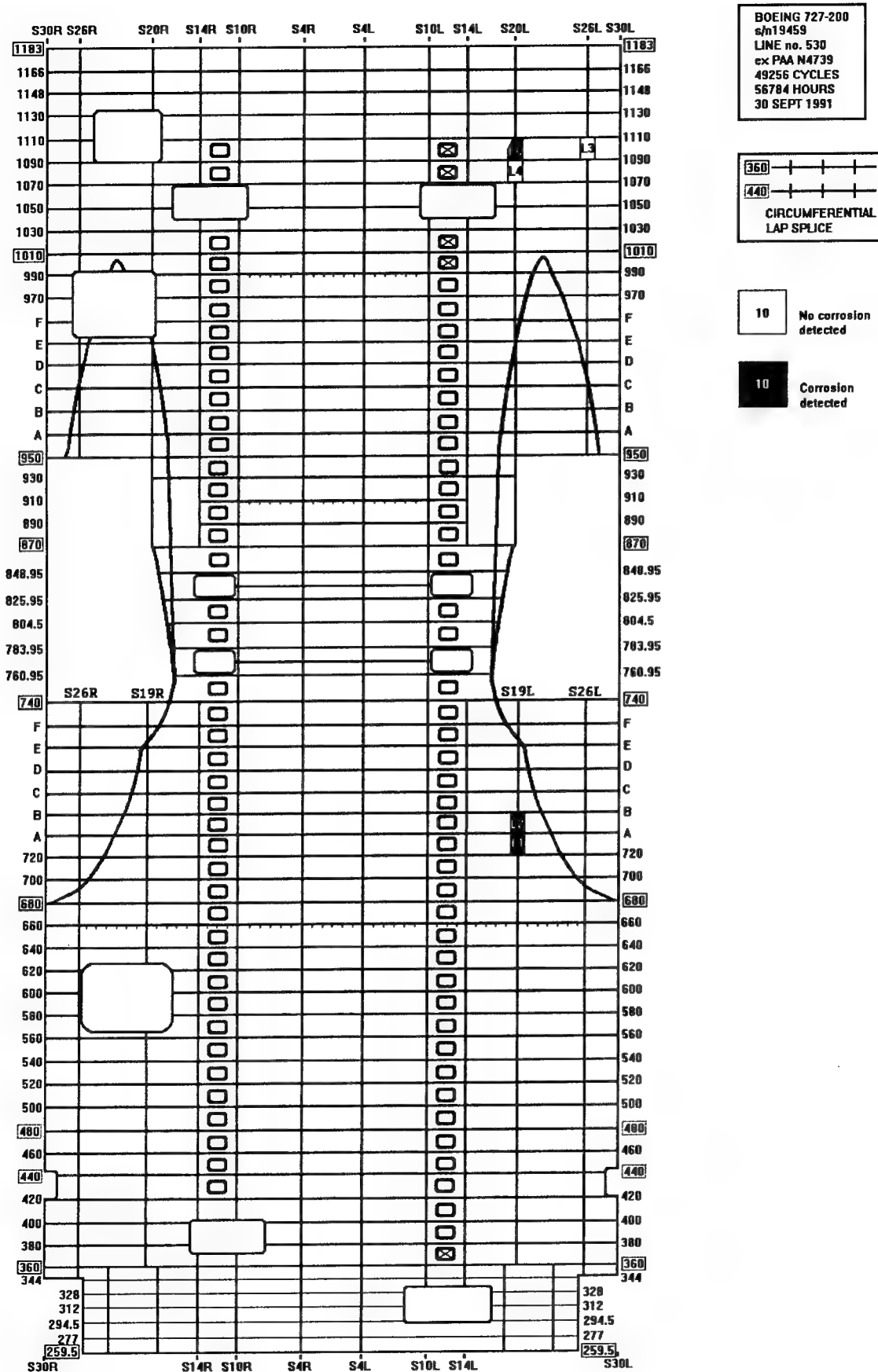


Figure 5.4 B727-N4739 specimens. Results of D Sight inspection for corrosion.

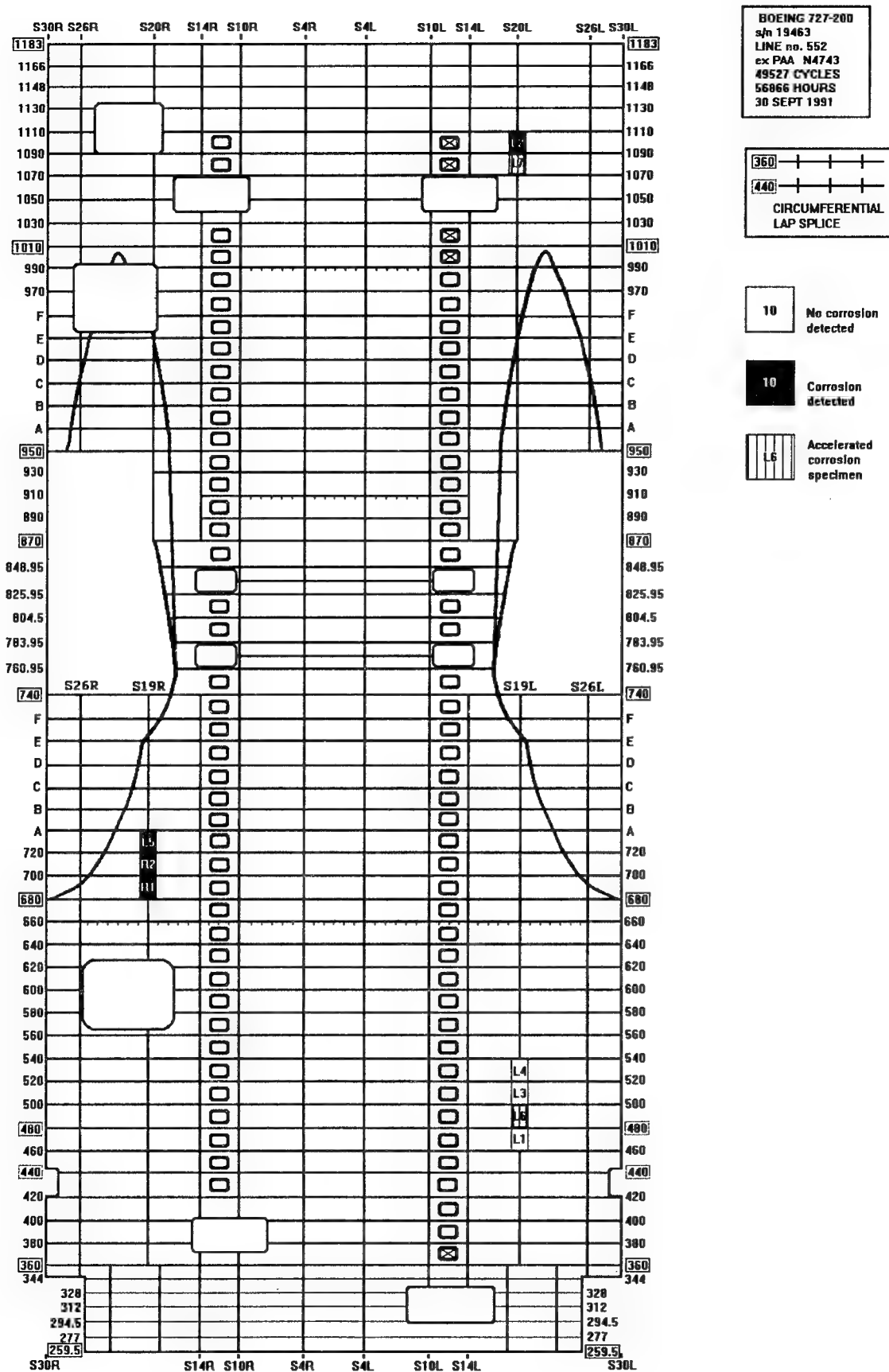


Figure 5.5 B727-N4743 specimens. Results of D Sight inspection for corrosion.

<b>Specimen Number</b>	<b>Image Number</b>	<b>D Sight Image Comment and (construction of the joint)</b>
L1A		
L1C		
L1E		five rivets top to bottom from left edge
L2		six rivets top to bottom middle of the specimen
L3A		
L3C		bottom row of rivets
L3E		middle row slight indication
L4A		two rivets bottom row from left specimen edge
L4C		some rivets in the top row
L4E		(teardown)(accelerated corrosion specimen)
L5		slight pillowing middle row right side three rivets
L6		
R3A		pillowing middle row
R3C		middle and top row
R3E		

**Table 5.6** D Sight Inspection of Specimens Retrieved from B727-200/N4746

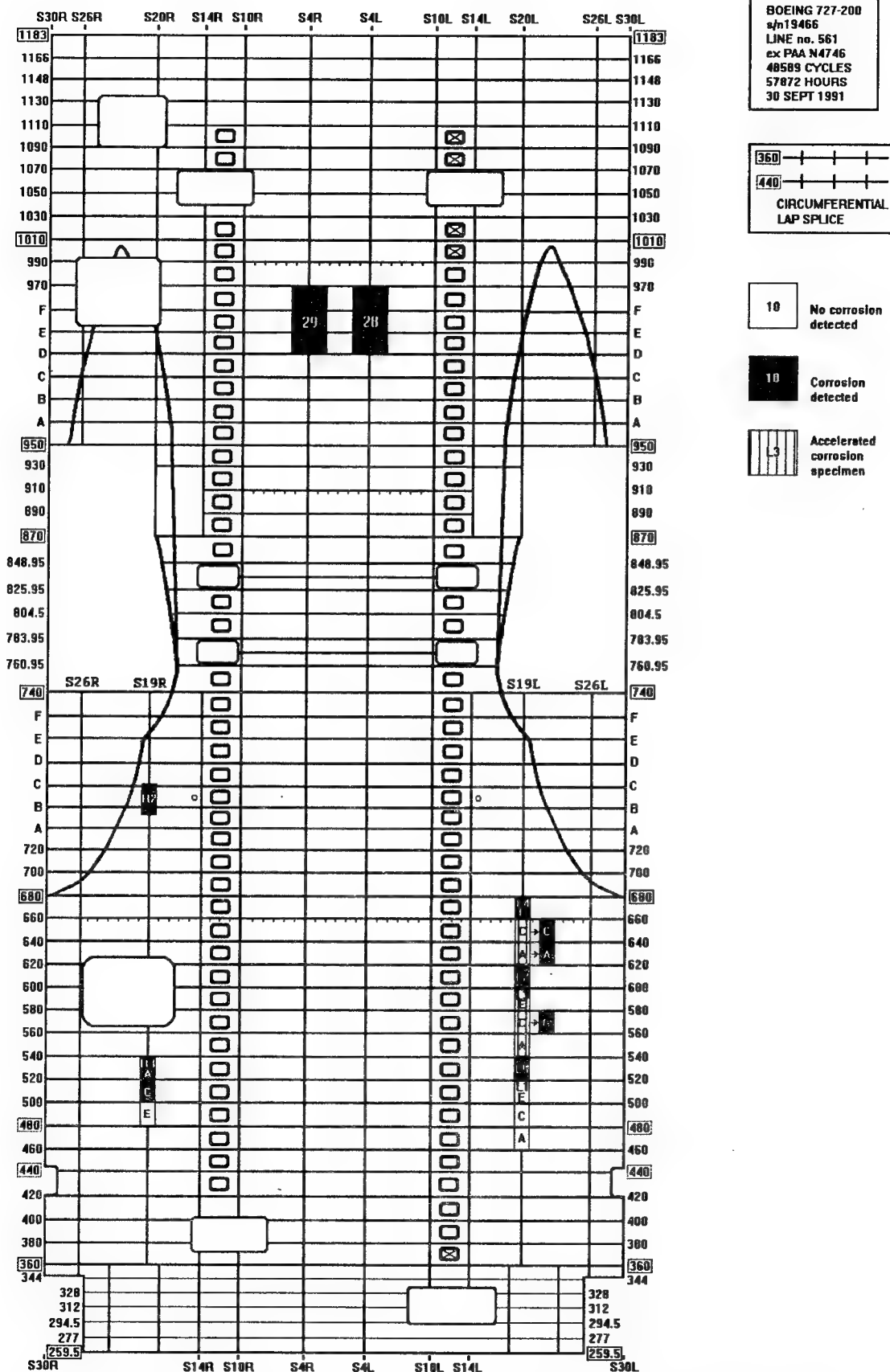


Figure 5.6 B727-N4746 specimens. Results of D Sight inspection for corrosion.

<b>Specimen Number</b>	<b>Image Number</b>	<b>D Sight Image Comment and (construction of the joint)</b>
1A	0-8	(circumferential)
2A	0-6	(circumferential)
2B	0-6	(circumferential)
	7-8	(lap splice) 5 rivets bottom row end of specimen
2C	0-5	
	6-10	(circumferential)
2D	0-5	(circumferential)
3	0-2	
	3	bottom row 5 rivets mark 4-8
	4-5	bottom and middle row slight pillowing
4	0-4	
5		(accelerated corrosion specimen)
6	0-5	
	6	3 rivets top to bottom mark 14-17
	7-8	
	9-11	slight pillowing top and middle row
7	0-1	middle row
	2-3	two rivets middle row
	4	
	5-6	two rivets top to bottom mark 8 (mark 18 on 6)
	7	(circumferential) top and botom rows
	8-11	
	12	(stringer adjacent to circumferential) 3 rivets
8	0-4	slight pillowing in many areas
9	0-2	slight pillowing
	3-4	

**Table 5.7 D Sight Inspection of Specimens Retrieved from B727-200/N4747**  
(continued on next page).

Specimen Number	Image Number	D Sight Image Comment and (construction of the joint)
10	0 - 3	
	4	two rivets top row mark 8 to 9
11	0	top row two rivets mark 7-9
	1	middle row two rivets mark 2-4
	2	middle and top row, mark 10-16
	3	
	4	three rows top to bottom, mark 6-8
	5	(this is the end of lap splice)
11	6	(begining of circumf) top row mark 12-14
	7	top row mark 6-8
	8-9	top and bottom rows
	10-12	
12	0-6	top two rows heavy pilowing sometimes all rows
	7-13	
13	0-3	pillowing throughout
	4-5	lighter pillowing
	6-11	(lap ends)
	12-17	(circumferential)
14	0-4	
	5-9	heavy pillowing (lap ends)
	10-16	(circumferential)
	17	2 rivets top to bottom pillowing mark 8-10
15	0	pillowing middle row mark 2 to 6
	1	pillowing from mark 6 - 18
	2	
	3	pillowing middle and top row mark 4 to 8
	4-6	(end lap splice)
	7-8	(start circumferential) pillowing top 4 rivets

Table 5.7 Continued .. D Sight Inspection of Specimens Retrieved from B727-200/ N4747 (continued on next page).

Specimen Number	Image Number	D Sight Image Comment and (construction of the joint)
16	0	6 rivets middle row from edge
	1-2	
	3	6 rivets top row
17	0-1	pillowing 4 rows top to bottom
	2-4	heavy pillowing
18	0-3	heavy pillowing
19	0-1	pillowing top to bottom 20 rivets from edge
	2-3	
	4	middle row 6 rivets
20	0-1	pillowing 8 rivets top and middle row
	2-4	
	5	3 rivets top and middle row mark 6-8
	6	
	7-8	pillowing 11 rivets top and middle mainly
21	0	2 rivets top row mark 8-10
	1	
	2	3 rivets middle row mark 6-8
	3-6	
	7	slight pillowing
22	0-1	(circumferential)
	2-3	pillowing top row
	4	
23	0	pillowing bottom rows (circumferential)
	1	
	2-4	pillowing bottom rows
	5-8	
24		(repaired, corrosion?)
25	0-8	heavy corrosion

**Table 5.7 Continued .. D Sight Inspection of Specimens Retrieved from B727-200/ N4747.**

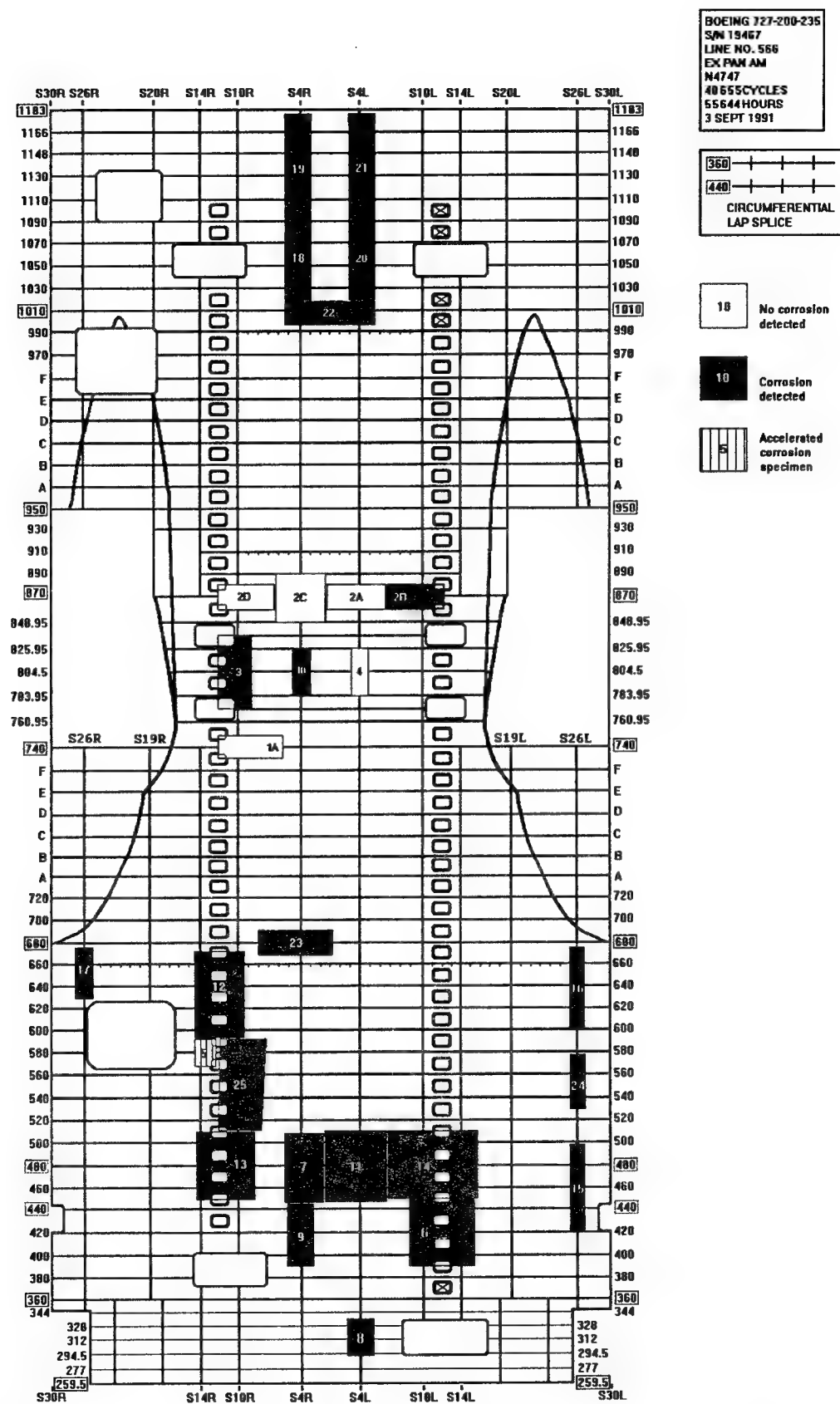


Figure 5.7 B727-N4747 specimens. Results of D Sight inspection for corrosion.

Specimen Number	Image Number	D Sight Image Comment and (construction of the joint)
L1		[teardown]
L2		slight pillowing throughout
L3		very slight pillowing
L4		pillowing throughout
L5		half of specimen pillowing top to bottom
L6		[teardown & neutron radiography]
R1		top to bottom except for left tree rivets
R2		
R3		
R4		five rivets top to bottom right side
R5		
R6		two rivets top to bottom on both sides of spec.

**Table 5.8** D Sight Inspection of Specimens Retrieved from B727-200/N4751.

Specimen Number	Image Number	D Sight Image Comment and (construction of the joint)
L1		
L2		
R1		middle row slight pillowing

**Table 5.9** D Sight Inspection of Specimens Retrieved from B727-200/N4752.



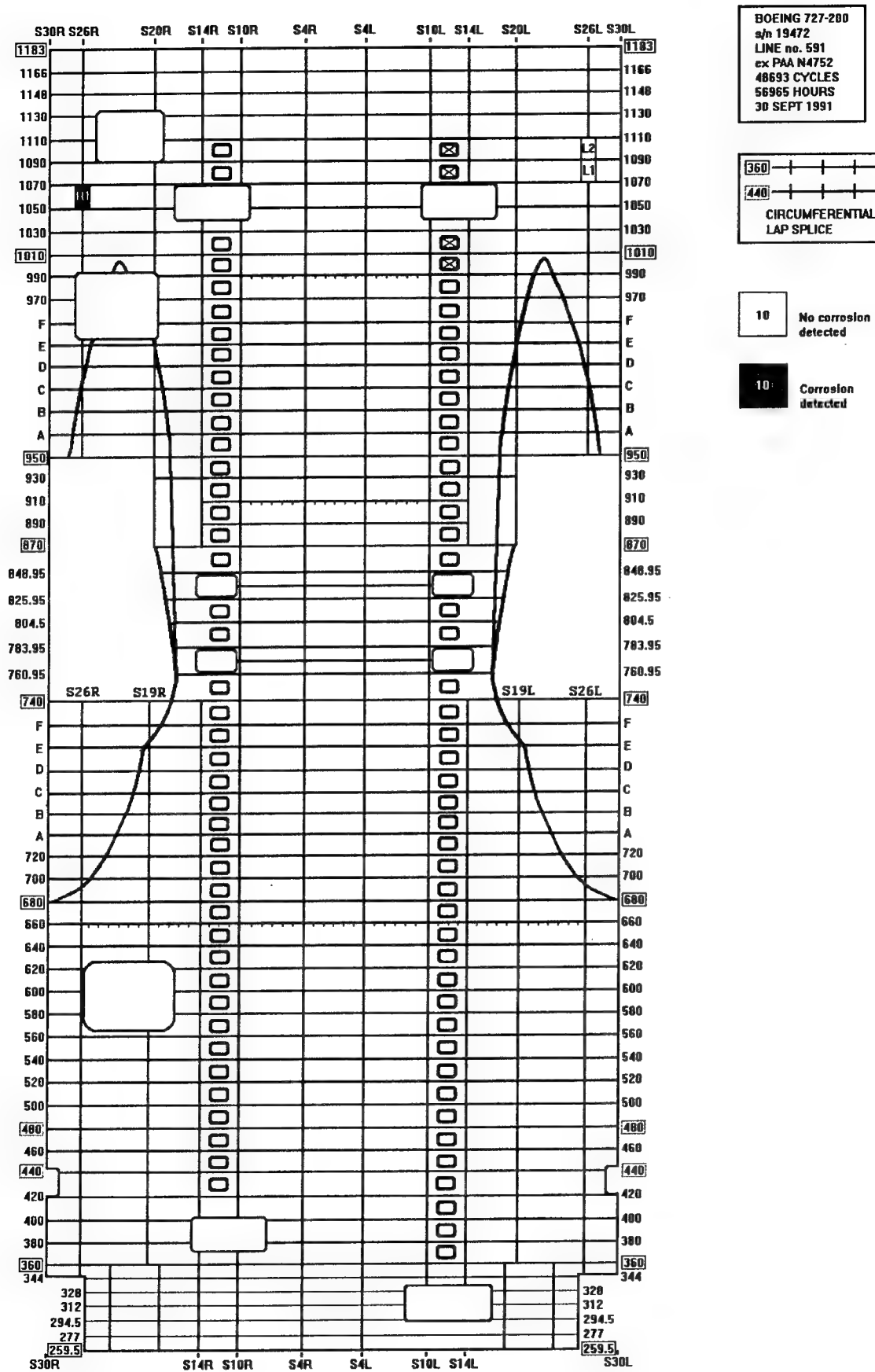


Figure 5.9 B727-N4752 specimens. Results of D Sight inspection for corrosion.

## 6.0 INSPECTION OF SPECIMENS SUBJECTED TO ACCELERATED CORROSION TESTING

The specimens which were subjected to accelerated corrosion testing in the laboratory were again inspected with D Sight before, at one or two intermediate stages and at the end of the corrosion application. Several of these specimens were also inspected by other NDE techniques for comparison with the D Sight results. The main techniques other than D Sight and visual inspection employed for monitoring the growth of corrosion in the specimens subjected to accelerated testing were x-ray radiography, eddy current and shadow moiré. The NDE methods used and the duration of exposures after which inspections were conducted are listed in Table 6.1 for all the specimens subjected to accelerated corrosion testing. The results of the D Sight inspection are presented in the next chapter along with their comparison with results from these other techniques. The specific details of the other NDE techniques applied are given below.

### 6.1 Radiography

Several naturally corroded specimens retrieved from aging aircraft were inspected by x-ray radiography. The x-ray results were largely disappointing, in that they failed to detect any corrosion in most of these specimens, even those that revealed significant amounts of corrosion on tear down and during visual inspection. Radiography was therefore employed only on two of the specimens that were subjected to accelerated corrosion: Boeing 727 specimen 43L6 and a DC-9 specimen 56T21A. The radiography was performed with a LORAD LPX-160 Series Portable Industrial x-ray Unit capable of applying an x-ray Potential of up to 160 kV and a maximum tube current of 5 mA. The specimens were placed at a distance of 43 inches from the x-ray tube on a table lined with lead to prevent back-scattering of the radiation. For most of the aircraft lap joint specimens, the applied voltage was 55 kV with the tube current at 2.5 mA for an exposure time of 60 secs. For some of the heavier specimens, a higher voltage of 60 kV, was applied. The x-ray images were recorded on Kodak Industrex M x-ray film and developed in-situ for immediate inspection.

The results of the radiography inspection are illustrated in Figs.6.1 to 6.6. The ambient view photographs of the exterior and interior surfaces of the two lap joint specimens DC-9 Specimen 21A and Boeing 727 Specimen 43L6, taken after exposure to salt spray for a total of 1104 hours, are shown in Figs.6.1, 6.2 and Figs.6.4, 6.5 respectively, along with close-up views of the most heavily corroded sections. Figs. 6.3 and 6.6 are x-ray images of the DC-9-21A and B727-43L6 specimens respectively recorded at the end of the test. Significant amounts of corrosion are obvious in the ambient views of the interior and exterior surfaces of both specimens. Virtually no corrosion is identified in the x-ray of the DC-9 specimen (Fig.6.3). The x-ray of the Boeing 727 specimen (Fig.6.6) however, exhibits several dark areas which are indicative of corrosion within the lap joint.

Serial Number	Specimen Number	D Sight			Shadow Moiré			Eddy Current			X-Ray	
		0 hrs	409 hrs	629 hrs	1104 hrs	409 hrs	629 hrs	1104 hrs	629 hrs	1104 hrs	0 hrs	1104 hrs
1	51L2	YES	YES	YES	YES	YES	YES	YES	YES	YES	YES	
2	43L6	YES	YES	YES	YES	YES	YES	YES	YES	YES	YES	YES
3	43L7R	YES	YES	YES	YES	YES	YES	YES	YES	YES		
4	46L3A	YES	YES	YES	YES	YES	YES	YES	YES	YES		
5	46L3C	YES	YES	YES	YES	YES	YES	YES	YES	YES		
6	46L3E	YES	311 hrs	532 hrs	1007 hrs	311 hrs	532 hrs	1007 hrs	532 hrs	1007 hrs		
7	46L4A	YES	YES	YES	YES	YES	YES	YES	YES	YES		
8	46L4C	YES	YES	YES	YES	YES	YES	YES	YES	YES		
9	47-5	YES	311 hrs	532 hrs	1007 hrs							
10	56T1A	YES	311 hrs	532 hrs	1007 hrs		532 hrs	1007 hrs	532 hrs			
11	56T1B	YES	311 hrs	532 hrs	1007 hrs		532 hrs	1007 hrs	532 hrs	1007 hrs		
12	56T1C	YES	311 hrs	532 hrs	1007 hrs	311 hrs	532 hrs	1007 hrs				
13	56T21A	YES	YES	YES	YES	YES	YES	YES	YES			YES
14	56T10A	YES	220 hrs	695 hrs		YES	220 hrs					
15	56T10B	YES	220 hrs	695 hrs		YES	220 hrs					
16	56T10C	YES	220 hrs	695 hrs			220 hrs	695 hrs				
17	56T19A	YES	YES	YES	YES	YES	YES	YES	YES			
18	56T19D	YES	311 hrs	532 hrs	1007 hrs		532 hrs	1007 hrs	532 hrs			
19	WA7A	YES	220 hrs	695 hrs		YES	220 hrs	695 hrs				
20	WA7B	YES	220 hrs	695 hrs			220 hrs	695 hrs				

Table 6.1 Inspection Matrix of Specimens Subjected to Accelerated Corrosion Testing

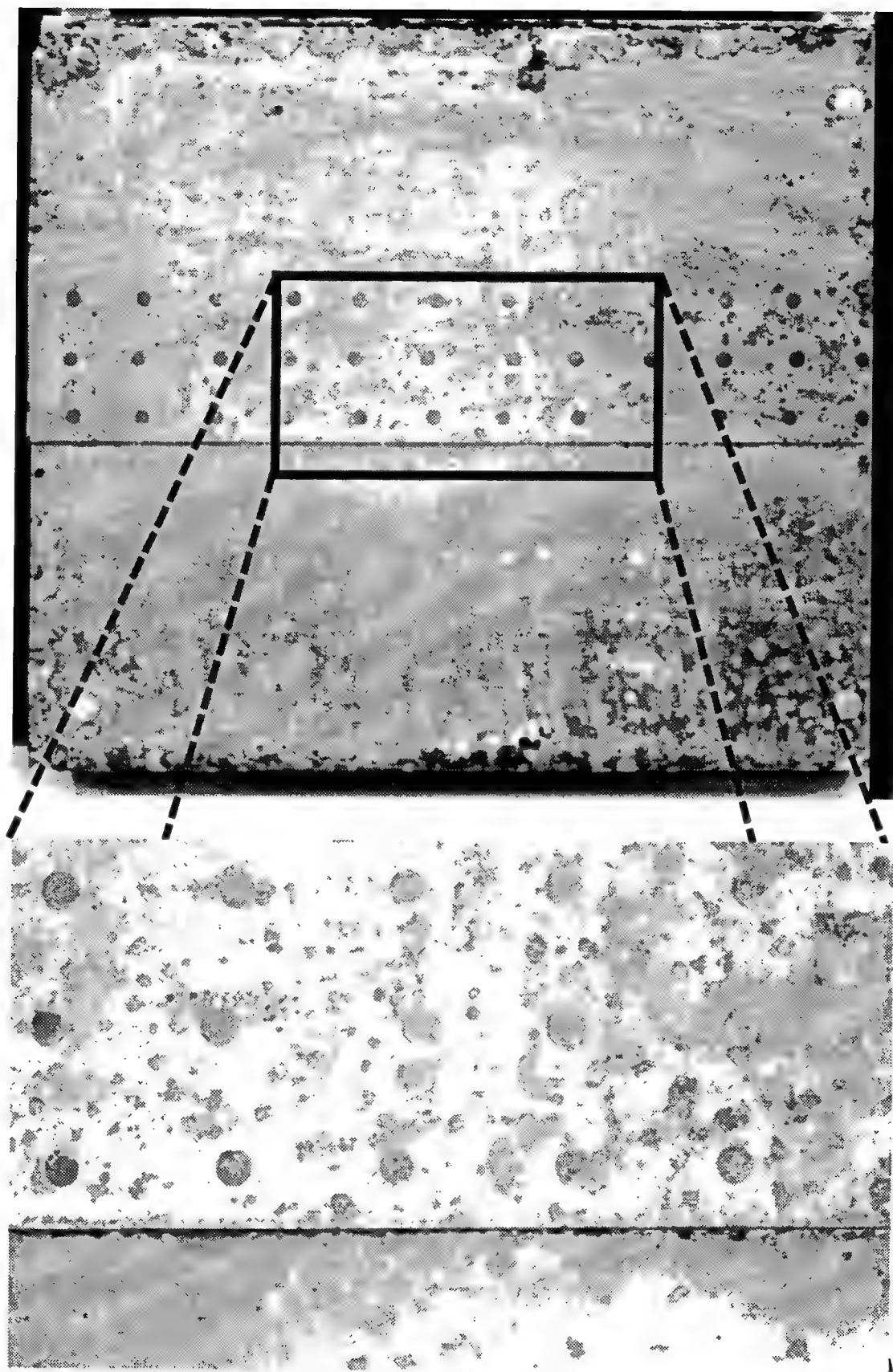


**Figure 6.1** B727 specimen 43L6 ambient exterior view and close up.

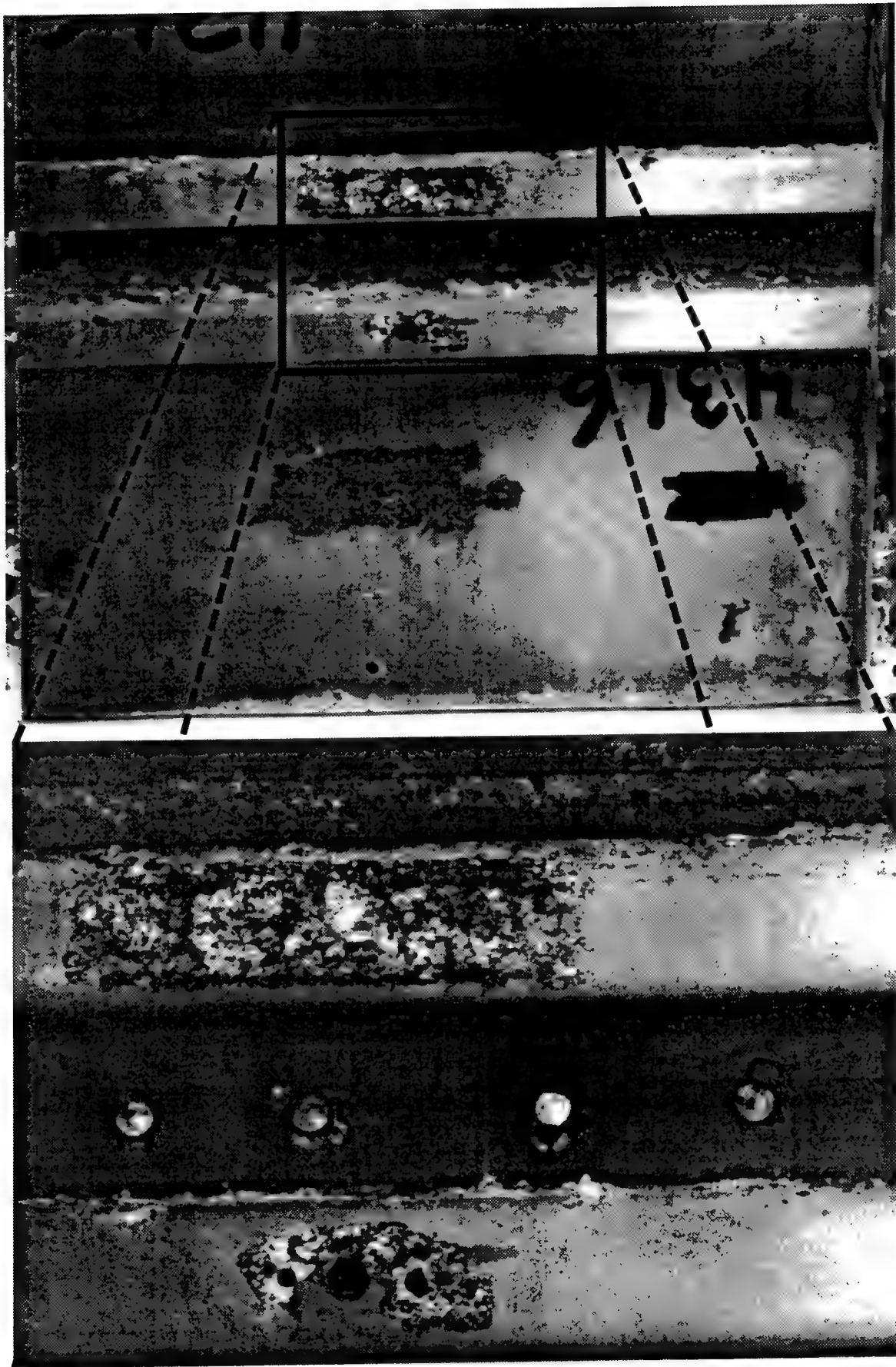


**Figure 6.2 B727 specimen 43L6 ambient view and close up - rear surface.**

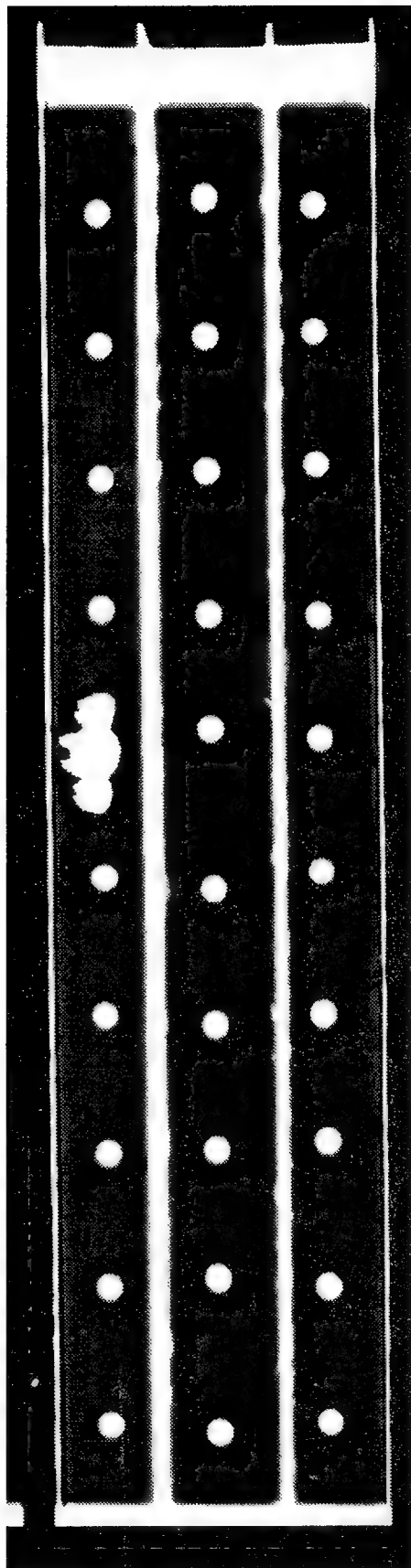


**Figure 6.3** B727 specimen 43L6 radiograph - 1104 hours exposure to accelerated corrosion.

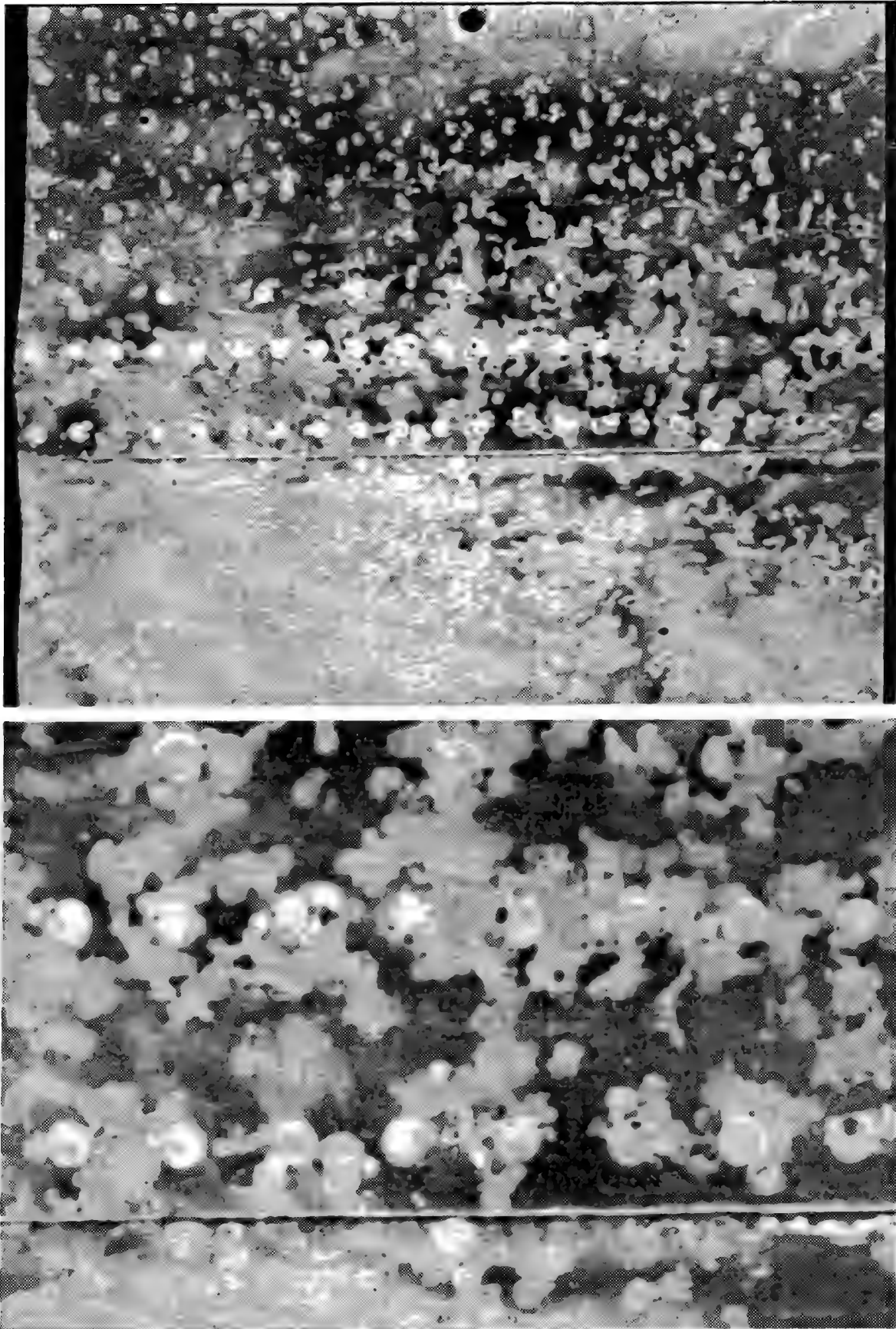


**Figure 6.4** DC-9 Specimen 21A exterior surface and close up view.

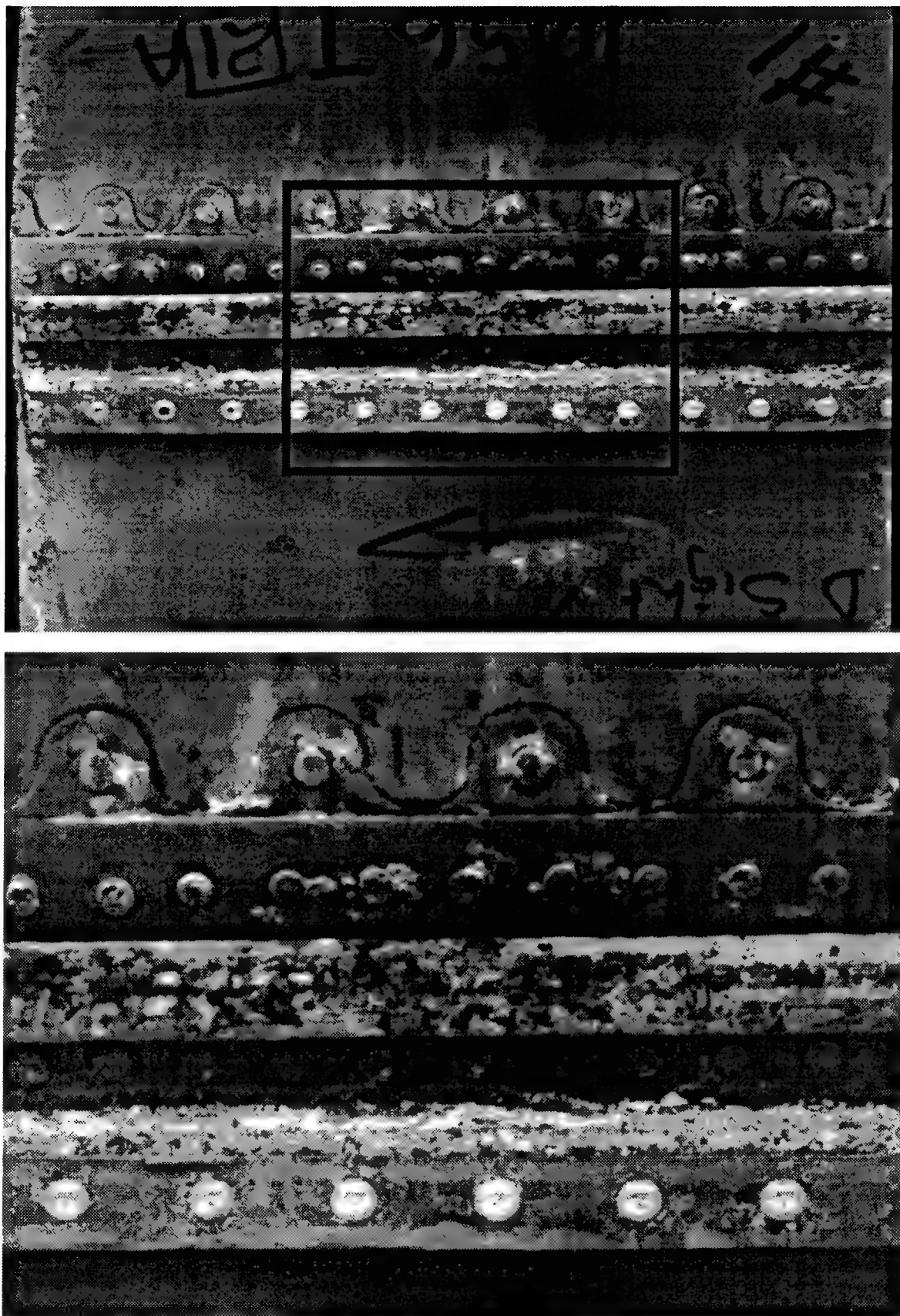


**Figure 6.5 DC-9 Specimen 21A inner surface and close up view.**

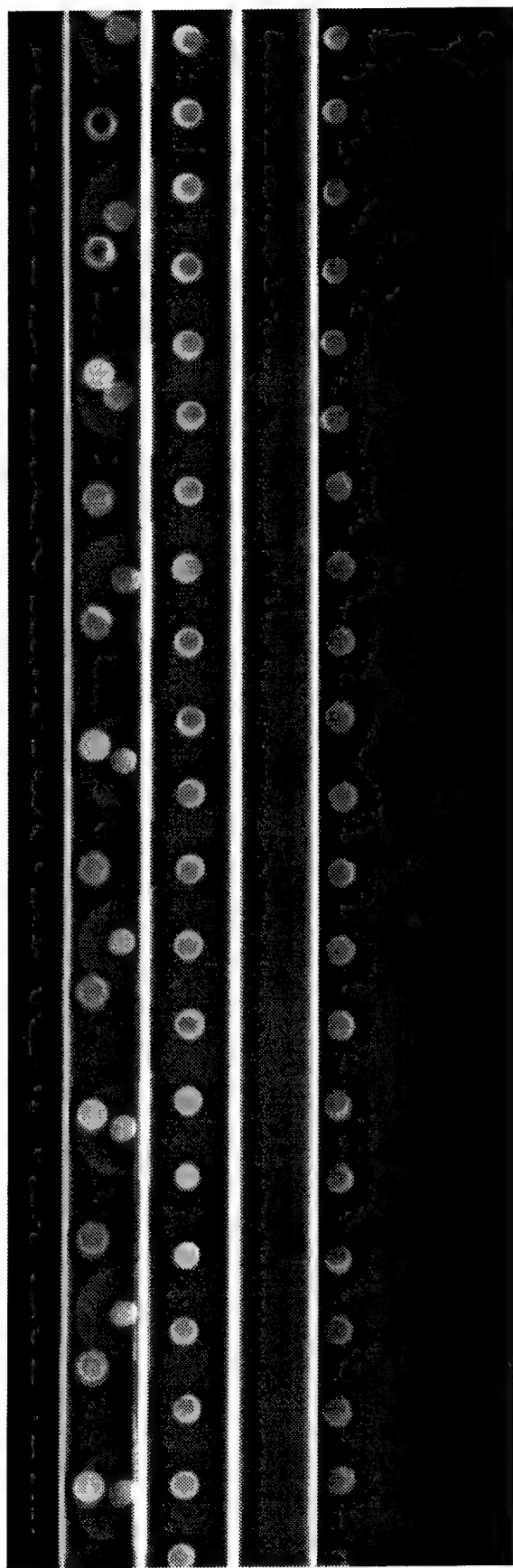


**Figure 6.6 DC-9 Specimen 21A radiograph - 1104 hours exposure to accelerated corrosion.**

## 6.2 Shadow Moiré

Shadow moiré is a simple and efficient means of obtaining whole-field contour maps of out of plane deformations. The surface topology of several of the corrosion specimens was mapped and recorded using this technique before, at an intermediate stage, and at the end of the accelerated corrosion process. The main problem in employing shadow moiré was to ensure that the grid was located and aligned the same way each time a specimen was examined. The location and alignment of the grid over the specimen with consistent repeatability was achieved by mounting the grid on a frame with locator screws and supporting legs fitted with dial gauges for accurate recording of their vertical movements. The specimen was placed horizontally on the ground and the locator screws on the grid mount were inserted into alignment holes drilled along its sides. The legs of the grid mount were adjusted to give the same readings on the dial gauges each time a specimen was mounted for shadow moiré inspection. The specimen was illuminated with a collimated light source from an angle of  $45^\circ$  and viewed through a high resolution CCD camera from vertically above. A grid with 200 lines per inch was used for the corrosion studies, which provided a sensitivity of 0.127 mm (0.005") per fringe.

Shadow moiré was found to be very sensitive to the pillowing deformation caused by artificially induced corrosion. Photographs of the moiré fringes obtained at different stages of exposure are displayed side by side for several specimens in Figs. 6.7 to 6.15. The increase in the number of fringes with increasing periods of exposure is readily observable in most of these figures. The shadow moiré technique not only readily indicates the presence of corrosion, but also provides a quantitative measure of the corrosion build-up, since the moiré fringes are contours of constant lateral deflection. It may be noted that since a fringe of the opposite colour lies halfway between two fringes of the same colour (black or white) one can reliably estimate changes in lateral heights equal to half the fringe sensitivity, i.e., of the order of 0.002"-0.003". The maximum pillowing deflections calculated from the fringe data from Figures 6.7 to 6.15 are tabulated in Table 6.2, along with some remarks on the qualitative nature of the results observable from the images of each specimen. For most of the Boeing specimens the maximum pillowing was observed between fasteners in the same row rather than across the rows. In the case of the Douglas specimen (56T21A) the shadow moiré showed evidence of appreciable upward curling (of the order of 0.005") of the free lip of the top splice, but did not indicate significant deformation of the strip between the top and bottom rivet rows. This appears to be due to the fact that the distance between the rivet rows in this specimen is three times as much as that between the rivets in the same row, which causes the curvature to be restricted to the ends, rendering the middle segments of the strip relatively flat (the modelling indicates that in the case of a rectangular panel of aspect ratio 2 pinned at the four corners, the deformation due to uniform

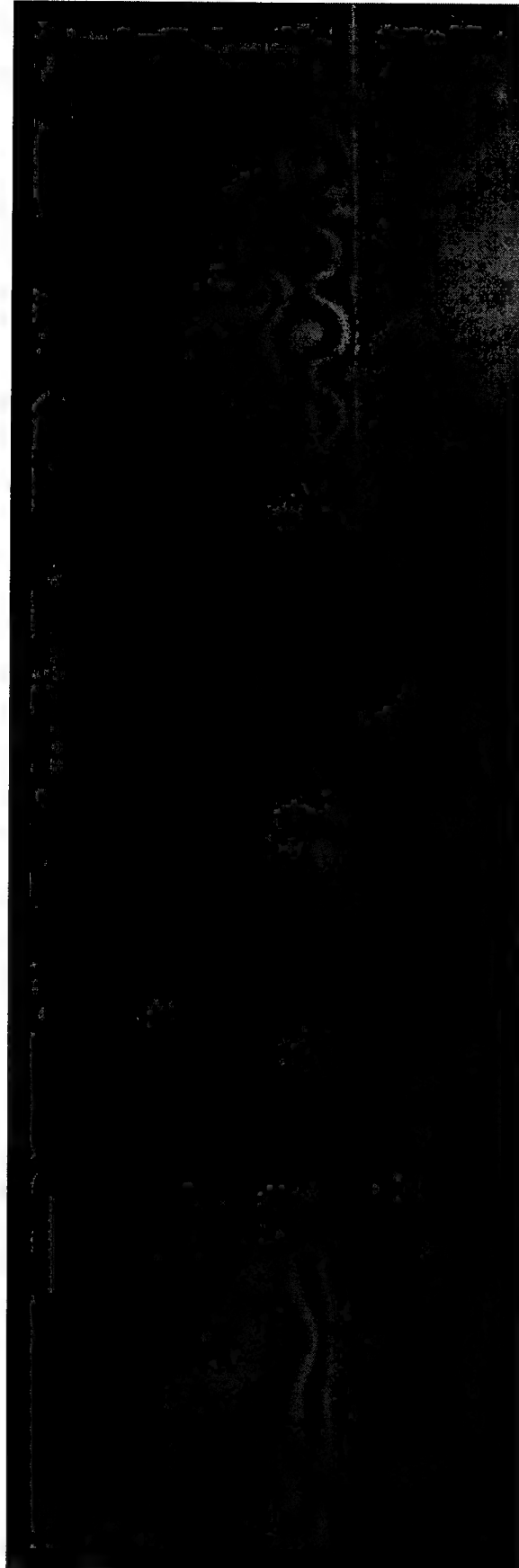
lateral pressure at the midpoints of the long edges is 99% of that at the centre of the panel, while it is only 18% at the mid-point of the short edges).

The comparisons of shadow moiré images taken before and after corrosion exposure was greatly facilitated through the development of a method of accurate specimen repositioning in relation to the shadow moiré grating. To illustrate the repositioning technique a specimen was placed twice in the shadow moiré set up, with the second position shifted sideways in relation to the first. Figure 6.16 illustrates the repeatability of shadow moiré test.

<b>Specimen Number</b>	<b>Figure Number</b>	<b>Maximum measured deflection</b>	<b>Remarks</b>
51L2	Fig.6.7	0.005"	Corrosion in the bottom row
43L6	Fig.6.8	0.007"	Corrosion evident
43L7R	Fig.6.9	0.007"	Corrosion throughout, max. in top row
46L3A	Fig.6.10	0.003"-0.004"	Corrosion less evident
46L3C	Fig.6.11	0.007"	Corrosion evident
46L3E	Fig.6.12	0.013"	Extensive corrosion, even across rows
46L4A	Fig.6.13	0.005"	Corrosion less evident
46L4C	Fig.6.14	0.010"	Corrosion very evident
56T21A	Fig.6.15	0.005"	Value indicates deflection of free lip

**Table 6.2** Deflection measurements from moiré fringe data.

SHADOW MOIRE (200 LINES PER INCH)



409 HRS

629 HRS

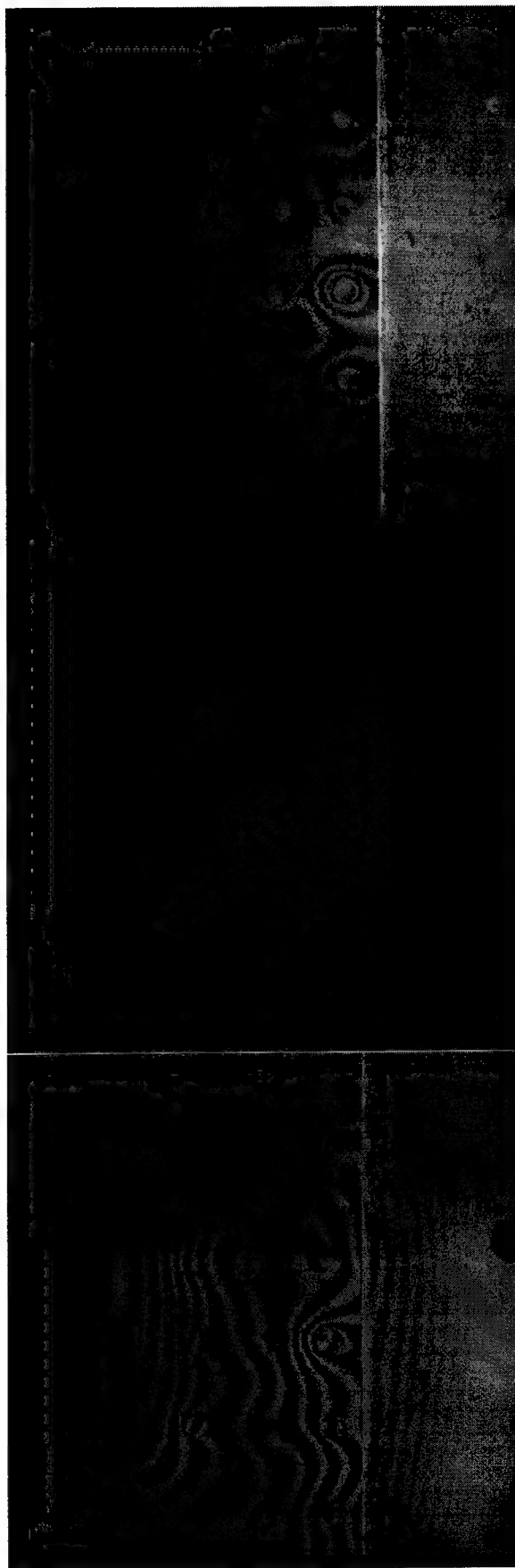
1104 HRS

ACCELERATED CORROSION EXPOSURE TIME

B727 SPECIMEN 43L6

**Figure 6.7** Shadow moiré inspection results at various corrosion exposure times.

SHADOW MOIRE (200 LINES PER INCH)



409 HRS

629 HRS

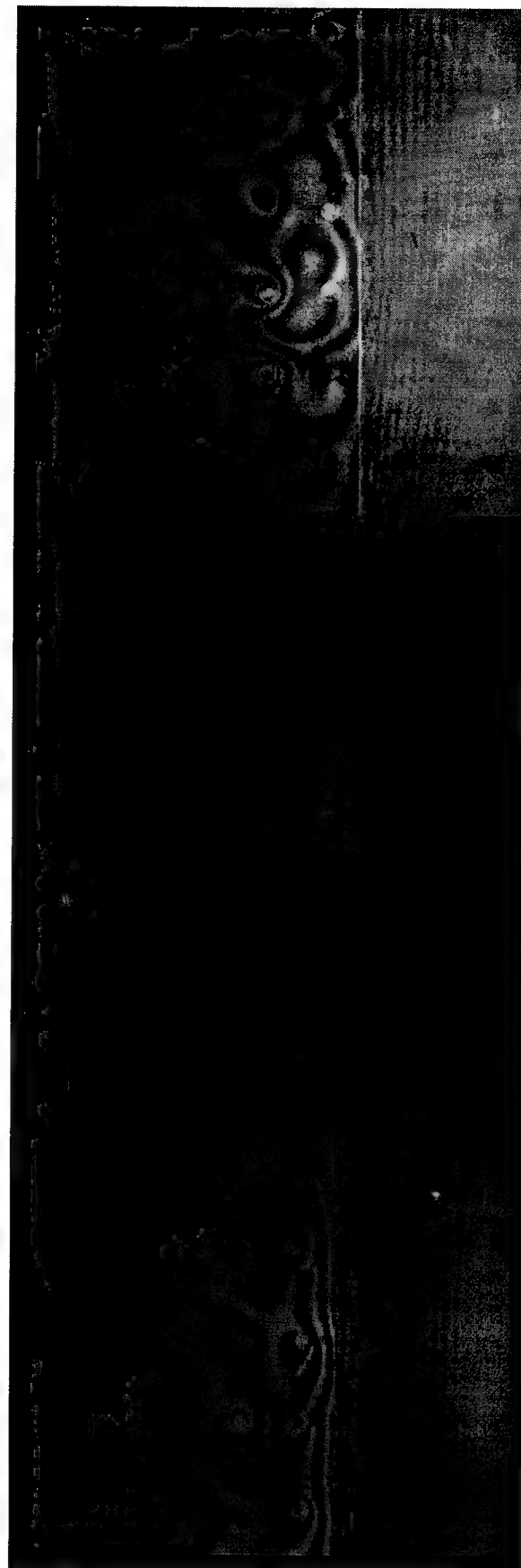
1104 HRS

ACCELERATED CORROSION EXPOSURE TIME

B727 SPECIMEN 43L7R

Figure 6.8 Shadow moiré inspection results at various corrosion exposure times.

SHADOW MOIRE (200 LINES PER INCH)



409 HRS

629 HRS

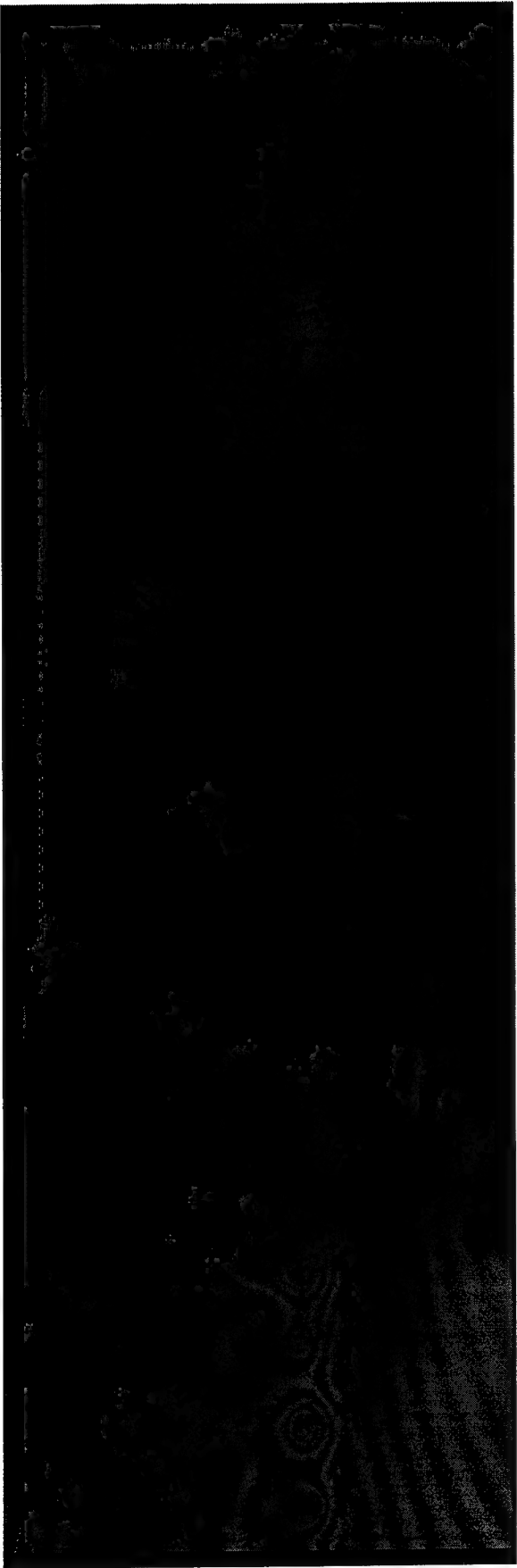
1104 HRS

ACCELERATED CORROSION EXPOSURE TIME

B727 SPECIMEN 46L3A

**Figure 6.9** Shadow moiré inspection results at various corrosion exposure times.

SHADOW MOIRE (200 LINES PER INCH)



409 HRS

629 HRS

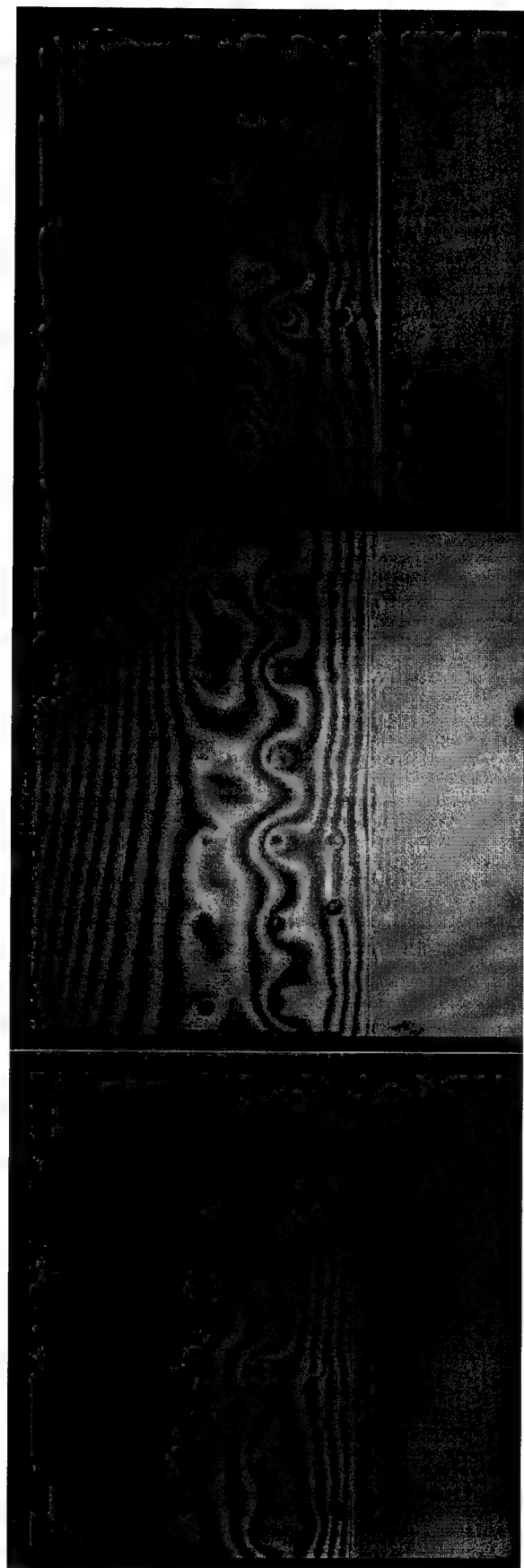
1104 HRS

ACCELERATED CORROSION EXPOSURE TIME

B727 SPECIMEN 46L3C

Figure 6.10 Shadow moiré inspection results at various corrosion exposure times.

SHADOW MOIRE (200 LINES PER INCH)



311 HRS

532 HRS

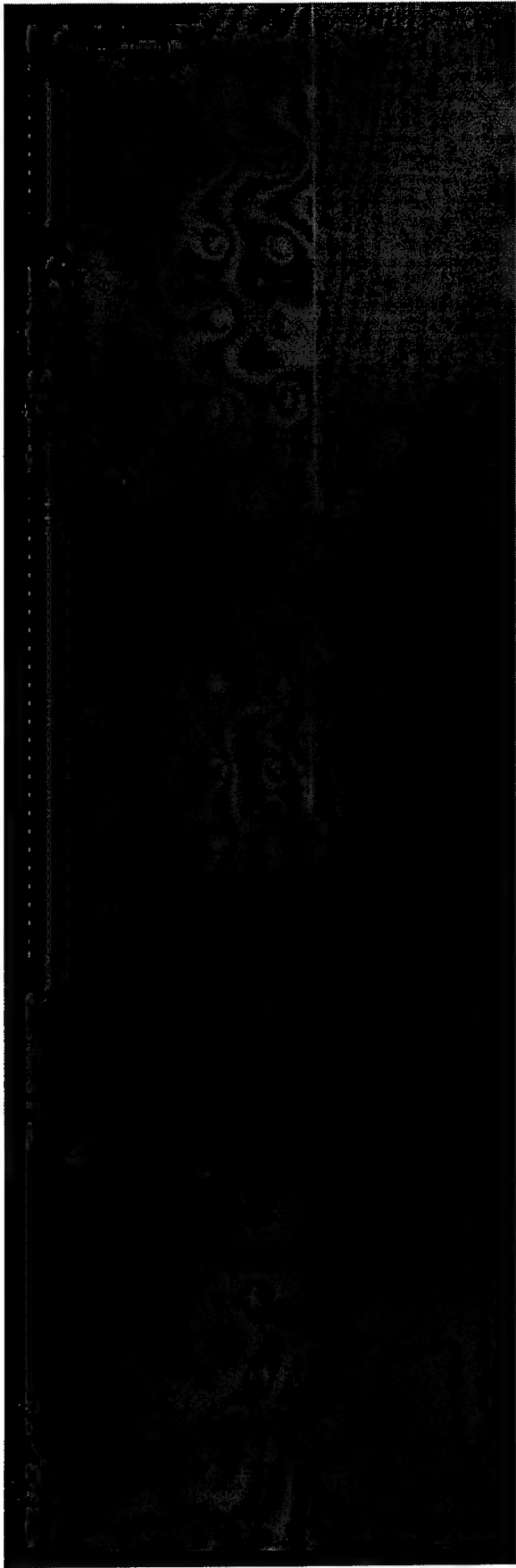
1007 HRS

ACCELERATED CORROSION EXPOSURE TIME

B727 SPECIMEN 46L3E

**Figure 6.11** Shadow moiré inspection results at various corrosion exposure times.

SHADOW MOIRE (200 LINES PER INCH)



409 HRS

629 HRS

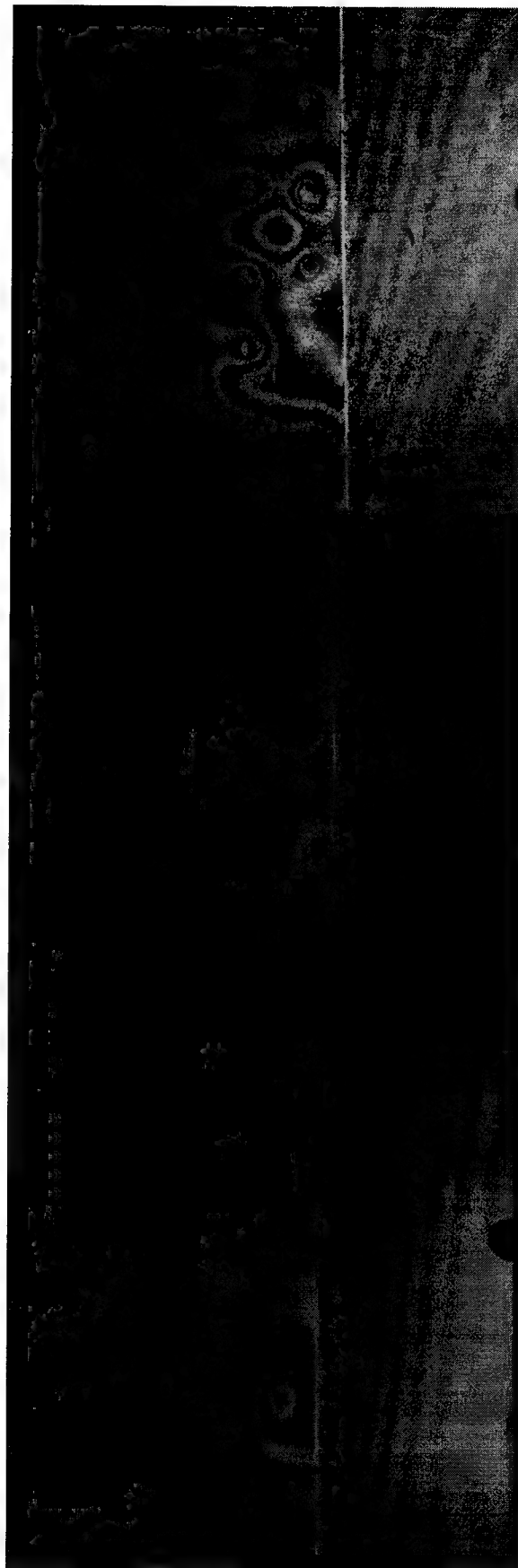
1104 HRS

ACCELERATED CORROSION EXPOSURE TIME

B727 SPECIMEN 46L4A

Figure 6.12 Shadow moiré inspection results at various corrosion exposure times.

SHADOW MOIRE (200 LINES PER INCH)



409 HRS

629 HRS

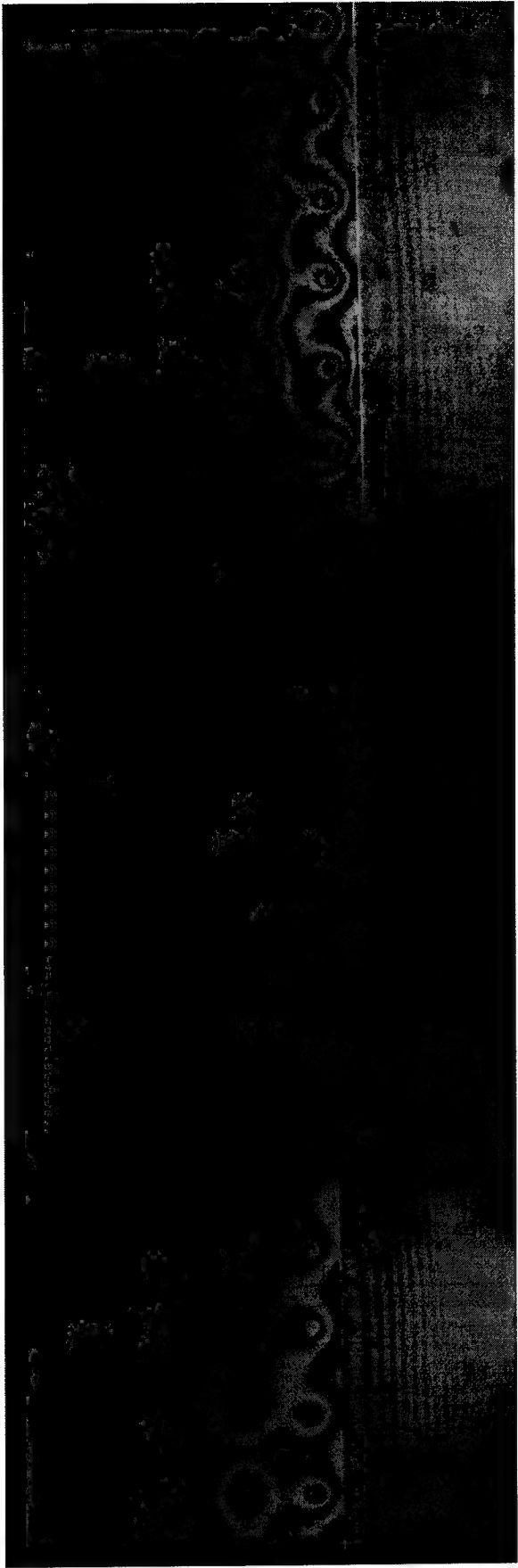
1104 HRS

ACCELERATED CORROSION EXPOSURE TIME

B727 SPECIMEN 46L4C

**Figure 6.13** Shadow moiré inspection results at various corrosion exposure times.

SHADOW MOIRE (200 LINES PER INCH)



409 HRS

629 HRS

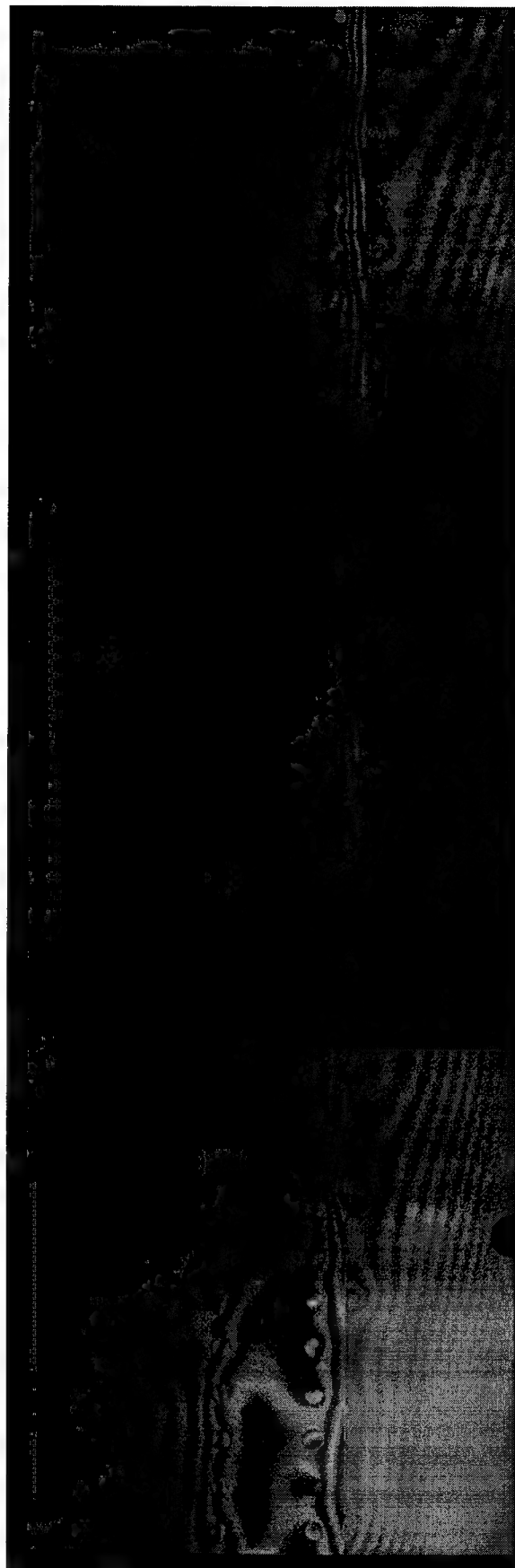
1104 HRS

ACCELERATED CORROSION EXPOSURE TIME

B727 SPECIMEN 51L2

Figure 6.14 Shadow moiré inspection results at various corrosion exposure times.

SHADOW MOIRE (200 LINES PER INCH)



409 HRS

629 HRS

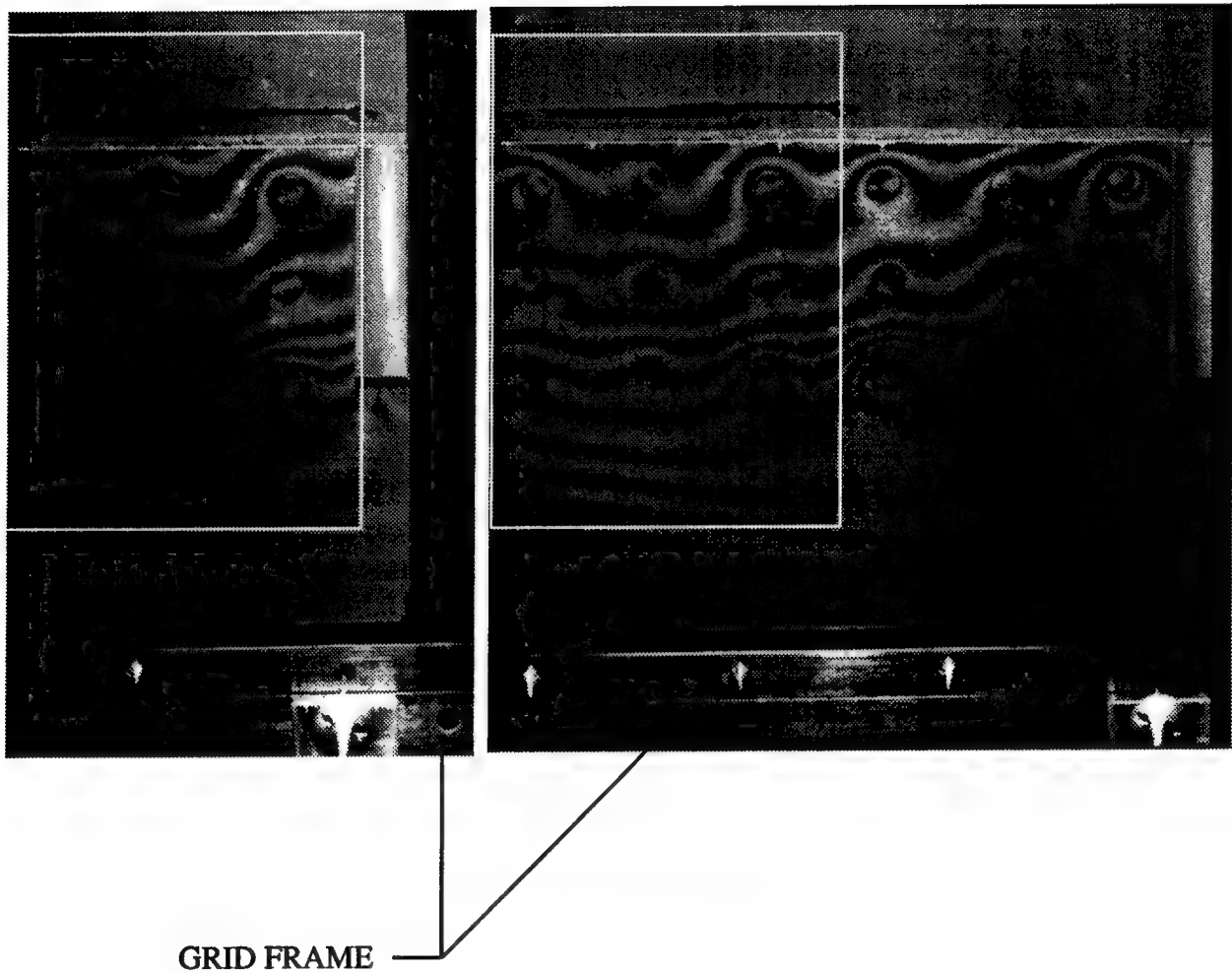
1104 HRS

ACCELERATED CORROSION EXPOSURE TIME

DC-9 SPECIMEN 56T21A

**Figure 6.15** Shadow moiré inspection results at various corrosion exposure times.

### REPEATABILITY OF SHADOW MOIRÉ IMAGING



Two images of the same panel, captured separately.  
In the right hand image the grid frame has been moved three rivet rows to the right.

**Figure 6.16** Shadow moiré repeatability.

### 6.3 Eddy Current

The eddy current inspection was performed as per Douglas specifications[14] using a Zetec MIZ-40 multi-frequency eddy current test instrument attached with a Tyvin LFSL-D low frequency differential eddy current probe (880 Hz to 10 KHz). An 18" manual XY positioner was used to locate the probe over the specimen. The data from the positioner and the analog X&Y information from the MIZ-40 was fed into a Dupont PortaScan PS1 portable colour scan imaging system, equipped with the PS1S-MIZ40 Eddy Current Software. The Portascan system provides an instant two-dimensional mapping of the information from the eddy current probe filtered through gates which can be set to any desired values to display flaws. The following settings were used on the MIZ-40 system for inspecting the corrosion specimens: Frequency = 10 KHZ, Gain 25 dB, Phase 80, H 2.0, V 1.6, Samples 500. The set up was calibrated using a reference specimen which consisted of two pieces of aircraft skin fastened together with screws, one of which had rectangular grooves of different depths cut into its inner surface at regular intervals. It was found that the sensitivity of the eddy current probe was limited to a minimum thickness loss of about 0.23 mm (0.009 inches), so this value was used to set the gates in the PS1 imaging software for the detection of flaws in the corrosion samples.

Comparisons of eddy current results with those of D Sight inspections for several naturally corroded specimens as well as specimens with artificially induced corrosion are illustrated in Chapter 7. In the case of specimens subjected to accelerated corrosion, images of D Sight and eddy current results obtained halfway through and at the end of the corrosion test period are placed side by side, for immediate appreciation of the corrosion build-up caused by salt fog exposure. The eddy current testing was less effective on the Douglas specimens than the Boeing specimens because of the higher aspect ratio of the fastener arrangements in the former. The Boeing lap joints normally have rivet spacings equal to about an inch in length, in the longitudinal as well as circumferential direction. The inter-rivet spacing on the Douglas specimens is only about an inch and a half in the circumferential direction and only a third of that in the longitudinal direction. This close spacing caused spurious results in the eddy current tests since a probe with a diameter of 3/8" had to be used for scanning the specimens. Similarly the proximity of the rivet row to the edge of the outer skin of the Douglas joints also resulted in loss of sensitivity of the eddy current probe in this region.

## 7.0 COMPARISON OF D SIGHT RESULTS WITH RESULTS OF OTHER INSPECTION TECHNIQUES

The comparison of D Sight, shadow moiré and eddy current inspection carried out on specimens exposed to accelerated corrosion is summarized in the following table:

Specime	D Sight result	Shadow Moiré	Eddy Current
56T21A	light corrosion	light corrosion	rivets too close for complete inspection
46L3E	mostly middle row but also light corrosion in top and bottom	mostly middle row (0.013")	no indication
43L6	all corroded	all corroded but less in top row (0.007")	all corroded (0.007")
51L2	bottom, middle and top rows corroded	bottom, middle but less in the top row (0.005")	weak indication in all rows
46L4C	top, middle and bottom but not everywhere	top, middle and bottom but not everywhere (0.010")	some corrosion indication
46L4A	all corroded	all but light (0.005")	some areas mostly middle row
46L3C	all corroded	all corroded (0.007")	most areas corroded
46L3A	middle and top row light corrosion	middle and top light corrosion (0.003-4")	no indication
43L7R	all corroded	all corroded (0.007")	little corrosion

**Table 71.** Comparison of D Sight with Shadow Moiré and Eddy Current.

The above results generally point to an excellent correlation between D Sight and shadow moiré. Corrosion mapping from shadow moiré was not attempted as only part of a specimen could be inspected with this technique. This was due to the limited size of the available gratings. Out of 9 specimens reported above 5 seemed to provide good comparison between eddy current and D Sight. In two specimens eddy current initially indicated less corrosion than D Sight but with increase in time of exposure to accelerated corrosion, eddy current also found more

corrosion. This suggests that D Sight is more sensitive to lap splice corrosion than eddy current. Figures 7.1 to 7.9 contain D Sight images along with D Sight and eddy current corrosion inspection maps taken at two stages during the accelerated corrosion process.

D Sight inspections of 39 specimens from the general specimen population and from the accelerated corrosion study were compared with their respective eddy current scan results. Based on their correlation's these may be tabulated into four categories (Table 7.2):

Good correlation between D Sight and eddy current maps		No correlation	
No corrosion found	Corrosion found	D Sight found corrosion but no eddy current confirmation	Eddy current found corrosion but no D Sight confirmation
56T19A		56T21A(c)	
		56T1B	
		56T1A	
51R5	46L4C(a)(c)	46L3A(a)(c)	51R2(b)
51R3	43L6(a)(c)	46L3E(a)(c)	51R1(b)
51L3	51R6	51L2(a)(c)	43L3
46R3E	51R4	51L2	
46L6	43L7R(a)(c)	39L3	
43L4	46L3C(a)(c)	43L2	
43L6	46L4A(a)(c)	46L4C	
46L3A	39L1	46L4A	
52L2	46R3C	43L7R	
52L1	46R3A		
	43L5		
	43R2		
	46L2		

(a) inspected after prolonged corrosion exposure, (b) eddy current signal due to paint, (c) corrosion found by shadow moiré

**Table 7.2** Comparison of D Sight and eddy current using naturally corroded and laboratory accelerated specimens. (D Sight images, D Sight corrosion maps and eddy current maps for these specimens can be found in the Appendix).

Total numbers of specimens in the above four categories are:

Good correlation between D Sight and eddy current maps		No correlation	
No corrosion found	Corrosion found	D Sight found corrosion but no eddy current confirmation	Eddy current found corrosion but no D Sight confirmation
11	13	12	3

**Table 7.3** Total number of specimens in each category (Table 7.2)

The above numbers can be further reduced to note that good correlation between D Sight and eddy current was obtained in 24 out of the total of 39 specimens (62%). The fact that a correlation was not observed in 15 specimens can be attributed to the greater sensitivity of D Sight (this was confirmed by shadow moiré in four of the specimens in this category), and possibly to a number of D Sight false calls as well as at least two eddy current false calls (which were attributed to paint patches on the specimen surface). The results indicate that the population of specimens was well balanced between non-corroded, corroded and lightly corroded specimens (11:13:12). If one were to assume that the fourth category contains non-corroded specimens then the last observation is still valid (14:13:12). The final observation which can be made at this time is that by adding the four confirmed corroded specimens to the second category (13+4) and adding the first and second category to suggest the total correct D Sight indication number (14+13+4=31). This translates to a nearly 80% (31/39) confirmed success rate for the D Sight inspections. The remaining 20% of specimens either contain a low level of corrosion or represent D Sight false calls.

It is suggested that with the increase in the number of specimens subjected to accelerated corrosion and periodic moiré inspections, the uncertainty regarding the number of D Sight false calls will be reduced substantially. Similar results could be achieved through tear down of this group of specimens. It is felt, however, that the number of destructive tests should be kept at a minimum, as the corroded specimens should be retained for future evaluations of improved D Sight and other NDI systems.

Only two specimens were subjected to tear down subsequent to D Sight inspections and these are shown in Figures 7.10 and 7.11. In both specimens the correlation is excellent.

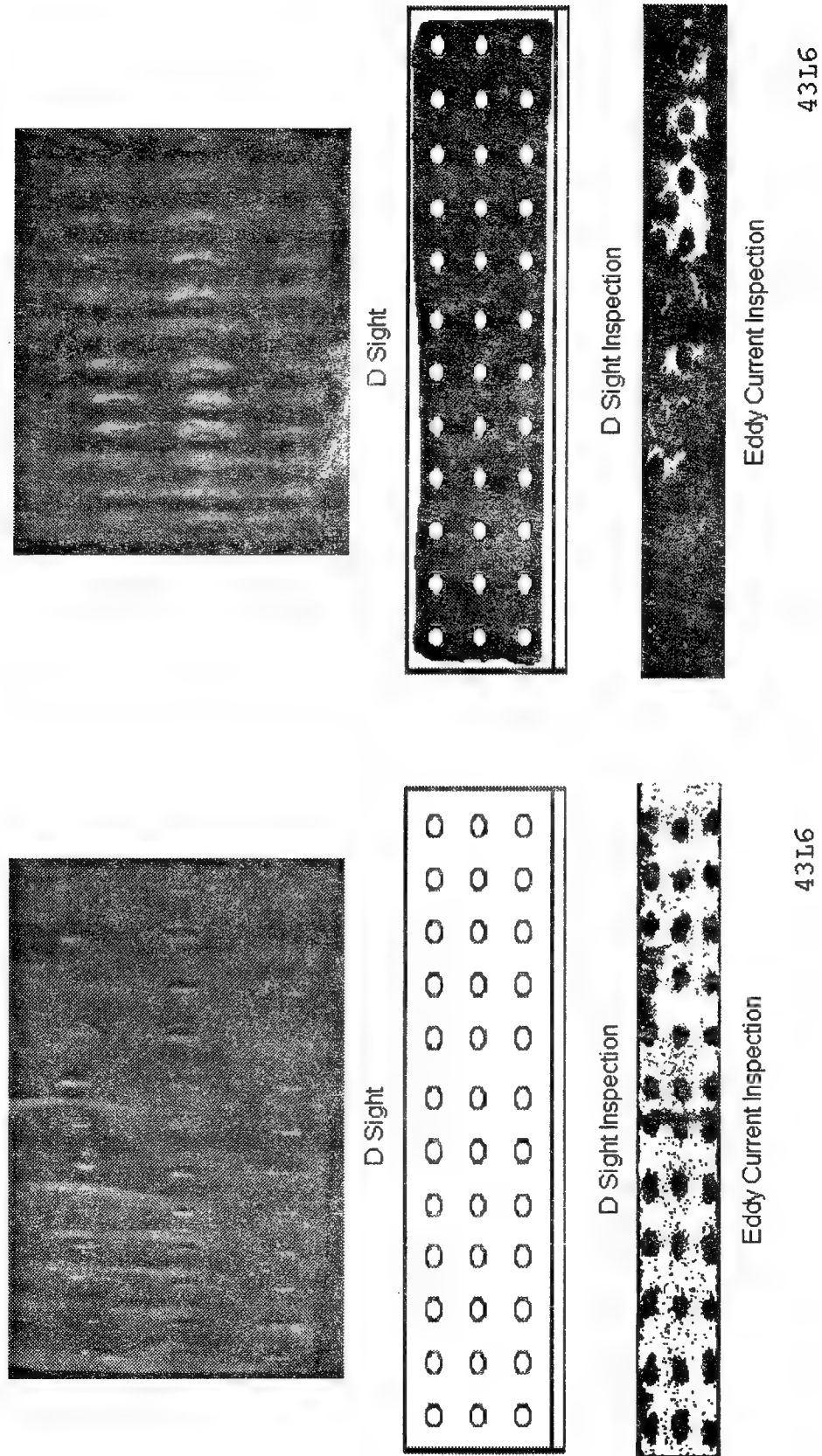


Figure 7.1 Specimen 43L6 pre- and post-corrosion inspection results. D Sight images, D Sight and Eddy Current corrosion maps.

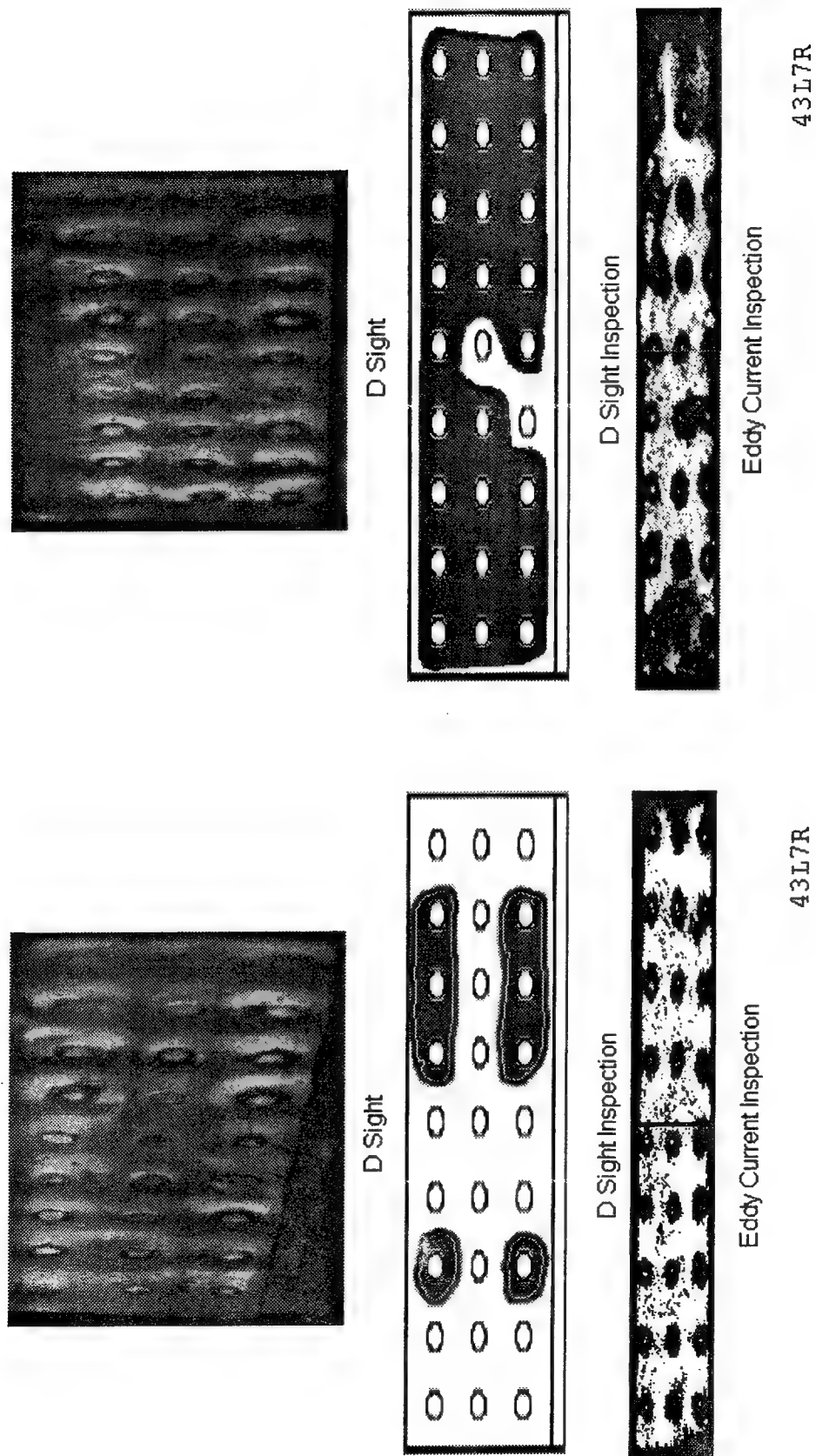
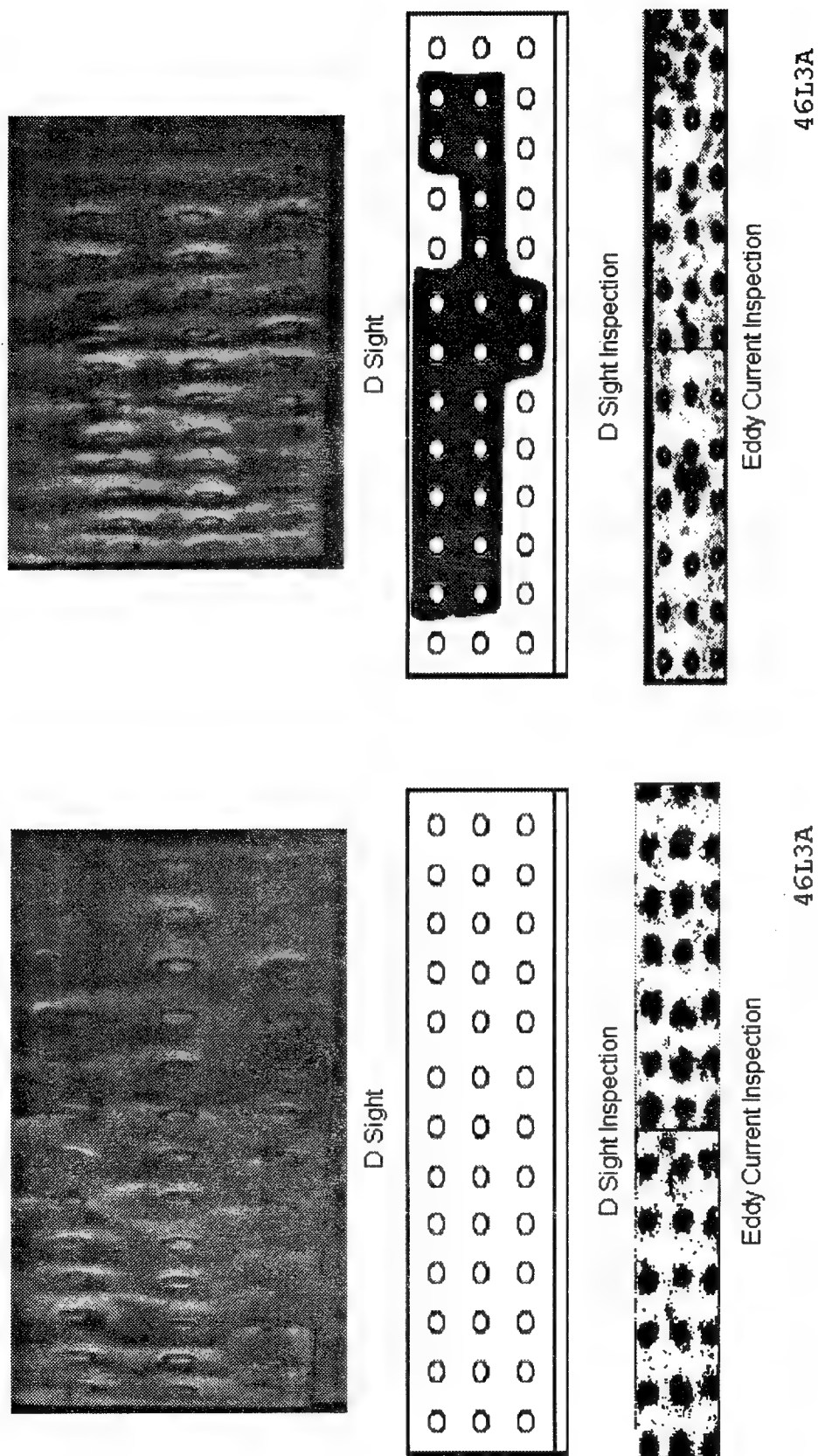
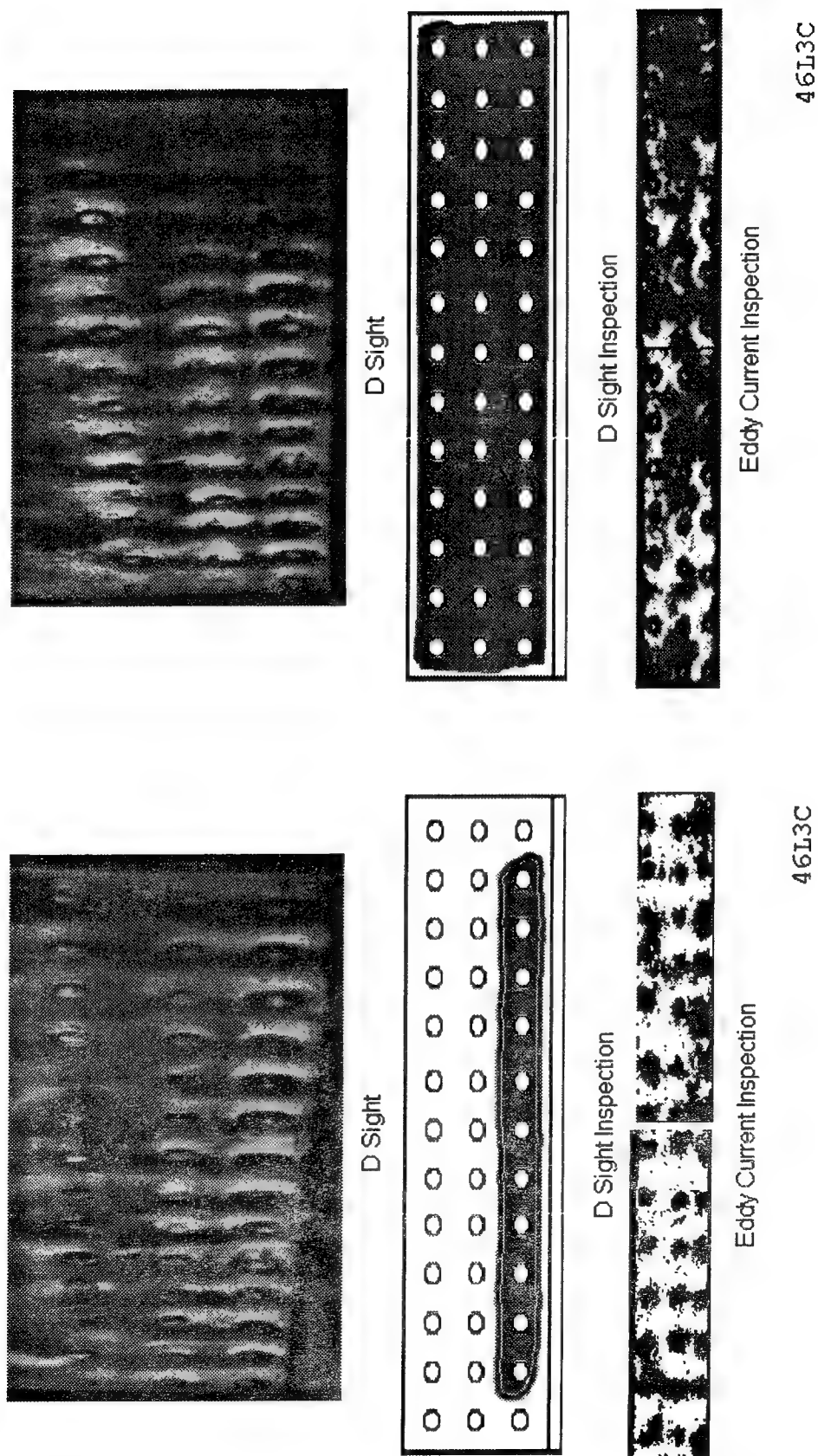


Figure 7.2 Specimen 43L7R pre- and post-corrosion inspection results. D Sight images, D Sight and Eddy Current corrosion maps.



**Figure 7.3** Specimen 46L3A pre- and post-corrosion inspection results. D Sight images, D Sight and Eddy Current corrosion maps.



**Figure 7.4** Specimen 46L3C pre- and post-corrosion inspection results. D Sight images, D Sight and Eddy Current corrosion maps.

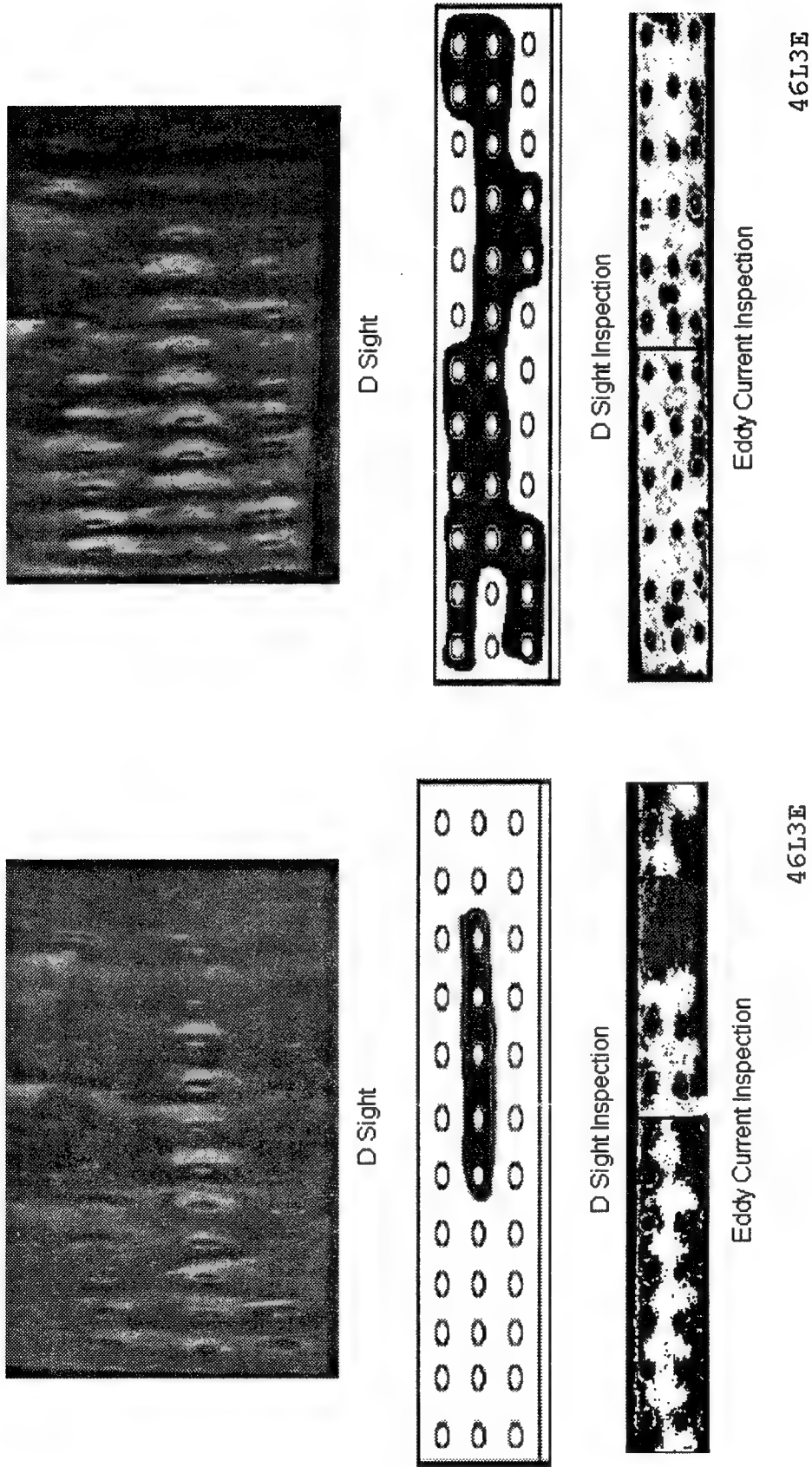


Figure 7.5 Specimen 46L3E pre- and post-corrosion inspection results. D Sight images, D Sight and Eddy Current corrosion maps.

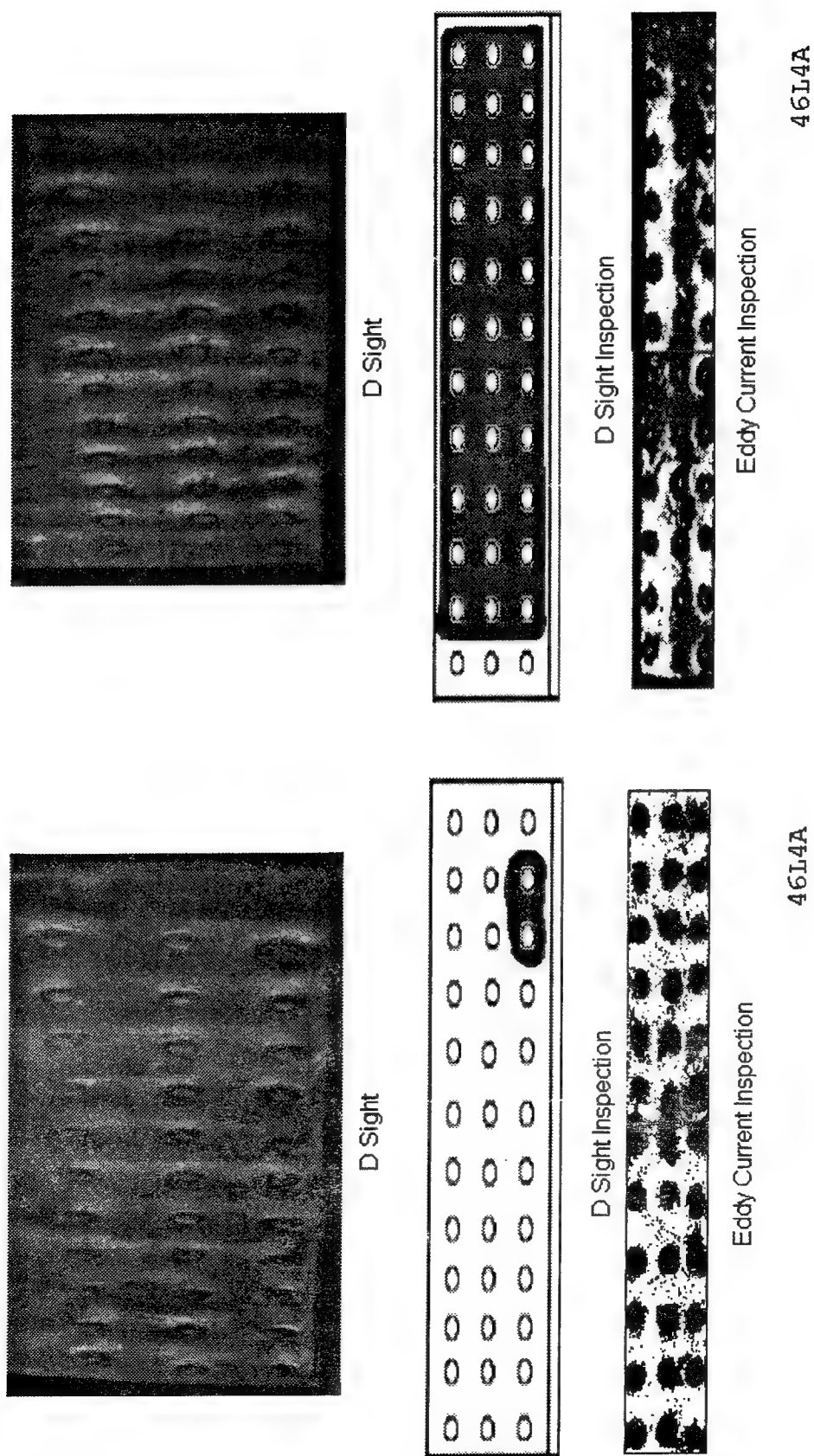
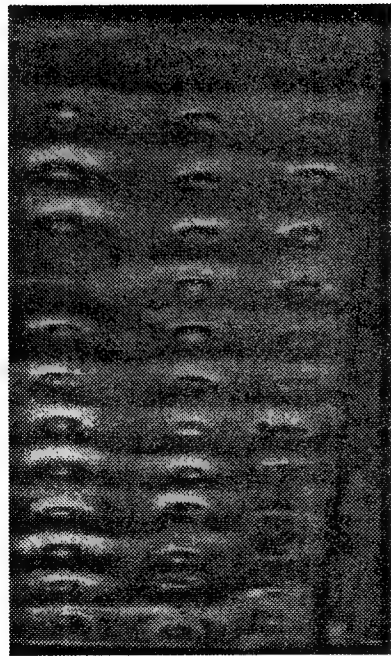
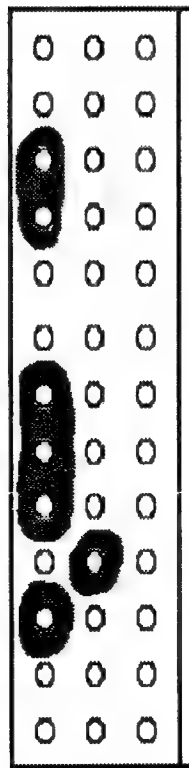


Figure 7.6 Specimen 46L4A pre- and post-corrosion inspection results. D Sight images, D Sight and Eddy Current corrosion maps.



D Sight

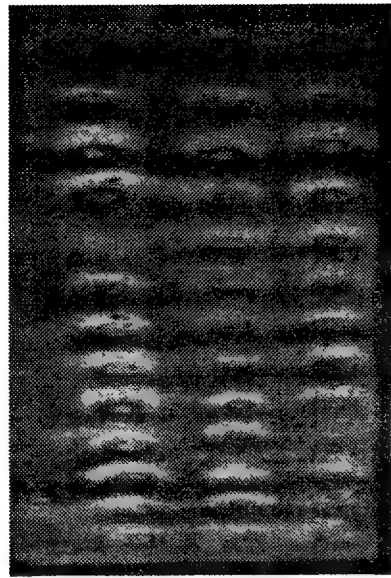


D Sight Inspection

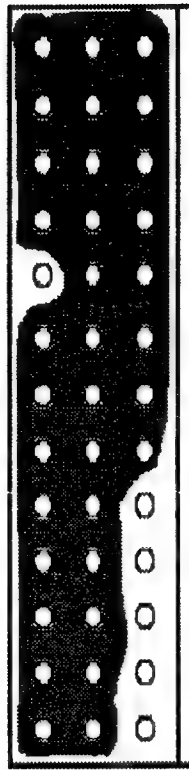


Eddy Current Inspection

46L4C



D Sight



D Sight Inspection



Eddy Current Inspection

46L4C

Figure 7.7 Specimen 46L4C pre- and post-corrosion inspection results. D Sight images, D Sight and Eddy Current corrosion maps.

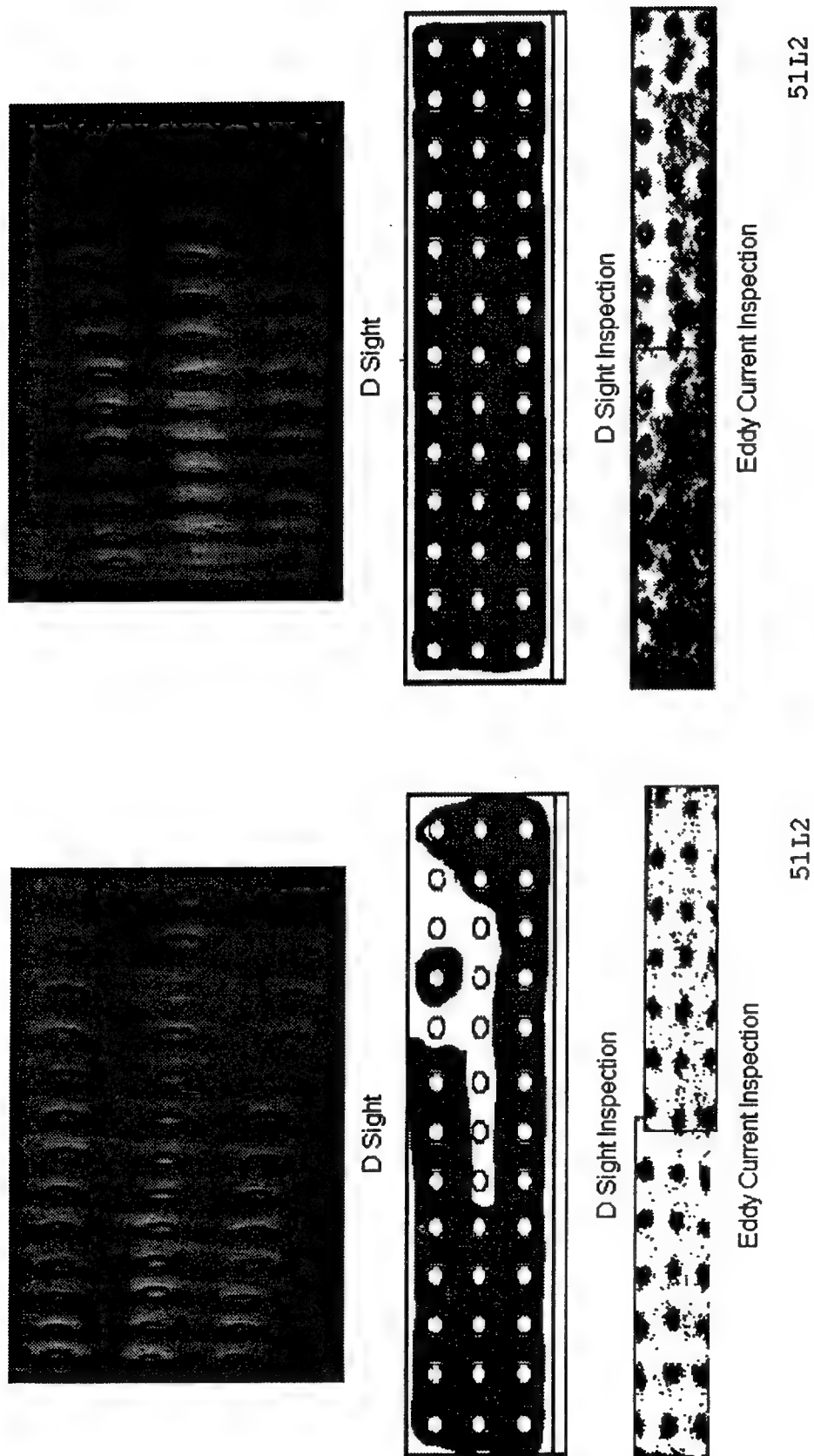


Figure 7.8 Specimen 51L2 pre- and post-corrosion inspection results. D Sight images, D Sight and Eddy Current corrosion maps.

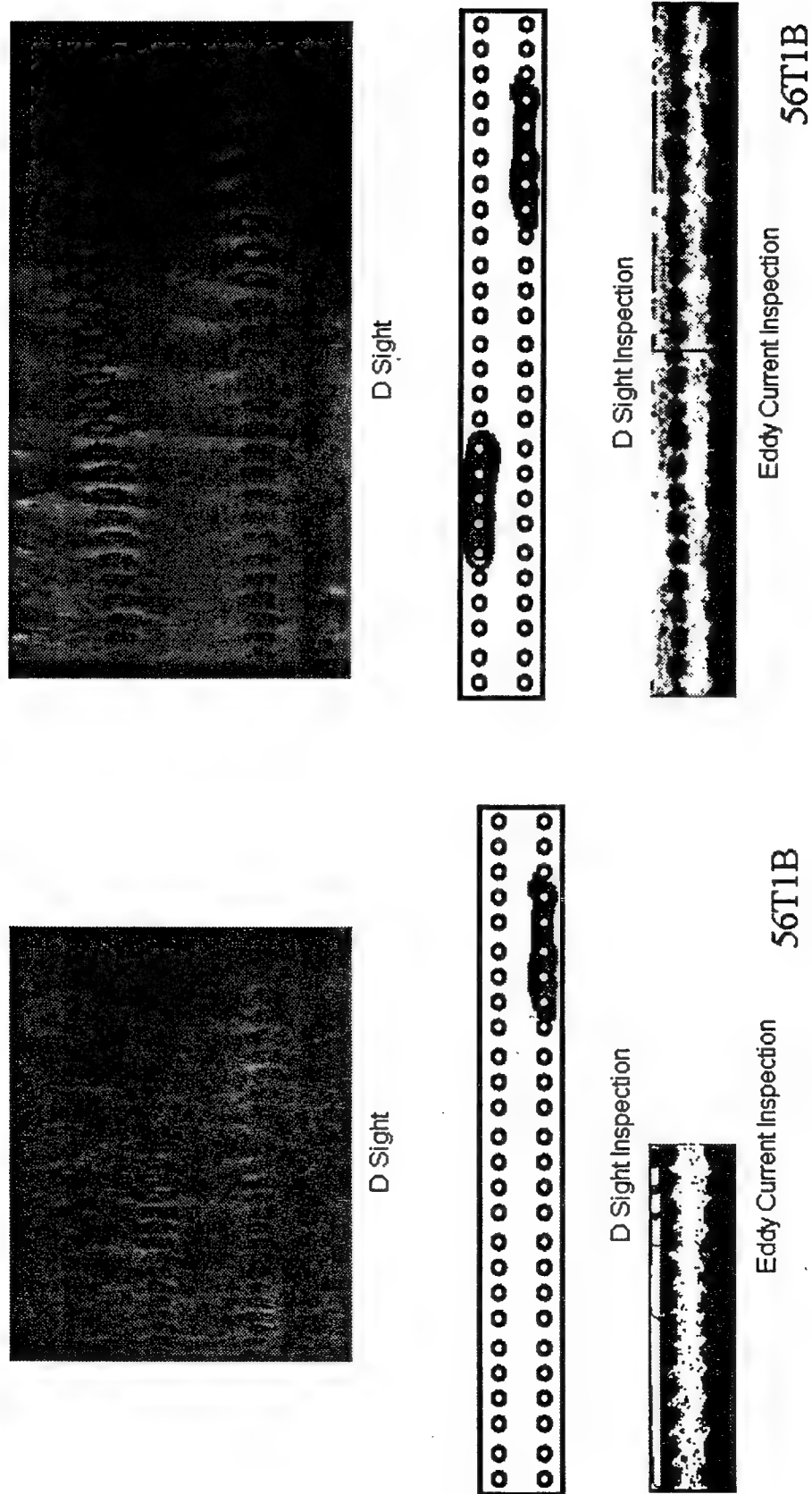
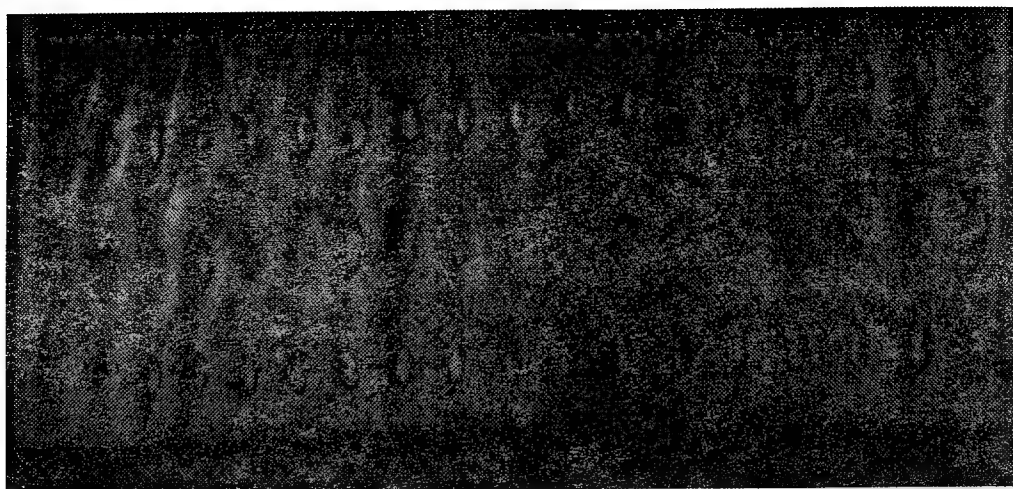
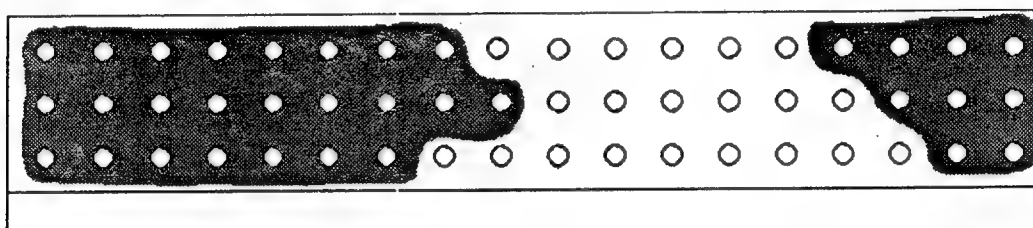


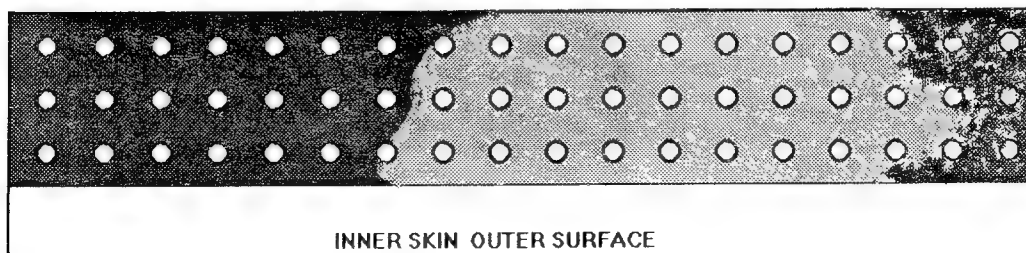
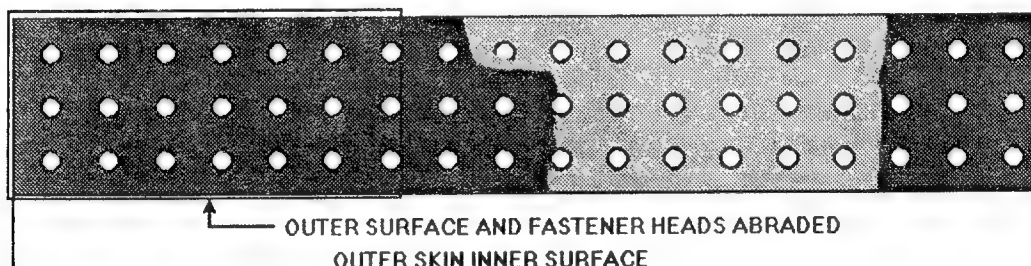
Figure 7.9 Specimen 56T1B pre- and post-corrosion inspection results. D Sight images, D Sight and Eddy Current corrosion maps.



D Sight image



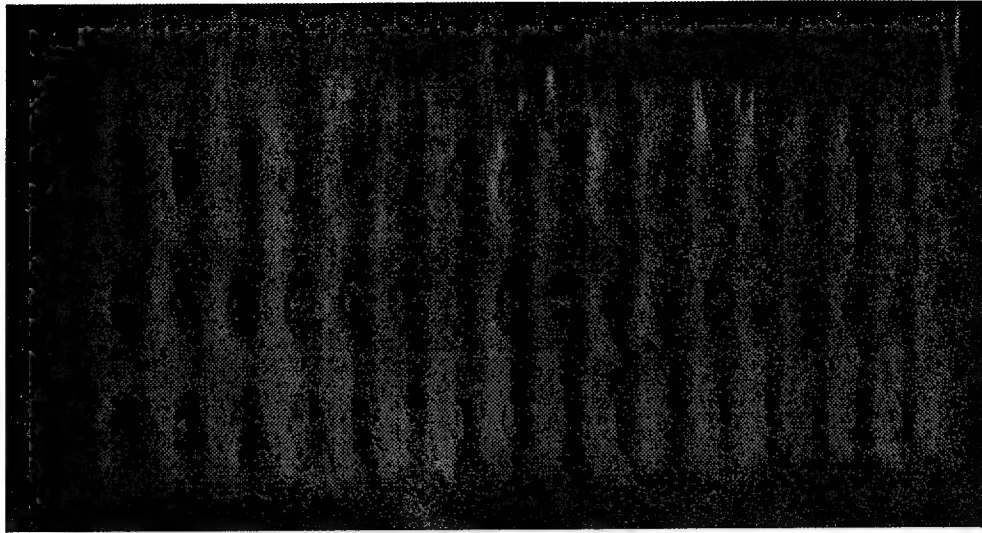
D Sight corrosion map



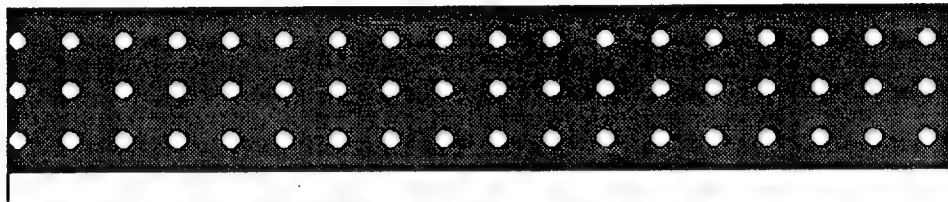
■ CORROSION  
 ■ NO CORROSION

TEARDOWN INSPECTION OF SPECIMEN B727 51L1

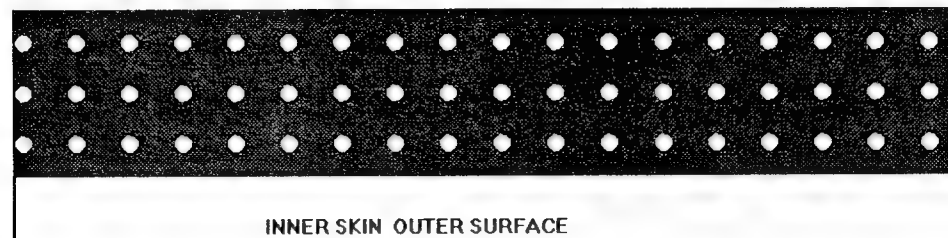
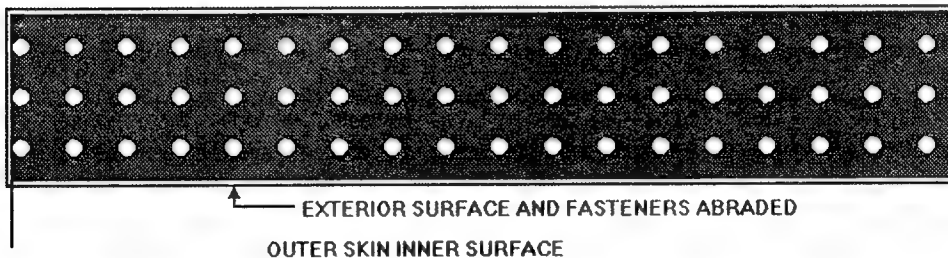
Figure 7.10 Specimen 51L1 D Sight and teardown maps of corrosion.



D Sight image



D Sight corrosion map



■ CORROSION  
 ■ NO CORROSION

TEARDOWN INSPECTION OF SPECIMEN B727 51L6

Figure 7.11 Specimen 51L6 D Sight and teardown maps of corrosion.

## 8.0 FUTURE WORK

The results obtained so far, in terms of generating corrosion by artificial means in the laboratory and detecting them with the D Sight inspection technique, have been quite successful. However, it is obvious that continued experimentation is necessary to generate more specimens with varying degrees of corrosion, for proper quantification and calibration of the D Sight set up in its application to corrosion detection. Experimentation with various standard techniques of accelerating corrosion in the laboratory has shown that the CASS technique employed is probably the fastest and most reliable means of simulating corrosion in aircraft structures. Unfortunately the CASS technique still requires considerable time (up to 2 months) to penetrate into the lap and butt joint specimens and induce corrosion within the splice. Further, considerable time is lost in disassembling and re-assembling the specimens for preparation of the interior surfaces to develop corrosion. In an effort to speed up the process, trials are underway to introduce the corrosive solution into the joint without having to disassemble and re-assemble the specimen. The method adopted is to open one of the rivets and to pump in the solution through the gap between the outboard skin and the inboard skin at the open rivet hole. A pneumatic pump capable of applying the required amount of pressure has been modified with end-fittings to suit this purpose. Initial trials in pumping in the solution in this manner have been successful. The corrosive solution needs to be pumped in at regular intervals to maintain its strength and concentration inside the joint. The method appears to be promising, but it is too early to judge how effective this new technique is and how much time saving it offers in comparison to the method of salt fog exposure in the corrosion chamber.

In the meantime the application of corrosion to aircraft specimens using the CASS technique is continuing, so that the degree of severity of corrosion in some of the previous samples can be increased and more new samples with corrosion can be produced for further studies on the application of D Sight to corrosion detection. The corrosion cabinet has been moved to an alternative location equipped with an exhaust system, so that the danger of salt contamination of other equipment is removed and the corrosion test chamber could be allowed to function continuously without interruption.

The data regarding the chemical composition of the corrosion product samples is being used to develop a mathematical model for correlating the amplitude of the pillowing deformation of the outer skin of the lap joint to the degree of corrosion inside the joint. This model is being developed with the idea that it will provide the tool for linking the D Sight measurements of the outer surface to the loss of aluminum material within the lap joint segment being interrogated. Ultimately it is expected that the model will offer the capability for

predicting the extent of corrosion within the joint, in terms of thickness loss at the internal surfaces of the outboard and inboard skins, from the measured magnitude of the amplitude of lateral deflection or "pillowing" of the outer skin.

The chemical characterization tests have produced conclusive evidence regarding the accuracy with which the laboratory process of exposure to acidified salt spray (as per ASTM B368) simulates the corrosion process in aging aircraft. However these studies could not establish the precise structure of the trihydrate phase in the samples (Gibbsite or Bayerite), nor were they sufficient for a precise quantification of the relative concentrations of the monohydrate and trihydrate phases. The latter is especially important from the point of view of mathematical modelling of the deformation caused by the corrosion build-up. A detailed study of the corrosion products at various stages of aging using the x-ray diffraction technique can not only resolve these issues but would also be helpful in determining the extent to which aging influences the composition of the corrosion products.

## 9.0 CONCLUSIONS

The results of the work carried out at the Institute for Aerospace Research in fulfilment of Tasks 5.4 to 5.10 of the collaborative agreement between the NRC, TDC and FAA on the Application of D Sight for Corrosion Detection have been presented in this report. The accomplishments of the IAR research team in this venture can be summarized as follows:

1. An extensive specimen library of fuselage lap and butt joints, consisting of both corroded and uncorroded specimens has been built up at IAR over the last year.
2. A procedure has been established for the application of accelerated corrosion in the laboratory that can reliably and successfully simulate the corrosion build-up occurring naturally in aging aircraft.
3. Comparative chemical analysis of corrosion products has verified the similarity between corrosion caused by exposure to acidified salt spray and that occurring on aircraft skin in the natural environment. The results of the chemical characterization tests are being used to develop a mathematical model of the pillowing deformation caused by corrosion build-up in fuselage lap joints.
4. A data base of D Sight inspection records on specimens with natural and artificially induced corrosion has been developed. For many of these specimens records of

inspection using alternative NDE techniques such as x-ray, eddy current and shadow moiré are also available for comparative evaluation.

5. In general reasonably good correlation has been obtained between D Sight and eddy current monitoring of corrosion in lap and butt joints. Where some lack of correlation is observed, it appears to be due to the higher sensitivity of D Sight or the higher threshold of thickness loss required for eddy current detection.
6. D Sight results are also well corroborated by shadow moiré mapping of the pillowing deformation caused by corrosion build-up. While the D Sight results are mainly qualitative, the application of shadow moiré facilitates quantitative interpretation of the effect of corrosion build-up. Further comparative studies between the two would be useful for the development and verification of a mathematical model for the quantitative interpretation of D Sight results.
7. There is significant disparity between the responses of the Boeing lap joints and those from McDonnell Douglas aircraft. The latter appear to be much less susceptible to corrosion than the Boeing splices. Further work with accelerated corrosion testing should concentrate more on Douglas specimens, so that a better understanding of their resistance to corrosion may be developed.
8. Further work could be done on increasing the reliability of eddy current inspection for corrosion application in terms of proper calibration of the set up and surface preparation of the specimens for noise reduction. This may assist in obtaining better correlation between D Sight and eddy current results. More specimens have to be subjected to tear down and visual inspection to obtain conclusive verification of both techniques of corrosion monitoring.
9. Development of a mathematical model for retrospective correlation between measured pillowing displacements and thickness loss due to corrosion will be the corner stone for application of the D Sight technology for corrosion monitoring. Starting with a simple linear approximation, the model would have to be progressively refined and verified at each stage for correctness and applicability. This calls for simultaneous attention to both experimental testing and analytical work.

## 10. ACKNOWLEDGEMENTS

The authors would like to thank: Mrs. J. Leonardo from Canadian Institute for Scientific

and Technical Information for identifying companies involved in parting and scrapping decommissioned aircraft; Mr. M. Micham of Soundair Inc. for his continued assistance in locating suitable airframes and Mr. C. E. Chapman for his guidance with eddy current and x-ray inspections.

## 11. REFERENCES

1. J.P.Komorowski and R.W.Gould, *D Sight for Aircraft Corrosion Inspection - Report on Tasks 5.1, 5.2 and 5.3*, Report Number LTR-ST-1943, Institute for Aerospace Research, National Research Council of Canada, August 1993.
2. *Standard Test Method for Exfoliation Corrosion Susceptibility in 2XXX and 7XXX Series Aluminum alloys (EXCO Test)*, ASTM G 34 - 90, Annual Book of ASTM Standards, Vol.03.02, 1993.
3. *Standard Practice for Evaluating Stress Corrosion Cracking Resistance of Metals and Alloys by Alternate Immersion in 3.5% Sodium Chloride Solution*, ASTM G 44 - 88, Annual Book of ASTM Standards, Vol.03.02, 1993.
4. *Standard Test Method for Salt Spray (Fog) Testing*, ASTM B 117 - 90, Annual Book of ASTM Standards, Vols.02.05, 03.02, 1993.
5. *Standard Practice for Modified Salt Spray (Fog) Testing*, ASTM G 85 - 85, Annual Book of ASTM Standards, Vol.03.02, 1993.
6. *Standard Method for Copper-Accelerated Acetic Acid-Salt Spray (Fog) Testing (CASS Test)*, ASTM B 368 - 85, Annual Book of ASTM Standards, Vol.02.05, 1993.
7. S.Krishnakumar, J.P.Komorowski and I.Sproule, *Chemical Characterization of Corrosion Products in Fuselage Lap Joints*, Rept. No. LTR-ST-1952, Institute for Aerospace Research, National Research Council of Canada, November 1993.
8. H.H.Uhlig and R.W. Revie, *Corrosion and Corrosion Control*, John Wiley and Sons, New York, 1971.
9. H.P. Godard, W.B. Jepson, M.R. Bothwell and R.L. Kane, *The Corrosion of Light Metals*, John Wiley and Sons, New York, 1967.
10. U.R. Evans, *The Corrosion and Oxidation of Metals: Scientific Principles and Practical Applications*, Edward Arnold (Publishers) Ltd., London, 1960.
11. E. Deltombe and M. Pourbaix, *Corrosion*, Vol.14, pp.496, 1958.
12. R.K. Hart, *Trans. Faraday Soc.*, Vol.53, pp.1020, 1957.
13. F.J. Shipko and R.M. Haag, Report KAPL-1740, General Electric Co., Knolls Atomic Power Laboratory, July 1957.

14. Eddy Current Inspection, Detection of Corrosion Manual, page 42, paragraph 2.1.6, McDonnell Douglas.